THE MECHANICS OF CREEP CRACK GROWTH IN A MAGNOX ALLOY

by

Neil Trigwell

Thesis submitted to the University of Aston in Birminham

for the degree of Doctor of Philosophy.

October 1979

The Mechanics of Creep Crack Growth in a Magnox Alloy

By Neil Trigwell - Submitted for the Degree of PhD. - October 1979

Summary

Magnox AL80 has been used for a study of creep crack propagation. A number of variables have been considered such as specimen geometry, notch root radius, material thickness, creep prestrain and stress level. The work has covered the material behaving under two values of the creep exponent, n=3.5 and n=7, according to the stress level.

As well as observing initiation times and crack growth rates, scribed grids have been used to examine the near crack tip strain levels and distributions. It was shown that estimations of COD from notch flank opening can give misleading indications of material behaviour and that a more informative method was to monitor displacements in the material surrounding the crack tip. Strong evidence was found for crack advance being displacement controlled, however it was shown that the COD approach should be considered geometry dependant. The summation of ε_{xx} and ε_{yy} provided the most successful description of crack advance as it produced a single value that described propagation in all the cases considered.

The strain distributions indicated that σ_{yy} was related to distance from a point ahead of the crack tip by the exponent $-(1/n+1)$ and that σ_{xx} is proportional to σ_{yy}. The constraint stresses arising in the DEN and CN specimens were evaluated.

Initiation time was found to be principally affected by the stress level but was modified by the constraints arising from specimen geometry. Crack growth was found not to obey either the empirical K or σ_{nett} relationships but was reviewed in context of the observed strain behaviour.

Key Words

Magnox AL80, Creep Crack Growth, Strain Distribution, Displacement Control

CONTENTS

1. GENERAL INTRODUCTION

Fracture mechanics allows the calculation of safe working stresses in components and structures at ambient temperatures which contain cracks. It would be of considerable benefit to the design engineer and to the plant engineer if these concepts could be applied to the operation of industrial plant at elevated temperatures. Under these 'creep' conditions a defect will almost always grow. The prediction of the growth rate of a crack like defect is a vital factor in the safe and economic operation of high temperature plant. The reliable knowledge that a small crack will not grow to critical size for fast fracture before the next scheduled maintenance period could save vast expense in unnecessary shut downs of high temperature plant.

This work is intended as a study of some of the factors which may influence creep crack growth predictions. The material under study is a nuclear reactor canning material, Magnox AL80. A brief review of the reactor systems in use of this country for power generation is given below as reference to the industrial application of Magnox AL80.

1.1 Nuclear Reactors

The nuclear reactor is already playing an important role in easing demand on fossil fuel supplies by using an economic alternative fuel and unlike oil and coal, nuclear fuel has little practical use other than for energy production.

The principles of all types of nuclear power station are basically the same. Electrical power is produced by a steam turbine driven generator. The steam is produced in a heat-exchanger, by heat taken from the reactor vessel by a transfer gas or liquid.

In the reactor vessel the fuel is bombarded with thermal neutrons causing it to decay into fission products releasing energy plus more thermal neutrons, which sustain the neutron flux giving a chain reaction. The thermal neutrons released are travelling too fast for efficient continuity of the reaction in a thermal reactor, so a moderator is used to slow down the neutrons. The thermal energy is removed by the cooling medium which in some reactors doubles as the moderator. In a fast reactor using plutonium fuel the fuel is sufficiently concentrated for the reaction to be maintained without a moderator. There are numerous variations on these themes[2,3] (see Table 1.1).

The development of the nuclear programme in this country has led to a logical progression through three main reactor types[2]. Firstly, the early Magnox type thermal reactor (fig. 1.1) fueled with uranium. This is being superseded by the Advanced Gas cooled Reactor (AGR). The AGR uses enriched uranium oxide fuel and has a higher operating temperature, giving more efficient generation than the Magnox Reactor. Thirdly, there are plans to introduce Fast Breeder Reactors using Plutonium fuel (fig. 1.2). These reactors should enable cheaper power generation than any other system, making use of the plutonium produced from the thermal reactors. The fueling arrangement of the Fast Breeder Reactor is such that more fissile material is produced than consumed. A fourth reactor type, the Light Water Reactor, is under consideration as a cheaper, less technologically demanding alternative to the AGR. However, decisions with regards the introduction of this reactor type are at present deferred.

CHARACTERISTICS OF MAJOR REACTOR TYPES TABLE.1.1

REACTOR	Magnox	AGR	CANDU	LWR	SGHWR	HTR	Fast Breeder
Country of Origin	Britian/ France	Britian	Canada	USA	Britain	Several	UK/USA
Fuel	Metal Natural	Oxide 2% enriched	Oxide Natural	Oxide 3–4% enriched	Oxide 2–3% enriched	Carbide 10% enriched	Plutonium
Cladding	Magnox	Stainless Steel	Zirc- aloy	Zirc- aloy	Zirc- aloy	Silicon- Carbide	Stainless Steel
Moderator	Graphite	Graphite	Heavy Water	Water	Heavy Water	Graphite	None
Coolant	CO_2	CO_2	Heavy Water	Water	Water	Helium	Sodium
Steam Cycle Efficiency	31%	42%	30%	32%	32%	39%	44%

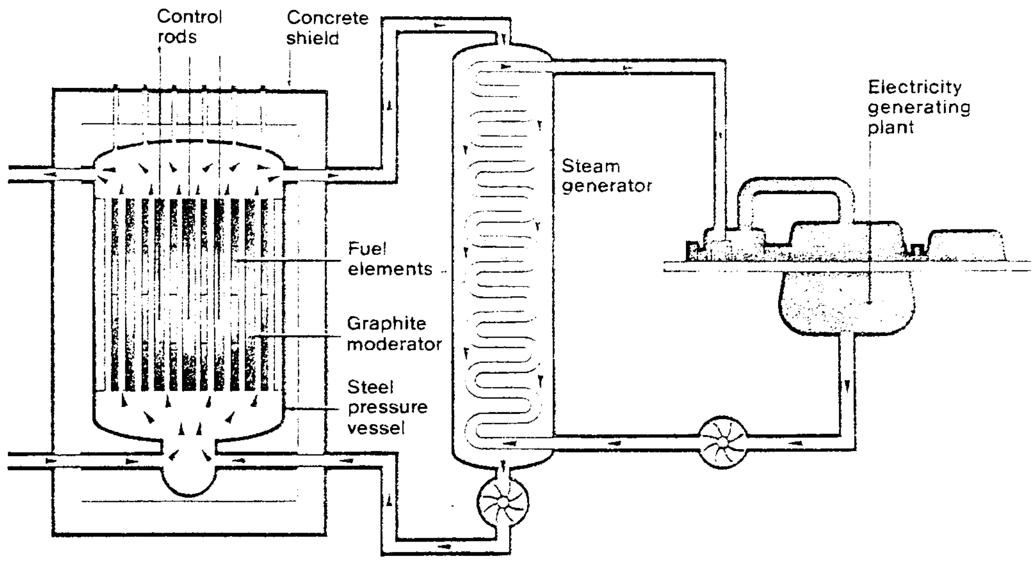

Magnox Thermal Reactor — Graphite Moderated (UK)

FIG. 1.1

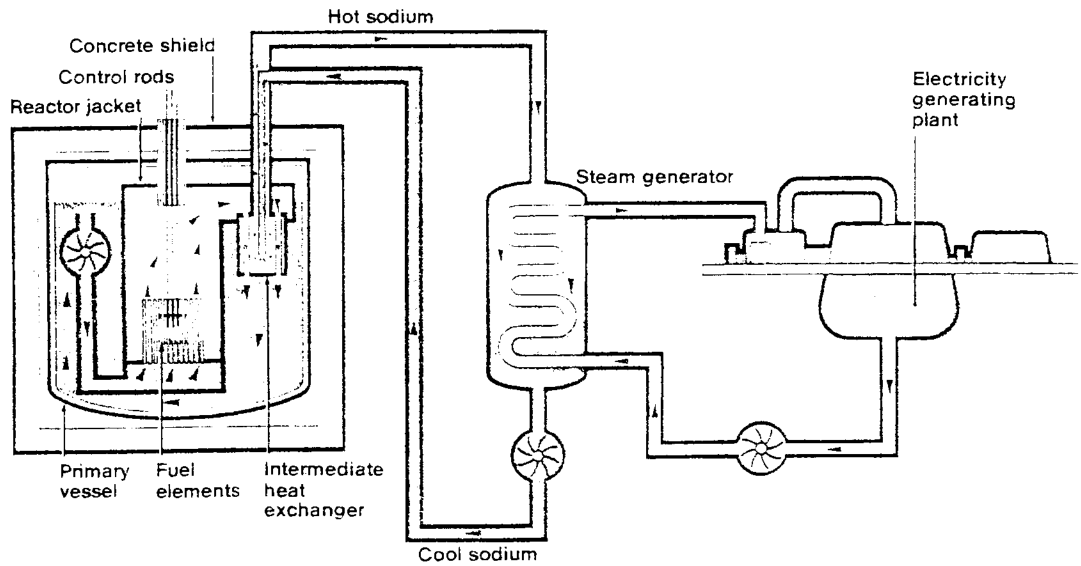

Fast Reactors — Sodium Cooled

FIG. 1.2

1.2 This Work

The development work involved in these reactor programmes has been on an immense scale with many components requiring resistance to an environment of a completely unprecedented nature. This work has been restricted to one material developed specifically for use as a fuel containing medium in the Magnox reactor, Magnox AL80. The more modern reactor systems utilising enriched fuels usually use a stainless steel for fuel cladding such as AISI 316. However, the extensive amount of existing data on Magnox AL80 suggested its particular suitability to a study of the stress and strain profiles preceeding defects growing under creep conditions. Knowledge of the nature of these profiles will be essential to the understanding of how creep crack growth rates may be predicted.

2. LITERATURE SURVEY

2.1 Development of Magnox AL80

A canning material must perform the following functions:[4]

1) Retain the fuel and fission products

2) Prevent oxidation of the fuel by the coolant (less important in the AGR where enriched oxide fuel is used).

It must also conform to the following requirements:

a) Present a low cross section to thermal neutrons (again less important with the more advanced reactors using enriched fuels).

b) Be resistant to corrosion in the cooling medium, including not forming low melting point constitu nts with particles carried in the coolant. It must also be resistant to corrosion in the cooling pond.

In the Magnox reactor operating conditions are such that can temperatures of around 460°C can be experienced,[5] with carbon dioxide pressures of up to 2.5MNm^{-2}.[6] Under these conditions, uranium when irradiated for long periods can undergo severe swelling due to evolution of gaseous fission products (such as iodine). It can also exhibit 'ratcheting' a form of distortion due to a growth along the [010] axis and contraction along the [100] axis of its orthorhombic crystal structure.[4]

Most creep applications require resistance to deformation. With a canning material it is more important that the can deforms with the fuel rather than cavitates or cracks which could result in fission product leakage into the coolant. The fuel cans are finned for better heat extraction and although mechanical strength is basically a secondary consideration some level of strength is required to ensure the heat transfer surfaces are reasonably resistant to deformation. Of the materials with a sufficiently low cross section to neutrons, beryllium is too brittle and aluminium reacts with uranium even at quite low temperatures. This left a magnesium based alloy as the most obvious possibility. This choice also had the advantage of good thermal conductivity and a low density. This enabled the effective cooling surface of the can to be much increased by finning at a very small weight penalty.[4]

The development of Magnox AL80, formerly A12 was performed by the United Kingdom Energy Authority and Magnesium Electron Ltd.[78] Primarily attention was paid to preventing oxidation in moist air and CO_2 leading to an alloy of:

$$Mg + 1\%Al + 0.01\%Be + 0.05\%Ca$$

Named MAGnesium Non OXidising. It proved difficult to obtain satisfactory welds with this alloy and it also proved more difficult to pressure shrink the can onto the fuel than envisaged. These problems were overcome by eliminating the calcium and decreasing the aluminium to give a final specification:

Al	0.7 - 0.9 Wt%
Be	0.002 - 0.03 Wt%
other metals	0.039 Wt%
Mg	Balance

This alloy is basically single phase. However, a very small volume of Al-5%Be second phase hardening particles may form with higher Beryllium levels. The solubility of Beryllium in magnesium is around 0.005%.[2]

Under pile conditions the oxidation resistance and fire resistance of pure magnesium were shown to be adequate.[10] This should apply to any magnesium alloy with a high enough melting point.

The main problems with Magnox AL80 were confined to low creep ductility around 200°C (see fig. 2.1)[4] and a pronounced tendency for grain growth around 400°C. These limitations do have practical significance. Cans near the gas inlet ports can be in the temperature range of this ductility trough. Shuffling cans from hot to cold regions and vice versa is desirable to obtain uniform burn up. However the cans from a hot zone may have undergone severe grain growth. This would present a serious possibility of leakage due to inter-granular cracking if they were then cooled to an operating temperature where the creep ductility was at a minimum. The shuffling of Magnox fuel cans can hence only be carried out on a limited scale.[4]

Some use has been made of Mg. Zirconium based alloys.[4] These alloys are fine grained and resistant to grain growth but on the whole, the sufficiently corrosion resistant alloys did not reach or maintain the same level of strength as AL80 under service conditions. Also the diffusion of plutonium through the Zr. alloy into the cooling gas is much greater than with AL80 as the Al alloy can form an Al/Plutonium intermetallic. Fig. 2.2 shows a typical Magnox fuel element.[5]

2.2 Creep Properties of Magnox AL80

The use of Magnox AL80 under conditions that were previously unexperienced resulted in a very full investigation programme. The results of many workers have been condensed and analysed by Harris & Jones.[12]

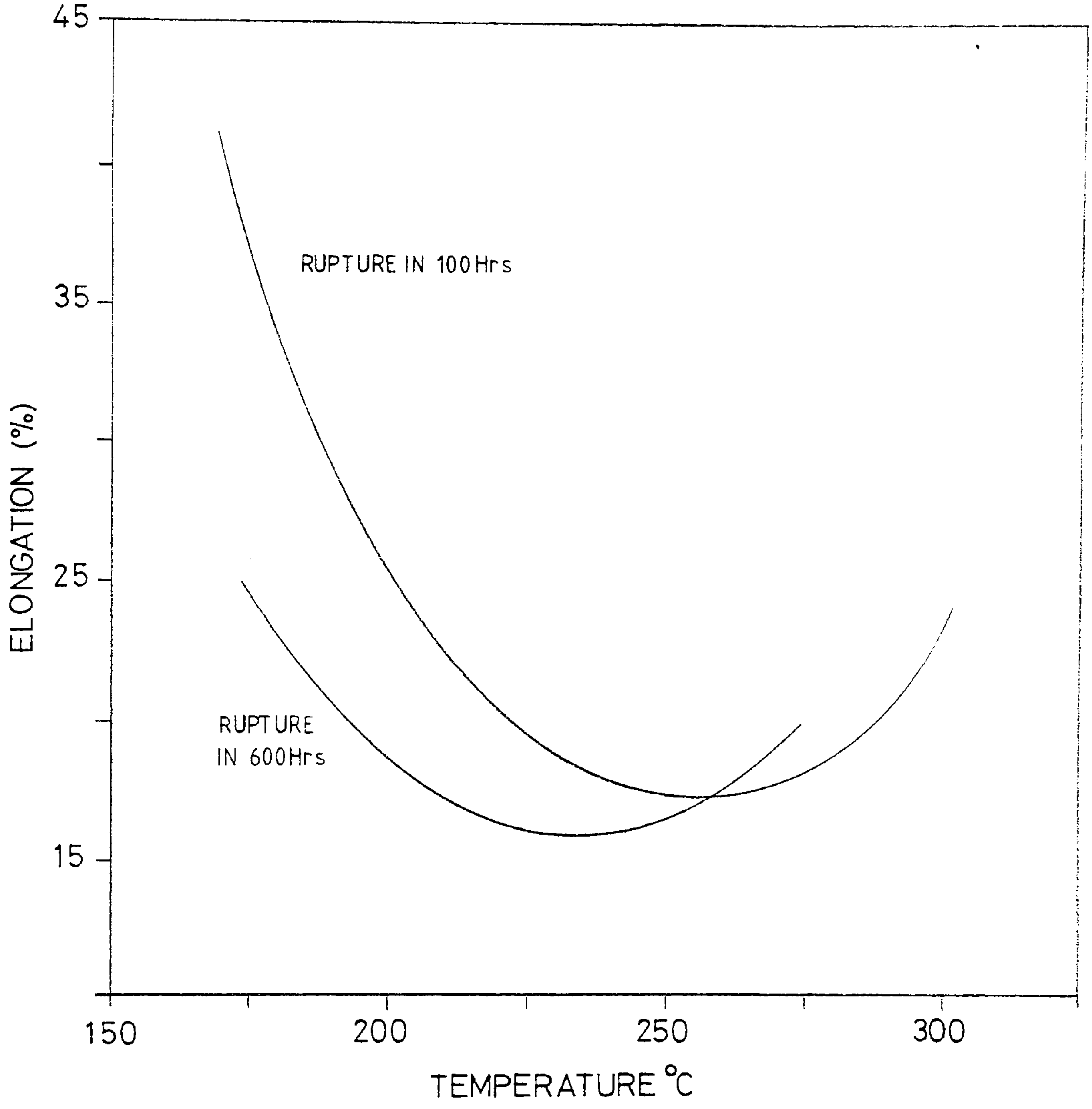

DUCTILITY .V. TEMPERATURE
FOR MAGNOX AL80

FIG.2.1

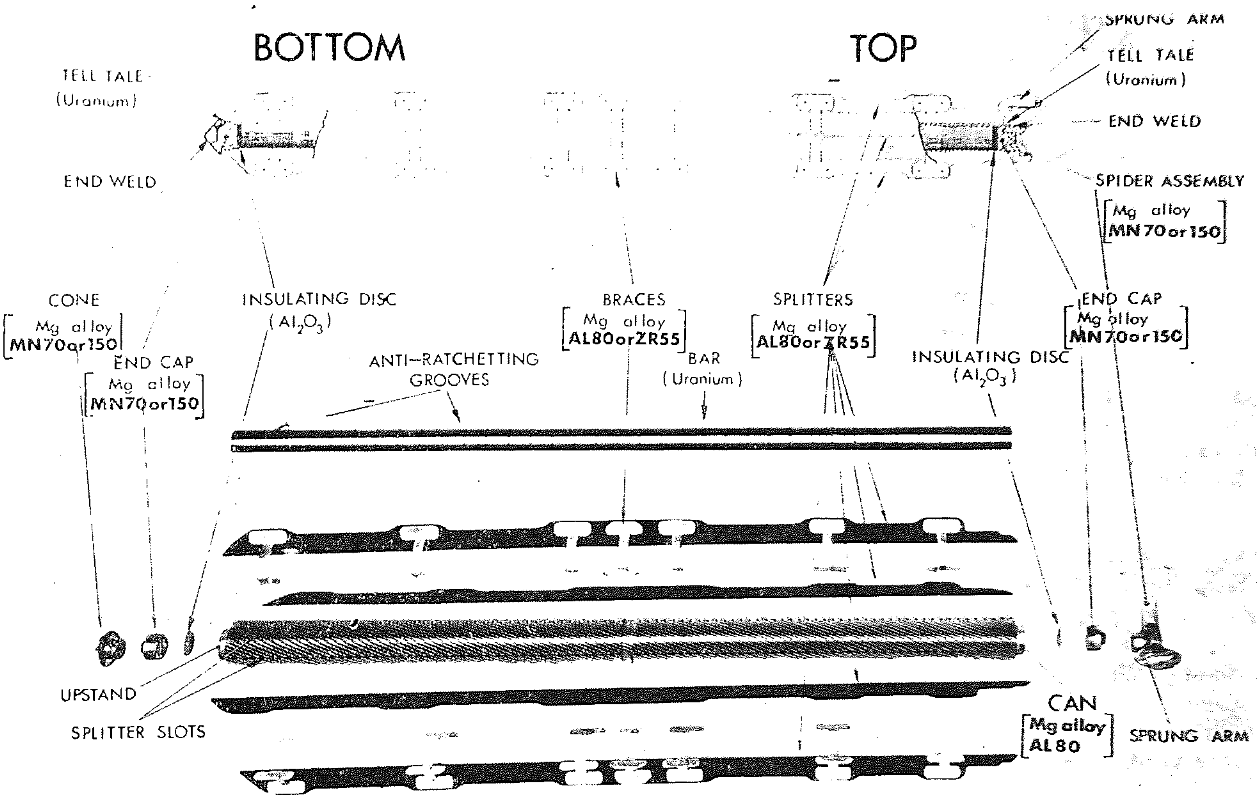

COMPONENTS OF A TYPICAL MAGNOX FUEL ELEMENT

FIG. 2.2

It was found that the creep behaviour of AL80 could be described by three basic equations depending upon the level of stress. This is possible because for many metals and alloys the activation energy for secondary creep is temperature independant above approximately half the absolute melting point (0.5_m ^oK).[13-16] This corresponds to a temperature of around 185^oC for Magnox AL80. It was found that the secondary creep behaviour could be expressed as follows:

Stresses above $15.5MNm^{-2}$,

$$\dot{\varepsilon} = 26.0 \times d^{-0.5} \times \sigma^{7.0} \times \exp(-32000/RT) \qquad 2.1$$

Stresses between $0.55 - 15.5MNm^{-2}$

$$\dot{\varepsilon} = 27.4 \times 10^{4} \times d^{-0.8} \times \sigma^{3.5} \times \exp(-32000/RT) \qquad 2.2$$

Stresses below $0.55MN^{-2}$

$$\dot{\varepsilon} = 84.3 \times 10^{5} \times d^{-2.0} \times \sigma \times T \times \exp(-32000/RT) \qquad 2.3$$

Where $\dot{\varepsilon}$ = secondary creep rate in Hr^{-1}

d = mean grain diameter in mm

σ = stress in MNm^{-2}

R = gas constant = 1.98 cals. $mol^{-1}deg^{-1}$

T = temperature in ^oK

All three of these equations are of the Norton Law type, that is secondary creep behaviour can be described by the generalised form:

$$\dot{\varepsilon} = A\sigma^{n} \qquad 2.4$$

Where A & n are constants

The importance of the structural feature, that is grain size, in equ. 2.1 & 2.2 is thought to be due to the greater number of high angle boundaries in finer grained material. This will allow more rapid sliding,[17] enhanced boundary diffusion,[18] and migration.[16]

At the low stress range the exponent of approximately unity and increased sensitivity to grain size suggests a directional diffusional creep mechanism[12] (i.e. Herring Nabarro type mechanism)[19,20]. It has been shown that a threshold stress exists for diffusion creep in many metals and alloys below which it will not occur.[21] For Magnox AL80 this stress will correspond to less than $0.1MNm^{-2}$ above $400^{\circ}C$. The effect of second phase particles has been shown to inhibit diffusion creep and the presence of such particles could raise this threshold stress significantly.[5,22]

The higher stress ranges, that is above $0.55MNm^{-2}$, will be controlled by slip creep mechanisms. Both stress dependancies in this slip creep regime exhibit the same activation energy for creep,[12,23] suggesting a similarity in the rate controlling mechanism. At the intermediate stress range the stress exponent is lower than for pure magnesium, 3.5 as opposed to 5.0.[21] Such a reduction in exponent is not uncommon in solid solution alloys and is probably due to the action of micro-mechanisms, such as solute drag, becoming the rate controlling factor.[24] The absence of any accurate energy data on the diffusion of Al in Mg has prevented precise definition of the micro mechanism operative in AL80.[25]

The increase in exponent above a certain stress is also common in metals and alloys.[24] It has been suggested that at the high stress levels behaviour could be better described by:[25]

$$\dot{\varepsilon} = A.\exp(B\sigma) \qquad 2.5$$

Where A & B are constants

However, any improvement in describing the creep rate of Magnox AL80 is slight, especially in view of the scatter in the accumulated data, and an expression of this form is less convenient in use.

The stress at which this deviation from the low exponent value occurs has been observed over several materials to be roughly proportional to the elastic modulus.[24] The exact reason for the deviation appears uncertain. It has been proposed that it is due to an increase in the number of vacancies at stresses above the transition. These will aid climb and diffusion thus assisting both conventional and micro-creep mechanisms.

2.3 Micro Aspects of Creep Fracture

There are two fundamental factors which cause creep deformation to differ from normal plastic behaviour. They are grain boundary sliding and diffusion. Both will be seen to be integral components in the models describing behaviour leading to creep fracture.

Grain Boundary Sliding

The concept of the equicohesive temperature has long been generally established. At low temperatures grain boundaries are stronger than the grains due to lack of conservative dislocation motion within the boundary. As the temperature rises the strength of both falls, but the strength of the boundary falls faster. This leads to a point where the strengths of the boundaries and the grains are equal. This point is called the equicohesive temperature T_E (fig. 2.3). Below T_E fracture is usually transgranular. Above T_E the fracture tends to become intergranular with a corresponding fall in ductility due to the failure stress being too low to cause any extensive deformation of the grains.[1]

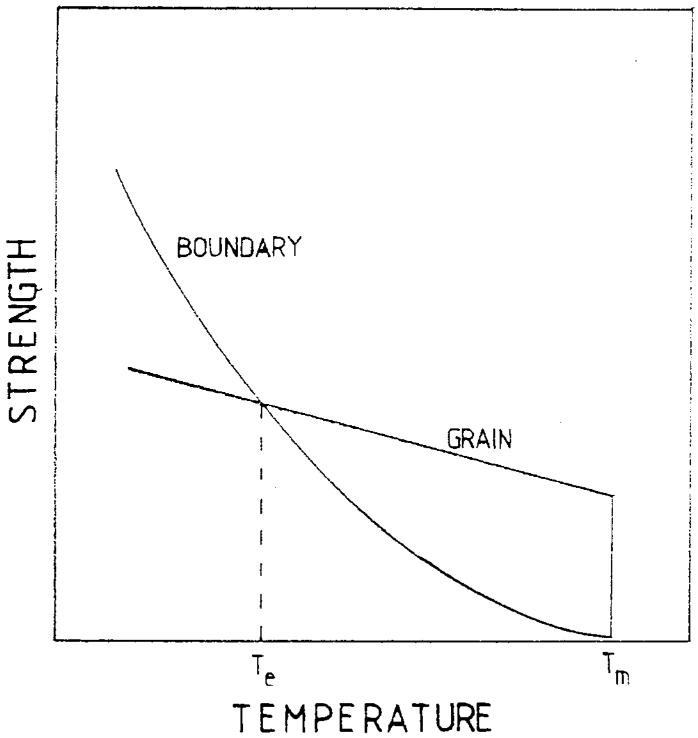

REPRESENTATION OF
THE EQUICOHESIVE TEMPERATURE

FIG.2.3

The modern concept of a grain boundary is that the two adjacent crystals maintain their specific spacing right up to a mono-atomic separation layer.[1] On the application of a sliding shear a nett flow is induced causing sliding. This is a thermally activated event and thus the equicohesive temperature will be strain rate dependant. It can be described by the following equation:[26]

$$\theta = T(C_1 - \text{Log}\,\dot{\gamma}) \qquad 2.6$$

Where θ = equicohesive point

$\dot{\gamma}$ = strain rate (shear)

C_1 = constant

Diffusion

This is also a thermally activated event and will hence become more predominant at high temperatures. Diffusion rates can be described by a classical Arrhenius equation:

$$D = D_o \exp(-Q/kT)$$

Where D = Diffusion coefficient

D_o = Correlation factor

Q = Activation energy

kT = Absolute temp. x Boltzmanns Const.

This indicates a strong rate dependance on temperature

2.3.1 Formation of Micro-Defects

The formation of voids under creep conditions was first observed by Jenkins.[27] However, their effect in limiting creep life was realised later by Greenwood.[28]

Since this time much work has been done in studying creep cavitation. Two basic types of cavity have been identified. Firstly, wedge shaped cavities or cracks situated on grain boundary triple points, in the same manner as the classic Zener Wedge Crack.[29] Secondly, rounded shaped voids situated in the grain boundary.[30] These are usually referred to as w (wedge) and r (rounded) cavities respectively.

It has been suggested that in fact w type cavities are no different from r cavities and are simply where a cavity has grown to meet a triple point. Stiegler[31] has made fractographic studies of cavities in tungsten and suggested that all cavities are initially polyhedral and change their shape according to the conditions of stress and temperature. Whilst it is very difficult to determine experimentally if a w crack actually nucleated at a triple point the work by McLean[32] does suggest the operation of two mechanisms. Examination of several high temperature alloys showed a predominance of w cracks at high stresses and low temperatures and r cavities at lower stresses and higher temperatures.

Stacey[33] working on Magnox AL80 has reported cracking below 150°C and cavitation above. Heal[34] using a much faster strain rate of 112% hr^{-1} on Magnesium determined a similar transition between 175 to 225°C. Hence there is considerable support for the existence of two distinct cavity morphologies.

2.3.1.1 Triple Point Cracking

Zener's initial theory stated that if slip along an interface was held up by an obstacle a stress concentration could build up, sufficient to initiate a crack. Eborall[35] and Chang & Grant[36] applied this concept to grain boundary triple points. Chang & Grant proposed the three classic ways a triple point crack can form. (Fig. 2.4) Seru & Grant[37] pointed out sliding on a grain boundary need not produce a triple point crack if a

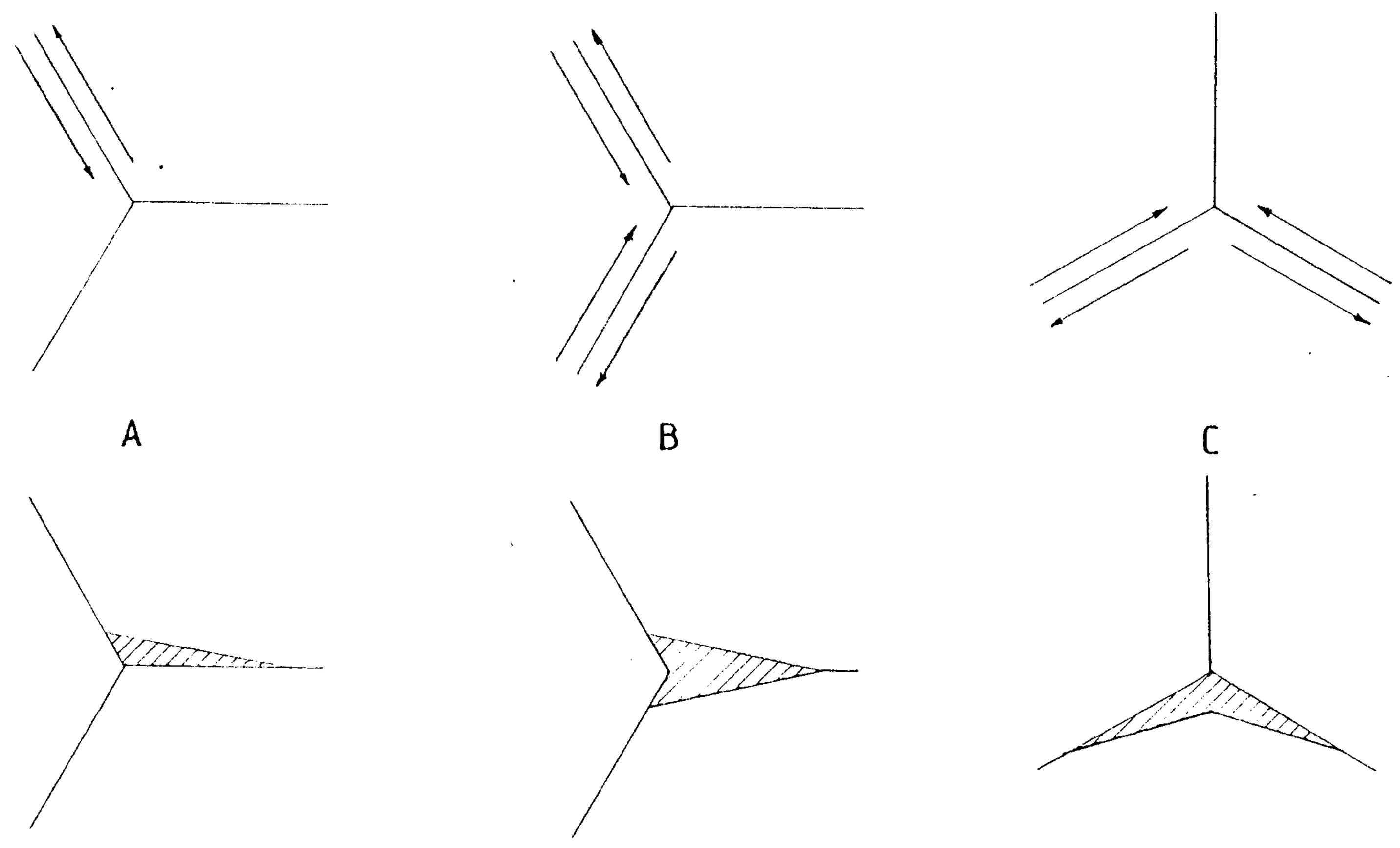

POSSIBLE MEANS OF TRIPLE POINT
CRACK NUCLEATION

FIG.24

plastic fold can occur instead.

The original fracture criterion was drawn up by Griffith,[38] based on the energy balance between, that required to produce a new surface against the stored elastic energy lost as a crack forms. The following equation was proposed:

$$\sigma_f \geqslant \sqrt{\frac{E\gamma}{c\pi}} \quad 2.8$$

Where:

σ_f = stress for cracking

E = Elastic modulus

γ = Surface energy

c = Crack Length/2 for a totally embedded crack

This implies a critical stress for fracture exists for a given crack length and vice versa. The equation only considers the elastic effects of the applied stress. Stroh[39] extended the work of Griffith to take account of the presence of dislocation pile-ups in a deformed metal. He drew up a fracture nucleation criteria as follows:

$$\tau_f \geqslant \sqrt{\frac{12\gamma\mu}{\pi(1-v)L}} \quad 2.9$$

Where:

μ = shear modulus

L = Length of sliding interface

τ_f = shear stress for crack formation

As this relationship is independant of the nature of the sliding interface it is possible to calculate an approximate value of the stress concentration at the end of a high angle boundary, necessary to nucleate a crack. Complete accuracy is not possible with this approach as no account is taken for energy dissipated as plastic work. McLean[40] applied the Stroh equation to a single dislocation pile-up model and found reasonable agreement with practical results. Application of equation 2.9 produced a value of μ about 0.3 of that expected. Stroh later amended his initial equation to:[41]

$$\tau_f \geq \sqrt{\frac{3\pi\mu}{8(1-v)L}} \qquad 2.10$$

where v = poissons ratio

Stroh stated that these equations will describe the fracture of a material giving a relationship between fracture stress and the inverse square of the grain diameter. (The sliding interface can represent the slip band length for the brittle cleavage case or the sliding grain boundary length for the creep situation, both of these will be directly proportional on average to the length to the grain diameter). Such a relationship was established by Hauser Landon & Dorn[42] for a magnesium 2% AL Alloy below 130°C. Smith & Barnby[43] examined a double pile-up model applicable to the Chang & Grant triple point crack type B in Fig. 2.4. They derived the following equation for nucleation:

$$\tau \geq \sqrt{\frac{2\gamma\mu}{n(1-v)L}} \qquad 2.11$$

This equation would reduce the level of McLean's calculated stress results as it predicts nucleation at much lower stresses. Such a reduction would have improved the agreement between McLean's calculated and practical results. The discrepancy had previously been attributed to segregated impurities.

2.3.1.2 Cavitation

This form of creep failure was recognised by Greenwood et al.[30] Small cavities were observed to form along grain boundaries, grow and coalesce. These cavities were not necessarily associated with triple points and were found mainly along grain boundaries perpendicular to the principal stress axis. This type of cavity was found by McLean[32] to favour higher temperatures and lower stress levels than the triple point cracks. It was concluded that a different process to triple point cracking was operating and it was called cavitation.

Early theories for the formation of r cavities were based on concepts of vacancies, produced by plastic deformation, condensing out on discontinuities, usually grain boundaries. It is now generally accepted that cavity nucleation is heterogenous. Grain boundary particles or ledges seem the most likely sites for nucleation but direct evidence is not particularly forthcoming. It is impossible to tell if a cavity nucleated at a particle or simply grew to meet it. Most theories advanced involve grain boundary sliding causing separation at a particle or a ledge,[45, 50, 46] as shown in Fig. 2.5. In fact grain boundary sliding must produce cavities at such points when ever plastic flow or diffusion is insufficient to prevent decohesion. Chen & Machlin[47] worked on copper bi-crystals and showed that some grain boundary sliding was necessary for cavity formation. Application of a shear stress along the boundary gave cavities, a tensile stress perpendicular to the boundary did not. Application of a combined stress produced many cavities.

Baluffi and Seigle[48] derived a critical nucleation condition for cavitation. In a simplified form, if a void radius r, in a material under a uniform stress σ, receives a vacancy from the boundary its surface energy increases by an amount $\Delta\gamma$ given by:

$$\Delta\gamma = \frac{2\gamma b^3}{r} \qquad 2.12$$

where γ_s = surface energy/unit area
b^3 = atomic volume

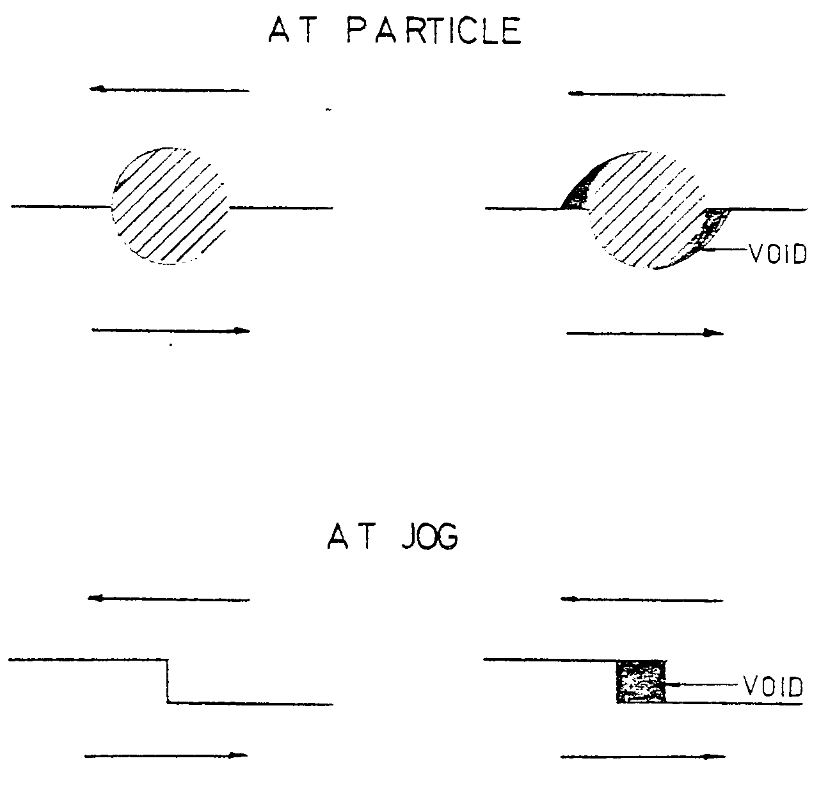

NUCLEATION OF VOIDS BY GRAIN BOUNDARY SLIDING

FIG. 2.5

The emission of a vacancy from the boundary is equivalent to the plating out of an atom on the boundary. This means a force σb^2 is moved through a distance b. If this work done exceeds the increase in surface energy cavity growth will be energetically favourable:

$$\sigma b^2 . b \geq \frac{2\gamma b^3}{r} \qquad 2.13$$

$$\sigma \geq \frac{2\gamma}{r} \qquad 2.14$$

Hence, a critical size of cavity nucleus, for a given stress level, must form before stable cavity growth can commence. It can be seen from this equation that a stress concentration will reduce this critical radius.

Rai[49] has pointed out that deformation induced decohesion is not the only mechanism for heterogenous cavity nucleation. He showed that thermodyamic considerations indicate the triple interface between a grain boundary and a non-coherent particle presents the lowest activation energy for nucleation by a vacancy cluster mechanism. Under such a mechanism, grain boundary sliding would only assist cavitation by providing a stress concentration at the particle interface. A minimum stress would be required for nucleation and there would be an incubation period whilst the critical size of vacancy cluster was accumulated by diffusion. Incubation periods and minimum stresses for cavitation have been observed.[50]

Smith & Barnby[51] considered the situation where a particle in the grain boundary could hold up sliding. The shear stresses acting on the particle may reach such a level as to fracture it, and hence form a cavity nuclei.

Fleck, Taplin & Beevers[50] used the 1M.V transmission electron microscope (TEM) to study cavities at early stages of growth in a copper alloy. The cavities observed were all associated with particles. They observed nucleation to be associated with a critical grain boundary sliding displacement. This suggested the importance of a stress concentration build-up at the particles during or before the nucleation process.

Weaver[52] pointed out that impurity particles or precipitate could form effective obstacles to grain boundary sliding. If particles were to act in cavity nucleation the distribution must be such as to enable sufficient stress build-up for nucleation and yet take the load off the triple points. If the particles stop grain boundary sliding effectively, cavitation will be delayed. This is supported by observations in Type 316 stainless steel[53] that show the effect of precipitate on cavity nucleation to be principally concerned with restricting grain boundary sliding and development of stress concentrations, providing heterogeneous nucleation sites was a secondary effect.

Cottrell[1] suggested that non-wetting precipitate would form easy nucleation sites for cavities forming by grain boundary sliding around particles. It was pointed out that aluminium which adheres particularly well to its oxide does not cavitate during creep. Following from this argument Eborall[54] suggested that the reason that titanium does not cavitate was because it dissolves its oxides and similar compounds.

At weakly coherent particles it has been shown that if the precipitate has a higher melting point than the matrix, diffusional flow around the particle will be inhibited.[55] This is due to there being little co-operative movement between the atoms of the precipitate and those of the matrix, which is necessary to enable such a boundary to act as a source or sink for vacancies. This will inhibit tendencies for a cavity formed by grain boundary sliding around a particle to sinter and hence aid the formation of a stable nucleus. This will not apply if the particle is completely non-coherent.

Harris[44] proposed that the mechanism of particle/matrix interface shearing by a grain boundary sliding induced stress concentration could account for all cavitation observed in Magnox AL80. Electron metallography revealed sufficient second phase particles to support this proposal.

Greenwood et al[30] observed that cavity spacing increased as temperature increased and was approximately equal to the slip band spacing. Slip processes can produce grain boundary ledges. Davies & Williams[56] produced a model for cavity nucleation in which secondary slip systems form small grain boundary ledges which are opened up into cavities by sliding. See Fig. 2.6. Using the 1M.V TEM to study copper Johanneson & Tholsen[46] showed cavities in very early stages of formation to be associated with grain boundary obstacles such as kinks and triple points. They proposed that the stress concentration at such points could be as high as 10^3.

Harris[44] considered nucleation at ledge type sites in Magnox AL80 unlikely as grain boundary diffusion rates are of a magnitude that would mean grain boundary sliding rates would have to be unrealistically high (1m/Hr) to prevent sintering. He favoured grain boundary separation at particles. However the electron microscopy

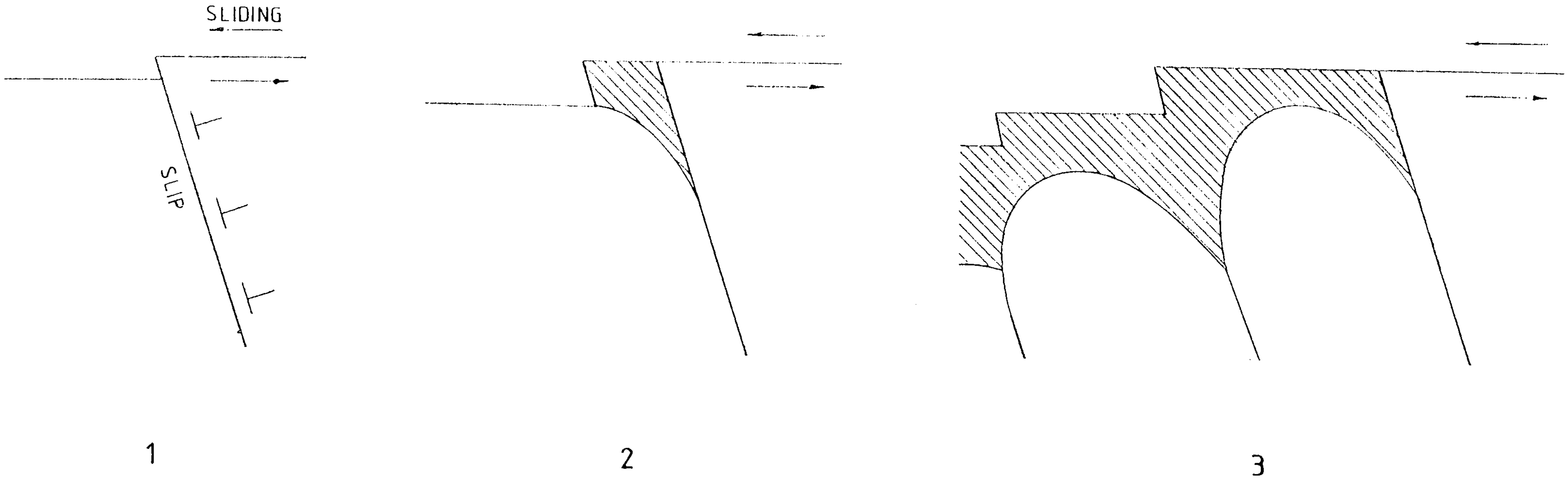

FORMATION OF CAVITIES BY
COMBINED DISLOCATION MOTION
AND GRAIN BOUNDARY SLIDING.

FIG. 2.6

study of Presland and Hutchinson [57] of cavities in pure magnesium deformed at 300°C showed that the majority of cavities were in no way associated with particles. They considered the intersection of grain boundaries with sub-grain boundaries to be the most common nucleation sites. See Fig. 2.7

2.3.2 Cavity Growth

Original theories of cavity growth were based on vacancy diffusion. Later mechanisms dependant upon deformation were advanced. Many relationships correlating cavity size, population, etc. with time related parameters have been drawn up. Table 2.1 includes some of these.

Cottrell [1] reviewed four of what he considered the most important possibilities by which a cavity could grow:

i) By spreading along the boundary like a cleavage crack through the breaking of atomic bonds by the concentrated stress at its end.

ii) By changing in volume through elastic deformation, as a result of changes in the applied stress or in the length of the cavity.

iii) By spreading along the boundary at constant volume (apart from elastic deformation) through the migration of atoms, mainly by surface diffusion from the sides of cavities to the ends.

iv) By spreading along the boundary, with changing volume, through the removal of atoms from the ends by atomic migration along the boundary or into the grains.

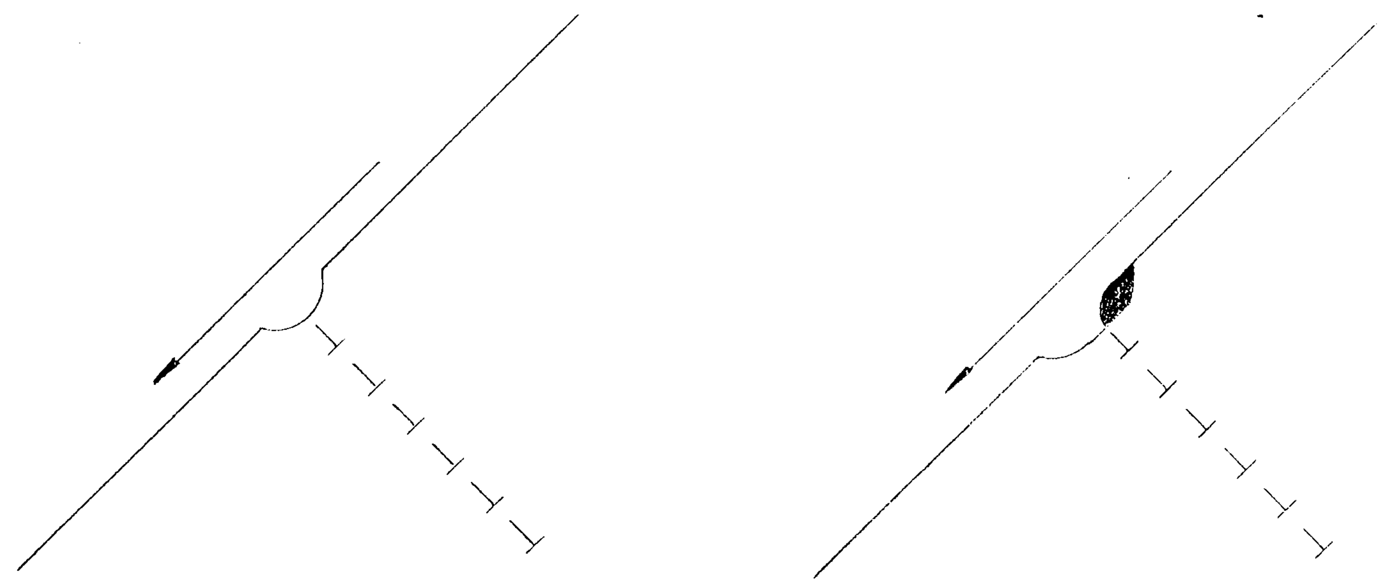

FORMATION OF CAVITIES AT
SUB-GRAIN BOUNDARIES DUE
TO SLIDING

FIG.2.7

WORKER	MATERIAL	RELATIONSHIP FOUND	COMMENTS
Greenwood[58]	Model	Cavity Vol $\propto$ (time x creep stress)	Applies to stages 1 & 11 of creep independant of shape of creep curve Assumed growth rate constant. Probably valid for widely spaced cavities.
Ratcliffe & Greenwood[59]	Magnesium	Creep strain & No. of cavities linearly related (approx)	
Ratcliffe & Greenwood[59]	Magnesium	Density change $\propto$ time$^{2.5}$	Exponent higher than expected for vacancy condensation at constant number of cavities. Must have continuous nucleation.
Price[60]	Oxygen free Silver	Creep strain & No. of cavities linearly related (approx)	
Intrater & Machlin[61]	Copper Bicrystals	Near linear relationship between cavity conc. & grain boundary sliding	
Boettner & Robertson[62]	Copper	Cavity vol. $\propto$ time$^{1.5}$	
Gittins[63]	Oxygen free Copper	Cavity No. $\propto$ time$^{0.5}$	Considered in reasonable agreement with Boettner & Robertson
Oliver & Cirifalco[64]	Silver	No. of cavities is constant	
Greenwood) Woodford)[65]	From Gittins	Linear relationship between No. of cavities & creep strain	For both stages 1 & 11 of creep

WORKER	MATERIAL	RELATIONSHIP FOUND	COMMENTS
Dyson & McLean[66]	Nimonic 80A	No. of cavities linearly increased with strain up to 75% of creep life	Considered useful in assessing remaining creep life.
Evans & Waddington[67]	Pointed out only cavities >1μm observed in metallography	Possible linear relationship between No. of observable cavities & creep strain, provided cavities followed a Log. normal size distribution and grew at uniform rate	Continuous nucleation not proven for optical microscopy studies (electron microscope studies have shown continuous nucleation)
Davies, Davies & Wilshire[68]	Nickel + Cobalt	Rupture life x creep rate = const.	Relationship independant of cobalt content, which affected stress for a given creep rate. Rupture life & hence cavity growth independant of stress, contradicting diffusion control growth by Hull Rimmer model.
Needham Wheatley & Greenwood[69]	Magnesium & Copper	Density change $\propto(\varepsilon.t.\sigma)^3$ for Cu & Mg $\propto(\varepsilon.t.\sigma)^{1.5}$ for Mg at later stages of test	Similar results suggested detailed structural features unimportant although cavities are often structually related.

TABLE OF RELATIONSHIPS CONCERNING CAVITY GROWTH

TABLE.2.1

Mode (ii) is of little interest as any contribution to crack growth by this mechanism will be small. However, it will occur in conjunction with changes in crack length by the other mechanisms. The remaining mechanisms may be considered in the context of the Griffith equation (equ. 2.8).

Mode (iv) enables a small cavity to grow, even if below the critical crack length as determined by the Griffith equation. This mechanism allows the applied load to do more work than is possible by just elastic deformation alone. The Griffith equation is based on only the stored elastic energy being available to produce a new surface.

Mode (i) The Griffith criteria is not a sufficient condition for crack growth to occur by this mode as it requires the crack tip to remain sharp. Some sharpness will be maintained at high temperature despite surface diffusion, but whether it would be sufficient for crack propagation is uncertain. This mode would result in fast fracture rates untypical of a creep situation.

Mode (iii) The Griffith criterion is always a sufficient criterion for crack growth by this mode. This is because the atomic bonds at the crack tip are overcome by thermal aggitation and hence a sharp crack tip is not required.

The observation of preferential cavity distribution along grain boundaries at 90° to the tensile stress axis and the tendency for cavities to elongate along these boundaries are strong evidence of a diffusion growth mechanism.[50,70] (i.e Mode iv) Such a mechanism could be described by the classic Herring-Nabarro model.

Baluffi & Siegle[48,71] considered the thermodynamic conditions for void growth by diffusion. They found a critical stress σ^* above which a cavity of radius r will grow by accepting vacancies from the grain boundary, as follows:

$$\sigma^* = \frac{2\gamma}{r.\cos^2\theta} \qquad 2.15$$

where θ = angle between the boundary normal and the tensile stress axis.

This treatment indicates a strong orientation dependance for cavity growth. As θ moves from 0° to 60° the stress factor will increase by 4 times. This can hence explain the observations of cavities lying preferentially on boundaries at 90° to the stress axis.

Many attempts have been made to estimate cavity growth rates based on vacancy diffusion models. A classic work performed by Hull & Rimmer[72] took the difference in chemical potential of a vacancy at a void surface and midway between voids as the driving force for diffusion. They derived the following equation for void growth rate:

$$\frac{dr}{dt} = \frac{Dg.z.\sigma.\Omega}{2kT.s.r} \qquad 2.16$$

Where: Dg = grain boundary diffusion rate
z = valency
Ω = volume of a vacancy
kT = Boltzmans constant X Absolute temperature
s = Average spacing between voids
r = cavity radius

The basic Hull Rimmer equation has since been refined by many workers to take account of several factors not considered in the original analysis. However, the relevance of exact calculation of cavity growth rates to this work suggests that these modifications do not warrant detailed examination. The most significant point of interest from these analyses based entirely upon diffusional growth is that the growth rate should be directly proportional to the stress.

The Hull Rimmer model was based on a constant number of voids, but the experimental results of Ratcliffe & Greenwood[59] indicated continuous nucleation. This concept of continuous nucleation was supported by other workers who observed cavity number / time or cavity number / strain relationships, see Table 2.1. With the acceptance of the importance of grain boundary sliding in nucleation and the advent of TEM techniques continuous nucleation has become generally accepted.[73]

Some observations show cavitation to give stronger connections with strain or strain rate than with time. This is not what would be expected if diffusion was the controlling mechanism. Work by Davies, Davies & Wilshire[68] on a range of nickel-cobalt alloys showed that for a given creep rate the fracture strain was independant of cobalt content. Additions of cobalt to the nickel increased the creep resistance and hence the stress required to produce a given creep rate. This meant that the failure strain and hence time to fail at a given strain rate were independant of stress. This is not consistent with the Hull Rimmer model even through fracture occurred by growth and linkage of voids. They suggested that under **these** conditions cavity growth was dependant upon other plastic deformation mechanisms, such as grain boundary sliding or dislocation motion.

It is a common observation that strain to failure is relatively insensitive to quite large changes in test conditions.[11] Also for a large number of materials the product of strain rate and time to failure is a constant. These observations seem to contradict a vacancy control model. A general questioning of diffusional controlled growth has resulted from these discrepancies, leading to development of an alternative approach based on deformation controlled growth.

Williams[74] experimentally determined crack growth rates in a single phase Al 20%Zn alloy as a function of stress and the angle between the crack plane and the tensile stress axis. For crack growth normal to the stress axis, the crack growth rate was found to be proportional to the opening rate of the widest part of the crack. This in turn was observed to have a 1:1 correlation with the grain boundary sliding vector parallel to the wedge opening. The crack growth was controlled by metallurgical features ahead of the crack tip. If these features restricted the plastic zone then instability would result and the crack would link off to another triple point crack. Observations of a similar nature were also made by Soderberg.[75]

Ratcliffe & Greenwood[59] observed that application of hydrostatic pressure equal in magnitude to the applied stress eliminated cavitation in pure magnesium. Hydrostatic pressure will affect the movement of vacancies but not dislocations. They considered that deformation growth was hence unproven.

Waddington & Williams[76] also studied the effect of hydrostatic pressure, using similar material to Williams. They observed that application of pressure reduced the crack growth rate and increased the rupture life and stability. They considered this was due to a reduction in the normal stresses at the crack tip. They considered the fact that cracks occurred at all in pressurised specimens as evidence of a deformation controlled process.

Needham & Greenwood[77] examined the effect of hydrostatic pressure on cavitation in copper at 500°C. They found that the application of this pressure affected the creep rate to a much greater extent than expected.

The change in creep rate was found to be reversible with changes in pressure, irrespective of the previous history of pressurisation. It was hence considered that the reduction in creep rate did not arise by the suppression of cavity growth. It was thought possible that the reduction in grain boundary sliding may account for the reduction in creep rate. Ratcliffe & Greenwood[59] had not considered the effect of pressure on grain boundary sliding, this could provide an alternative explanation for their failure to observe cavity growth in pressurised specimens.

Diffusion controlled growth does not easily account for McLean's[78] observation that small alloying additions can radically affect cavity growth rates. These additions should have little effect on the diffusion rates but can have a marked effect on mechanical properties and the nature of the grain boundaries. However, it has been proposed that second phase particles in the grain boundary may inhibit diffusional cavity growth.[55,79] If the diffusional properties of the particle and the boundary differ then back stresses may be generated around the particles inhibiting cavity growth.

Davies & Dutton[80] performed a series of experiments on Cu-15% Al at 400°C in which the stress direction was changed. The material was stressed to tertiary creep in the orientation shown in Fig. 2.8a. During this stressing grain boundary sliding occurred. A cube of the material was then cut out and tested in compression as shown in Fig. 2.8b. They found that many cavities closed and much of the density loss was recovered. A second cube was cut from the original block and compressed at 90° to the original axis, which was equivalent to the initial tensile condition. Fig. 2.8c. Cavity

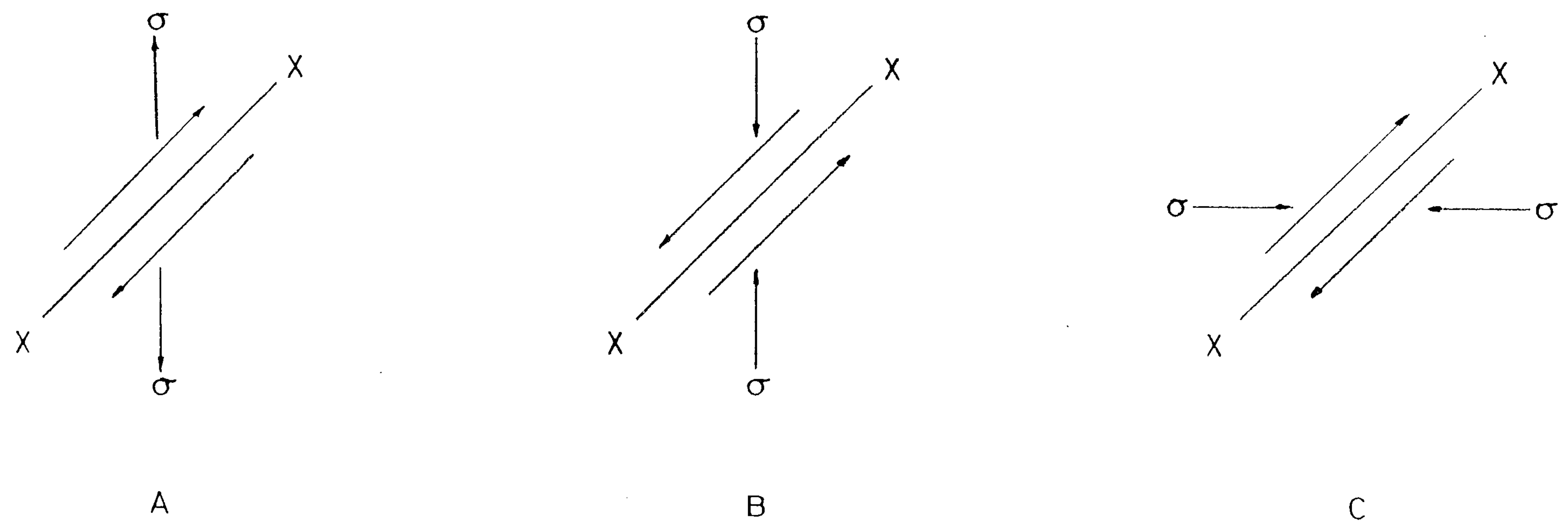

SEQUENCE OF STRESSING RELATIVE
TO GRAIN BOUNDARY (XX)

FIG.2.8

growth in this block was observed to continue. They concluded that only grain boundary sliding was contributing to cavity growth and that diffusion processes were unimportant.

This work was criticised by Taplin & Gifkin[61] on the grounds that void closure could have occurred by sintering and not grain boundary sliding on reversed stressing. Gittins[63] considered the void closure could have occurred by plastic deformation on compression. He stressed copper well into the tertiary creep stage up to a point where some void linking had occurred. On reversed stressing at room temperature some density loss was recovered. As minimal grain boundary sliding will occur at ambient temperature a sintering mechanism for void closure was proposed.

Davies & Williams[82] repeated the Davies Dutton test using copper and obtained similar results to the original work. They also performed the compression tests at room temperature with material containing isolated voids. Essentially, no shrinkage was observed indicating that the voids were not readily closed by a sintering mechanism. They suggested that the density recovery observed by Gittins could be attributed to the partial closure of the very large cavities where several voids had coalesced and not the sintering of isolated cavities.

Davies & Williams[56] proposed a model for cavity formation based on dislocation motion and grain boundary sliding as shown in Fig. 2.6. In this model slip dislocations enter the boundary and form jogs which are opened into cavities by sliding. This model can account for a relationship between cavity size and creep strain. Ishida

& McLean[83] proposed a similar model in which a dislocation moves along its glide-plane until it is stopped by a boundary. Under the action of the applied stress the dislocation continues to move by a combination of glide and climb, emitting vacancies due to non-conservative motion. The cavity can thus open out despite a tendency for it to sinter.

Hancock[84] proposed that void growth under creep conditions could be described by the McClintock[85] model more normally applied to ductile plastic conditions. The McClintock model is a mathematical approach which shows that pre-existing voids can elongate in the direction of the tensile axis and increase in volume by the action of the tensile and radial stresses.

Hancock showed this approach to be applicable to hole growth when the ratio of stress over strain rate is low, as is often seen during tertiary creep. It was also considered important in regions of localised high strain rates such as at locations of grain boundary sliding.

Unlike the diffusion growth models, the predicted growth rate by this approach does not decrease with cavity size (equ. 2.16 and 2.17). It was shown that for a linear viscous solid the growth rate can be expressed as:

$$\frac{dR}{dt} = R - \left(\frac{3\gamma}{2o}\right) \quad \text{with a through thickness stress } \sigma_{zz} = 0 \qquad 2.17$$

Where R = (length + width of cavity /2)

The cavity will shrink due to surface tension producing a hoop strain if:

$$\sigma < \frac{3\gamma}{2R} \qquad 2.18$$

Above this value growth rates show a non-linear correlation with stress.

McLean, Dyson & Taplin[86] considered that this mechanism will be unimportant at engineering strain rates but could arise under fast laboratory tests particularly at low temperatures, or at crack tips where high stress and strain rates can occur.

The orientation of creep cavities to the tensile stress axis (TSA) has been used to attempt to distinguish between diffusion or deformation controlled growth.

The following angles to the TSA should be obtained for respective mechanisms:

Diffusion	90 Degrees
Shear	45
Chang & Grant[87]	
type a	70
type b	90
type c	45
Hancock/McLintock	0

Hence this approach cannot definitely discriminate between diffusion or deformation processes unless the angular distribution observed is very small. Lower ranged stresses have been observed to cause the distribution of cavities to peak at around 90° to the TSA rather than 45° for higher stresses. This follows from the earlier discussion on the stress dependance of the formation or either r or w type cavities.

The effect of grain size on cavitation has been studied. Rama Rao et al[88] found for Cr-Ni stainless steel there was a shift in the cavity distribution from 90° to 45° to the tensile stress axis as grain size was decreased. This suggested the importance of grain boundary sliding in establishing the controlling mechanisms for nucleation and growth. However, for a Cr-Mn-N steel the distribution remained constant at around 90°. They considered this behaviour to be due to the operation of a precipitate/matrix interface nucleation as the precipitate was the common factor of all the specimens of this steel.

Fleck, Beever & Taplin[45] found for copper alloys that smaller grain size, increasing the effect of grain boundary sliding, resulted in an increased volume of cavitation.

Gittins[63] working on copper reported that the number of cavities observed followed the same time dependance as grain boundary sliding, but once nucleated grew at a constant rate. This was interpreted as indicating a dependance of nucleation on grain boundary sliding but growth being entirely diffusion controlled.

Good & Nix[89] introduced regular size and spaced bubbles of water vapour into silver creep specimens. They considered these to act as pre-existing cavities. For cavities around 1µm in size the activation energy for creep failure was found to be in very close agreement with the activation energy for free surface diffusion. They hence considered a diffusion type cavity growth model appropriate. For larger cavities, around 12µm diameter, under similar test conditions, the stress and temperature dependance of rupture were identical to those of creep. From this observation they suggested that the final stages of cavity growth consisted of plastic tearing between cavities. In both cases SEM examination of the fracture surfaces showed cavitation to have been exclusively from the pre-existing sites. The presence of the water vapour bubbles severely reduced creep ductility. They also commented that observations by other workers[90,91] on helium bubbles much less than 1μm diameter suggested that cavity growth may be creep controlled. For these very small cavities capillary action will be so strong a stress concentration will be essential for growth.

Cane[92] examined cavitation in alpha iron at 700°C. It was observed that the strain rate contribution of grain boundary sliding and cavitation followed the same stress dependance. This indicated that the factors controlling deformation and cavitation are related. It was also observed that by pre-straining the test pieces to increase the flow stress reduced both creep strain and cavitation for the same test time, temperature, and stress. This is inconsistent with the Hull Rimmer model. However, the largest cavities formed on boundaries at 90° to the tensile stress axis which supports a diffusion mechanism. Cane proposed that dislocations entering grain boundaries maintain their Burgers vectors and during grain boundary sliding, deformation occurs by a mixture of climb and slip. During this non-conservative motion vacancies are produced dependant upon the deformation. At very low stresses, below the regime of slip creep the classic Herring Nabarro[19,20] vacancy production process would be expected to predominate.

The works by Good & Nix and that by Cane are clear indications that it is rapidly becoming accepted that the mechanism of cavity growth cannot be adequately described by only a vacancy diffusion or only a deformation process. Cavity nucleation must also be considered devoid of a single mechanism. The possibility of transitions from one mechanism to another or inter-play between mechanism must clearly be considered.

Such a transition between diffusional growth and deformation growth is a feature of a model proposed by Beere and Speight.[93] They considered diffusional void growth in a material where the grains were undergoing slip creep as opposed to the Hull Rimmer model in which the grains were behaving in an elastic manner and the creep deformation was principally diffusional. Because the grains are deformed by dislocation creep the need for the atom plating/ vacancy source distribution to be spread evenly across the boundary no longer applies. Hence, shorter diffusion paths are possible allowing faster cavity growth. At low stresses the situation was considered similar to the Hull Rimmer model because the amount of slip creep is low. As the stress increases the proportion of slip creep increases reducing the radius around the cavity from which diffusional contributions of vacancies to the cavity can operate. In the limit of high stresses, cavity growth was considered to become identical to Hancock's non-diffusive cavity growth in a plastic body.

The importance of grain boundary sliding in nucleation seems easy to accept, even if it only serves to provide a stress concentration rather than actually be responsible for decohesion. The arguments over the relative importance of diffusion and other deformation mechanisms to cavity growth must be viewed in context of the creep situation. Creep testing can cover a very wide range of temperatures, even in terms of fractions of T_{mp}. The stresses used can also cover a wide range. Both diffusion rates and grain boundary sliding rates are temperature dependant. They are also stress dependant, diffusional processes having a stress dependancy exponent of unity and grain boundary sliding a higher value.[94] Diffusional cavity growth can utilise a very high proportion of the work done by the applied load. Hence, growth of this kind is possible at very low levels of stress provided nucleation can occur. Sliding mechanisms would be expected to increase in importance at higher stresses and strain rates. A change in the relative importance of these parameters with test conditions is possible for a single material. This must be even more likely to occur when considering the many different materials that have been studied in the works reviewed here.

2.3.3 Cavity Linking

So far the mechanisms for cavity nucleation and growth have been considered but not the actual processes by which cavities link up to exhibit creep crack growth. In practice it has been observed that at least two distinct failure modes may occur:

i) Void growth then a cracking mode of linkage similar to a Griffith cracking type process.

ii) Voids continue to grow and final fracture is by an internal necking mechanism or a ductile tearing process. The fracture process is considered to arise from the formation of intense shear bands between neighbouring cavities, which eventually exceed the work hardening capacity of the material.[95] This type of failure mode is known as the void-sheet mechanism.

A preference for the void-sheet mechanism has been observed in ductile materials, such as magnox[96] and copper, and also with finer grain sizes. For example, Morris[97] examined the effect of grain size on the creep failure of 316 stainless steel and found void sheet fractures below 25μm from r type cavities. At larger grain sizes, greater densities of larger cracks were observed, forming from w type cavities and failures only occurred after some crack growth. Similar observations have been made by Cocks & Taplin[98] and also Fleck et al.[45] Morris measured the uncavitated cross section area and hence calculated the nett section stress acting. For the larger grain size specimens (greater than 25µm) the nett section stress did not correlate with the occurrence of fracture. However, a longest crack length at fracture. versa stress criteria was observed with the larger grain sizes suggesting a Griffith type mechanism. It was considered that the Griffith equation was modified under creep conditions by relaxation of the crack tip stresses. In 316 it was proposed that this relaxation was controlled by the size and distribution of the carbide network.

Soderberg[99] observed a relationship between longest crack length and fracture in 20Cr-35Ni Stainless Steel at 700°C as follows:

$$\sigma . c^{b} = \text{constant} \qquad 2.19$$

where σ = applied stress

c = crack length

It was found that $b = 0.55$ which is in close agreement with the value of 0.5 expected by a Griffith criterion. The stresses used in this work were relatively high, giving rupture times of 3.5 to 535 hours, producing a wedge type cracking mechanism.

The void sheet mechanism probably occurs in ductile and fine grained materials because in such cases the increase in nett section stress with cavity growth causes the creep strength of the material to be exceeded before a crack in excess of the critical size can form. This is expecially likely where creep relaxation is easy as this will increase the critical crack length.[97]

McMahon[100] suggested fracture could be classified as stress controlled or strain controlled. It was suggested by Knott[101] that fracture classification could be between cracking processes and rupture processes. Unfortunately it has been shown that these classifications are not synonymous in that rupture can be either stress or strain controlled, as can cracking.[102, 103]

Johnson[104, 105] examined the effect of biaxial stress on creep fracture and found it was possible to classify materials into two types of behaviour.

1) The function describing fracture was a function of the Von Mises equivalent stress $\bar{\sigma}$ and fracture is considered to be controlled by the magnitude of the octahedral shear stress. These materials normally exhibited only a single crack with little or no subsidiary cracking. Tertiary creep in these materials could be described by:

$$\dot{\varepsilon}^{t}_{ij} = A(\bar{\sigma})^{n-1}.\sigma'_{ij} \; f'(t) \qquad 2.20$$

Materials shown to exhibit this type of behaviour, at least within certain temperature ranges, include 0.2% carbon steel, magnesium and some aluminium alloys.

2) The function describing fracture was a function of the principal tensile stress σ_1. These materials exhibited grain boundary cracking which accumulated during tertiary creep. Tertiary creep in these materials could be described by:

$$\dot{\varepsilon}^{t}_{ij} = A' \, f(\sigma_1) \, \sigma'_{ij} \, \exp.B'f(\sigma_1)t \qquad 2.21$$

Materials following this type of behaviour at least within certain temperature ranges include Mo. steel, copper and Nimonic 75.

It was noted that dependance on σ_1 did not correlate with the degree of intergranular fracture or with tensile ductility. Unfortunately there appears to be little knowledge as to the micro mechanism that determine which stress system will characterise failure. The action of octahedral shear stresses in the void sheet mechanism and the principal stress in a Griffith type case seem logical correlations. However, this is not consistent with high ductility tending to produce void sheet failures and the absence of such a ductility correlation with the controlling stress function. This serves to illustrate the complications of material behaviour under multi-axial stress states.

2.3.4 Metallographic Techniques

Optical microscopy is seriously limited in the information it can supply relating to cavities. Resolution is limited to around lum. Detailed information regarding shape and crystallographic orientation is not available.

Conventional use of the Transmission Electron Microscope (TEM) requires production of thin films, often far less than lum thick. Any cavity must be very small to be contained within the foil. A shadowgraph technique was developed by Taplin & Barker[73] in which non-transparent foils were examined (similar to a conventional radiographic technique). However, even in these thick films one side of a cavity would probably be exposed to the polishing solution which could have caused enlargement and distortion. Cocks & Taplin[98] later showed that when using this technique a small change in beam angle could result in a severe change in cavity appearance, for example, an equiaxed cavity could change in appearance to look elongated with a sharp corner. This technique cannot supply information regarding the structural features of the adjacent grains. The use of the 1M.V TEM has proved to have considerable scope in overcoming many of these difficulties.[46 50]

Electron fractography using the Scanning Electron Microscope (SEM) has proved a useful technique for examining cavity shape, size and distribution.[56 106 107] If a material is brittle at low temperatures it can be broken open after creep testing and examined. This technique allows easy sample preparation with little chance of seriously deforming the cavity features. However, again the technique is unable to detect features of the crystal structure or orientation.

2.4 Mechanical Aspects of Creep Fracture

2.4.1 Effect of Notches

The first indication of any effect of notches under creep conditions came from the failure of boiler flange bolts, in the threads or at abrupt changes in section. These failures were considerably premature when compared with smooth bar data. It was found that these failures could not be predicted from smooth bar or short term notched tensile tests.[108]

An increasing amount of creep rupture work has followed from the early investigations into these failures, primarily on notched round bar specimens. The effect of the notch on the creep life was expressed as the ratio of time to failure of the notched bar over the time to failure of a smooth bar of the same nett section area. If this ratio exceeded a value of one notch strengthening was considered to have occurred and notch weakening with a value of less than one.

The results of studies of the notch phenomena are conflicting, some tests showing a weakening effect others a strengthening effect. During these early works the effects of most of the possible variables were investigated (i.e. notch depth[109,110,111], notch acuteness[110,112,113], plain bar ductility[108,114,115,116], grain size[114], precipitate[115]). However, it was about 20 years after the original investigation before the phenomena started to really be rationalised.

It was recognised that the principal effect of a notch on creep life was any change that it may cause in the time to initiate a crack, rather than in the time taken for this crack to propagate across the section.[116] Work by Taira & Ohtani,[117] described in detail later, showed that for the circumferentially notched bar geometry under creep conditions the maximum value of the axial stress moved to a point some distance from the notch root. It had already been observed that in many cases failure started by formation of micro cracks ahead of the notch that then linked back onto the notch tip. Taira & Ohtani also showed that the value of the equivalent stress (as given by the Von Mises criterion equ. 2.22) was lower than the nominal stress at notch tip.

$$\bar{\sigma} = \frac{1}{2}\left((\sigma_1 - \sigma_2)^2 + (\sigma_2 - \sigma_3)^2 + (\sigma_3 - \sigma_1)^2\right)^{0.5} \qquad 2.22$$

This could result in delaying the formation of cracks at the notch tip and hence increase the time to rupture. Where complete relaxation is not possible either due to inhibition by precipitate or inadequate ductility there will be a tendency for notch weakening.

Hayhurst et al[118,119] extended this approach and proposed that the tendency for notch weakening with sharper notches is because the strain required for the relaxed state to be reached is greater and hence there is a more chance that the ductility of the material will be exceeded before this state can be attained. They also considered the stress systems controlling final fracture as outlined in section 2.3.3, that is either octahedral shear stress or maximum principal stress. They considered that weakening will be promoted where the peak stresses have the same multi-axial character as the multi-axial stress rupture criterion of the material.[120]

This again illustrates the complexity of rupture under multi-axial stress states under creep conditions such as those that may arise with the presence of a notch or crack.

Conventions

The convention of co-ordinates shown in Fig. 2.9 is the system used throughout. Three basic types of stress state are generally considered:

1) Plane stress where the stress σ_{zz} is equal to zero.
2) Plane strain where the strain ε_{zz} is equal to zero.
3) Anti-plane strain from displacements only in the z direction of the body.

In addition to these three stress states there are also three modes of loading considered.

Mode I	Normal tensile loading
Mode II	Shear or sliding loading
Mode III	Loading to produce displacements that are skewed around the crack plane normal.

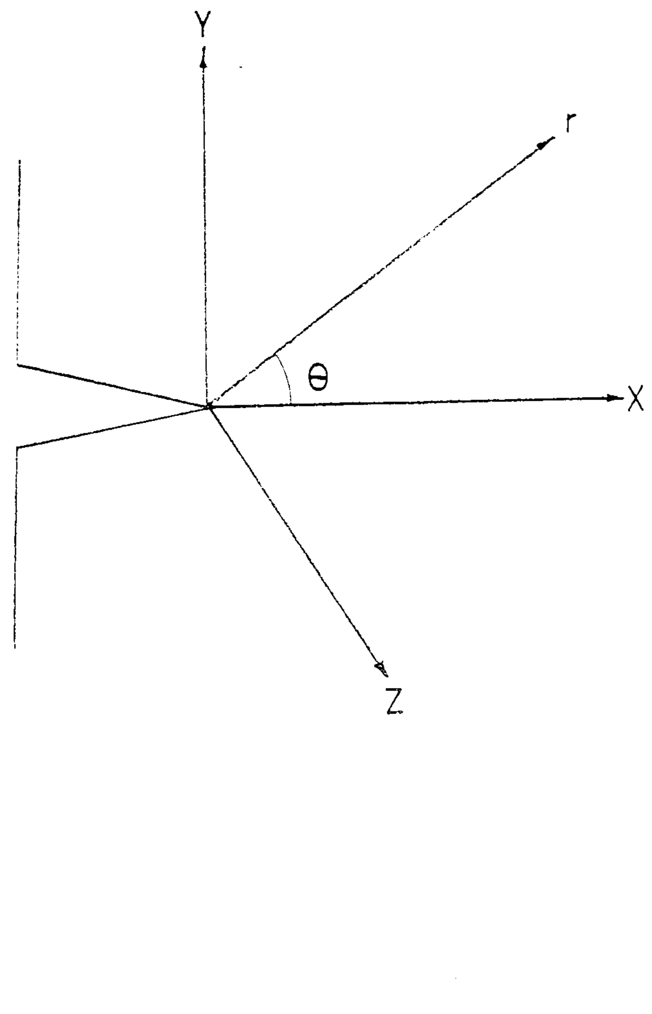

SYSTEM OF CO-ORDINATES

FIG.2.9

Each of these loading modes corresponds to a basic type of stress field in the vicinity of the crack tip. It is conventional to subscript fracture mechanics parameters with the appropriate loading mode number i.e. K_I, K_{II}, K_{III} for modes I, II, III respectively.

2.4.2 Stress Fields Preceding Cracks

Irwin[121] developed work by Westergaard[122] to express the stress σ_{ij} in an infinite body undergoing extension of a slit crack length $2a$. Under plane stress conditions the resulting formulae are of the general form:

$$\sigma_{ij} = \frac{\sigma\sqrt{\pi a}}{\sqrt{(2\pi r)}} \cdot f_{ij}(\theta) \qquad 2.23$$

where σ = applied stress

In mode I loading for σ_{xx} $\quad f_{ij}(\theta) = \text{Cos}\,\frac{\theta}{2}\left(1-\text{Sin}\,\frac{\theta}{2}\,.\,\text{Sin}\,\frac{3\theta}{2}\right)$ 2.24

σ_{yy} $\quad f_{ij}(\theta) = \text{Cos}\,\frac{\theta}{2}\left(1+\text{Sin}\,\frac{\theta}{2}\,.\,\text{Sin}\,\frac{3\theta}{2}\right)$ 2.25

σ_{xy} $\quad f_{ij}(\theta) = \text{Cos}\,\frac{\theta}{2}\left(\text{Sin}\,\frac{\theta}{2}\,.\,\text{Cos}\,\frac{3\theta}{2}\right)$ 2.26

Commonly $\sigma\sqrt{\pi a}$ is represented by K which is referred to as the stress intensity factor. This is an important parameter in fracture mechanics.

$$\sigma_{ij} = \frac{K}{(2\pi r)^{0.5}} \cdot f_{ij}(\theta) \qquad 2.27$$

where $K = \sigma\sqrt{\pi a}$

This represents the stress distribution that will exist under Linear Elastic conditions. Plastic or creep behaviour will result in redistribution of these stress profiles. Solution of the stress profile preceding a crack after creep relaxation has been attempted by several approaches.

Rice & Rosengren[123] applied the J integral (this parameter is described in more detail in section 2.4.3.3) to a circular path radius r. The J

Integral is a path independant line integral.

$$J = \int_{\Gamma} \left(W(e)dy - T.\frac{du}{dx} ds \right) \qquad 2.28$$

where
Γ = line path
T = traction vector
$W(e)$ = energy density
u = displacement
s = arc length

By choosing a circular path radius r it was shown

$$\frac{J}{r} = \int_{-\pi}^{+\pi} \left(W(e(r\ \theta)\cos\theta - T(r\ \theta)\frac{du}{dx}.(r\ \theta)\right)d\theta \qquad 2.29$$

Each of the terms in the integrand has the dimensions of stress x strain. The integrand must exhibit a singularity at the crack tip which at least on an angular average depends inversely on the distance from the crack tip. It seems reasonable to conclude that:

$$\sigma_{ij} \ . \ \varepsilon_{ij} = \frac{f(\theta)}{r} \text{ as } r \rightarrow 0 \qquad 2.30$$

That is, the strain energy follows a 1/r dependance from the crack tip. It should be noted however, that although this relationship has been shown to be applicable in many cases, rigorous proof of its general applicability has not been possible. If plastic behaviour of the form described by equ. 2.31. can be assumed:

$$\varepsilon = A\sigma^{n} \qquad 2.31$$

Then from equ. 2.30 it follows that:

$$\sigma.\sigma^{n} \propto \frac{J}{r} \qquad 2.32$$

$$\sigma^{n+1} \propto \frac{J}{r} \qquad 2.33$$

$$\text{i.e. } \sigma \propto \left(\frac{r}{J}\right)^{-(1/n+1)} \qquad 2.34$$

$$\text{and } \varepsilon \propto \left(\frac{r}{J}\right)^{-(n/n+1)} \qquad 2.35$$

Barnby[124, 125] has attempted to predict the steady state stress distribution ahead of a creep crack by use of the Hoff[126] analogy. This analogy provides a means of solving creep problems by analogy to the non-linear elastic situation. Hoff proposed that the stress distribution in a body undergoing deformation by a non-linear creep law will be the same as that in a non-linear perfectly elastic body following the time derivative of the creep law. The non-linear elastic strains will be numerically equal to the creep strain rate and can hence be used to represent creep strain rate behaviour, i.e.:

$\dot{\varepsilon} = A\sigma^n$ for the creep situation is replaced by

$\varepsilon = A\sigma^n$ for the non-linear elastic solution

The analogy is considered valid provided the creep strains are large compared to any linear elastic strains in the body. In Barnby's[124] initial model relaxation was considered to occur by replacement of elastic strain by creep strain. That is, relaxation down the line AB in Fig. 2.10 Non-dimensionalising stress and strain by dividing the stress by a reference stress σ_o such that:

$$\sigma' = (\sigma/\sigma_o) = \varepsilon' = (\varepsilon/\varepsilon_o) \qquad 2.36$$

The initial elastic solution as given by equ. 2.27 becomes:

$$\sigma' = \frac{K}{\sigma_o\ (2\pi r)} \qquad \theta = 0 \qquad 2.37$$

From equ. 2.36 $$\varepsilon' = \frac{K}{\sigma_o\ (2\pi r)}$$

Using the analogy to a non-linear elastic material and converting from elastic strain to creep strain where :

$$\dot{\varepsilon}' = (\dot{\varepsilon}/\dot{\varepsilon}_o) = (\sigma/\sigma_o)^n = \sigma'^n$$

$$\sigma'^n_{ss} = \frac{K}{\sigma_o\ (2\pi r)} \qquad 2.38$$

$$\sigma'_{ss} = \left(\frac{K}{\sigma_o\ (2\pi r)}\right)^{(1/n)} \qquad 2.39$$

where σ'_{ss} = the non-dimensionalised steady state stress

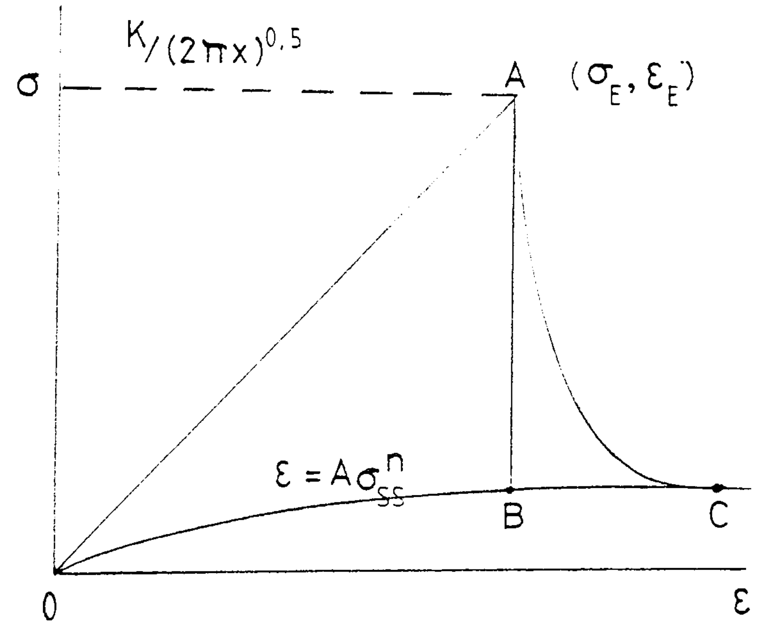

SCHEMATIC RELAXATION OF LOCAL STRESS FROM LEFM VALUE TO STEADY STATE.

FIG. 2.10

By applying the equilibrium criterion

$$\text{Applied Load} = B.\int_0^{W-a} \sigma.dx \qquad 2.40$$

Where B = breadth of section
(i.e. z direction measurement)

To maintain equilibrium it was found necessary to replace K in equ. 2.31 with a function K' which resulted in the solution:

$$\sigma_{ss} = \sigma_{gross}\,\frac{(2n-1)}{2n\,\sigma_0}.(w-a)^{-(2n-1)/2n}.(w)^{(2n-1)/2n}.(x/w)^{-(1/2n)} \qquad 2.41$$

The dependance on x, however, remains unchanged.

For the situation of n=1 the stress distribution has the same dependance on x as for LEFM conditions.

$$\sigma_{ss} \propto \frac{1}{x}^{(1/2n)} \qquad 2.42$$

assuming $\varepsilon = A\sigma^{n}$ (non-linear elastic)

$$\varepsilon_{ss} \propto \frac{1}{x}^{(1/2n)^{n}} = \frac{1}{x}^{(1/2)} \qquad 2.43$$

However, considering the strain energy

$$\sigma_{ss}.\ \varepsilon_{ss} = \frac{1}{x}^{(1/2n)} . \frac{1}{x}^{(1/2)} \qquad 2.44$$

This is not consistent with the Rice & Rosengren proposal of a 1/x dependance on strain energy except at n=1.

Whilst Barnby considered relaxation at constant strain may be possible under a rapid creep transient, it was considered desirable to try and reconcile the approach with the result of Rice & Rosengren for the general case $n \neq 1$. To this end Barnby and Nicholson[125] proposed that relaxation followed the Neuber rule rather than occurred at constant strain. The Neuber rule states that the product of the stress and strain concentrations at a point ahead of a notch is a constant. This is equivalent to relaxation down the hyperbola AC in Fig. 2.11.

$$\varepsilon_p . \sigma_p = Q_p^2 \qquad 2.45$$

Where ε_p = strain concentration at point p

σ_p = stress concentration at point p

The Neuber rule can be maintained by equating the elastic strain energy to the creep strain energy.

$$\sigma_E . \varepsilon_E = \sigma_{ss} . \varepsilon_{ss} \qquad 2.46$$

If $\varepsilon_E = \sigma_E / E$ then applying the Hoff analogy:

$$\frac{K}{\sqrt{(2\pi x)}} \cdot \frac{K}{E\sqrt{(2\pi x)}} = \sigma_{ss} \cdot A\sigma_{ss}^{n} \qquad 2.47$$

Thus

$$\sigma_{ss} = \frac{K^2}{2\pi EA}^{(1/1+n)} . x^{-(1/1+n)} \qquad 2.48$$

This dependance on x is compatible with the Rice & Rosengren strain energy dependance:

$$\sigma_{ss} . \varepsilon_{ss} \propto \frac{1}{x}^{(1/1+n)} \cdot \frac{1}{x}^{(n/1+n)} = \frac{1}{x} \qquad 2.49$$

Experimental work by Barnby & Nicholson[125] on AISI 316 stainless steel between 650°C to 750°C (with n varying from 7 to 9.5) showed the stress profile preceding a crack was closer to the:

$$\sigma_{ss} \propto x^{-(1/1+n)}$$

than

$$\sigma_{ss} \propto x^{-(1/2n)}$$

As expected in the near tip region where high stresses are predicted behaviour deviated from these distributions to produce a flat plateau region as shown in Fig. 2.11.

It is of interest to note that both of these distributions revert back to the Linear Elastic dependance of x for the case of n = 1.

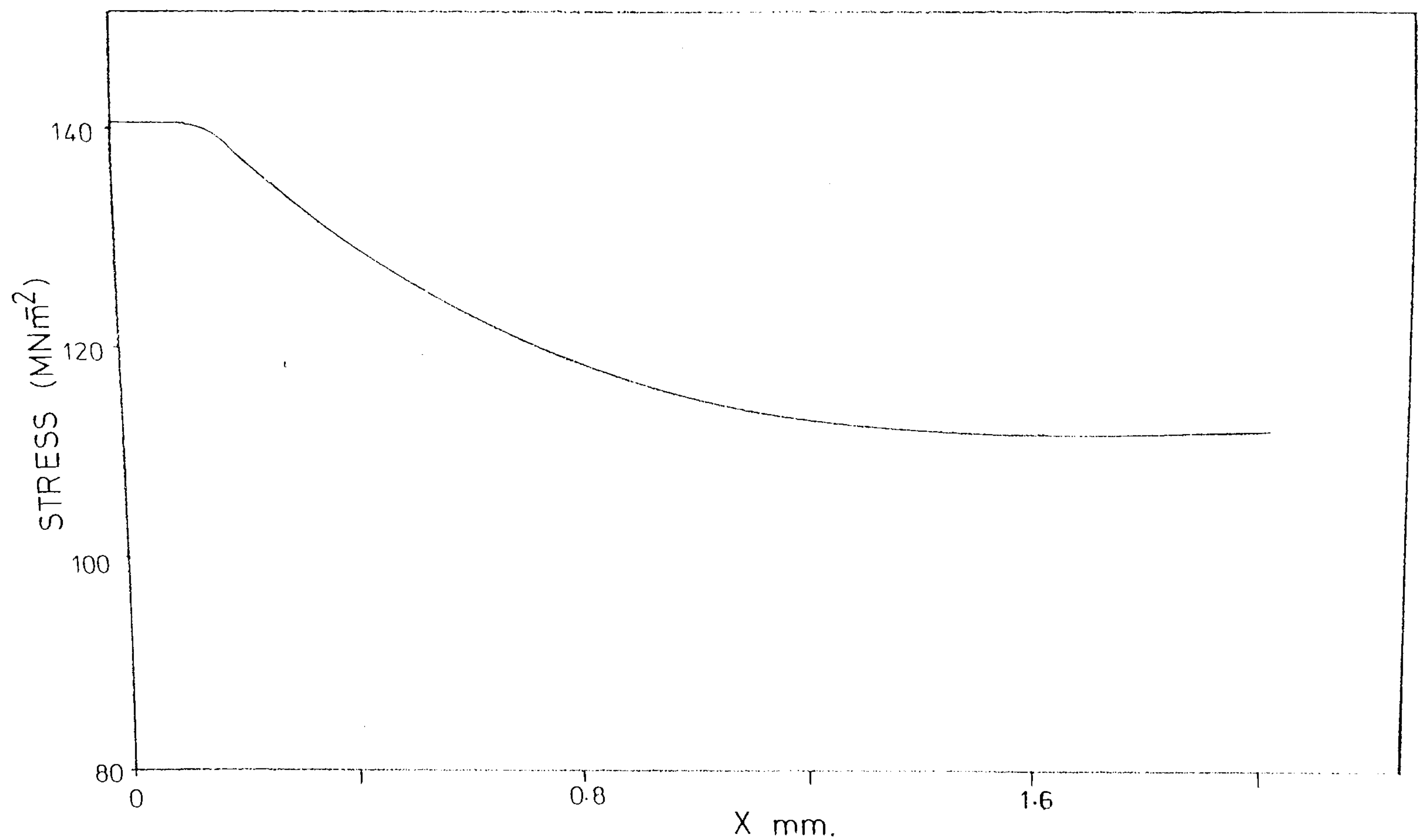

STRESS.V.DISTANCE FROM CRACK TIP DISTRIBUTION (BARNBY AND NICHOLSON

FIG.2.11

The Hoff[128] analogue can also be applied to the J integral and the C* parameter (C* is discussed in section 2.4.4.3, it is basically the J function in which strain and displacement have been replaced with their respective rate functions). The equations describing the distribution of stress and strain under plastic conditions 2.34 and 2.35 can be replaced for the creep situation by:

$$\sigma \propto \left(\frac{r}{C*}\right)^{-(1/n+1)} \qquad 2.50$$

$$\dot{\varepsilon} \propto \left(\frac{r}{C*}\right)^{-(n/n+1)} \qquad 2.51$$

That is, stress and strain rate have the same dependance on r as from the analysis by Barnby.

Vitek[129] utilised a computer simulation technique for predicting the time dependant formation of a 'plastic zone' ahead of a crack. The local stress was based on a function of distance from the crack tip and time. Dislocation densities and time dependant changes to these densities were then predicted and used to estimate the level of the stress.

The simulation was found to produce stress profiles extremely similar to those derived from the Bilby Cottrell Swinden model[130] for the instantaneous formation of a plastic zone. A region of constant or near constant stress ahead of the crack was observed as in the BCS model. This region was found to extend with time and the magnitude decreased, approaching a flat line at a stress level equal to the nett section stress, see Fig. 2.12. It was considered that the time dependant formation a plastic zone could be described by the BCS model if the stress is represented by an apparent friction stress that is both time and stress dependant.

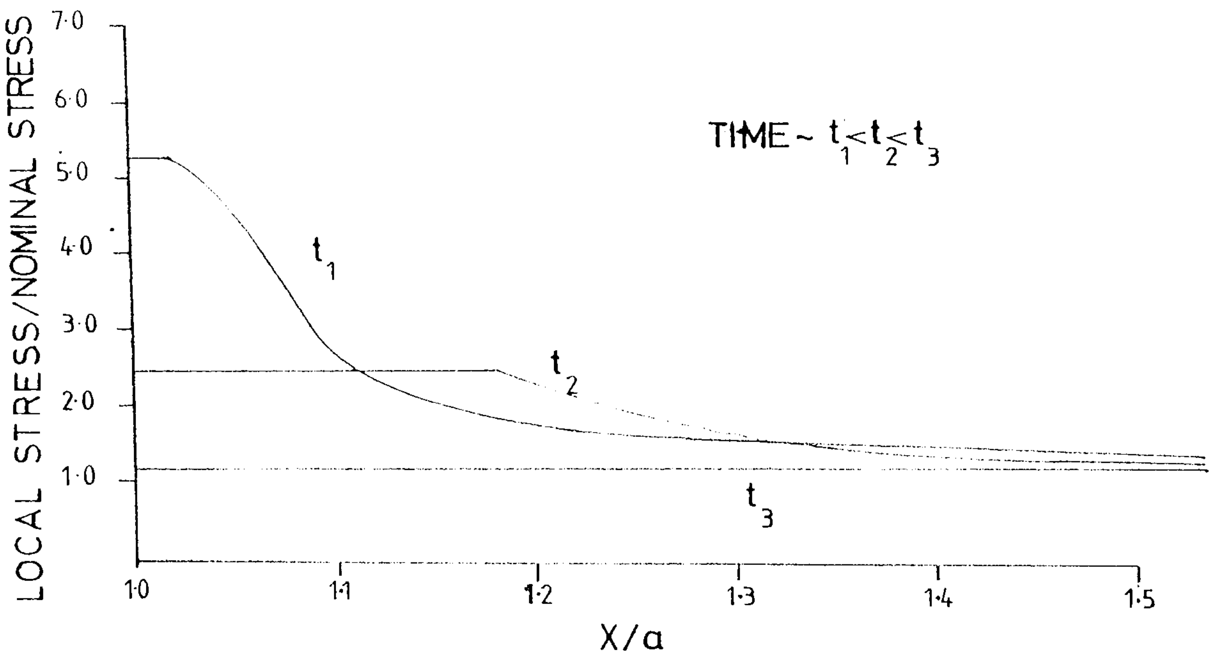

TIME DEPENDANT FORMATION OF
PLASTIC ZONE (BY VITEC)

FIG. 2.12

This model is for a stationary crack not for one undergoing steady state growth. Unlike the models of Barnby & Nicholson[125] this model predicts the total removal of the effect of the stress concentration at the notch tip by relaxation. Whilst the concept of a plastic zone in material behaving totally in a viscous manner has conceptual difficulties, a region of uniform stress at the crack tip was observed by Barnby & Nicholson. This work by Vitek may enable a quantification of this observed effect.

Solution of the stress profiles ahead of cracks by numerical techniques, such as finite element analysis, is certain to increase with the advent of computers and with the increasing dexterity of engineers in their use. Taira & Ohtani[117] have performed such an analysis for the circumferentially notched round bar geometry using the 'Displacement' or 'Direct Stiffness' finite element analysis method. Creep by Nortons law was then applied, based on the elastic stresses over a small time interval. The changes in the elastic strains were then used to recalculate the stresses by Hookes law to produce a new stress distribution. This process was then repeated for successive time intervals and finally yielded steady state stress and strain profiles. The important factors emerging from this work are that the maximum relaxed value of σ_y is some distance in from the crack tip and that the equivalent stress is at a maximum at the crack tip, but because of the constraints of the notches it is at a level lower than the nominal stress. See Fig. 2.13.

Unfortunately the dependance of the steady state stress on x for these profiles was not evaluated in the form of a function of the distance x, neither was the strain energy dependance on x. It is thus

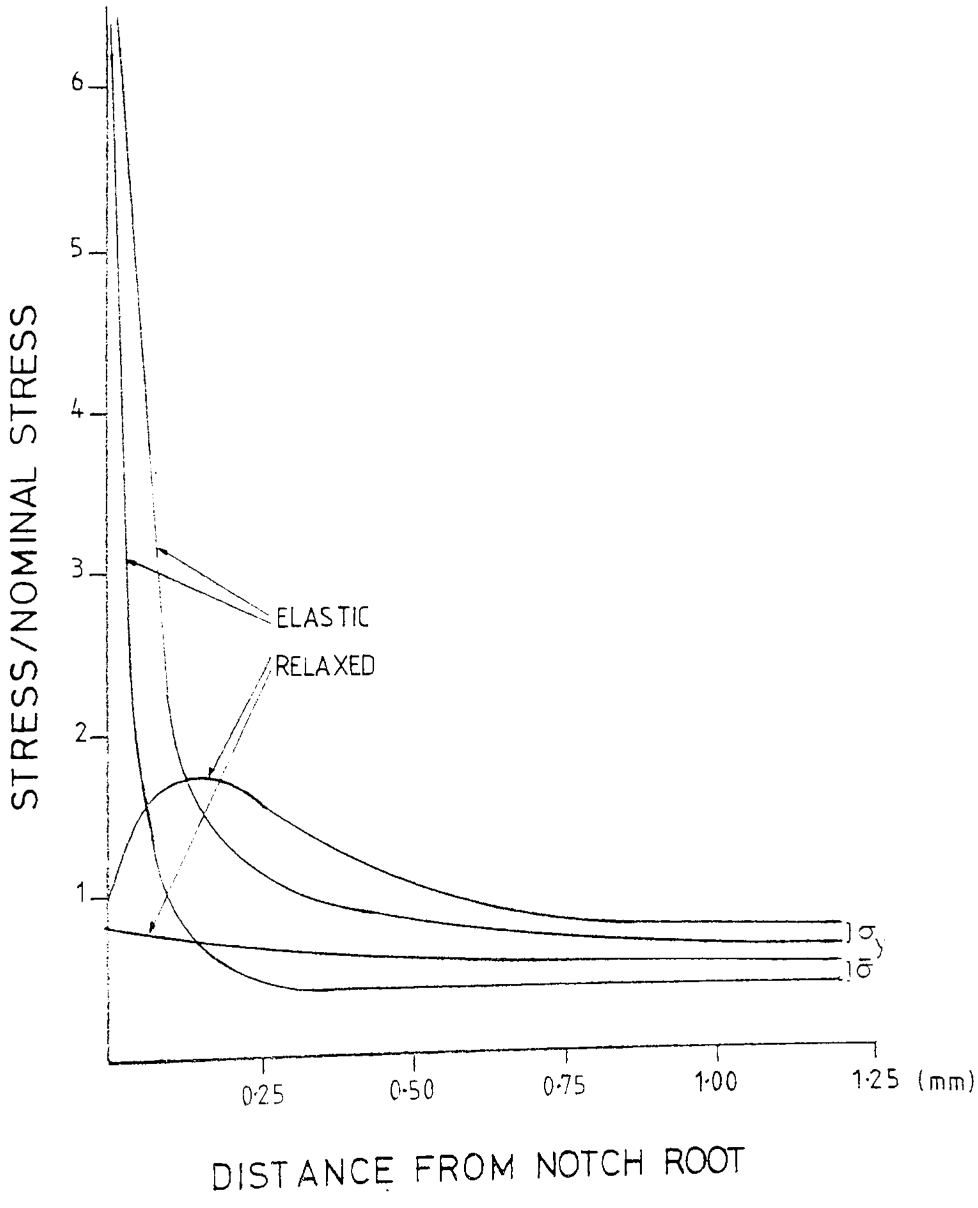

STRESS.V.DISTANCE FROM CRACK TIP DISTRIBUTION (TAIRA AND OHTANI).

FIG.2.13

not possible to compare this approach with the results of Barnby & Nicholson or Rice & Rosengren.

2.4.3 Ambient Temperature Fracture Mechanics

The original energy balance approach to fracture was proposed by Griffith.[38] It was based on the elastic strain energy lost on cracking balancing the energy required to produce two new surfaces. The following relationship was drawn up:

$$\sigma_{crit} \propto \frac{1}{\sqrt{a}} \qquad \text{Where } a = 0.5 \text{ crack length in centre of infinite body} \qquad 2.52$$

or

$$\sigma\sqrt{a} = \text{const} \qquad \text{or} = \text{crack length for an edge crack} \qquad 2.53$$

$$\text{where const.} = \sqrt{\frac{2E\gamma}{\pi}} \qquad \text{for plane stress} \qquad 2.54$$

$$\text{const.} = \sqrt{\frac{2E\gamma}{\pi(1-\nu)}} \qquad \text{for plane strain} \qquad 2.55$$

ν = poisson's ratio

This predicts a critical stress to propagate a crack of a given size or a critical maximum defect size for a given stress level. Although the Griffith criterion has been subsequently modified the concept of these inter-related criticals is still applicable.

The work of Griffith is only applicable where there are no non-linear effects prior to fracture. This prevents accurate application to most engineering situations.

Irwin[131] and Orowan[132] modified the Griffith approach to accommodate limited plastic deformation prior to failure. The $2\gamma_{surface}$ energy term was replaced by γ_p so the energy balance was now between elastic energy stored and the energy required to do a critical amount of plastic work, necessary to cause crack growth. This γ_p term was found to exceed $\gamma_{surface}$ by around three orders of magnitude and hence $\gamma_{surface}$ can be neglected.[133]

It was considered by both Irwin[134] and Orowan[133] that provided this plastic work was confined to a small region compared to both the crack length and the body then the elastic energy release would still be represented sufficiently accurately by elastic analysis.

Irwin[134] considered that fracture could be characterised by the strain energy release rate. This can be interpreted as a force G:

$$G = \frac{dU}{da} \qquad 2.56$$

G represents the irreversible energy loss/unit area of newly created surface area. There will be a critical value, G_c to initiate crack propagation.

2.4.3.1 <u>Stress Intensity Factor Approach</u>

The basis of Linear Elastic Fracture Mechanics (LEFM) is that the stress field ahead of a sharp crack can be characterised by a single parameter K the stress intensity (equ. 2.27). Irwin showed that the crack extension force could be related to K:

$$G = \frac{1 + b}{c\mu} \cdot K^2 \qquad 2.57$$

Where $b = 3 - 4\nu$ for plane strain

$b = \frac{3-\nu}{1+\nu}$ for plane stress

μ = shear modulus

Hence if fracture can be characterised by a critical value of G, it can also be characterised by a critical value of K. This is to be expected as the analysis is based on Linear Elastic conditions so that K will not only describe the elastic stress field but also the elastic strains and the strain environment. This means that K will also describe the strain energy density on which G is based.

For an infinite plate in uniform tension:

$$K_I = \sigma\sqrt{\pi a} \qquad 2.58$$

It should be noted K bears the same stress and crack length dependance as the original Griffith criterion Usually a geometric correction has to be made to relate K to specific geometric conditions

$$K = Y.\sigma\sqrt{a} \qquad 2.59$$

Where Y = Constant or a function of a/w, depending on the geometry under consideration, which converts the situation to the case of an infinite plate.

The critical value of K for fracture will depend upon the stress conditions developed in the specimen. Plane strain conditions representing the minimum resistance to fracture and hence results in a minimum value of K for fracture. For mode I opening the plane strain value of K for fracture is referred to as the K_{IC} value.

The Westergaard equations predict an increase to an infinitely high level of stress as the crack tip is approached. This is obviously impossible and in a normal material plasticity will occur at the crack tip to give a plastic zone radius r_y, with a redistribution of the crack tip stresses as shown in Fig. 2.14. The value of r_y can be calculated by setting the σ_y component of the stress equal to yield stress.

$$\sigma_{ys} = \frac{K}{(2\pi r)^{0.5}} \qquad 2.60$$

$$r_y = \frac{1}{2\pi} \cdot \left(\frac{K}{\sigma_{ys}}\right)^2 \quad \text{plane stress} \qquad 2.61$$

Irwin[137] considered that for plane strain the increase in tensile strength for plastic yield due to the elastic constraint would raise the yield strength by ×3 hence the plastic zone size is reduced accordingly:

$$r_y = \frac{1}{6\pi} \cdot \left(\frac{K}{\sigma_{ys}}\right)^2 \quad \text{plane strain} \qquad 2.62$$

It was suggested[138] that the effect of a small plastic zone corresponded to an apparent increase in crack length by an increment r_y.

$$K = Y\sigma\sqrt{a + r_y} \qquad 2.63$$

This plastic zone correction is only valid for small plastic zones contained within the stressed ligament, however it enables LEFM criteria to be applied to cases of limited yielding.

2.4.3.2 Crack Opening Displacement

Wells[139] proposed that the amount the crack faces displace at the crack tip prior to fracture could be used as a failure criterion. That is, there will be a critical Crack Opening Displacement (COD_{crit}) to initiate crack propagation.

This approach can be viewed in the context of the Dugdale Strip Yield model.[140] This model accommodates the occurence of crack tip plasticity in a basically elastically loaded body and hence COD is an

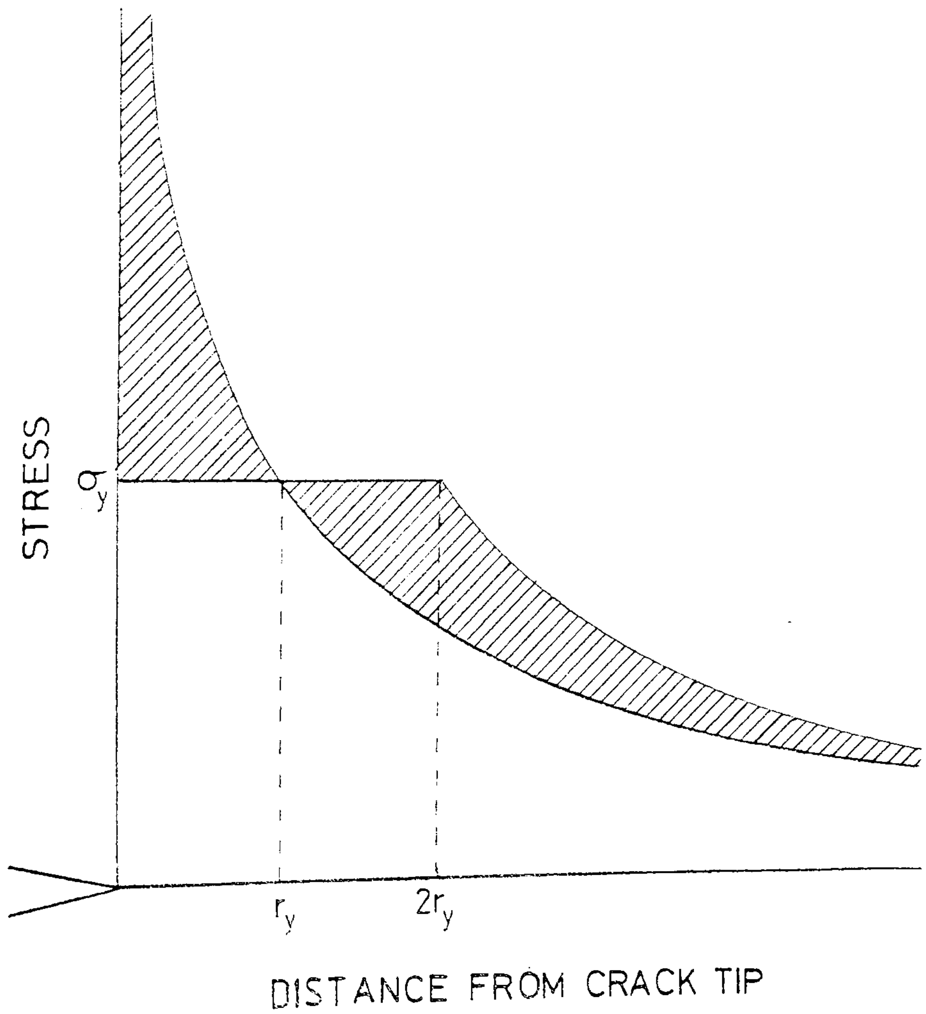

REDISTRIBUTION OF LEFM
STRESS LEVELS DUE TO FORMATION
OF A PLASTIC ZONE

FIG. 2.14

indication of the plastic work done. The crack tip is partly restrained from opening by a stress which for purposes of the fracture model is usually equated to the yield stress. It is then possible to show by use of the Dugdale analysis:[141]

$$G = \sigma_{ys} \cdot d \qquad \text{(approximately)}$$

$$\text{Where } d = \text{COD} \qquad 2.64$$

This approach is hence analogous to the energy balance criteria. Irwin[137] noted that this linear relationship between G and d will apply even when the ligament net section is approaching general yield.

Cottrell[142] considered the possibility that the COD should be composed of the product of a critical strain ε_c and gauge length. It was considered that as the strain would act over the notch root diameter 2ρ, this would approximate to the gauge length:

$$d_{crit} = 2\rho \cdot \varepsilon_c \qquad 2.65$$

Under conditions where large plastic strains can occur it was suggested that an equilibrium notch root radius will exist, blunt notches will sharpen to this value and sharp notches blunt to it. Such an approach was found applicable in analysing fractures in a 1000 MNm^{-2} steel.

2.4.3.3 J. Integral

This is a method of characterising the crack tip stress/strain fields by use of a path independant line integral.[143] It is the path independance that is the key to this method. This enables the conditions at the crack tip to be characterised by integrating along a path remote from the complications in the stress strain fields near the crack tip.

J can be considered to represent the potential energy difference between two identically loaded bodies, differing in crack length by a small amount da:

$$J = -\frac{1}{B} \cdot \frac{dU}{da} \qquad 2.66$$

Where U = displacement vector

B = thickness

This is represented in Fig. 2.15. The shaded area corresponds to dU = J.B.da. For Linear elastic behaviour the J integral is identical to G and hence a J_{crit} criteria, related to K_c is possible:

$$J_{IC} = G_{IC} = \frac{(1-\nu^2)K^2_{IC}}{E} \quad \text{for plane strain} \qquad 2.67$$

The J integral is valid however for both linear elastic and elastic-plastic materials provided the non-elastic behaviour can be treated by deformation theory of plasticity. Thus J can be used to extend fracture mechanics concepts from LEFM into the elastic-plastic regime for many materials.

2.4.4 Macroscopic Creep Crack Growth

The derivation of a fracture mechanics approach applicable to creep situations would be of much use to operators of high temperature plant. It would enable the prediction of defect growth rates in components of complex shape and enable more efficient, safe operation of such plant with the elimination of unnecessary down-time periods for repair of substantially sub-critical defects. The fracture mechanics parameters described above (K, J and CCD) are basically for the prediction of fast fracture. Successful correlations of crack growth with fracture toughness parameters had been observed during fatigue testing.[144] This prompted attempts to examine the possibility of obtaining similar

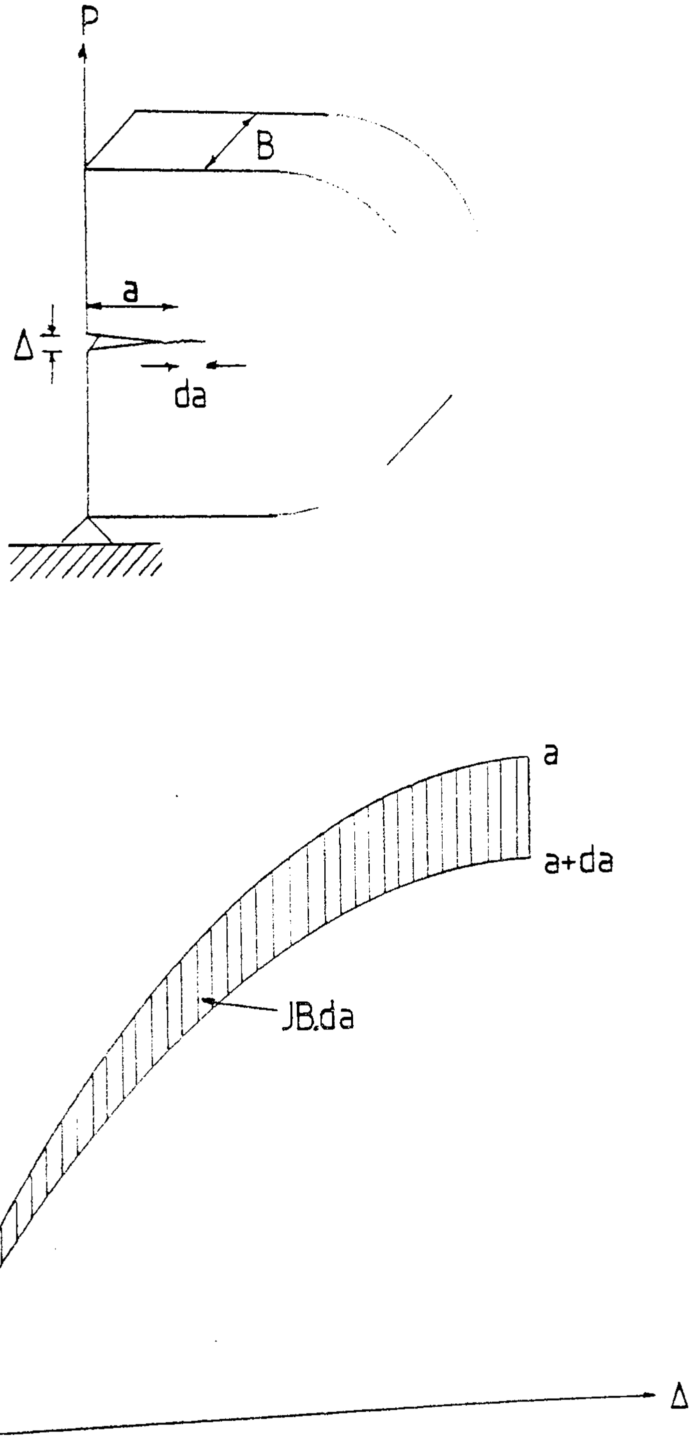

INTERPRETATION OF J INTEGRAL FIG.2.15

correlations under creep conditions. Several approaches have been attempted as outlined below and some of the earlier correlations obtained are listed in Table 2.2.

2.4.4.1 Stress Intensity Approach

Correlations of creep crack growth with the K parameter were observed by Popps & Coles[145] and Siverns & Price[146] in 1970 and this type of correlation has since attracted much attention:

$$\frac{da}{dt} = DK^m \qquad 2.68$$

where $\frac{da}{dt}$ = crack growth rate

D = constant

m = constant

Various studies using this approach are listed in Table 2.2. For a K parameter to apply it would seem a prerequisite that the stress profile preceeding the creep crack followed a linear elastic distribution despite creep relaxation. However good correlations of crack growth with K seem fairly common. Few workers used more than one specimen geometry and hence varied the geometrical compliance function. Where this precaution has been neglected the general applicability of K must be considered unproven. James[148] did find good correlation of K with growth rates in Centre Cracked Plate and Compact Tension specimens indicating validity in this case.

Nicholson & Formby[158] found that a K approach was unsatisfactory for AISI 316 as using CN and SENT specimens failed to give a single da/dt verse K correlation. Similarly, both Gooch[163] and Bain[164] found the exponent m to be geometry dependant. Keneyon et al[152] reported a K correlation for constant K specimens but all the data did not fall on a single curve and hence like the work of Nicholson & Formby

WORKER	MATERIAL	T/T_m	GEOMETRY	RELATED PARAMETER	COMMENTS
Popp & Coles [145]	Inconel 718		CCP	K	K = 100 - 160 da/dt exp. = 7
Siverns & Price [146]	$2\frac{1}{4}$Cr. 1Mo V	0.46	SENT	K	K = 10 - 90 = 5.5
Harrison & Sandor [147]	1Cr Mo V Wrought	0.45	CCP	K	K = 2.5 - 60 = 4.5 Both K & σ_{nett} give reasonable correlation for σ_{nett} da/dt exponent = 10
James [148]	316 Cold Worked	0.47	CCP CTS	K	K = 25 - 40 = 20
Robson [149]	0.2%C Steel Cast Cast Wrought	0.41	CTS SENT CTS	K	K = 40 - 50 = 20 K = 40 - 50 = 20 K = 30 - 40 = 14
Thornton [150]	$\frac{1}{2}$Cr Mo V Wrought Cast Wrought (f.g) Wrought (c.g)	0.46	SENB	K	K = 30 - 70 = 8 K = 40 - 50 = 16 K = 17 - 40 = 6 K = 35 - 50 = 6
Neate & Siverns [151]	$2\frac{1}{4}$Cr Mo Quen. $\frac{1}{2}$Cr Mo V	0.46	SENT (2 widths)	K	K = 10 - 90 = 5 K = 12 - 70 = 3.4 (K reported but σ_{nett} also gives correlation)
Kenyon et al [152]	Al. Alloy	0.47	Const.K	Not K	K reported but data did not all fall on one line.
Taira & Ohanti [117]	1Cr Mo V Norm.& Temp.	0.50	Cir.NB	σ_{nett}	exp. not necessarily same as creep exp. da/dt exp. = 8.9

Ellison & Walton[153]	1Cr Mo V Norm. & Temp	0.46	SEN	K	$da/dt = A \times t^{0.98} \times K^{7.46}$
Haigh[154]	1Cr Mo V $\frac{1}{2}$Cr Mo V	0.45	WOL	COD	$da/dt = A \times (dd/dt)^{0.8}$
Neate[155]	$\frac{1}{2}$Cr Mo V	0.46	SEN CCP WOL	Equ.σ Equ.σ K	$da/dt = A \times \sigma^{7.4}$ $da/dt = A \times t^{0.5} \times K^{3.24}$
Pilkington et al.[156]	$\frac{1}{2}$Cr Mo V	0.45	SEN	K	da/dt K^m but also d K^m
Webster[157]	$\frac{1}{2}$Cr Mo V	0.46	Double Cant. beam	C*	$da/dt = A \times C^{*m}$ where m = 1 or (n/n+1)
Nicholson & Formby[158]	$\frac{1}{2}$Cr Mo V	0.59	SEN CN	σ_{nett}	da/dt exp. approx. = creep exp.
Koterazawa[159]	304 Stainless Steel	0.54	Cir. NB DEN	K	da/dt exp. = 7.7
Harper & Ellison[160]	1Cr Mo V	0.46	SEN CTS	C*	da/da exp. approx. = 1
Landes & Begley[162]	Discalloy		CTS CCP	C*	= 1
Sadananda & Shahiasian[161]	Inconel 718	0.44 - 0.56	CTS	C*	= 1

TABLE OF FRACTURE MECHANICS PARAMETER BASED CORRELATIONS WITH CRACK GROWTH

TABLE.2.2

must be considered to dispute K control.

2.4.4.2 Nett Section Stress Approach

Taira & Ohtani[117] obtained a correlation of growth rates with the nett section stress of the form:

$$\frac{da}{dt} = A \cdot \sigma^{p}_{nett} \qquad 2.69$$

Where A & p = constants

On failure to obtain a valid K correlation Nicholson & Formby[158] found that the crack growth rates for both specimen geometries correlated with a single nett section stress expression of the above type. They found the constant p to approximately equal n in the 2nd creep law and considered this could apply generally. However, this is not totally consistent with the results Taira & Ohtani.

Neate & Siverns[151] had obtained K correlations for SEN specimens of two different widths but DiMelfi & Nix[165] indicated that for one material reasonable correlation with σ_{nett} could also be obtained. Correlations with both σ_{nett} and K also applied to the analysis by Harrison & Sandon[147] of the work by Brothers. It is likely that this illustrates the curve fitting ability of a Log/Log plot rather than has physical significance.

2.4.4.3 J Integral Approach

For application to the creep regime an extension of the J integral is more generally used than J itself. This extension is usually referred to a C* but in some cases $\dot{J}$ is used instead. This parameter is obtained by employing a non linear elastic/creep analogue, so replacing the strains and displacements in the J function by strain rates and displacement rates.[161, 166, 167] $\dot{J}$ characterises the stress/strain fields around the crack tip and represents the energy leak rate during crack growth. Similarly C* characterises the stress/strain rate fields around the crack tip, but is not necessarily equal to the rate differential of J and hence C* cannot immediately be related to the energy leakage associated with crack growth. This is basically because the analogue is mathematical, not physical.[128]

$$J = \frac{dU}{da} \qquad \text{(unit thickness)} \qquad (2.66)$$

$$C^* = \frac{-dU^*}{da} \qquad \text{Where } U = \text{Potential energy}$$

$$\text{but } U^* \neq dU/dt \qquad 2.70$$

However, U* is related to the power input at the load points, so it can be shown that C* may be considered as the rate of change of creep energy dissipation rate with crack length. This can only be related to the energy releases rate with crack growth if stress redistribution effects are negligible.

C* has found reasonable support in several later works.[161 162 167 169] One major disadvantage, is that the parameter is not easy to evaluate. C* has been found to give correlations of growth rate for two specimen geometries. This was not possible using either K or σ_{nett}.[162] Harper and Ellison[160] also found this parameter to describe crack growth rates for two different geometries but only after the effects of stress redistribution had become negligible. Correlations with this parameter usually show approximate direct proportionality:

$$\frac{da}{dt} = AC^* \qquad 2.71$$

Where A = constant

However, Nikbin, Webster and Turner[170] considered the correlation could be of the form:

$$\frac{da}{dt} = AC*^{(n/n+1)} \qquad 2.72$$

As the exponent (n/n+1) will approximately equal unity this could not definitely be established.

2.4.4.4 Displacement Approaches

The possibility that crack growth rates were controlled by local displacements at the crack tip was proposed by Wells & McBride.[7] They considered the accumulation of strain to be a specific feature of creep fracture. COD has shown fair success in characterising crack initiation. Under creep conditions this is not immediately consistent with the operation of a K, σ_{nett} or C* parameter. Correlations with crack growth have been attempted. Equations of the following type have been [103 154 173] proposed:

$$\frac{da}{dt} = B \frac{dd}{dt}^{p} \qquad p = 0.8 \rightarrow 1.0 \qquad 2.73$$

$$\text{or} \quad \frac{da}{dd} = B' \qquad 2.74$$

Where B & B' = constants
d = displacement

These relationships have been proposed to support displacement control of crack growth. However, this does not appear to follow at first sight as the crack appears to be growing into increasingly more ductile material. Under such relationships crack extension controlled by displacements at the crack tip is only possible if the deformation zone at the crack tip is increasing in size. This would be expected from simply analogue to LEFM plastic zone size consideration. Also the effect will be amplified by viscous flow of material into the deformation zone as the stress level increases. In these analyses dd/dt represents the rate of opening along a line through the crack tip. It is assumed that displacement occurs entirely at the crack tip, not in the material either side of tip.[154] A critical strain criterion would appear to be a simple solution to the problem of increasing deformation zone size as these increases could be accommodated by increasing the gauge length over which the strain acts:

$$COD = \varepsilon_{crit} \cdot h \qquad 2.75$$

Where ε_{crit} = critical strain

h = gauge length (variable)

Such an approach was supported by Floreen & Kane[174] from work on tensile and torsion loading. However, the critical strain approach has been criticised due to its inability to exhibit geometric size effects.[175]

Nicholson[172] considered that even when crack growth following a σ_{nett} correlation the crack growth was ultimately controlled by the crack tip displacements.

2.4.4.5 Reference Stress Approach

This approach compares creep deformation in a complex geometry with deformation in a standard geometry and relates the two by an arithmetic function. The relevance of this approach is basically limited to situations of extreme ductility leading to total plastic collapse of the load supporting ligament. It has more validity in predicting rupture times of sections rather than crack growth rates.[173 176]

2.4.5 Application of Fracture Criteria to Creep Conditions

The observation of crack growth correlations with the various fracture mechanics parameters have led to attempts to rationalise the results into generalised conditions.

The application of a K parameter requires that the stress conditions in the specimen are approximately of an LEFM type distribution. The obvious case where this may occur is under conditions where the creep strains are unable to relax the elastic stresses significantly prior to crack growth. This would require an extremely creep brittle material. However, K control has been reported in materials that exhibit reasonable ductility before fracture.[149,150] Nicholson and Formby, who observed a σ_{nett} correlation, showed that the relaxation of stresses in their material under creep conditions occurred extremely rapidly.[158]

Neate and Siverns[151] considered K control could result with ductile materials under conditions of constraint and low applied stress. At high stresses they observed that for a ductile $\frac{1}{2}$Cr $\frac{1}{2}$Mo $\frac{1}{4}$V steel correlations with K were geometry dependant. At low stresses this geometry dependance was less noticable. They considered that under conditions of low stress and constraint the deformation becomes localised near the crack tip. When this occurs they considered the effective plastic zone size to be comparable with that allowed for by LEFM. However, unless creep relaxation is prevented it is difficult to see how the K parameter can provide a valid description of the crack tip stresses and displacements on this basis alone. The proposal by Neate and Siverns is contrary to the conclusion of DiMelfi & Nix[165] who reviewed work on creep crack growth and found that low values of stress tended to produce σ_{nett} correlations.

Koterazawa[159] considered geometries that localise the stress intensity to the crack tip to favour K control. Under dynamic crack growth these geometries would require stress relaxation to occur more rapidly if

LEFM conditions were not to apply. Koterazawa considered the c* results from Landes & Begley[162] bend test specimens. These values were replotted using an effective stress parameter to compensate for the stress concentration preceeding the crack far into the specimen ligament, where relaxation could occur. It was found that the behaviour of these specimens could be characterised by a $K_{effective}$ parameter. Gooch[163] observed K correlations in SEN tension and SEN bend specimens.(although the K index was slightly higher for the later geometry). On breaking open specimens at -196°C that had undergone some creep crack growth the cryogenic fractures were transgranular. This indicated that the grain boundaries had not been substantially weakened away from the crack tip and that grain boundary damage for these geometries is concentrated in this region.

Barnby[124,125,177] has shown that an LEFM type stress distribution can occur as a special case under totally non-elastic conditions. Using an elastic analogy by Hoff, it was shown that for a creep exponent of n equal to 1 in the 2nd creep law this case will arise. (see section 2.4.2). It was proposed that for values of n below around 5, K control will apply. For values of in excess of 5 the stress distribution will be relaxed down to form which has little resemblance to an LEFM profile and will result in σ_{nett} providing a more valid description of crack growth.

Williams & Price[178] also considered the time dependant stress distribution around a crack tip. Their conclusions were similar to those of Barnby, that is, K control would arise at low values of the exponent.

As the value of the exponent rises the relaxed stress distribution will progressively approach that described by perfect plasticity. They considered that under such conditions use of a reference stress approach was applicable. In a geometry devoid of a bending moment this will be equivalent to the nett section stress.

DiMelfi & Nix[165] pointed out that the theories of Barnby and of Williams & Price do not explain the observation of a K control by Koterazawa in a material of high n value. These theories also fail to explain the variation of behaviour of a material under slightly different conditions observed by DiMelfi & Nix when comparing the results of other workers.

One difficulty in accepting the C* parameter is in visualising its physical significance, although a parameter based on non-linear behaviour clearly warrants examination for use in the creep regime. It has been shown C* will be consistent with K for brittle conditions and with σ_{nett} for ductile conditions and high values of n[169]. A parameter that accurately characterises the crack tip stress field under creep conditions would clearly be useful especially between the extremes of applicability proposed for K and σ_{nett}. However, C* can only characterise the stress field under steady state conditions. Any creep energy consumed in relaxation of stresses not directly affecting crack growth will result in over estimation of C*. The C* parameter relies on steady state conditions and therefore its significance is likely to be through its stress characterisation. Although it has been shown that through C*[169] :

$$\frac{da}{dt} \propto \dot{E}_{crack\ tip} \qquad 2.76$$

C* does not account theoretically for the energy expended in an increasing volume of deformation zone as the crack grows. Hence, an apparent increasing correlation with strain rates and crack length will appear in the same way as COD is seen to increase with crack length. This means the characterisation of the strain rate field may not always be completely valid.

Gooch, Haigh & King[179] considered crack growth characteristics to be a function of both metallurgical (i.e. microstructure) and geometric (i.e. dimensional) factors. They considered a diagramatical representation of creep crack behaviour, see Fig. 2.16. This diagram suggested that LEFM* conditions only apply where relaxation of the elastic stresses by creep is avoided. The use of a reference stress approach is considered desirable where extensive creep deformation occurs at the notch tip. Where plastic deformation as opposed to creep deformation tends to occur they considered the general yield criteria may find a level of applicability.

Vitek[181] proposed a dependance of crack growth on K based on diffusional crack growth, consistent with observed processes of damage growth discussed earlier in section 2.3.2. In this model the crack grows by the diffusion of atoms from the crack tip. These plate out on the boundaries along the crack plane causing a stress redistribution. The mechanism proposed is analogous to the diffusional growth of r type cavities. The analysis is for a brittle material as plasticity at the crack tip which could also redistribute stress is ignored, as is the possibility of interaction between plastic tearing and diffusional crack growth. Under this model crack growth was found to be dependant upon K^4. Whilst accepting this model to be an extreme

* Linear Elastic Fracture Mechanics

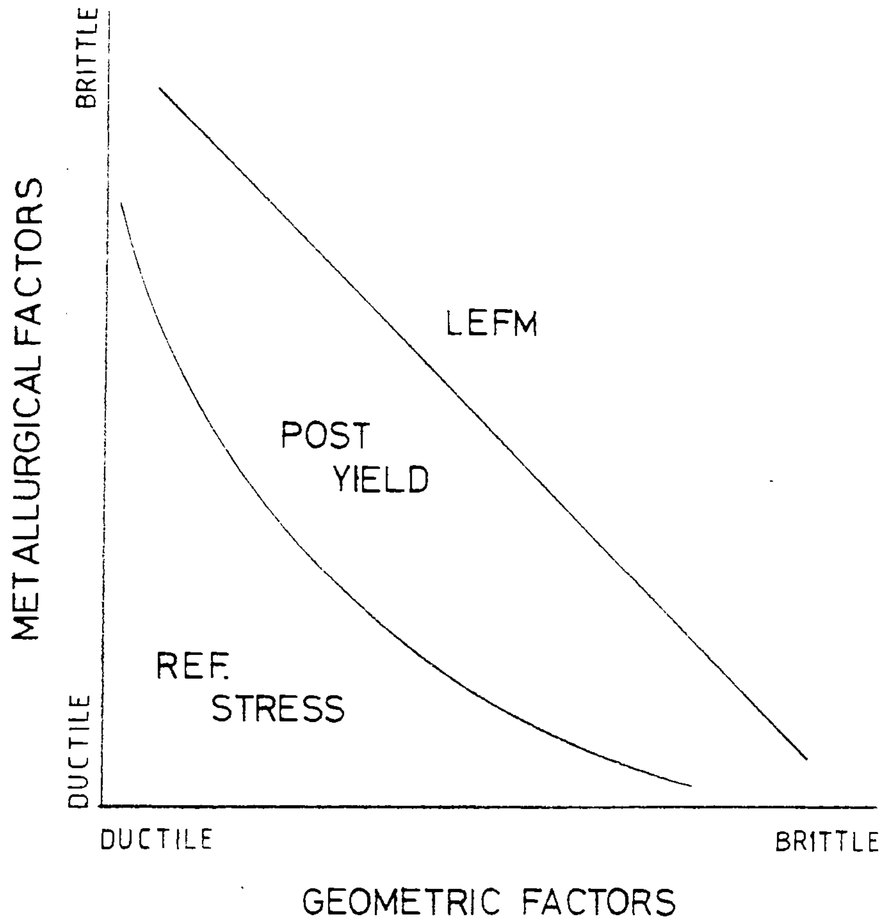

APPLICABILITY OF FRACTURE
MECHANICS PARAMETERS RELATIVE
TO DUCTILITY CONSTRAINTS.

FIG.2.16

simplification Vitek considered that diffusional growth of cracks may well be a possible mechanism. Metallographic observations have shown crack paths following grain boundaries perpendicular to the tensile stress axis and where boundaries were orientated at a low angle to the tensile axis crack path tended to become discontinuous. This behaviour was considered similar to the growth of r type voids. Comparison with growth rates in a brittle Cr-Mo-V steel were made. The results indicated that the main crack was too wide to enable predictions made by this analysis to agree with observed behaviour but the microcracks observed in front of the main crack were of the correct order.

The concept of diffusional crack growth was supported by Sadonanda & Shahinian[161]. By observation of the effect of temperature on crack growth rate for a given value of K they considered it to be a balance between diffusion of point defects contributing to crack growth and deformation processes causing retardation and even crack arrest due to blunting effects. This retardation occurred at the higher temperatures where deformation processes were faster than the crack growth processes. A minimum value of K for crack growth was observed as was predicted from Vitek's analysis. The activation energy for crack growth was approximately that expected for grain boundary diffusion.

Vitek[181] reviewed the growth correlations with K for more ductile materials and commented on observations of a high exponent for low values of K and vice versa. It was considered that this is more consistent with crack growth driven by plastic processes. The extent of diffusion processes in these cases is uncertain. Plasticity will interact with diffusion as dislocations may act as sinks for point defects influencing the vacancy flux in the plastically deformed region.

Another theory to account for the observation of LEFM and σ_{nett} control was drawn up by DiMelfi & Nix[165] based on void distribution in the region ahead of the crack. It was assumed that cavities grew by power law creep in the elastic stress field. A stress dependance of crack velocity is derived through the elastic stress intensity factor.

$$\frac{da}{dt} = BK^{n} \tag{2.68}$$

The cavity spacing appears to be an important factor in the constant B. At large intercavity spacings corresponding to less severe creep damage the derived equation predicts very low values of the crack velocity. Under such conditions it was proposed that another stress dependance becomes operative based entirely on σ_{nett}. Under this theory K control is observed at high stress levels and with small inter-void spacing, σ_{nett} control is observed at low stresses where the inter-void spacing is large. The heavy reliance on the LEFM stress distribution in this theory without taking account of relaxation must cast some doubt on its applicability. However the importance of cavitation in creep fracture is well accepted for many materials so an approach that considers this phenomenon has much in its favour.

The consideration of damage caused by creep leads to a very major criticism of all K σ_{nett} or J type approaches to creep crack growth predictions. These approaches imply that at any stage of crack growth, a given value of the parameter in question will result in a given crack growth rate. Under creep conditions a material will be accumulating damage. In section 2.3.1 this damage was shown to start at a very early stage in the creep life. Hence, it is likely that during crack growth the crack will be moving through increasingly more pre-damaged and thus less crack resistant material. This is supported by observations that even in a brittle material growth rate has been shown to depend on starting stress.[173] Growth rates for a given K being faster for a lower starting stress. Layering of crack growth rate data verse K or σ_{nett} is a common observation in many of these studies.

It has been observed by many workers that creep crack growth only starts after a definite incubation period.[117 147 149 152] However, it has been shown that isolated crack growth and cavitation close to the crack tip can start very rapidly but there is a protracted period before a single complete crack forms across the thickness.[161 173] This rapid formation of isolated cracks may be due to machining or pre-fatigue damage acting in conjunction with a high unrelaxed stress concentration in the early stages of a test. An apparent incubation period is always observed before steady crack growth occurs. This suggests the need to accumulate a damage zone prior to the onset of stable cracking.

As the importance of creep damage to the fracture process is well accepted it seems desirable to formulate an approach in which full account is taken of the phenomenon of accumulating damage. Displacement approaches are the most obvious manner in which this can be accommodated.

It is a common observation that the exponent in the K control and

σ_{nett} control laws are often approximately equal to the exponent in the second creep law. This suggests a similar stress dependance for crack growth as for straightforward creep displacement. Bain[164] observed the crack growth exponent for K and σ_{nett} to be geometry dependant in centrifugally cast HK40. In this material crack growth was thought to be influenced by oxidation of interdendritic carbides. In such cases geometric factors affecting crack opening will influence the growth rate. But where crack growth is controlled entirely by tip displacements the concept of related stress dependancies of crack growth and creep displacements seems consistent.

Vitek[128] worked from the Bilby, Cottrell, Swinden model for the formation of a plastic zone in order to extend to the model to the time dependant case. Supported by experimental results it was concluded that COD concepts are good criteria to predict the onset of crack growth. Vitek also compared COD and J criteria from the theoretical view point and found that J was more applicable to fast fracture. It was considered that COD was the better parameter to apply to a situation of cumulative damage as in **creep**.

The work by Vitek using a time dependant Dugdale strip yield model for initiation and a similar approach for growth by Heaton and Chan have been unified and extended by Ewing.[175] A critical COD criteria is employed for both initiation and growth. A critical strain criteria was rejected on the basis of its inability to accommodate size effects. Despite the tendency of experimental results, reported in the literature, not to support a constant COD, (see section 2.4.4.4), this approach may be valid here.

The analysis is based on a small scale deformation model. If the effect of increasing deformation zone size in practice is the cause of increasing COD whilst in fact a critical strain type concept is operative, the use of a critical COD in the model is analagous as the width of the deformation zone is assumed constant.

i.e. $$COD = h.\varepsilon_{crit} \tag{2.75}$$

in the analysis h = constant

in practise h = increases

Both this model and a similar approach by Riedel[183] predict that under certain conditions initiation time and crack growth rate can be predicted by K. Both predict:

$$\frac{da}{dt} = AK^{2n-2} \tag{2.77}$$

$$t_i = A'K^{-2n} \tag{2.78}$$

The initiation relationship is based on accumulation of strain at a point with the plastic zone stationary. The growth law is based on the accumulation of strain at a point as the crack tip moves towards that point. This indicates K may at least be applicable for describing local crack growth under conditions of accumulating strain, but for values of n greater than 3 the exponent in the growth law will be greater than in the creep law. It should be noted that these predictions are for local correlations of growth rate with K. Unless crack propagation is at a constant velocity the growth rate will depend not only on the value of K but on the prior history of K.

For low stresses Ewing predicted a change to dependance on σ_{nett}. Riedel predicted change to σ_{nett} control when relaxation and redistribution of stress and strain is more likely. That is, when small scale yielding breaks down. On this basis K control is again favoured by high initial K values and also by increasing geometrical features (i.e. size). For initiation to occur under conditions of small scale yielding the following inequality must be satisfied.

$$d > 4(\bar{\phi}.E/K)^2 \qquad 2.79$$

Where d = either 0.5 the remaining ligament length or 0.5 the crack length which ever is smaller.
$\bar{\phi}$ = critical COD

Whether C* allows for accumulating damage is not straightforward. Webster used the formula:[157]

$$C^* = \frac{1}{B} \cdot \frac{P}{n+1} \cdot \frac{d\dot{\Delta}}{da} \qquad 2.80$$

Where $\dot{\Delta}$ = Load point displacement rate

$d\dot{\Delta}/da$ can be calculated from non-linear beam theory. This approach takes no account of deformation ahead of the crack and is hence only applicable where this is small relative to the total deformation seen at the load points and no account is made for material degradation. These limitations restrict the applicability of this method under usual creep conditions.

Other methods calculate C* from measurements of P, a/w, and $\dot{\Delta}$ during the test. Some indication of material degradation may hence be incorporated in the $\dot{\Delta}$/load measurements. However, it is difficult to see how on this basis the effect of the damage can be separated, thus enabling reliable predictive calculations. It is interesting to note that Harper and Ellison[128] reported layering of results at low growth rates where relaxation and damage spread is more likely.

One point in favour of C* in the respect of damage accumulation is that it has been shown that this parameter may have some degree of applicability in predicting the propagation of a damage front.[160] The damage front concept was originally proposed by Kachenov[184] on a phenomenological mechanics type basis. Rupture occurs when the damage parameter increases from its virgin condition of zero to the exhausted state of unity. The spread of a damage front has been considered by Shiro Kubo et al,[185] they found the damage rate $\dot{\rho}$ to be described by:

$$\dot{\rho} = \frac{C^*}{r}(b/n+1) \qquad 2.81$$

n = Nortons law exponent

b = exponent relating rupture life to stress

It was found that crack growth behaviour could be expressed as a function of C* only when $(b/n+1) > 1$ (i.e. $b > n+1$). When $(b/n+1) < 1$ the crack growth rate is dependant upon the amount of prior crack growth as well as C*. This is because for values of $b > n+1$ the accumulating damage is saturated to a constant steady state value, uneffected by the previous stress/strain history. Under such conditions crack growth will be determined solely by the crack tip stress/strain rate fields, characterised by C*. However, when $b < n+1$ (which they considered may be the general case in metals), the damage value rather than saturating at a steady state approaches to unity and hence crack growth is dependant upon prior history.

The extent of any accumulated damage effect will depend on many factors. The nature of the stress/strain profiles preceding the crack will determine the extent of the damage in the ligament prior to the arrival of the crack tip. The effect of these profiles will depend on the mechanisms by which damage occurs as diffusion and sliding mechanisms have different stress dependancies.

The actual nature of these stress/strain profiles are clearly important. The determination of the nature of these profiles will be of essential importance in reviewing creep fracture from a damage accumulation view point.

2.5 Summary with respect to this work

The essential features of the formation and growth of micro defects appear to be fairly well identified. The behaviour of micro defects has been described by theories with sound basis and for which there is substantial experimental support. Although no single approach can explain all the observed behaviour this is to be expected as the creep environment is a situation where the exact behaviour may depend on the balance of temperature and stress.

Magnox AL80 is a material where at low stresses creep deformation can become diffusion controlled with the characteristic creep exponent value for this type of behaviour of n=1. Under these conditions any cavitation must be predominantly by diffusion as this is the only mechanism operating to any extent. As diffusional growth of cavities is an extremely efficient means of utilising the work done in deformation for cavitation, the process has credence at these low stresses. Nucleation of cavities under these low stresses with minimal sliding would not be easy. However, Kirkendall voids are observed to form in diffusion experiments with zero applied stress.

At higher stresses the importance of sliding on the cavitation process is likely to increase for all metals and alloys. The action of grain boundary sliding in assisting cavity nucleation is easy to accept. In some cases growth entirely by deformation processes may apply.

This may be the case for the formation of wedge cracks in some materials. Where cavitation is entirely deformation controlled it would be expected to be strongly related to strain. The possible existence of an intermediate range cannot be dismissed out of hand and such an approachs appear to be gaining support. In the intermediate range, sliding will probably control nucleation and hence cavity number would be expected to be related to strain. The effect of diffusion on growth would not be easily identified from cavity density studies due to continuous nucleation and also plasticity interacting with diffusion modifying the kinetics. Cavity morphology would probably give the best indication as to the operation of both deformation and diffusion processes. In this work the stresses will be above those associated with purely diffusional creep for Magnox AL80 so sliding would be expected to be influencing cavitation. The presence of a notch has been seen to give rise to a stress concentration and an intensification of shear. The material is ductile and around the notch tip intense plastic behaviour is probable. This could inhibit diffusion processes in the near tip region. The void sheet cavity linkage mechanism has been associated with Magnox. It hence seems probable that deformation and shear processes are likely to have more influence on macroscopic crack growth than diffusion. However, in the region away from the immediate crack tip region the intermediate behaviour of deformation controlled nucleation with deformation/diffusion growth is not ruled out.

For the growth of macroscopic defects the current situation is very indefinite. Most theoretical considerations are attempts at justifying empirical relationships. Very few of the theoretical proposals concerning creep crack growth take much account of the micro processes that occur during creep and may well play an integral role in the control of crack advance.

It appears that prediction of creep crack growth will require the knowledge of at least the following points:

1) The mechanism or criteria controlling crack advance.
2) The nature of the stress distribution preceding a creep crack. The mechanism controlling crack advance is likely to be related to stress or displacement. A knowledge of the stress distribution ahead of the crack tip will enable estimation of the rate at which the criteria controlling crack advance will be satisfied.
3) The effect of geometry on (1) and (2) above. This will be essential if crack growth rate predictions are to be made for service components from laboratory test specimens.

The following work is a study of the growth of macro cracks and has concentrated on the points (1) to (3) above. This seemed the best way to progress towards a sound understanding of how creep crack growth rates may be reliably predicted. The material used was Magnox AL80, a nuclear reactor canning material. This is a ductile material for which creep crack growth is not normally an associated problem. However, it was considered that the high ductility of the material would facilitate the study of strain distributions ahead of crack tips which could lead to an insight to these points outlined above.

3. EXPERIMENTAL PROCEDURE

All the experimental work has been performed on Magnox AL80 sheet of either 1.6, 3.2 or 6.4 mm thickness. The material was of analysis as shown in Table 3.1. With the exception of one test the material was used in the as-supplied condition with a mean grain size of 0.04mm for the 1.6mm thick sheet and 0.08mm for the 3.2 and 6.4mm material.

3.1 Crack Growth Testing

These tests were performed to examine two distinct aspects. Firstly, to examine the strains in the region of the crack tip and the distribution of strain with distance from the crack tip. Secondly, to examine the crack extension rates under creep conditions.

The majority of the work has considered two basic specimen geometries, the Double Edge Notched geometry (DEN) and the Centre Notched geometry (CN). A third geometry has also been considered to a lesser extent, the Single Edge Notched geometry (SEN). The test specimen geometries were based on the standard fracture toughness test piece designs as described in ASTM 410. For the first two tests the specimen profile used was as indicated by the dotted outline in Fig. 3.1. This specimen profile proved unsatisfactory as for total crack length, a, to width, w, ratios a/w of up to around 0.45 a/w fracture occurred through the pinholes. The modified design shown by the solid outline in Fig. 3.1 was hence adopted for subsequent tests. This enabled an a/w ratio of around 0.33 to be used as the starting notch length due to the reduced pin-hole loading.

The notches were produced by spark machining using a thin copper foil. The resulting notches were typically 0.4mm wide with a root radius of

TABLE OF CHEMICAL ANALYSE.

ELEMENT	%
Aluminium	0.77
Beryllium	0.004
Iron	0.006
Silicon	0.06
Manganese	0.003
Zinc	0.008
Calcium	0.01
Magnesium	Balance

Table 3.1

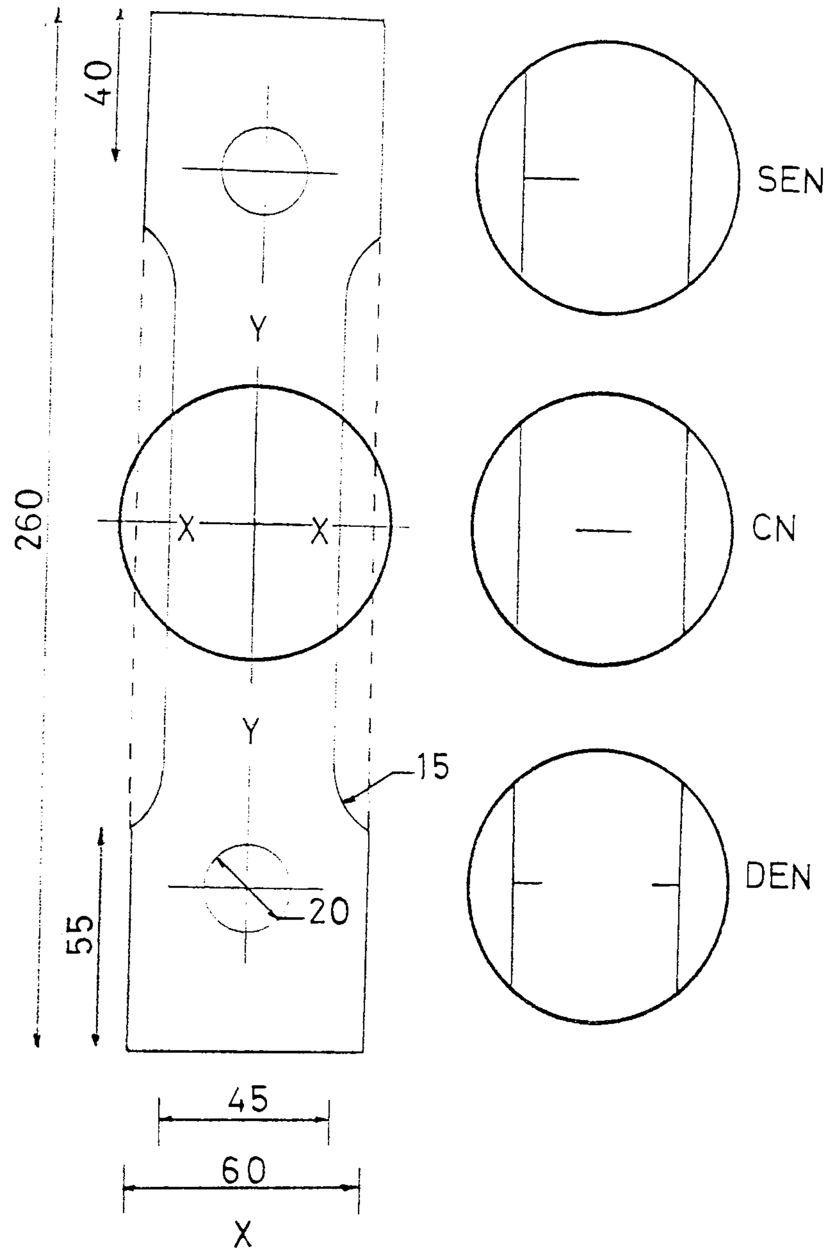

DIMENSIONS IN MM.

NOTCHED TEST SPECIMEN DESIGN

FIG. 3.1

around 0.1mm. Three specimens were tested using very large radius, semi-circular notch roots. These notches were also produced by spark machining. Attempts at modifying the tips of normal spark machined notches by hot fatigue cracking at 300°C using a mean load and amptitude of 400N were made for two specimens.

The early work was performed on a Denison T48 creep testing machine. This machine was grossly over capacity with a lever arm ratio of 44·8:1 However at that time it was the only machine available. The last 21 tests were performed on a 10KN ESH creep testing machine with a 10:1 lever arm ratio. This rig had a ported furnace through which continuous observation of the notched region of the specimen was possible. Temperature monitoring of the specimen surface was also performed through this port. Along the central 60mm the 3 zone furnace control was adequate to ensure that no two points varied in temperature by more than 5°C and the overall temperature was maintained at 300°C ± 3°C. The load was applied to the specimen by means of the automatic lever arm levelling mechanism. Specimen grips were of a pin loading design and machined from a nickel free tool steel to avoid any interaction between the specimen and the grip material. Specimen identifications for these tests are prefixed TS.

Specimens that were creep pre-strained prior to notching were cooled from pre-straining under load, and then reheated under load after the notches had been cut. Normally the load was only applied after the specimen temperature was observed to have stabilised at 300°C for a period of at least 1 hour. The cooling and re-heating intervals for the pre-strained specimens were fairly **short**, that is around 0.75 hours. The furnace was of a counter balanced vertically split and hinged variety and at 300°C could safely be opened and raised clear of the specimen to allow fast cooling and pre-heated before lowering for rapid re-heating. Timing for these pre-strained specimens was the total time that the specimen was under load above 280°C.

3.1.1 Production and Recording of Grids

In order to examine the strain field ahead of the notches it was necessary to produce a grid on the specimens that could be photographed before and during creep testing.

Trials were made using a photo-resist material commercially available for the production of electronic printed circuit boards. A negative for contact printing onto the specimen was producing by photographically reducing a perforated card template illuminated from behind. This produced an array of dots spaced at 0.5mm intervals. Initial tests indicated that the photo-resist was sufficiently temperature stable to be used directly as the position markers. On longer term tests however, the resist proved unstable and faded. Etching up the grid pattern was considered but discounted as the contrast obtained would be insufficient in view of the surface deformation encountered under test conditions. The photographic method was rejected in favour using a scribed grid of 0.5mm spaced lines produced with a vernier height gauge.

The grids were recorded photographically using a 35mm single lens reflex camera with a 135mm focal length lens and 175mm tube extension. This system produced a magnification of approximately x6 when the 35mm film negative was enlarged to the standard photographic half plate size. The specimen could be photographed in-situ in the furnace through the observation port. The selection of a 175mm tube extension length was a deliberate compromise between optimium magnification, depth of focus and adequate working distance to allow photography of the specimen through the furnace port. The specimen was illuminated with a quartz halogen light source with fiber-optic light guides. See Fig.3.2a and 3.2b. Focussing of the camera system was by moving the entire camera and lens system towards or away from the specimen by means of a screw feed table. The lens distance adjustment was always left on a constant setting (maximum) to minimise variation in the magnification between photographs. Where possible, all the photographs pertaining to a particular specimen were processed and printed as a single batch. This was also to avoid variation in the magnification between photographs.

It was attempted to analyse the grid displacements using a digitising computer. However, it was found that this method was in fact less convenient than simply making measurements with a ruler and only of compatible or even inferior accuracy. The principal difficulty with the computer system was that the digitising sight could not be moved easily over short distances and so could not be positioned accurately over the points. The actual method used for analyising grid displacements and estimations of the accuracy of the method are discussed in conjunction with the results.

3.1.2 Crack Length Monitoring

The monitoring of crack length was originally by means of the D.C. potential drop technique.[186] This was however later abandoned completely for several reasons. The accuracy of the P.D. technique for this application was considered suspect in view of the degree of ductility and hence change in probe spacing that occurred during each test.

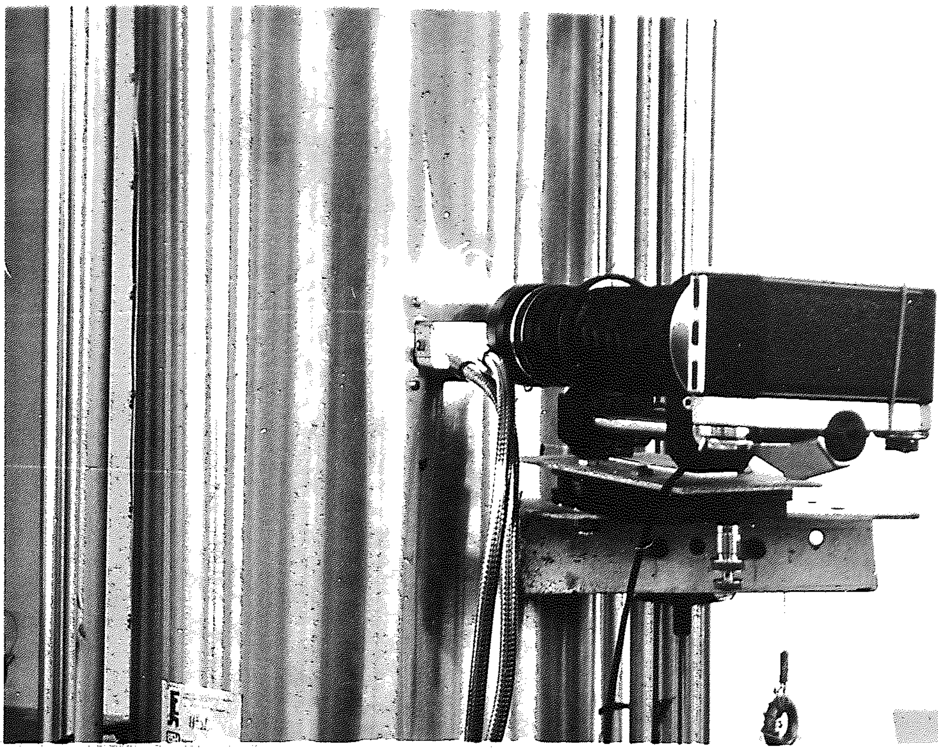

A

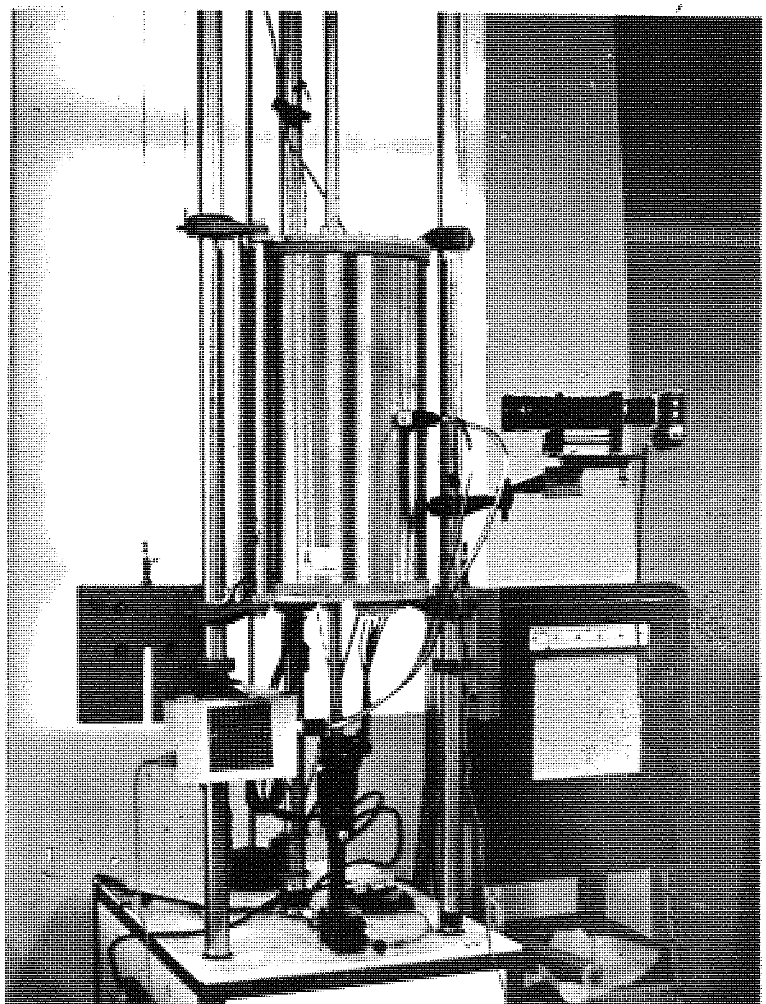

It proved impossible to calibrate to an adequate degree of accuracy for these changes in the distance between the probe wires. Also the high conductivity of Magnox AL80 combined with a large specimen size required a high current for a reasonable potential drop across the crack. Oxide formation in combination with this large current resulted in resistance heating at the pin-holes. This caused general temperature instability and a tendency for pin-hole failures.

With the advent of the ESH creep rig with a ported furnace it was decided to rely on optical monitoring of the crack. Although this method proved open to a degree of personal interpretation, estimation of the surface position of the crack tip to within 0.75mm was consistently repeatable from the photographs taken. This represents a better degree of accuracy than was possible using the potential drop technique on such a ductile material.

3.1.3 Experimental Design

A Latin square or orthogonal type of design was applied to the study of the variables considered where ever possible. The blocks were usually of four specimens or six specimens but with some specimens occurring in several blocks, for instance:

i) effect of stress level

DEN low stress, CN low stress, SEN low stress, DEN high stress, CN high stress, SEN high stress. (all 3.2mm thick).

or

DEN low stress, CN low stress, DEN intermediate stress, CN intermediate stress, DEN high stress, CN high stress (all 3.2mm thick).

ii) effect of thickness

DEN thin, CN thin, DEN intermediate, CN intermediate, DEN thick, CN thick

(all low stress)

Similarly with notch root radius and pre-strain. The technique for analysising Latin square experiments statistically was not considered to offer any advantage in processing the results. However, use of an orthogonal type design ensured that the maximum chance of detecting significant trends arising from a number of variables was obtained from the minimum number of specimens. This was considered especially important for a project such as this which involved the need for a series of long term tests to be performed in a finite time period and with limited resources available.

3.2 Smooth Bar Creep Testing

These tests were performed to provide supporting information for the notched, crack growth test specimens. Three factors were considered of interest:

i) Verification of the values of the creep exponent operative in the stress regimes considered.

ii) To provide an indication of the extent of the primary creep regime.

iii) To provide metallographic specimens for a quantitative assessment of the extent of cavitation as a function of strain.

The specimens used in these tests were of the design shown in Fig. 3.3 These tests were performed on a Denison T47 creep rig with a thyristor controlled furnace. Temperature control was normally better than $\pm 3^{\circ}C$ on $300^{\circ}C$ with a variation along the specimen length controlled

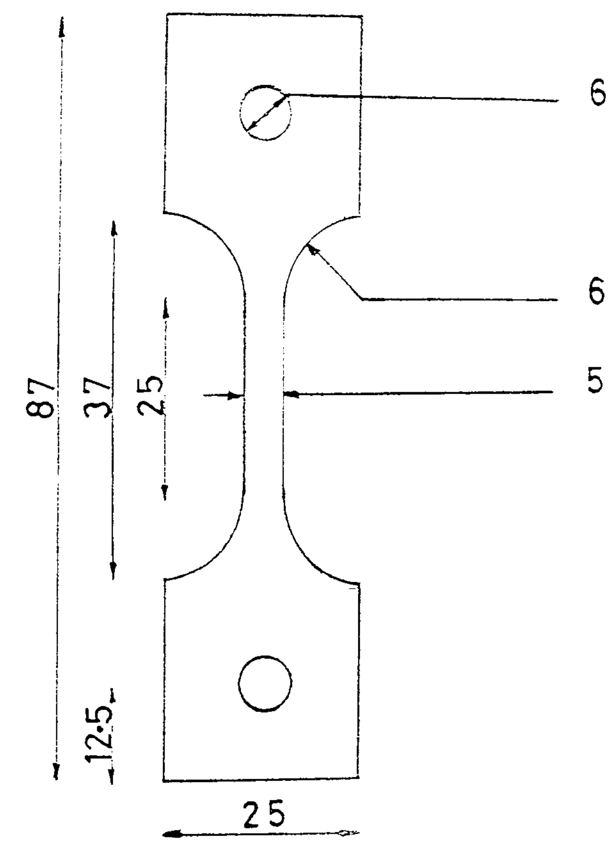

DIMENSIONS IN MM.

SMOOTH BAR TEST SPECIMEN
DESIGN

FIG. 3.3

to less than $3^{o}C$. Elongation was recorded by monitoring the lever arm displacement with either a dial-gauge or with a transducer depending upon the test duration. Although not as accurate as the use of extensometers, this method was considered adequate in view of the comparatively undemanding aims of these tests. The greatest disadvantage in not using extensometers was that no indication of primary extension occurring immediately on loading could be obtained by simply monitoring the lever arm displacement. All the tests were performed under approximate constant stress conditions. The constant stress was maintained by adjusting the scale pan weight at frequent intervals to off-set the reduction in area, calculated from the elongation on a constant volume basis. Specimen identification for these tests were prefixed SME.

3.3 Metallography

Basic metallography was performed to examine grain size, the regions preceding crack tips and similar general points of interest. Specimens were prepared by conventional mechanical polishing techniques, but avoiding excessive pressure, to a 1μm diamond paste finish. The surface was then etched in saturated oxalic acid solution (aqueous) and then repolished with 1μm diamond paste then an Alumina based metallurgical polishing medium before re-etching with oxalic acid solution. Where specimens were required for quantitative metallographic examination all the specimens were first assembled and mounted together in a single mount of a cold setting medium. This ensured that during preparation each specimen in the mount received as near as possible the same treatment. Where cavitation was to be examined an inferior quality of finish was often accepted rather than prolonging the preparation treatment and possibly distorting or enlarging the cavities in such a soft and ductile matrix. Often a small piece of untested material was mounted with a creep tested sample so that any tendency to form etch pits could be noted to avoid confusing these with true creep cavities.

The scanning electron microscope has been used to examine fracture surfaces as well as metallographic specimens of the region surrounding creep crack tips.

A quantitative metallographic study of the extent of cavitation seen in the smooth bar creep specimens was made. The analysis was made from photographs using a Joyce Loebl Magiscan Image Analyising Computer system programmed in Basic language to give average cavity number, length, height and area measurements for a given field.

4. RESULTS

4.1 Smooth Bar Creep Tests

These tests were performed to provide supporting information for the notched tensile tests. Three factors were of particular interest i) to check the values of the creep exponent operative for the stress levels encountered in the notched tensile tests. ii) to assess the extent of primary creep deformation. iii) obtain an indication of the relationship between creep damage and uni-axial creep strain ε_{yy}.

4.1.1 Assessment of the Creep Exponent Values

The secondary creep rates are shown in Table 4.1 From metallographic examination of SMB3 and 15 it was observed the grain size had increased by a factor of about*2 during creep testing. The creep rates shown for these two specimens have been corrected by the application of the grain size dependance on creep rate given in equation 2.2. This equation predicts that for this stress regime the creep rate is proportional to $d^{-0.8}$. The creep exponents were evaluated as the gradient from linear regression analysis of $\log.\dot{\varepsilon}$ versus log.stress Separate regression analysis were performed for stresses below $15.5 MNm^{-2}$ and stresses above this value, exponents of 3.69 and 7.1 were obtained respectively. These agree well with the commonly reported values for Magnox AL80 of 3.5 and 7 for the same conditions of stress.

4.1.2 Assessment of the Extent of Primary Creep

A measure of the strain arising from primary creep deformation and the duration of the primary interval for these specimens are also shown in Table 4.1. The duration of the primary creep interval is

TABLE OF RESULTS FROM SMOOTH BAR TESTS AT 300°C

STRESS MNm^{-2}	SME. NO.	TOTAL STRAIN %	STRAIN RATE $Hr.^{-1}$	PRIMARY CONTRIB. % (Apprx)	TIME FOR PRIMARY. Hrs. (Apprx)	COMMENTS
5	2		2.19×10^{-4}	0.3	100	
	13	33	1.56×10^{-4}	0.25	100	
	14	10	1.76×10^{-4}	0.25	50	
6	6		3.26×10^{-4}	0.5	50	
7.5	3	11	7.41×10^{-4}	0.7	50	Strain rate corrected for gr.growth
	15	10	8.18×10^{-4}	0.79	20	" " " " " "
	16		7.60×10^{-4}		20	Furnace failure
	17	34	9.24×10^{-4}		20	Primary contr. too small to record.
20	9	33	3.8×10^{-2}	3.0		
	12	7	5.2×10^{-2}	2.8	0.2	
30	10	56	7.5×10^{-1}	6	0.1	
	11	17	8.5×10^{-1}	4	0.05	

TABLE.4.1

the time before secondary creep became established. The contribution to strain from primary creep shown in Table 4.1 is not the total strain accumulated during the primary creep interval. The contribution from primary creep shown represents the strain above that which would be expected had secondary creep started immediately. If the line of creep strain versus time for secondary creep is extrapolated back to t=0 the primary contribution is given by the value of the intercept with the strain axis. This is shown schematically in Fig. 4.1. This will be less than the total strain accumulated during the primary period. The contribution from primary creep evaluated here has more pertinence to considerations of steady state deformation than the total primary creep strain as the important factor is the deviation from the steady state.

Only very small primary strain contributions were observed at the low stress range (5 to 7.5 MNm^{-2}). This contribution was observed to increase with stress, to around 4% strain in the range of 20 to 30 MNm^{-2}. The variation in the primary creep contribution across this stress level was about 3%.

4.1.3 Quantitative Metallography of Smooth Bar Creep Specimens

A limited quantitative metallographic examination was made on some of the smooth bar specimens. The extent of the cavitation present was observed to be both stress and strain dependant. The difference in cavitation between a high stress and low stress specimen deformed to similar extents was apparent to the naked eye for fairly high strains. The high stress specimens showed noticably less damage than their low stress counterparts. The damage was in the form of grain boundary cavities elongated at 90° to the tensile axis, as shown by Fig. 4.2. The results of the quantitative metallographic examination are shown

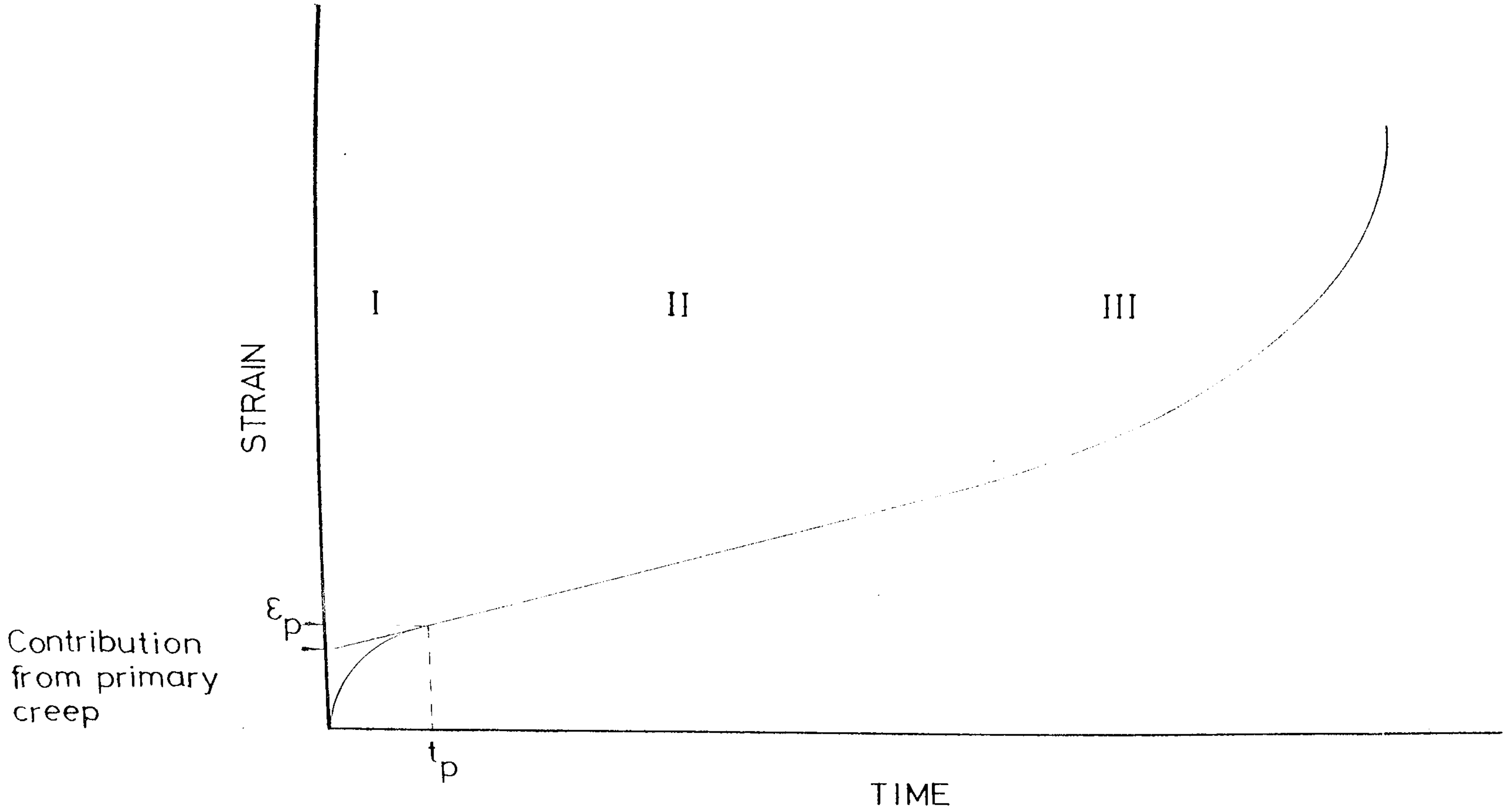

SCHEMATIC REPRESENTATION OF
A SMOOTH BAR CREEP CURVE

FIG. 4.1

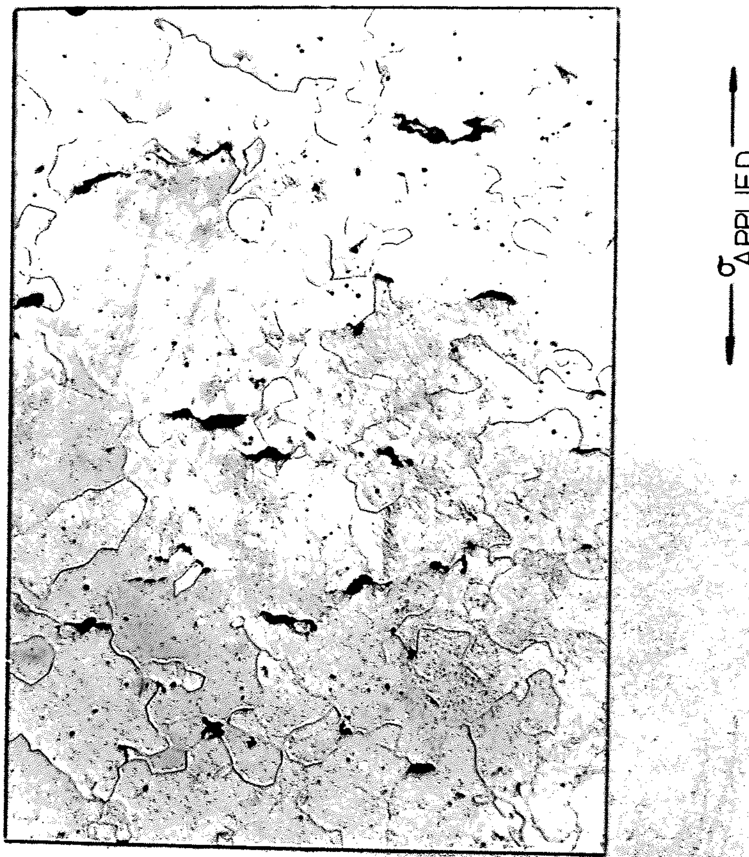

X100

CREEP DAMAGE IN A SMOOTH BAR
CREEP SPECIMEN (SMB 4)

in Fig. 4.3. The damage has been expressed as an estimate of the effective loss of ligament computed as follows:
Consider a square section of side Fl on a specimen. Within this frame there is an average cavity density for the specimen in question. There are N cavities of average length L and average height H. (length being perpendicular to the tensile stress axis and height parallel).

It was considered that fracture would occur along a path through adjacent voids. For a void to be instrumental in reducing the load bearing capacity of the ligament it would have to be contained within a band of finite width from the mean crack path. Based on an approach by Widgery & Knott[187] the width of this band has been set to 6 times the average cavity height. See Fig. 4.4

As a fraction of the frame height this fracture path band represents

$$\frac{6H}{Fl}$$

Assuming an even distribution of voids in the strip. The number of voids in the strip equals $\frac{6HN}{Fl}$

Assuming all the voids in the strip contribute to the reduction in the load bearing capacity of the ligament, then multiplying by the average length of a void L, gives the total effective length of cavity in the strip. This can be expressed as a fraction by dividing by the frame length

$$\text{Fractional loss of ligament} = \frac{6HNL}{Fl^2} \qquad 4.1$$

Joining experimental points of the same stress level in Fig. 4.3 with straight lines produced the following indications of the effective loss of ligament for a 20% strain.

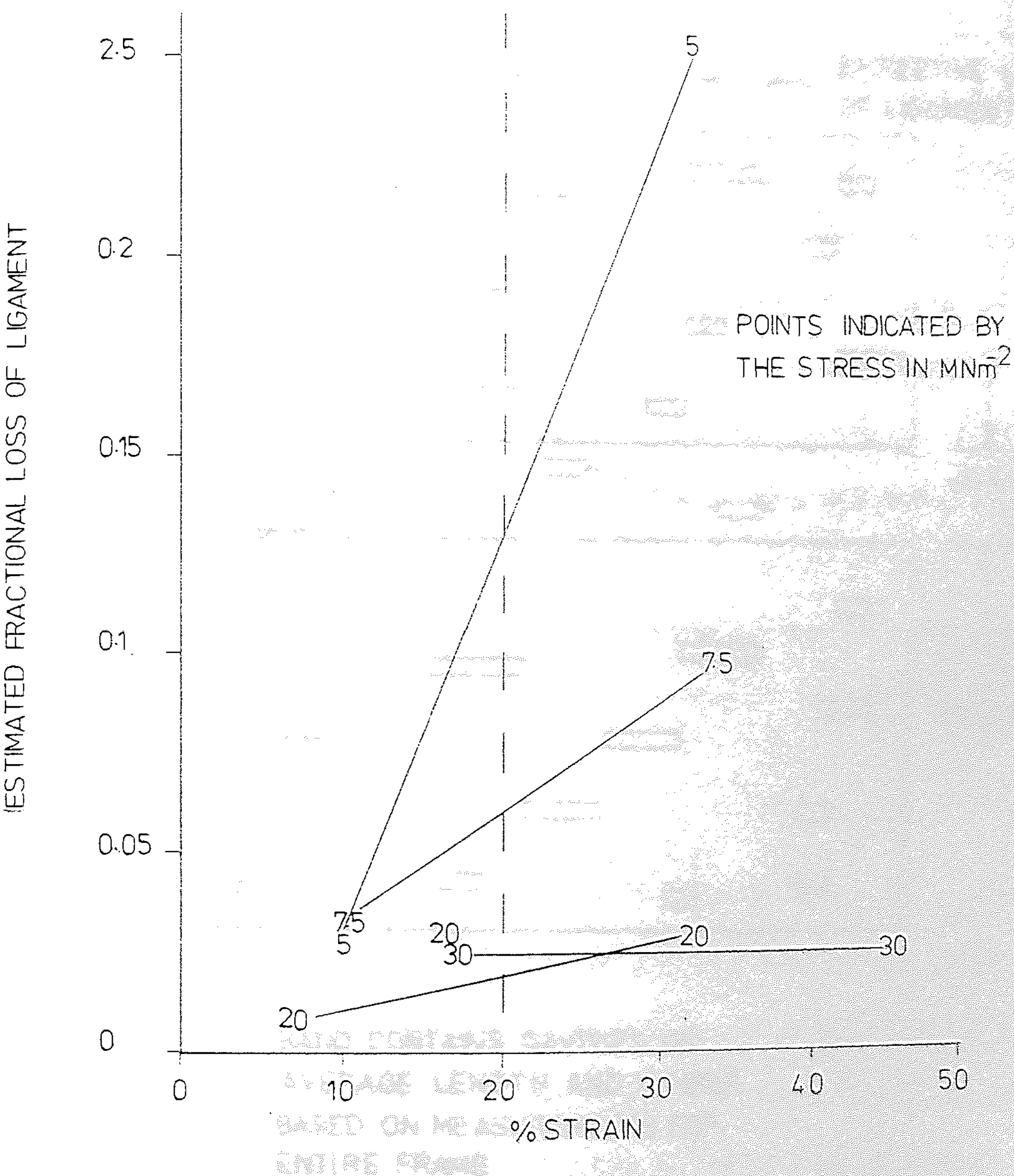

EFFECTIVE LOSS OF LIGAMENT DUE
TO CREEP CAVITATION.V.STRAIN
(FROM SMB TESTS)

FIG.43

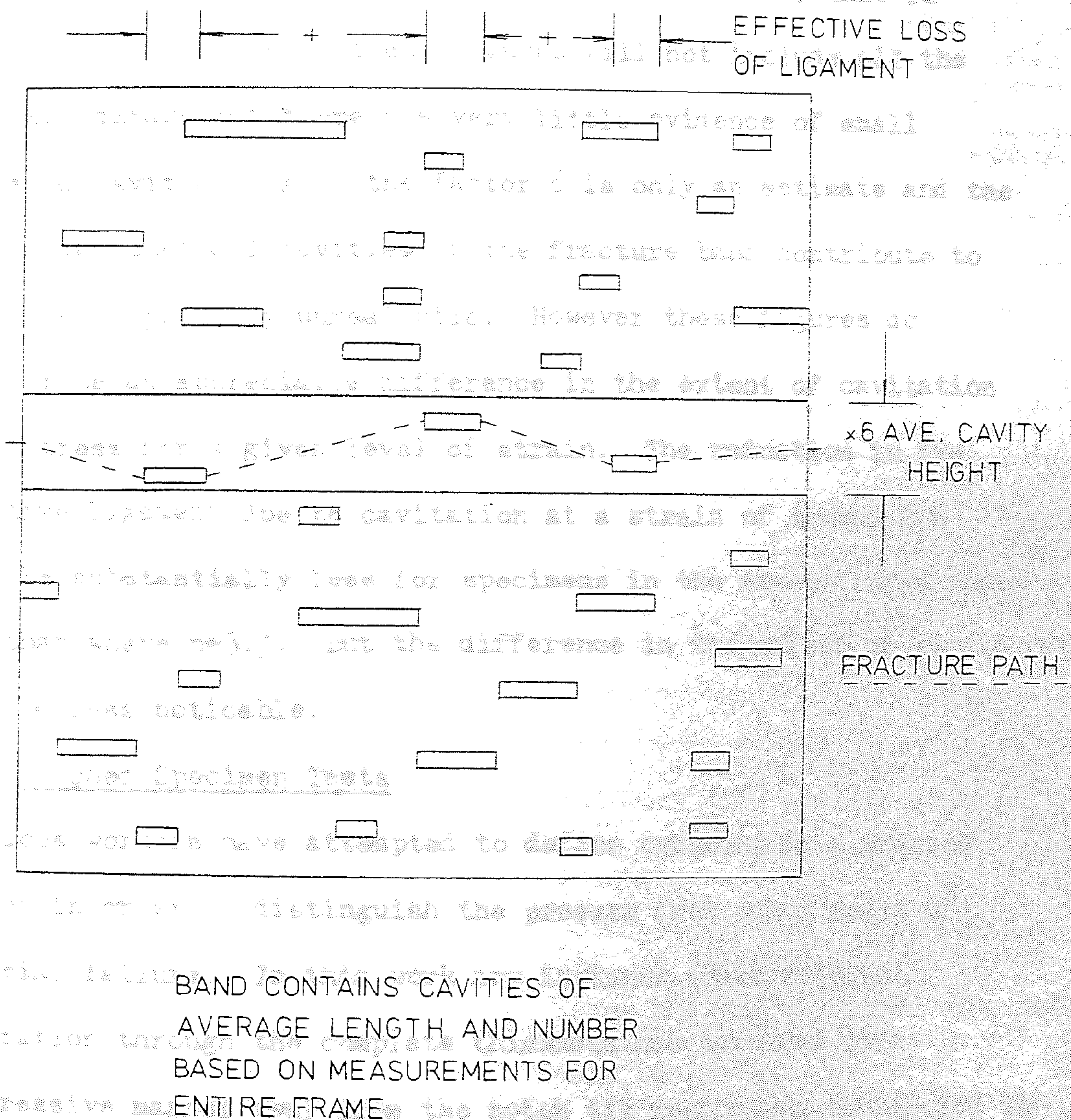

EVALUATION OF LOSS OF LIGAMENT
DUE TO CAVITATION

FIG.4.4

Stress MNm^{-2}	%Loss
5	13
7.5	6
greater than 20	2.5

This analysis only considered fairly large cavities, that is greater than 3um, hence these figures will not include all the ligament damage but there was very little evidence of small isolated cavities. Also the factor 6 is only an estimate and the assumption that all cavities in the fracture band contribute to fracture is probably unrealistic. However these figures do illustrate an appreciable difference in the extent of cavitation with stress for a given level of strain. The reduction in the effective ligament due to cavitation at a strain of around 20% will be substantially less for specimens in the stress range where n=7 than where n=3.5. But the difference in the effect on strain rate will be less noticable.

4.2 Notched Specimen Tests

Previous workers have attempted to define cracking in a precise manner in order to distinguish the process from other modes of material failure. In this work any instance where material separation through the complete thickness has occurred in a progressive manner away from the notch tip region was considered to constitute crack growth. Where a crack has formed under creep conditions it is considered to constitute a creep crack. Fracture normally showed a greater resemblance to a ductile tearing process than what might classically be defined as a cracking process.

Details of the notched specimen test program are shown in Table 4.2.

TABLE OF NOTCHED TEST SPECIMEN PROGRAMME

TABLE.4.2

TS NO.	GEOMETRY	NOMINAL STARTING STRESS(MNm^{-2})	COMMENTS
1	DEN	15	
2	DEN	30	
3	DEN	10	Not stopped before fracture
4	DEN	10	Notches sharpened by hot-fatigue Results not considered in detail
5	DEN	10	Not stopped before fracture
6	CN	13	Photographic records inadequate quality for analysis.
7	DEN	10	
8	CN	10	
9	DEN	10	
10	CN	5	Pin-hole failure
11	DEN	5	
12	DEN	20	
13	CN	20	
14	DEN	20	Notch root radii = 3mm
15	DEN	20	Notch root radii = 2mm
16	CN	5	
17	SEN	5	
18	DEN	20	Creep pre-strained prior to notching(grid quality poor)
19	DEN	5	Creep pre-strained prior to notching
20	DEN	20	Notches sharpened by hot fatigue Results not consiered in detail
21	DEN	20	Large Grain Size-Caused very bad orange peel, grid analysis not very accurate
22	DEN	5	6.4mm thick sheet
23	DEN	5	1.6mm thick sheet
24	SEN	20	
25	DEN	20	Very high starting a/w (0.65)
26	CN	20	Creep pre-strained prior to notching
27	SEN	20	Notch root radius = 3mm
28	CN	5	6.4mm thick sheet
29	DEN	5	1.6mm thick sheet

4.2.1 General Observations

The most immediately apparent difference in behaviour between the Double Edge Notched (DEN) and Centre Notched (CN) geometries was in the location of the maximum contraction in the X-direction. This maximum contraction occurred along the plane of the notch for the CN geometry, but was displaced some distance in the Y-direction above and below the notch plane for the DEN case. Fig. 4.5 shows an example of a deformed CN and DEN specimen. For crack growth in the DEN specimens the crack remained fairly straight, growing roughly along the specimen centre line XX. The CN specimens showed initially straight crack growth along the centre line XX, followed by a tendency for the final fracture path to run along the 45^{o} shear bands. This trend can be observed in Fig. 4.5.

All three specimen geometries underwent a definite period of time under creep conditions before a complete through thickness crack was observed at the notch tip. This period is hereinafter referred to as the initiation time. In the thicker sections tested some evidence of tunnelling was observed prior to the formation of a through thickness crack. Crack growth started by the formation of a small nick in the notch tip (see Fig. 4.6). There was then a period of slow crack growth. This was followed in the DEN and CN geometries by rapid collapse of the remaining ligament. Visual observations of this collapse phenomenon suggested that this event could not be classed as crack growth as in many cases failure across the ligament was virtually simultaneous and not by progressive growth of the cracks.

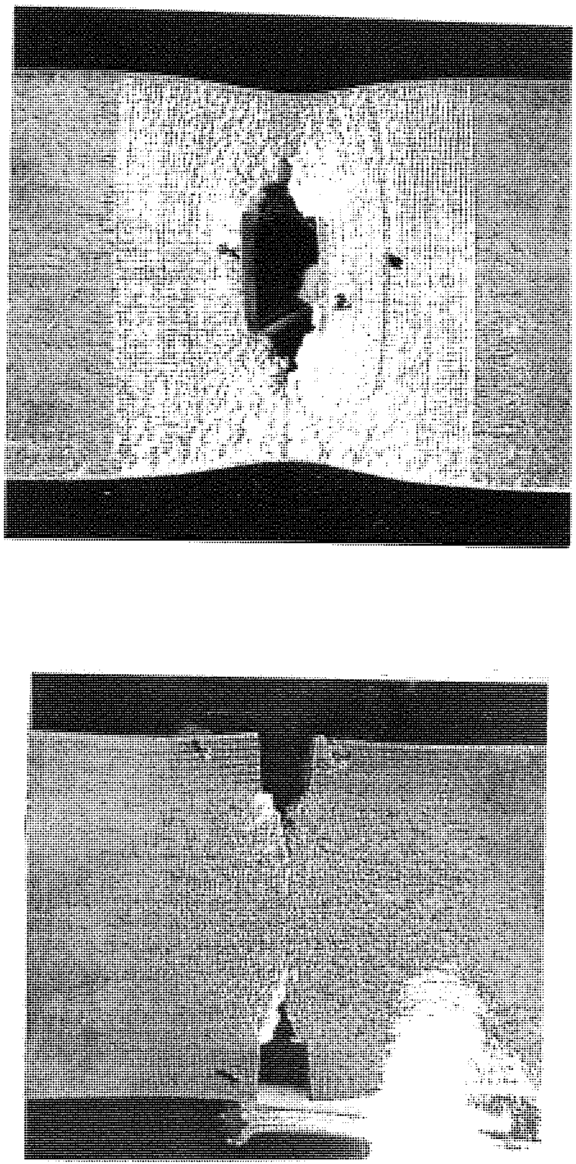

COMPARISION OF LATERAL
CONTRACTION FOR CN AND
DEN GEOMETRIES

FIG.

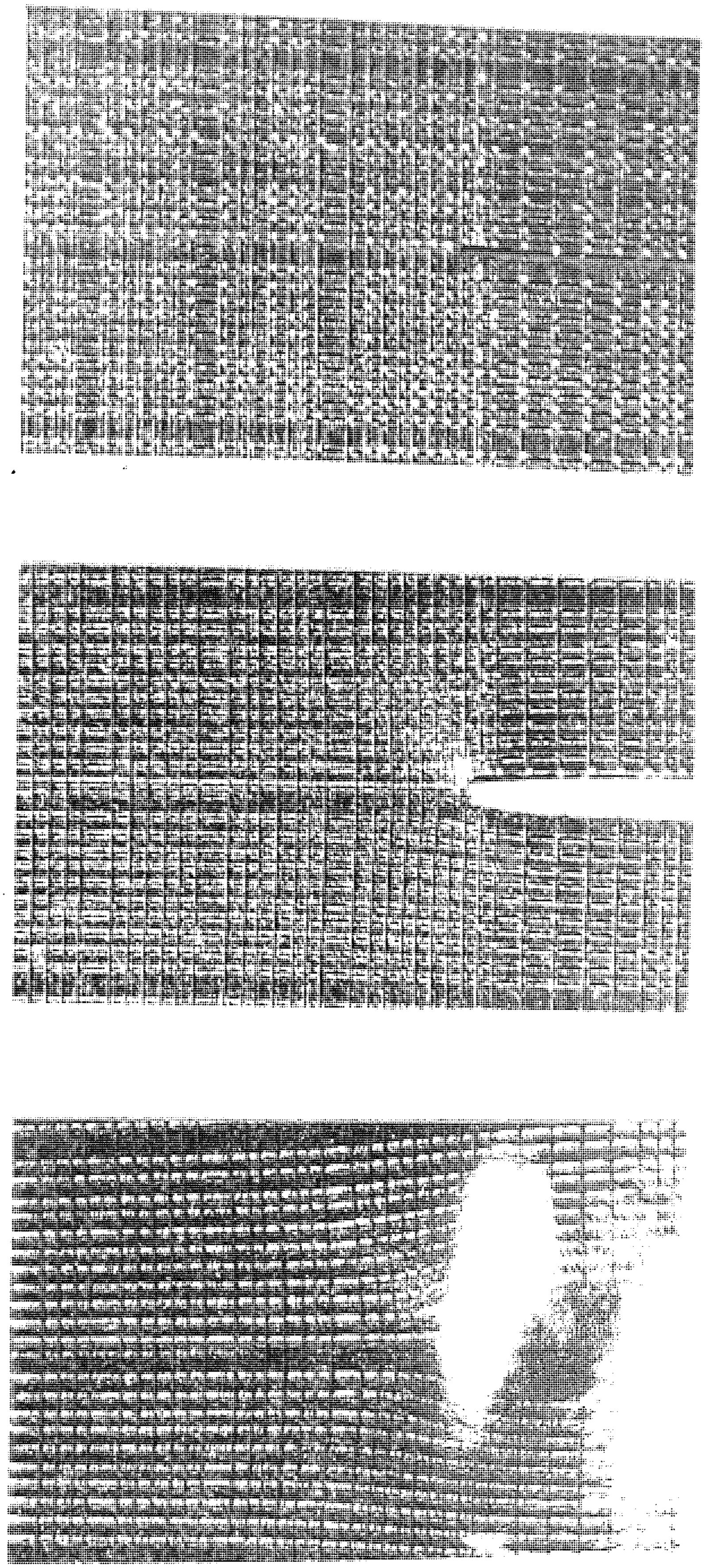

TYPICAL CRACK GROWTH SEQUENCE

FIG. 46

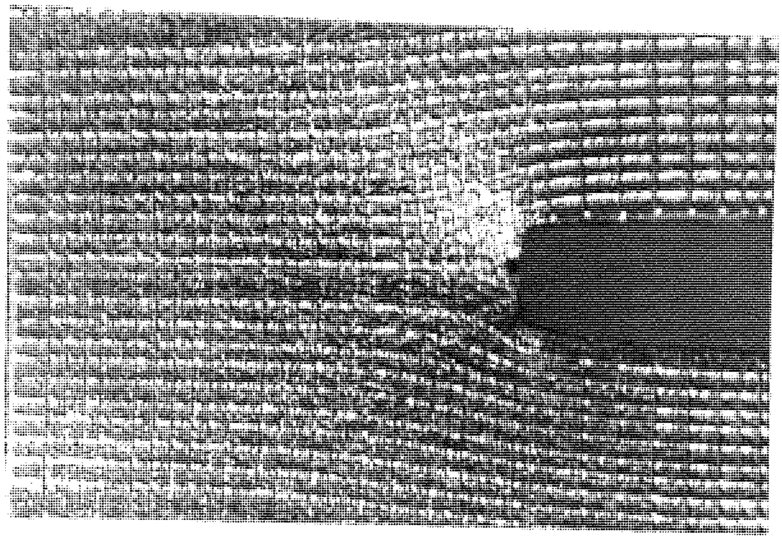

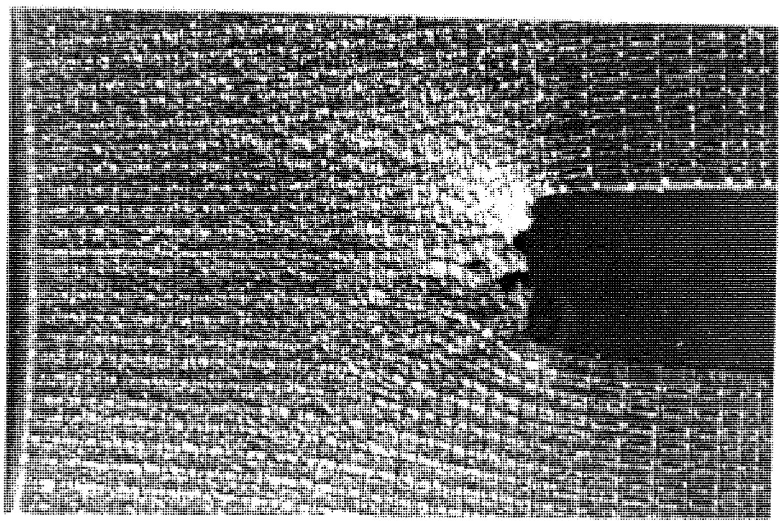

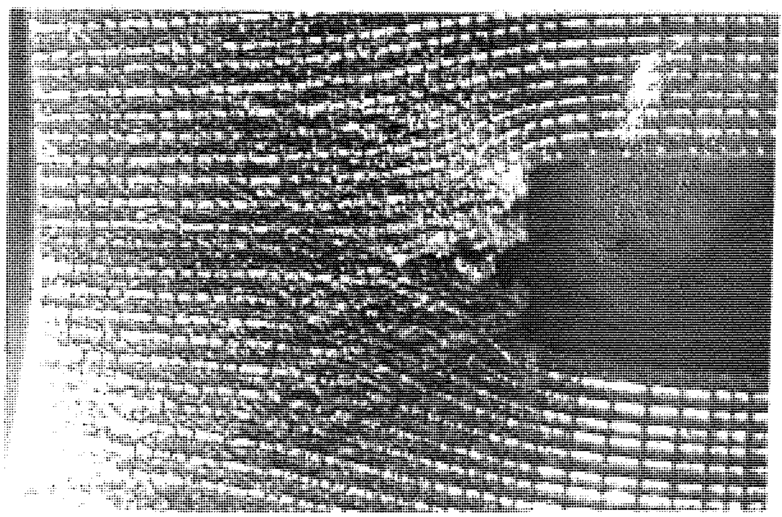

Post fracture examination of the fracture surfaces showed boundaries between light and heavier oxidation. These boundaries were considered to represent the approximate positions of the crack fronts at the onset of ligament collapse. However this estimation will be less reliable for the higher stress tests. The ligament collapse stresses could be calculated on the basis of these crack front positions. These collapse stresses have been grouped according to the starting stress level and are shown in Fig. 4.7. (Starting nett section stresses of $5MNm^{-2}$ = low, $10MNm^{-2}$ = intermediate, $20MNm^{-2}$ = high). Also shown in Fig. 4.7 are the UTS levels for magnox AL80 at $300^{\circ}C$ at various strain rates (taken from reference11). As can be seen from this figure the ligament collapse stress was dependant upon the initial starting stress. If the starting stress was low then the collapse stress would also tend to be low. For the $20MNm^{-2}$ starting stress level the average ligament collapse stress approximately corresponded to the hot tensile strength of the material (measured at a strain rate of 1000% Hr^{-1}).

The average ligament collapse loads corresponded to a/w values of 0.72, 0.59, 0.60 a/w for the low, intermediate and high stress levels respectively. This phenomenon of ligament collapse made it extremely difficult to obtain photographic records of cracks between 0.6a/w and final fracture for these geometries.

Ligament collapse was not observed with the SEN geometry even at a/w values in excess of 0.8 . For the high stress SEN cases crack growth increased to a high rate but material separation was still of a definitely progressive nature away from the notch tip.

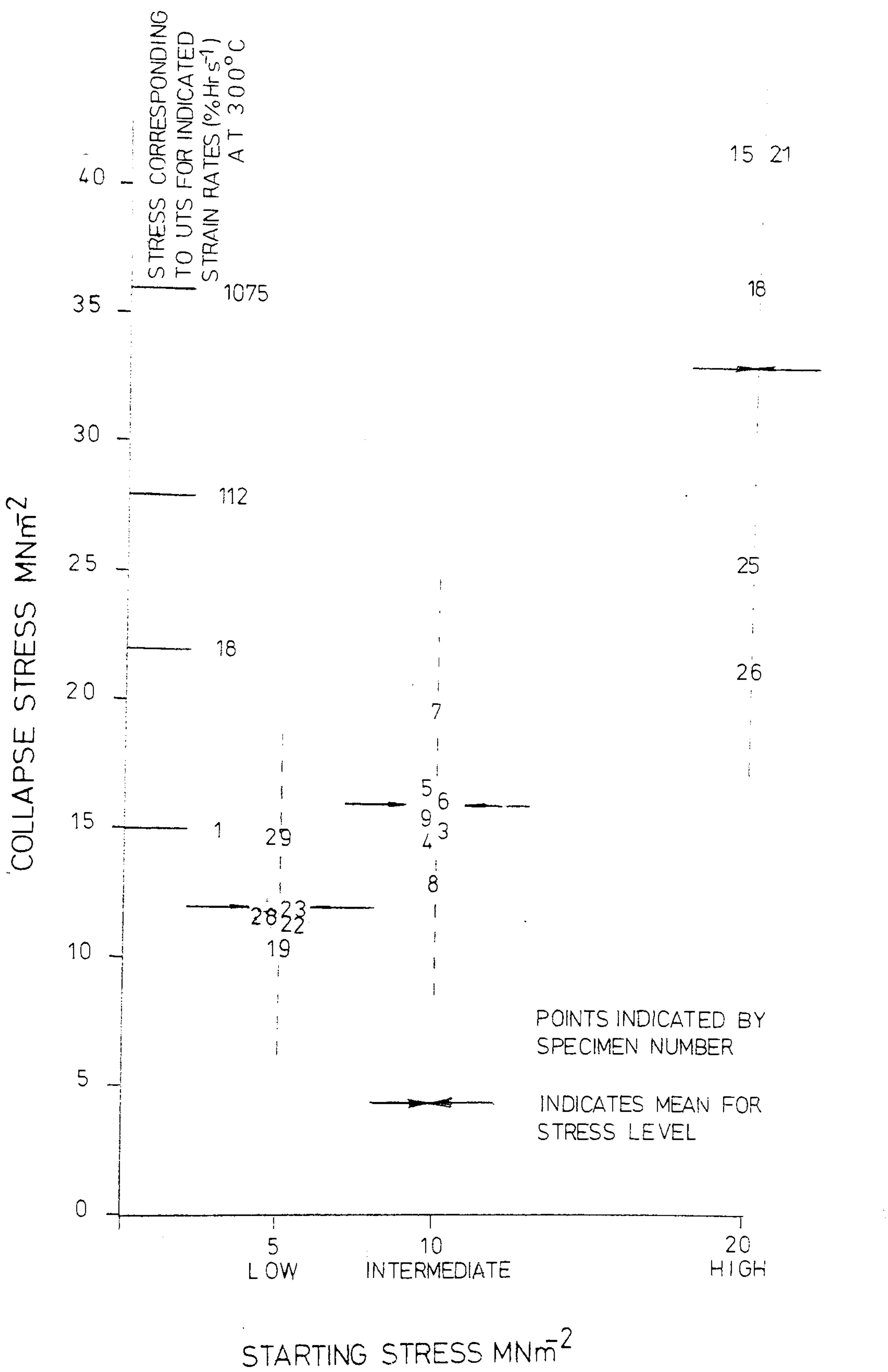

NETT SECTION STRESS
FOR LIGAMENT COLLAPSE

FIG.4.7

4.2.2 Notched Specimen Tests - Measurements Relating to Time

In this section the results of the observations of crack initiation time and the crack length versus time studies from the notched tensile tests will be presented.

4.2.2.1 Crack Initiation Times

Crack initiation time was taken as the first observable occurrence of a complete through section crack. The exact time when a complete through section crack formed was estimated by a combination of visual examination and 'back extrapolation' of the crack length/time plots for each case. The estimated accuracy of these predictions, based on the range of the first and last possible instance for initiation was approximately $\pm$ 0.25Hrs for the high stress tests and $\pm$25Hrs for the low stress tests. As can be seen these accuracies are far from ideal. In the analysis of the crack length versus time observations the critical factor was the estimate of the time when the crack length equalled 0.35a/w. This could normally be estimated with much greater accuracy than initiation, see Fig. 4.8.

Despite the experimental inaccuracies, initiation times were considered to warrant inspection. From examination of the initiation times it seemed probable that the times were influenced by both the stress level and geometrical features. Correlations of the type $t_i \propto K^{-m}$ had been proposed in the literature.[175,183] As K is a function of both stress and geometry, correlations of initiation time with K seemed a logical starting point. Linear regression analysis of $\log.t_i$ versus $\log.K$ were attempted, also regressions of $\log.t_i$ versus $\log.\sigma_{nett}$ were made. The initiation times had to be divided into two groups according to the n value operative. Specimens for which the starting

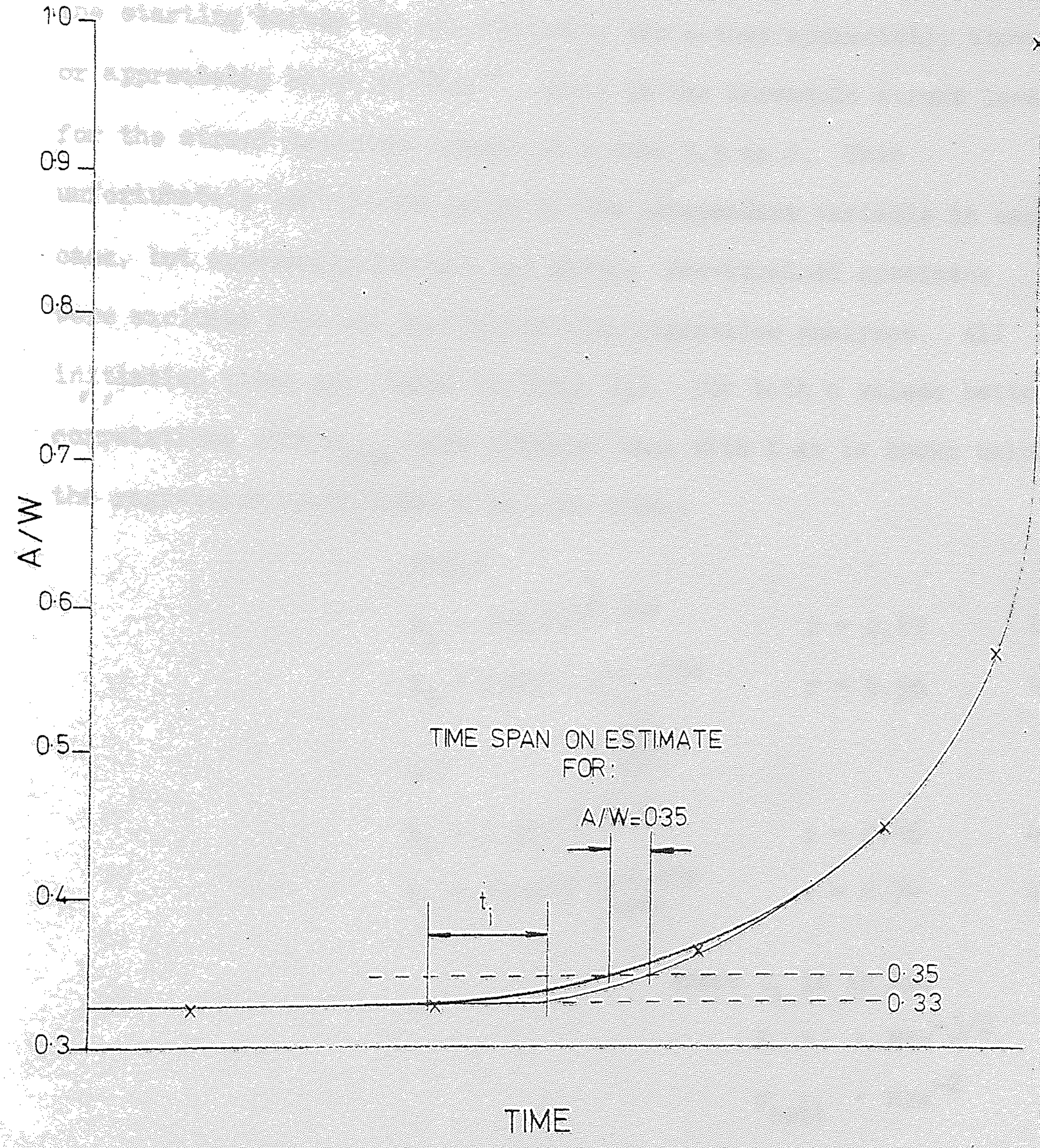

COMPARISION OF THE ACCURACY OF
PREDICTING TIMES TO INITIATION
AND TO 0.35A/W

FIG.4.8

nett section stress was below 15.5MNm^{-2} were treated as one group with n=3.5 and specimens with a starting nett section stress above this value were treated as another group with n=7. In practice the starting stress for all specimens was either appreciably above or appreciably below 15.5MNm^{-2}, which is the threshold stress level for the stress dependant change in n from 3.5 to 7. This unfortunately limited the range of the independant variable in each case, but especially for the n=7 group. Pre-strained specimens were excluded from all initiation time regression analyses. All initiation times are listed in Table 4.3. For both n values better correlations with σ_{nett} were obtained than with K as is shown below, the regression coefficient r is also shown:

n=3.5

$$t_i = 105.8K^{-0.92n} \qquad r = 0.87 \qquad 4.2$$

$$t_i = 217500\ \sigma_{nett}^{-1.035n} \qquad r = 0.96 \qquad 4.3$$

n=7

$$t_i = 2.58K^{-0.063n} \qquad r = 0.46 \qquad 4.4$$

$$t_i = 33\times10^5\ \sigma_{nett}^{-0.67n} \qquad r = 0.74 \qquad 4.5$$

Where t_i is in Hrs

K " " MNm$^{-3/2}$

σ_{nett} " " MNm^{-2}

Despite the better correlation with σ_{nett} than with K it was still considered that geometry was important in crack initiation time. In order to investigate this possibility the geometric and the stress factors in the K expression were separated.

$$K = \sigma . f(a)$$

Where the f(a) is given by a value Y which incorporates a correction for finite geometry

INITIATION AND THROUGH FAILURE TIMES

SPECIMEN NUMBER	t_i	STARTING K	STARTING σ_{nett}	n	t_{fail}
1	5.5	1.97	15.0	7.0	/
2	0.25	3.89	30.0	7.0	/
5	40.0	1.2	10.38	3.5	67.0
6	29.0	1.47	13.24	3.5	30.6
7	40.0	1.19	10.33	3.5	81.6
8	32.0	1.12	10.39	3.5	72.0
9	40.0	1.19	10.39	3.5	56.1
11	700	0.599	5.27	3.5	/
12	3.0	2.49	21.88	7.0	4.33
13	1.85	2.19	20.19	7.0	4.35
15	2.75		20.45	7.0	5.12
16	525	0.566	5.38	3.5	1049.4
17	275	1.30	5.15	3.5	629.8
22	775	0.597	5.18	3.5	2421.4
23	337	0.61	5.29	3.5	1007.0
24	0.6	5.31	20.46	7.0	5.7
25	10	1.87	19.75	7.0	20.3
27	4.5		19.66	7.0	7.0
28	625	0.624	5.7	3.5	1248.0
29	500	0.629	5.78	3.5	729.4

TABLE.4.3

For unit thickness and width

$$K = \sigma_{gross} . Y$$

$$K^n = \sigma^n_{gross} . Y^n \qquad 4.7$$

Multiple regression analysis was performed on the following basis:

$$\log . t_i = \log . A + B_1 \log . Y^n + B_2 \log . \sigma^n_{nett} \qquad 4.8$$

i.e. $$t_i = A . Y^{B_1 n} . \sigma^{B_2 n}_{nett} \qquad 4.9$$

and $$\log . t_i = \log . A + B_1 \log . Y^n + B_2 \log . \sigma^n_{gross} \qquad 4.10$$

i.e. $$t_i = A . Y^{B_1 n} . \sigma^{B_2 n}_{gross} \qquad 4.11$$

Where A, B_1 and B_2 are constants

σ_{gross} is in MNm^{-2}

The regressions were made using σ_{gross} in place of σ_{nett} because K is based on σ_{gross} and not σ_{nett}.

If B_1 approximately equalled zero in these regression analyses then initiation would be purely stress controlled. If B_1 is found to approximately equal B_2 then this constitutes evidence that initiation is strongly dependant upon the value of K operating. Again the two levels of n presented a problem as the constant 'A' would probably only be constant for a single value of n. The exponent n could not be introduced as a separate variable as it would not be independant of the stress term. This meant that regression analysis to show the individual effects of stress and geometry on initiation time had to be confined to a single n value. However to demonstrate better the effect of geometry, regression across both n values was performed but in this case the stress term dependance will also be compensating for the change that the n values should have made on the constant A. The results are as follows:

For all cases of n=3.5 (i.e. low and intermediate stress tests)

$$t_i = 2.3 \times 10^5 Y^{-0.22n} . \sigma_{nett}^{-1.06n} \qquad r = 0.97 \qquad 4.12$$

or

$$t_i = 7.8 \times 10^4 Y^{-0.27n} . \sigma_{gross}^{-1.15n} \qquad r = 0.99 \qquad 4.13$$

For all cases of n=7 (i.e. high stress tests only)

These analyses include two large notch root radius specimens for which Y = 0.07 was used, corresponding to what was considered a suitably low value of K.

$$t_i = 2.1 \times 10^6 Y^{-0.02n} . \sigma_{nett}^{-0.66n} \qquad r = 0.93 \qquad 4.14$$

$$t_i = 1.2 \times 10^4 Y^{-0.06n} . \sigma_{gross}^{-0.513n} \qquad r = 0.75 \qquad 4.15$$

Analysis across the two n values

Only the low and high stress regime results have been considered so that the stress term and the creep exponent will correlate almost exactly, and excluding the large notch root radius specimens.

$$t_i = 3500 Y^{-0.165n} . \sigma_{nett}^{-0.34n} \qquad r = 0.71 \qquad 4.16$$

The significance of the factors in the regression analyses can be estimated from T test values computed from B/(est. standard deviation of B). The T values obtained for the geometric and stress terms are as follows:

	T for Y term	T for stress term
from equation 4.12	1.69	12.4
4.13	3.34	20.8
4.14	0.68	2.5
4.15	2.19	3.5
4.16	1.32	11.2

For equation 4.14 and 4.15 the significance of the stress term is less than for the other cases because the variation in stress for these cases is slight. Also at n=7 the errors in predicting the initiation time represent a greater percentage of the average time for this event with this group of specimens than for the specimen where n=3.5. Excluding equation 4.14 and 4.15 the load factor is highly significant in all cases. By comparison with standard T-tables on a one sided basis (that is, increasing Y can only decrease initiation time, the possibility that it might increase initiation time is not considered to exist) the geometric factor in the equations using σ_{nett} will just about find significance at the 10% level. That is, the variation observed in initiation time with change in Y could have occurred purely by chance 1 time in 10. For the regressions using σ_{gross} values in place of σ_{nett} values higher significance was observed for the geometric factor. For equation 4.13 for n=3.5 the variation in initiation time with change in the Y function could only have occurred by chance 1 time in 200 (i.e. 0.5% significance). For equation 4.15 for n=7 the significance was lower than for the corresponding n=3.5 case but significance of the Y term was still around 4 times better than for the correlations with σ_{nett}. That is for equation 4.15 the variation in initiation time with Y could have occurred purely by chance slightly more often than 1 time in 40 (i.e. around 2.5% significance).

In all cases the exponent for Y was considerably less than the exponent for the stress term. This means that initiation time is not described by K. The predominant factor affecting initiation time is the stress. Geometry described by the Y function has been seen to have some effect on initiation time, but to a lesser degree than would be expected if K was controlling the initiation event.

Specimen thickness was also observed to affect initiation time. This is of particular interest as this is not compensated for by K. Increasing specimen thickness was observed to increase initiation time. This effect can be seen from Table 4.4 which shows specimens grouped as corresponding DEN and CN specimens. It can also be seen from Table 4.4 that in all but one of these groups shown the centre notch specimen initiated faster than the DEN specimen and in three of the comparisons the starting K was lower for the CN case. This suggests that the Y function is not an adequate description of the effect of geometrical variation on initiation time.

4.2.2.2 Crack Length Versus Time Data

It was not feasible to take sufficient photographs of each specimen to produce a reliable plot of crack growth rate versus crack length. For such a plot to be accurate a very precise plot of crack length versus time would be required first. A method of examining the crack growth data was required which would avoid the errors involved in deriving growth rates from the crack length time data. This was done by taking theoretical predictions of crack growth rate and converting them to crack length versus time functions. This enabled the experimental crack length time data to be directly compared with the theoretical predictions.

INITIATION TIMES AND CRACK GROWTH INTERVALS FOR SPECIMENS IN GROUPS

SPECIMEN NUMBER	t_i	$t_{fail} - t_i$	STRESS LEVEL	REMARKS
17	275	355	L	SEN
24	0.6	5.1	H	SEN
27	4.5	2.5	H	SEN - Large notch root radii
22	775	1646	L	DEN - 6.4mm thick
28	625	623	L	CN - 6.4mm thick
11	700	/	L	DEN - 3.2mm thick
16	525	524	I	CN - 3.2mm thick
23	337	670	L	DEN - 1.6mm thick
29	500	229	L	CN - 1.6mm thick
12	3.0	1.3	H	DEN - 3.2mm thick
13	1.85	2.5	H	CN - 3.2mm thick
8	·32	40	I	CN - 3.2mm thick
9	40	16	I	DEN - 3.2mm thick
7	40	41	I	DEN - 3.2mm thick
PRE-STRAINED SPECIMENS NOT INCLUDING TIME FOR PRE-STRAINING				
19	200	210	L	DEN
18	1.75	2.58	H	DEN
26	2.7	2.8	H	CN - 6.4mm thick

TABLE.4.4

Correlations between crack growth rate and either K or σ_{nett} have been proposed, principally on an empirical basis as follows:

$$\frac{da}{dt} = AK^m \qquad 4.17$$

$$\frac{da}{dt} = B\sigma^m_{nett} \qquad 4.18$$

It has also been proposed that m may approximately equal n, the exponent in Norton's law. It seems reasonable that m and n should be related if crack growth is displacement controlled. From equations 4.17 and 4.18 it follows that for crack growth between a_1 and a_2:

$$t = \int_{a_2}^{a_1} \frac{1}{AK^m}.da \qquad 4.19$$

or

$$t = \int_{a_2}^{a_1} \frac{1}{B\sigma^m_{nett}}.da \qquad 4.20$$

Both K and σ_{nett} can be expressed as functions of the crack length a. Using the expression of K for an infinite plate and using m=n:

$$t = \int_{a_2}^{a_1} \frac{1}{A'a^{(n/2)}}.da \qquad 4.21$$

or

$$t = \int_{a_2}^{a_1} \frac{(1 - a)^n}{B'}.da \qquad 4.22$$

Where A' and B' are functions of the applied load.

These integrals were solved to give theoretical relationships between crack length and time for each of the crack growth laws. The analyses were confined to between 0.35 and 0.7 a/w. The limits were set to eliminate effects from crack initiation or ligament collapse. However it became apparent that tertiary effects were operative below 0.7a/w.

These limits also kept the analysis within the normal range of the K-calibration of the specimen geometries considered.

For both of the σ^{n}_{nett} and K^{n} growth relationships considered the time interval for growth between 0.35 to 0.7 a/w was set to 100 units and graphs of crack length versus time were constructed on the basis of equations 4.21 and 4.22. The time scale for each experimental crack length time plot was normalised so that the time for crack growth between 0.35 and 0.7 a/w represented 100 units and could hence be directly compared with the theoretically derived curves for σ_{nett} and K control.

As for the study of initiation time the specimens were divided into two groups depending upon n value (section 4.2.2.1). Specimens from the intermediate stress range were not considered as a change in the exponent level could occur within the crack growth range considered. The results are shown in the figure 4.9a for the cases of n=3.5 and figure 4.9b for cases of n=7.

The effect of finite geometry on the K-control curve was estimated using K-calibration tables. Fig. 4.10 shows the percentage increase in K for each geometry from the value at 0.35 a/w as the crack length increases. The corresponding percentage increases are also shown for $K_{infinite}$ and σ_{nett}. If K control is applying the crack growth will be described by equation 4.17. The exponent m will be a material constant for that temperature, at least over the stress range for which the creep exponent n is constant. The essential factor of these predictive approaches is that the exponent m should not be geometry dependant. Either K or σ_{nett} should provide a totally adequate description of geometry if either of these approaches are valid. This means that regardless of the value of m,

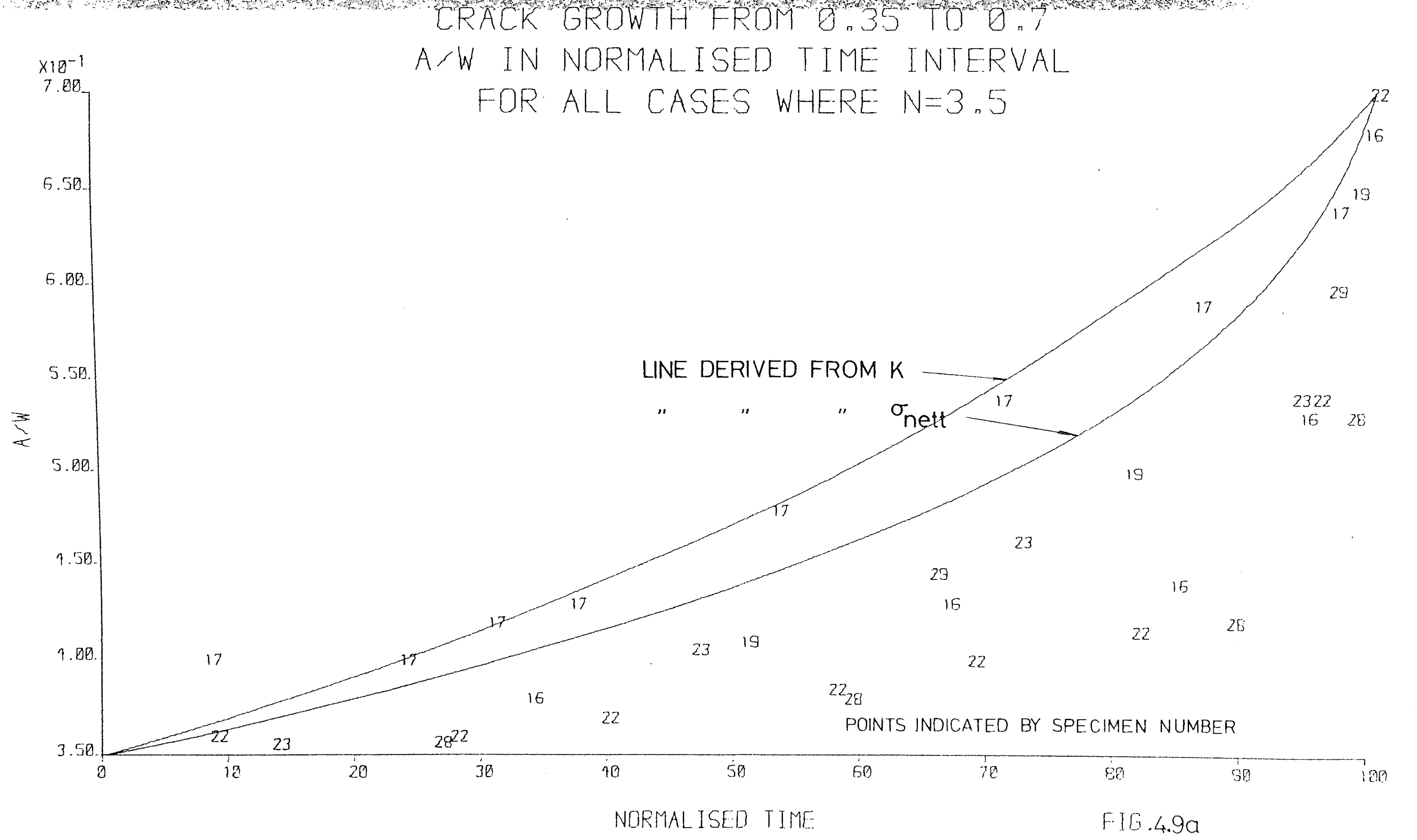
CRACK GROWTH FROM 0.35 TO 0.7
A/W IN NORMALISED TIME INTERVAL
FOR ALL CASES WHERE N=3.5
X10^-1
7.00
6.50
6.00
5.50
5.00
4.50
4.00
3.50
A/W
LINE DERIVED FROM K
" " " σnett
POINTS INDICATED BY SPECIMEN NUMBER
0
10
20
30
40
50
60
70
80
90
100
NORMALISED TIME

FIG.4.9a

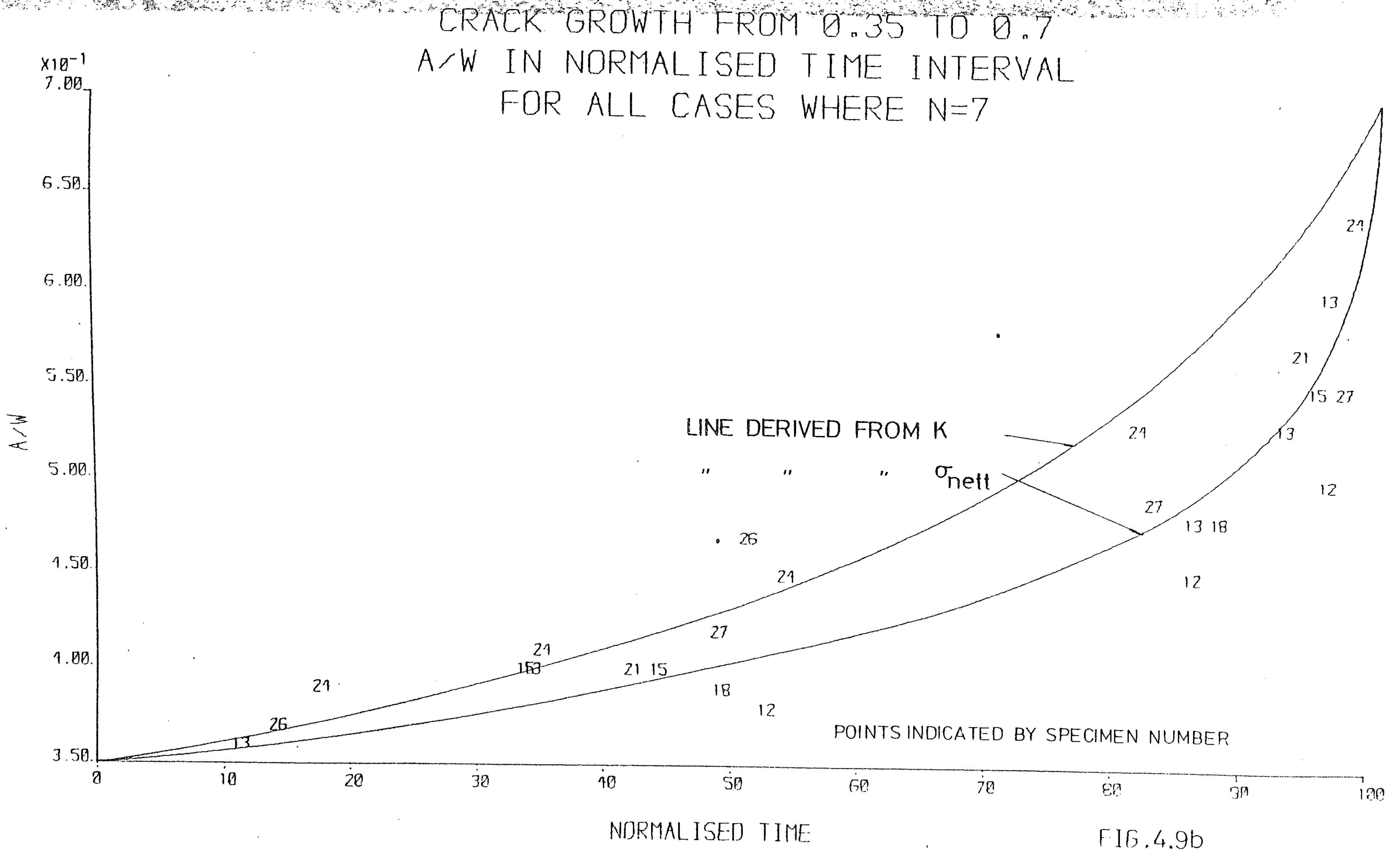
CRACK GROWTH FROM 0.35 TO 0.7
A/W IN NORMALISED TIME INTERVAL
FOR ALL CASES WHERE N=7
X10^-1
7.00
6.50
6.00
5.50
5.00
4.50
4.00
3.50
A/W
0
10
20
30
40
50
60
70
80
90
100
NORMALISED TIME
LINE DERIVED FROM K
" " " σnett
POINTS INDICATED BY SPECIMEN NUMBER

FIG.4.9b

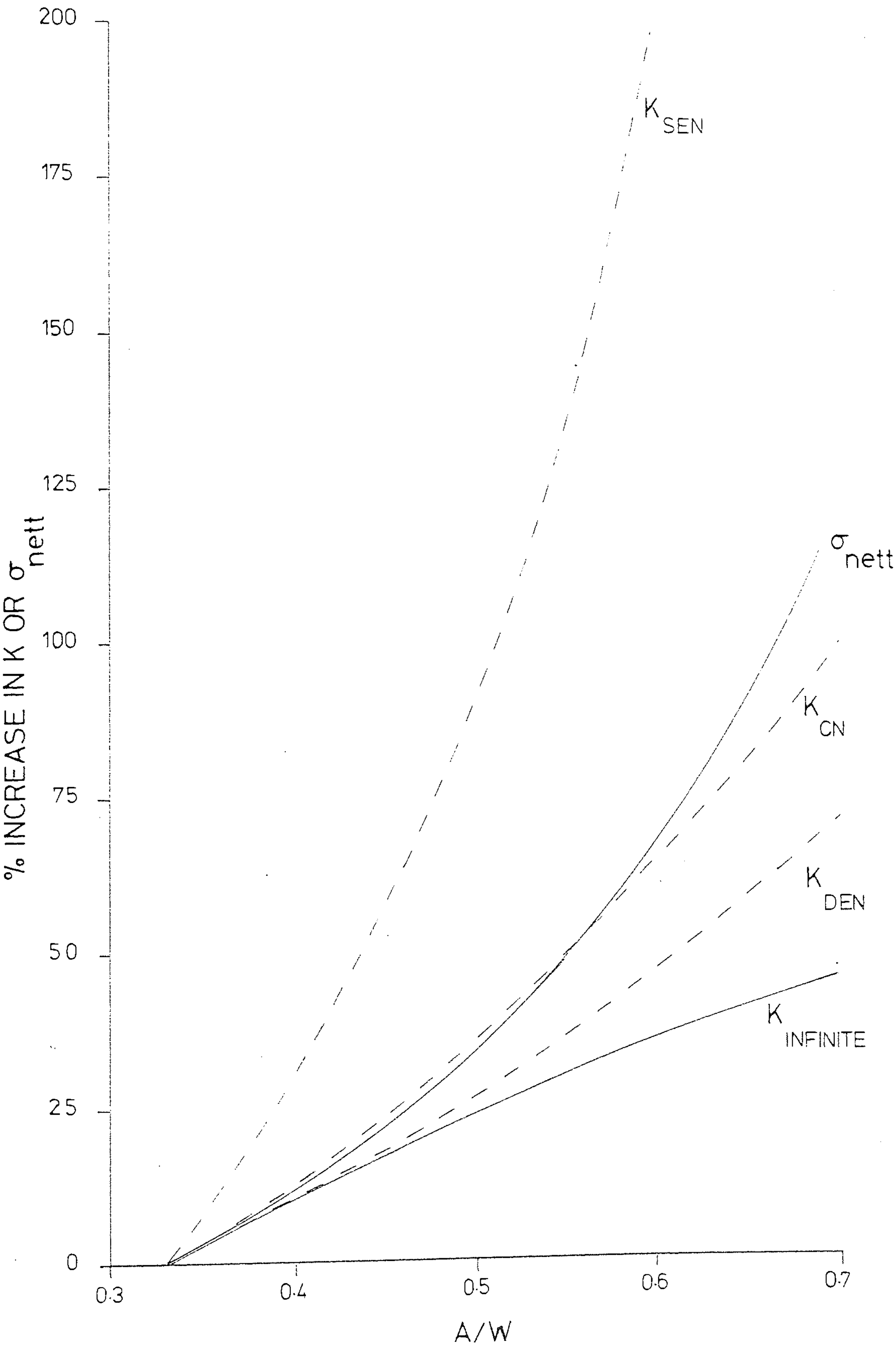

PERCENTAGE INCREASE IN K AND NETT SECTION STRESS WITH CRACK LENGTH FROM VALUES FOR 0.33A/W

FIG.4.10

under K control the geometry which shows the greatest percentage change in K over an interval of crack growth should show the most change in crack growth rate. Conversely, the geometry showing the least change in crack growth rate would be expected to show the least change in K. Behaviour other than this would dispute that crack growth is controlled entirely by the value of K. The tendency for large changes in K to cause large changes in growth rate will increase as the exponent m increases.

The lines of percentage increase in K for the DEN and CN geometries fall between those of σ_{nett} and $K_{infinite}$ indicating that K control for these specimens would produce a change in crack growth rate with crack length between that predicted by σ_{nett} and $K_{infinite}$. The SEN geometry showed the greatest percentage change in K and under K control would hence be expected to show the greatest change in crack growth rate.

Under a straightforward σ_{nett} relationship all the specimens should show identical behaviour. However, a bending moment is present with the SEN geometry due to its asymmetric design but a proportion of this moment is relaxed by rotation of the specimen around the loading pins. The magnitude of the bending moment increases with increasing crack length. From plane beam theory, ignoring the effect of stress concentrations arising from the notch, the fibre stress at the crack tip will increase more for the SEN geometry than for the other two with crack growth. Hence, under σ_{nett} control the SEN geometry would be expected to show a similar or greater change in growth rate than the other two geometries over the same interval of crack growth.

It can be seen from the Fig. 4.9 that for n=3.5 only one specimen produced a crack length versus time curve resembling those derived from equation 4.21 and 4.22, and this was the SEN specimen TS17. As discussed above, true K control behaviour for this geometry would be expected to show the maximum change in growth rate not the least as shown here. This observation tends to discount the operation of a K or σ_{nett} control law under any single value of the exponent m and not just for m=n. This is because even with allowance for geometry dependance of K and the effect of the bending moment present with the SEN geometry, the data from all the specimens would not fall on a single line.

For n=7 agreement with the predictive theories is better, but again the SEN geometry (TS24 & 27), even with a very large notch root radius, produced the most uniform crack growth rate of the specimens that had not been pre-strained. This again disputes that the crack growth behaviour over this a/w interval could be described by either the K or σ_{nett} crack growth law using a single value of m.

The possibility that the exponent m should equal (2n - 2) rather than n has been proposed[175 183] but there seems little point in investigating the use of such values of m as it has already been shown that neither the K nor the σ_{nett} growth law will describe crack growth for all the geometries for a single value of m.

It was decided to consider the effect of accumulating damage on the theoretical relationships. To modify the K law to accommodate degradation of the ligament would have required detailed knowledge of the manner in which this damage is distributed across the ligament.

Details of the strain distribution across the various specimen geometries was available from this work. However, the results of the Quantitative metallographic examination of the smooth bar test specimens (section 4.1.3) had indicated that the relationship between damage and strain is dependant upon the level of the stress. The basis of the σ_{nett} approach is such that it may be considered that the damage is uniformly distributed across the ligament. This means that the damage can be incorporated as an additional increment of crack length, that is, crack growth between $0.35 + D_1$ to $0.7 + D_2$ a/w is normalised into 100 time units with the initial damage value increasing to D_2 by a function of a/w. The function relating D_1 and D_2 used was simply a linear one. The main disadvantage of this method was that the percentage loss of ligament through damage incorporated in the growth law accumulates at a very high rate with increasing a/w unless D_1 and D_2 are set close together.

The application of a range of damage allowances are shown in Fig. 4.11a and 4.11b. Minor corrections to the theoretical σ_{nett} curve improved the general agreement between the theoretical and experimental results for the CN and DEN specimens with n=7. However when applied to the case for n=3.5 a massive final damage correction proved necessary in order to bring about general agreement with the experimental results of the DEN and CN specimens.

The observations with regards ligament collapse made in section 4.2.1 suggested that this phenomenon may have been influencing crack growth rate at high a/w values. Examination of the experimental results and theoretical predicted crack length time distributions

CRACK LENGTH.V.NORMALISED TIME
INCORPORATING A DAMAGE
CORRECTION (N=3.5)

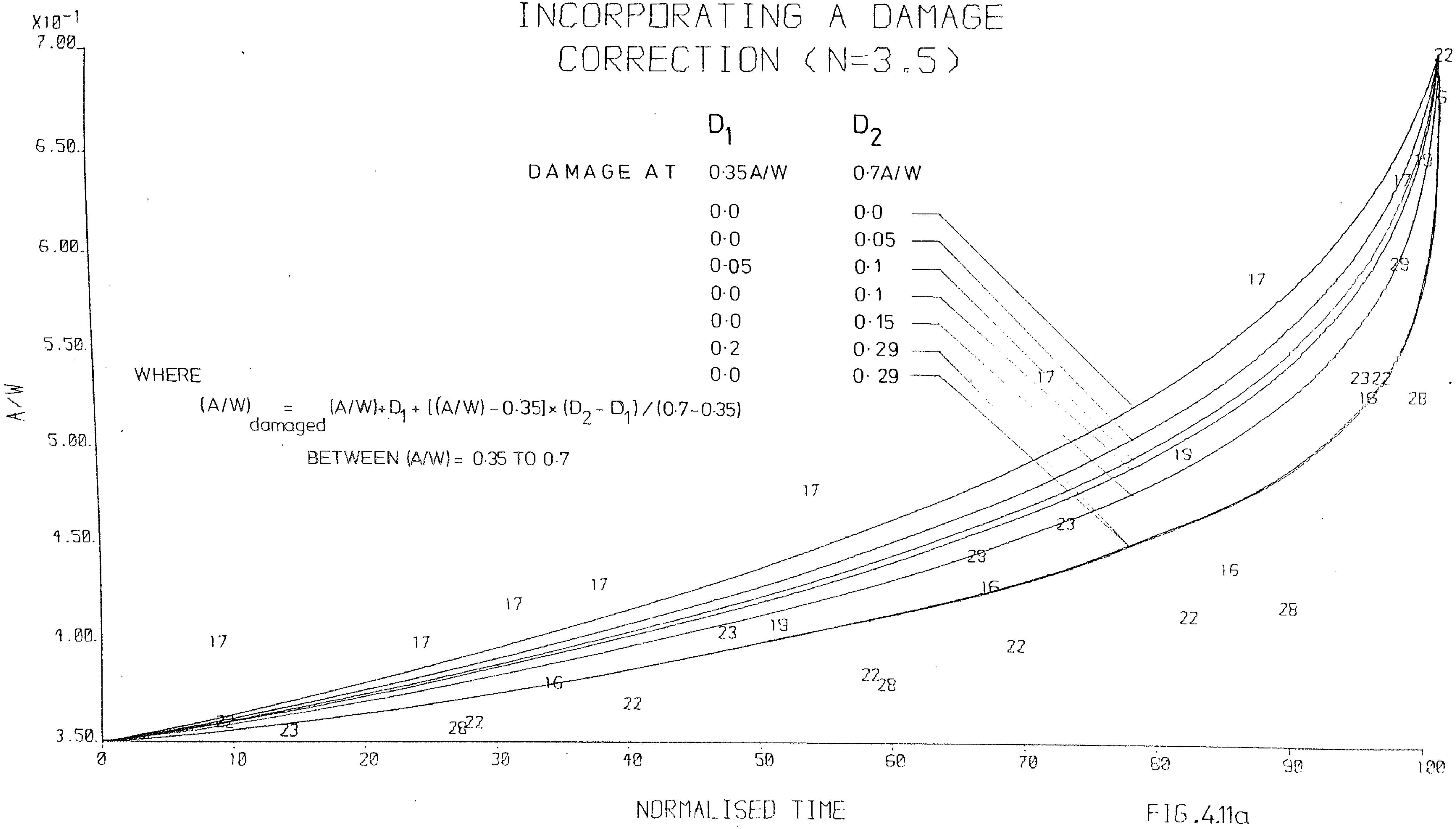

FIG.4.11a

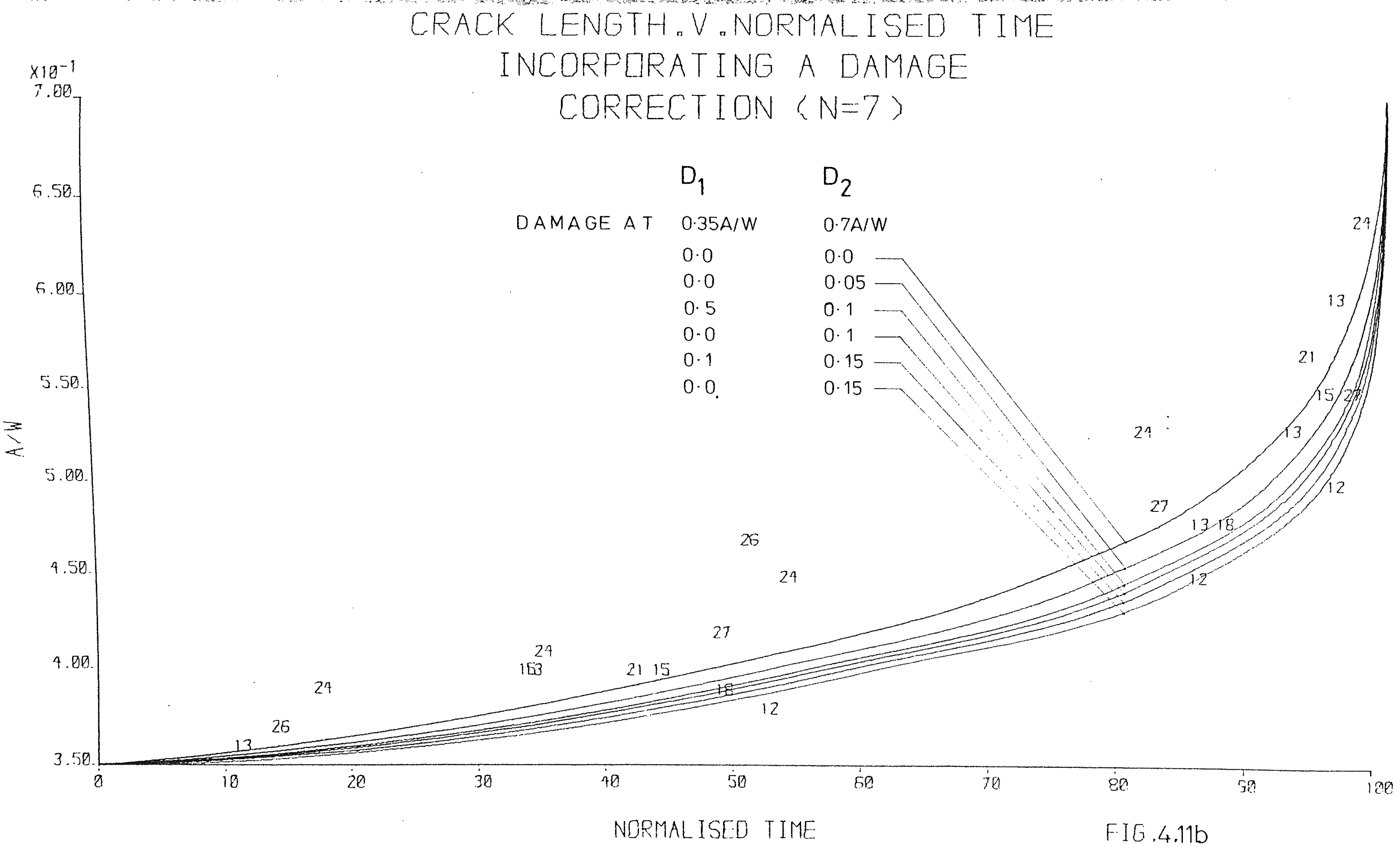

CRACK LENGTH.V.NORMALISED TIME
INCORPORATING A DAMAGE
CORRECTION (N=7)
X10^-1
7.00
6.50
6.00
5.50
5.00
4.50
4.00
3.50
A/W
D1
D2
DAMAGE AT
0·35A/W
0·7A/W
0·0
0·0
0·5
0·0
0·1
0·0
0·0
0·05
0·1
0·1
0·15
0·15
0
10
20
30
40
50
60
70
80
90
100
NORMALISED TIME

FIG.4.11b

showed that even by reducing the growth interval to between 0.35 and 0.55 a/w would not lead to crack growth being described by either K or σ_{nett} control, based on a single value of the exponent for all the geometries for either the case of n=3.5 or n=7. The basic differences in the trends of crack growth behaviour observed over the interval of 0.35 to 0.7 a/w would still be observed over the shorter interval of 0.35 to 0.5 a/w.

Some observations with regards crack growth behaviour were made as follows. The pre-strained specimens, in particular TS19 and 26 showed less change in growth rate than was normal for specimens of their respective geometries. Thinner specimens were observed to show less change in growth rate than their thicker counterparts, compare TS 23 and 29 (both 1.66mm thick) with TS22 and 28 (both 6.4mm thick) Fig. 4.9.

4.2.3 Grid Analysis

Grid displacements in both the X-direction and Y-direction have been analysed. The displacements in the Y-direction, d_{yy}, were analysed over a standard interval of the first 6 lines between 1 and 4mm either side of the XX centre line. Measurements of the distance between lines of corresponding interval either side of the XX centre line were made from photographs of the specimens taken during testing. See Fig. 4.12a. This meant that the calculated displacement would be an average for the corresponding points above and below the crack plane. This was considered desirable in order to reduce the effect of inaccuracy in measurement and to accommodate any minor deviation of the crack tip from the XX centre line. The displacement d_{yy} for each point was calculated by dividing the measurement of the distance

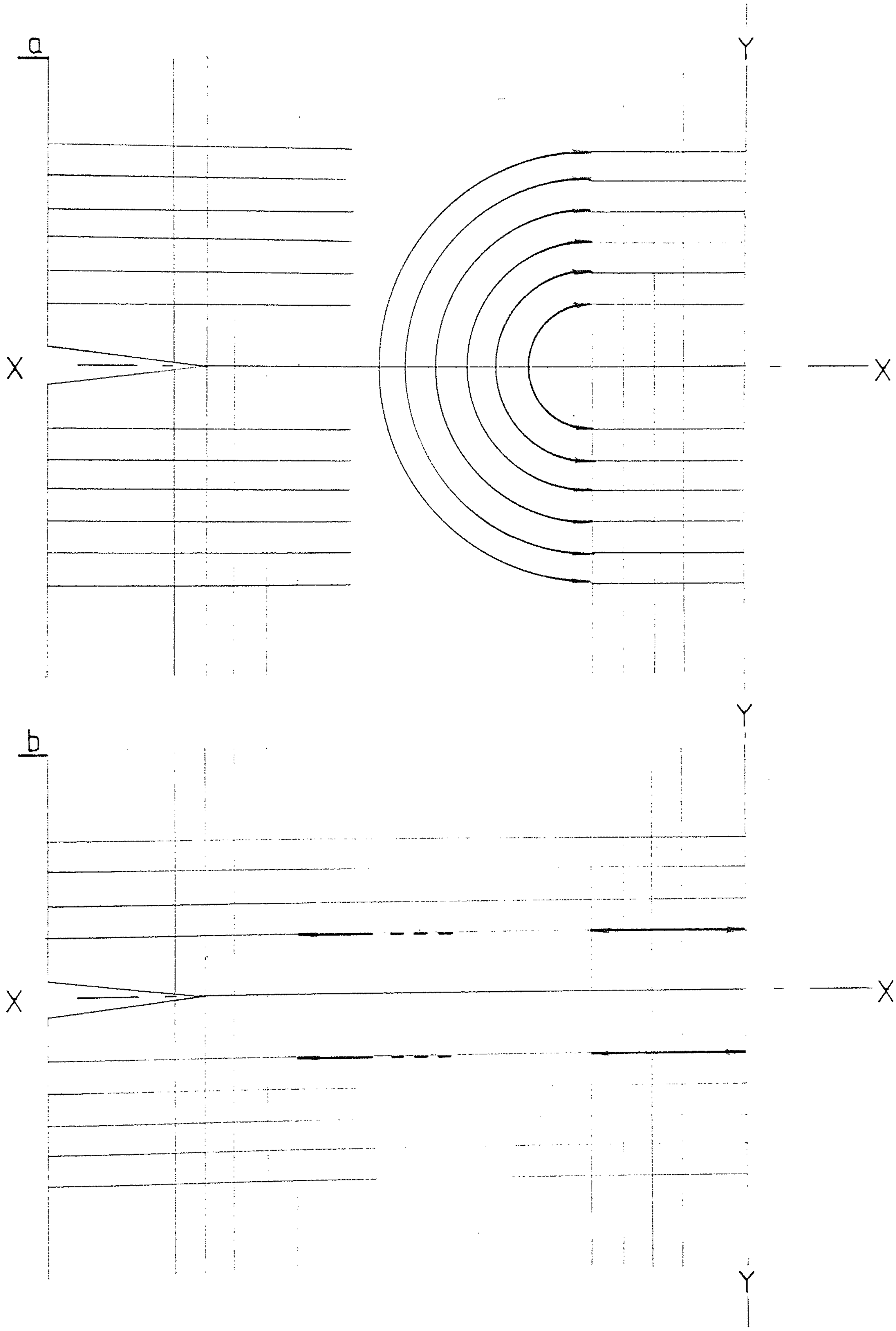

MEASUREMENT OF GRID LINES FOR THE ASSESMENT OF DISPLACEMENT

FIG.4.12

between the two corresponding points by the magnification of the photograph, then subtracting the equivalent distance measured from the photographs of the unstrained specimen also divided by the relevant magnification. The result of this subtraction was then divided by two to compensate for the measurements having been made across two quandrants, i.e.:

$$d_{yy} = \left(\frac{\text{measurement}_{t=t_1}}{\text{mag}_{t=t_1}} - \frac{\text{measurement}_{t=t_0}}{\text{mag}_{t=t_0}} \right) \Big/ 2 \qquad 4.23$$

Wherever possible the magnifications $\text{mag}_{t=t_0}$ and $\text{mag}_{t=t_1}$ would be the same.

The displacements in the X -direction d_{xx} were derived from measurements from the YY centre line of the specimen for the CN and DEN geometries. This line was used as it could be considered to be free of lateral displacement in these geometries. For the SEN case measurements were made from the first line in from the specimen edge remote from the notch tip. For all geometries, measurements for corresponding points above and below the XX centre line were averaged to improve accuracy. See Fig. 4.12b. Measurements were not made along the XX centre line as deformation near the crack tip usually obliterated the grid markings. Where strains are quoted they have been calculated from displacement between 1 and 1.5mm from the XX centre line. As for the case of the displacements d_{yy} the values of d_{xx} were calculated by dividing by the magnification and then subtracting the relevant distance of the points in question from the reference line before deformation.

$$d_{xx} = \frac{\text{measurement1}_{t=t_1} + \text{measurement2}_{t=t_1}}{2\text{mag}_{t=t_1}} - \frac{\text{measurement}_{t=t_0}}{\text{mag}_{t=t_0}} \qquad 4.24$$

Engineering extensional strain e_{ii} is equivalent to the gradient of displacement d_{ii} with distance in the i-direction. The displacements d_{xx} and d_{yy} were used to calculate values of ε_{xx} and ε_{yy} on this basis.

It was found that d_{yy} increased in a linear manner with Y-distance from the XX centre line, for example see Fig. 4.13. The degree of linearity was particularly good within the confines of the 45° shear bands but the gradient of a straight line, fitted by a least squares method to displacement versus distance measurements, within the limits of 1 to 4mm either side of the XX centre line indicated earlier, was considered a good description of uniform strain at all points across the ligament. With the exception of the near tip region, the linear regression of displacement versus distance produced negligible intercept value. That is, the product of the regression gradient and distance form the XX centre line to a point, described approximately all the displacement that had occurred over this distance. This means that provided the degree of linearity is acceptable then it can be considered that a uniform strain exists along the line of measurement, across the XX centre line.

Near the crack tip or notch tip a definite displacement additional to the uniform strain was observed in the form of an intercept value in the regression analysis. When approaching the crack tip along the XX centre line the last point through which displacement analysis showed a negligible non-uniform contribution, that is less than 0.08mm was referred to as the D-point (deviant). The general trend of the displacement d_{yy} versus Y-distance is shown schematically for various positions across the ligament in Fig. 4.14a. The trends in

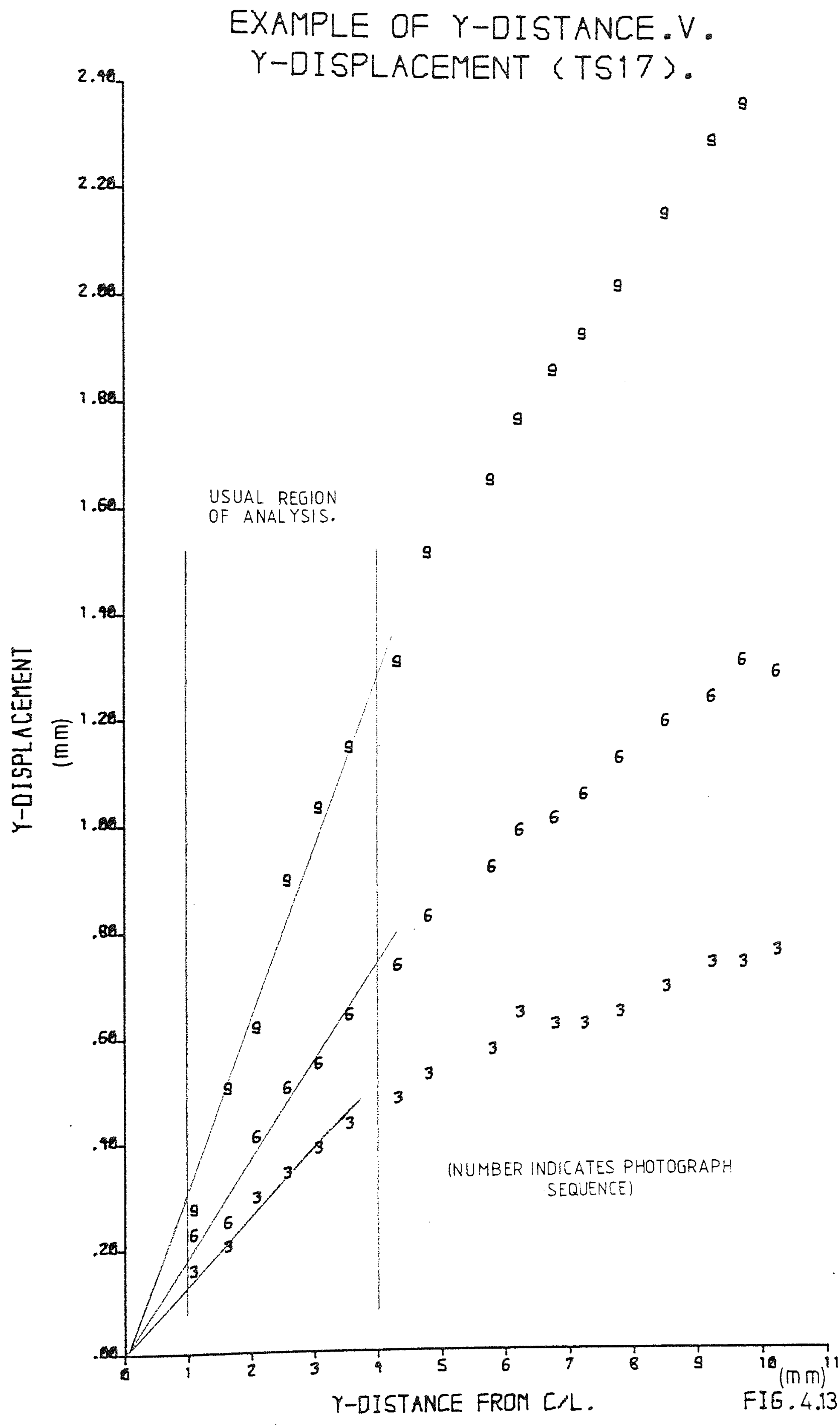
EXAMPLE OF Y-DISTANCE.V.
Y-DISPLACEMENT (TS17).
Y-DISPLACEMENT
(mm)
2.40
2.20
2.00
1.80
1.60
1.40
1.20
1.00
.80
.60
.40
.20
.00
0 1 2 3 4 5 6 7 8 9 10 11
(mm)
USUAL REGION
OF ANALYSIS.
(NUMBER INDICATES PHOTOGRAPH
SEQUENCE)
Y-DISTANCE FROM C/L.

FIG. 4.13

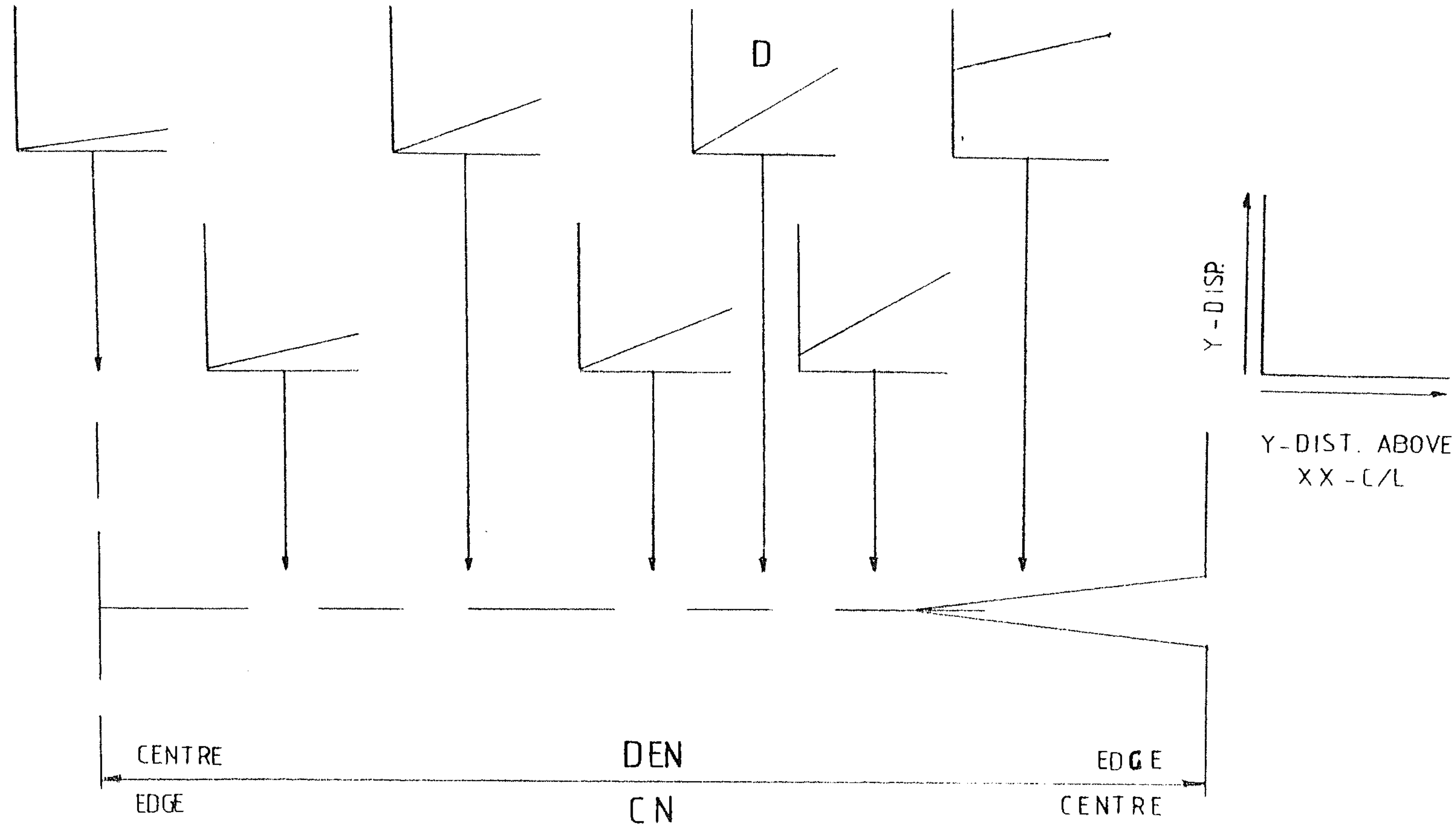

SCHEMATIC REPRESENTATION OF
DISPLACEMENT.V.(YY)DISTANCE
ACROSS LIGAMENT

FIG.4.14a

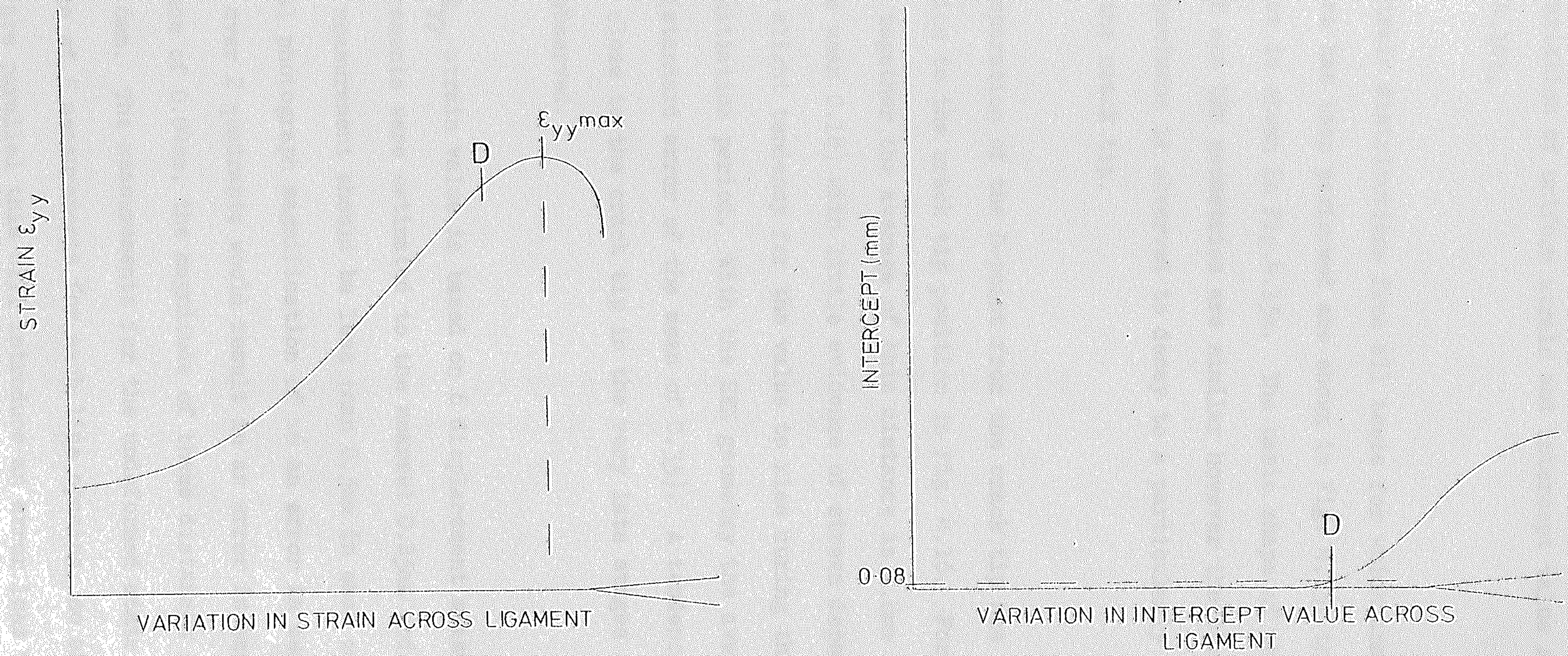

SCHEMATIC REPRESENTATION OF
VARIATION IN STRAIN AND
INTERCEPT VALUES

FIG. 4.14b

the variation of uniform strain and intercept value are shown in Fig. 4.14b.

The strain distributions from all tests for which analysis of the ε_{yy} strains has been performed are shown in Fig. 4.15, the key to these figures is shown in Fig.4.15a. The basic shape of these profiles for the CN and DEN geometries are similar however the strain ε_{yy} for the SEN specimens is observed to decay to a particularly low value remote from the crack tip.

The separation of the D-point from the crack tip has been shown in relation to the crack tip position in Fig. 4.16. For the CN and DEN cases together the average of this distance is 1.8mm (standard error of the mean 0.18) with little evidence of stress dependance. There was a slight tendency for the value to rise during the early stages of the initiation period. With the SEN geometry the average was lower, 0.98 (standard error of the mean of 0.35). A tendency for the D-point to be close to the crack tip in the very late stages of crack growth were observed.

Each ε_{yy} strain value is based on 6 displacement measurements. Measurements were estimated to the nearest 0.25mm and the error on each ruler measurement should be less than 0.5mm in each case. For a typical photograph magnification of x6 an error in measurement of 0.5mm over 2 quadrants would result in an error in assessing each distance of 0.04mm, the magnitude of these distances will be between 1 and 6mm. The measurements for the undeformed state are based on the average of 5 measurements for each line spacing, so assuming the scribe lines are parallel this will introduce an error less than 0.01mm in

KEY TO FIGS. 4.15

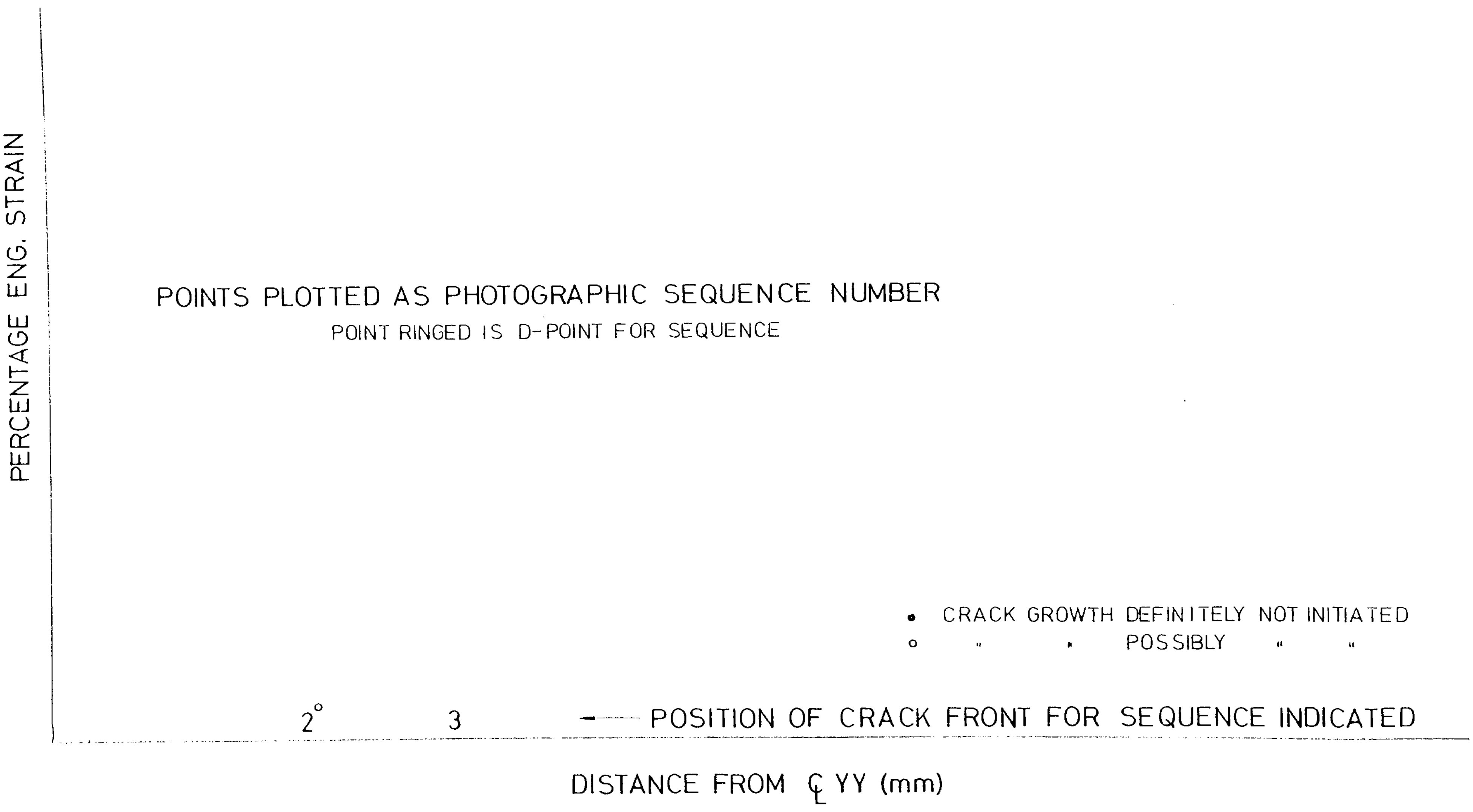

ENG. STRAIN(YY).V.X-DISTANCE
FROM CENTRE LINE YY FOR TS 1

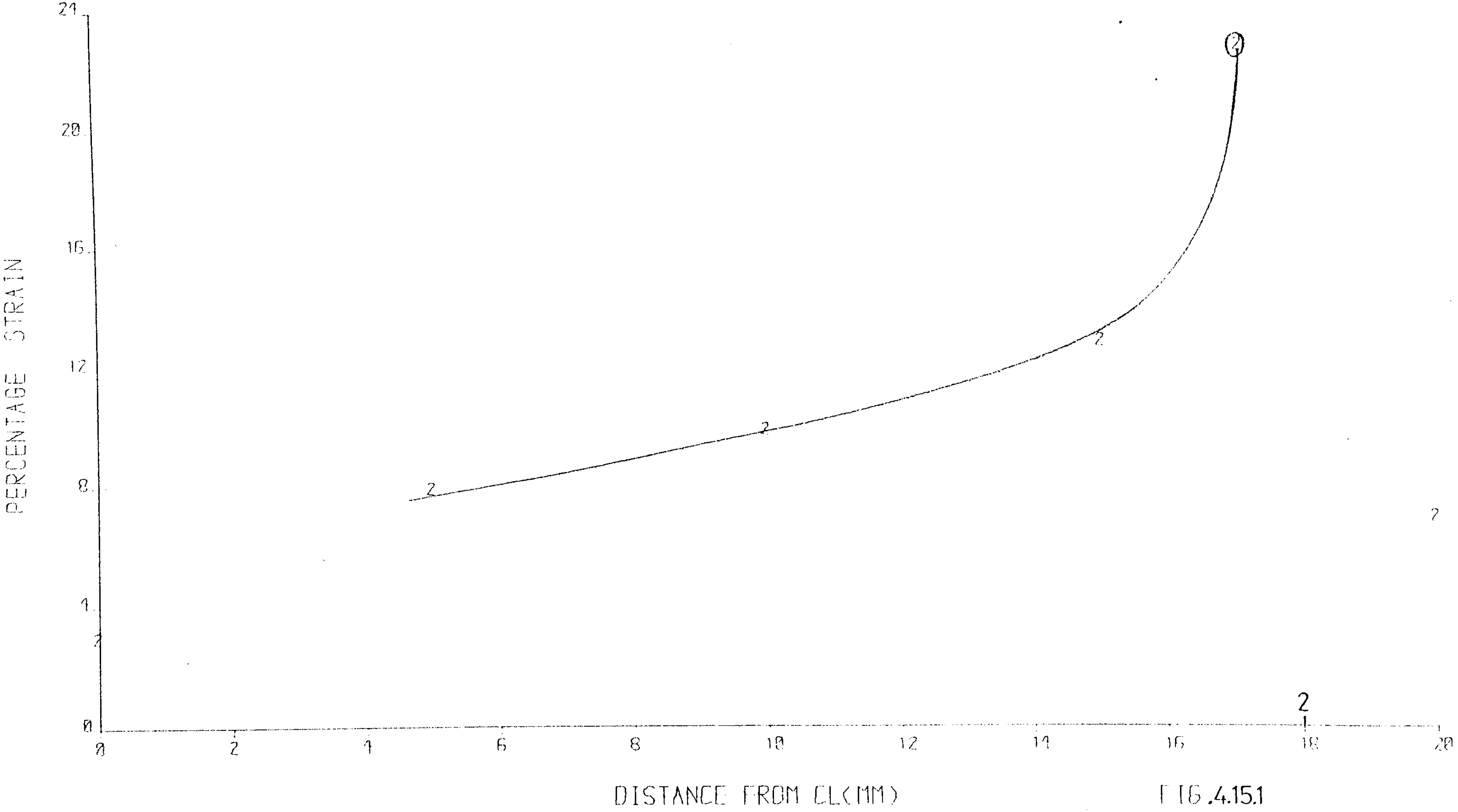

FIG.4.15.1

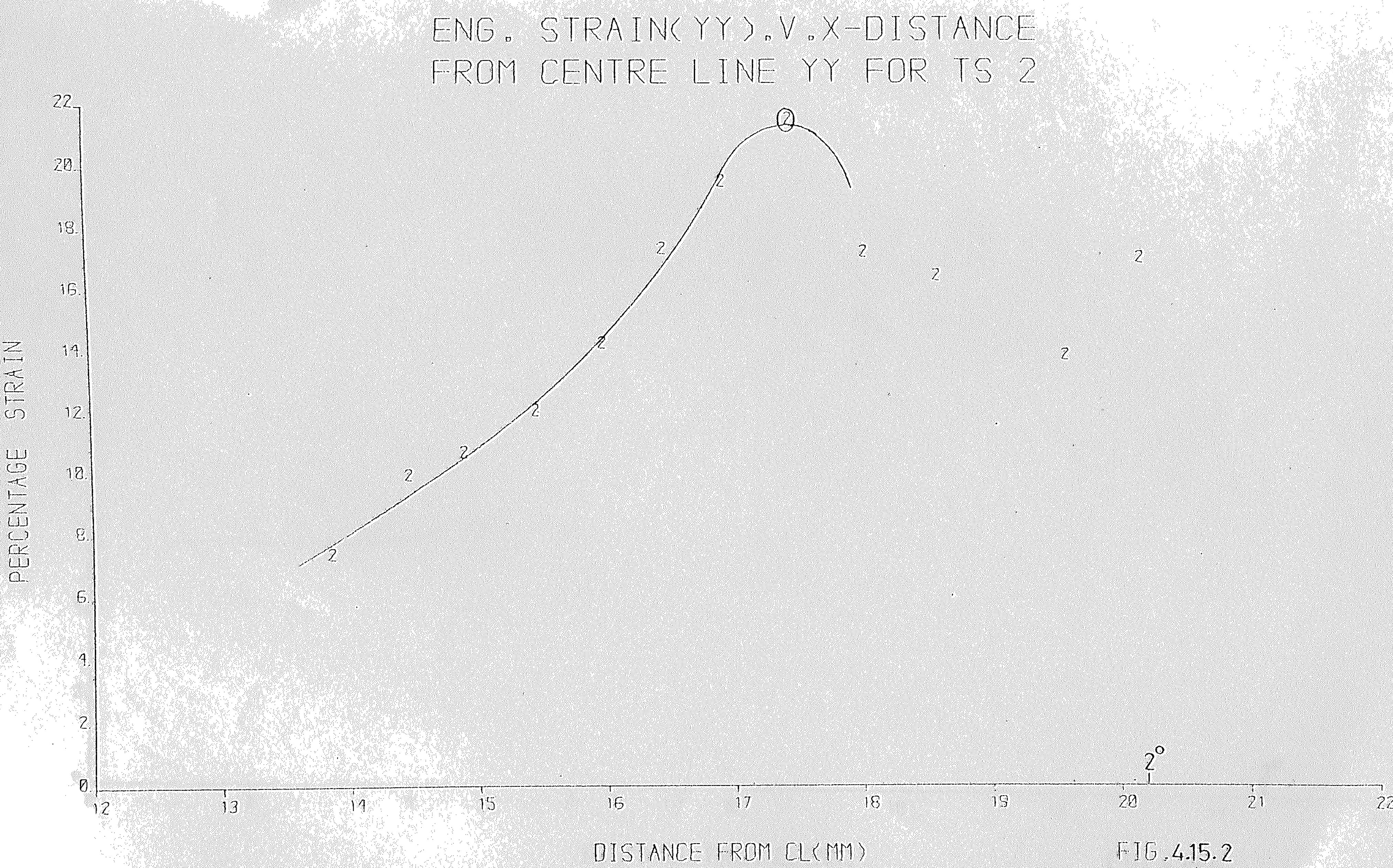

ENG. STRAIN(YY).V.X-DISTANCE
FROM CENTRE LINE YY FOR TS 2
PERCENTAGE STRAIN
DISTANCE FROM CL(MM)

FIG.4.15.2

ENG. STRAIN(YY).V.X-DISTANCE
FROM CENTRE LINE YY FOR TS 4

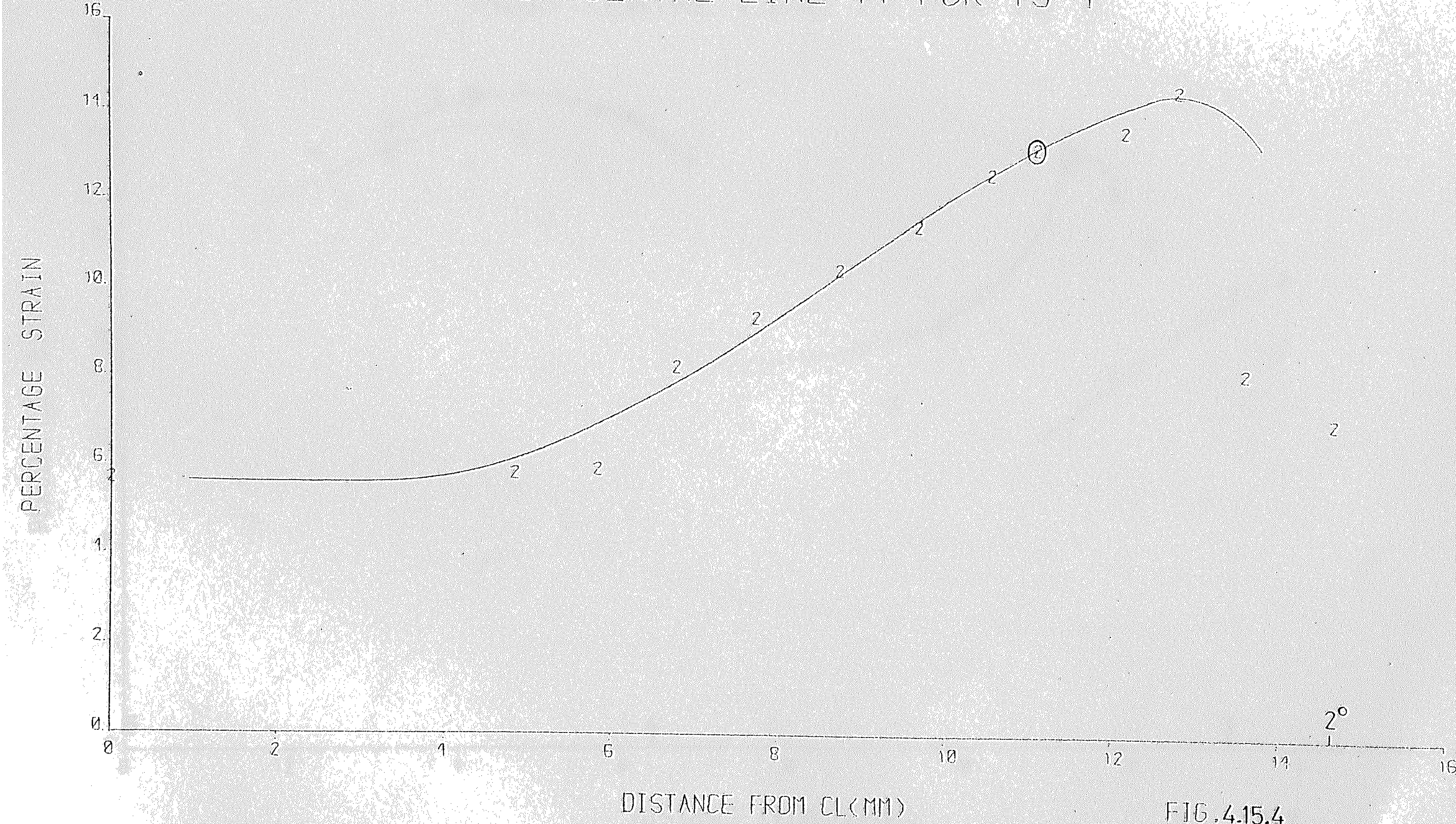

FIG.4.15.4

ENG. STRAIN(YY).V.X-DISTANCE
FROM CENTRE LINE YY FOR TS 7

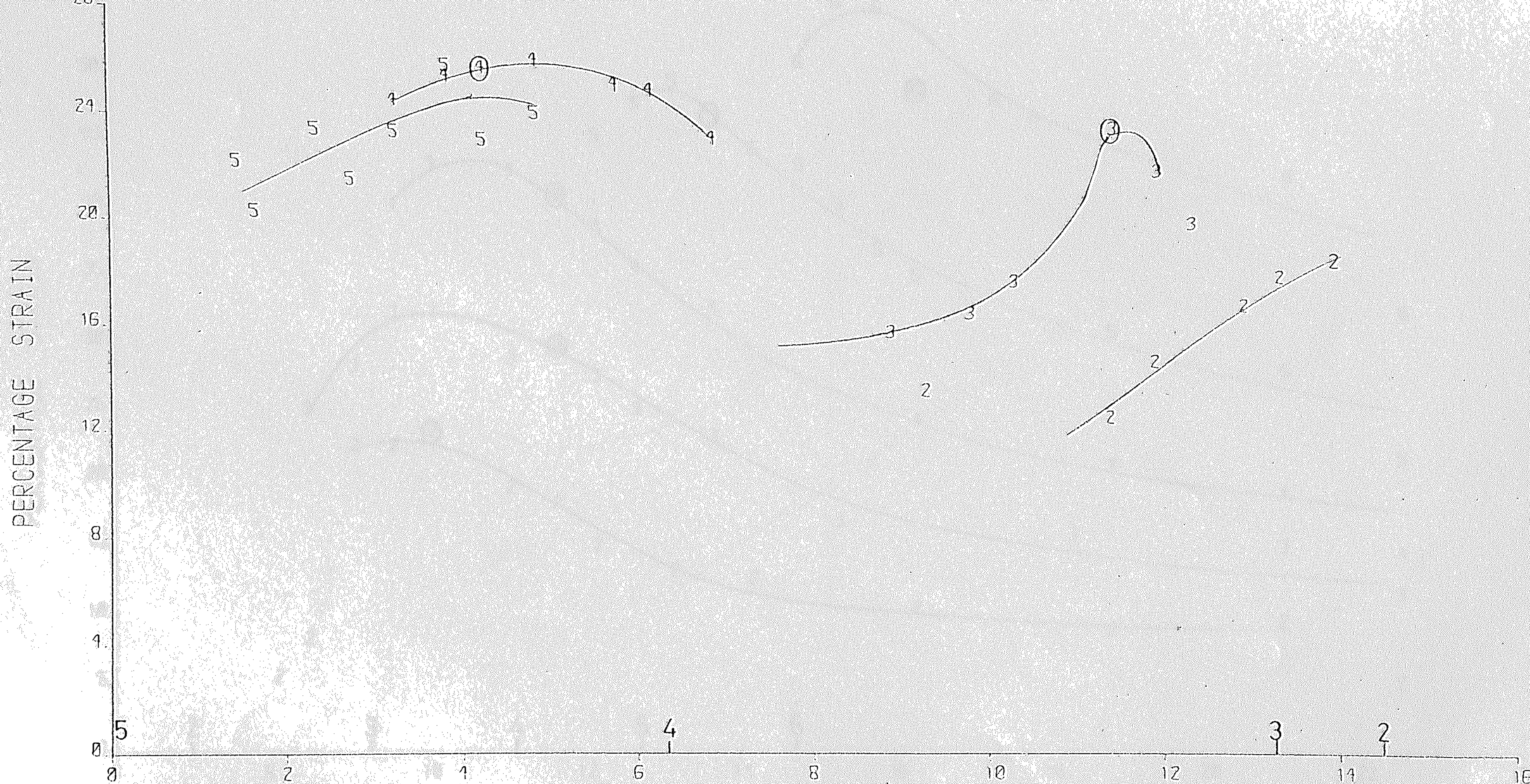

FIG. 4.15.7

ENG. STRAIN(YY).V.X-DISTANCE
FROM CENTRE LINE YY FOR TS 8

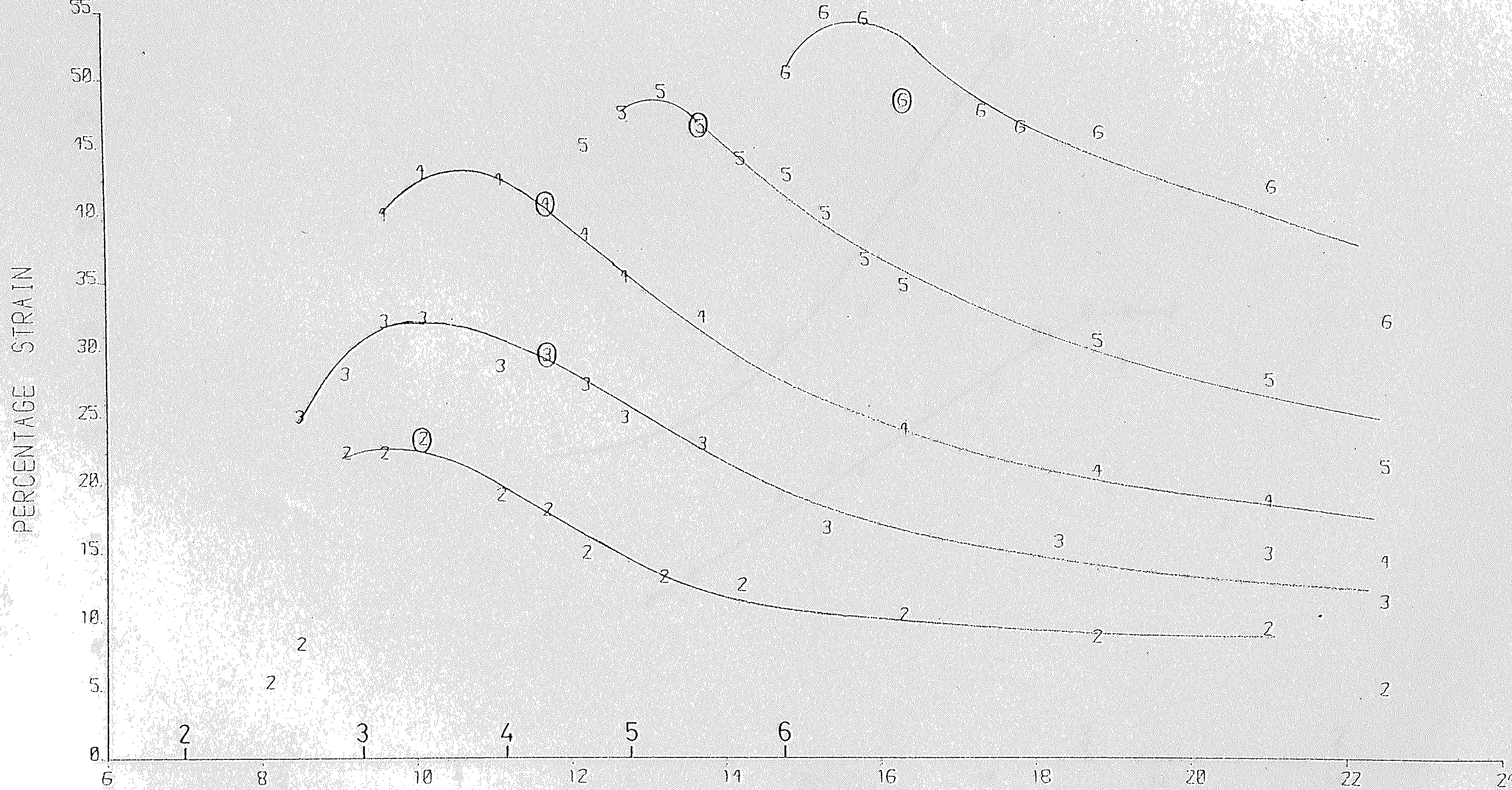

FIG.4.15.8

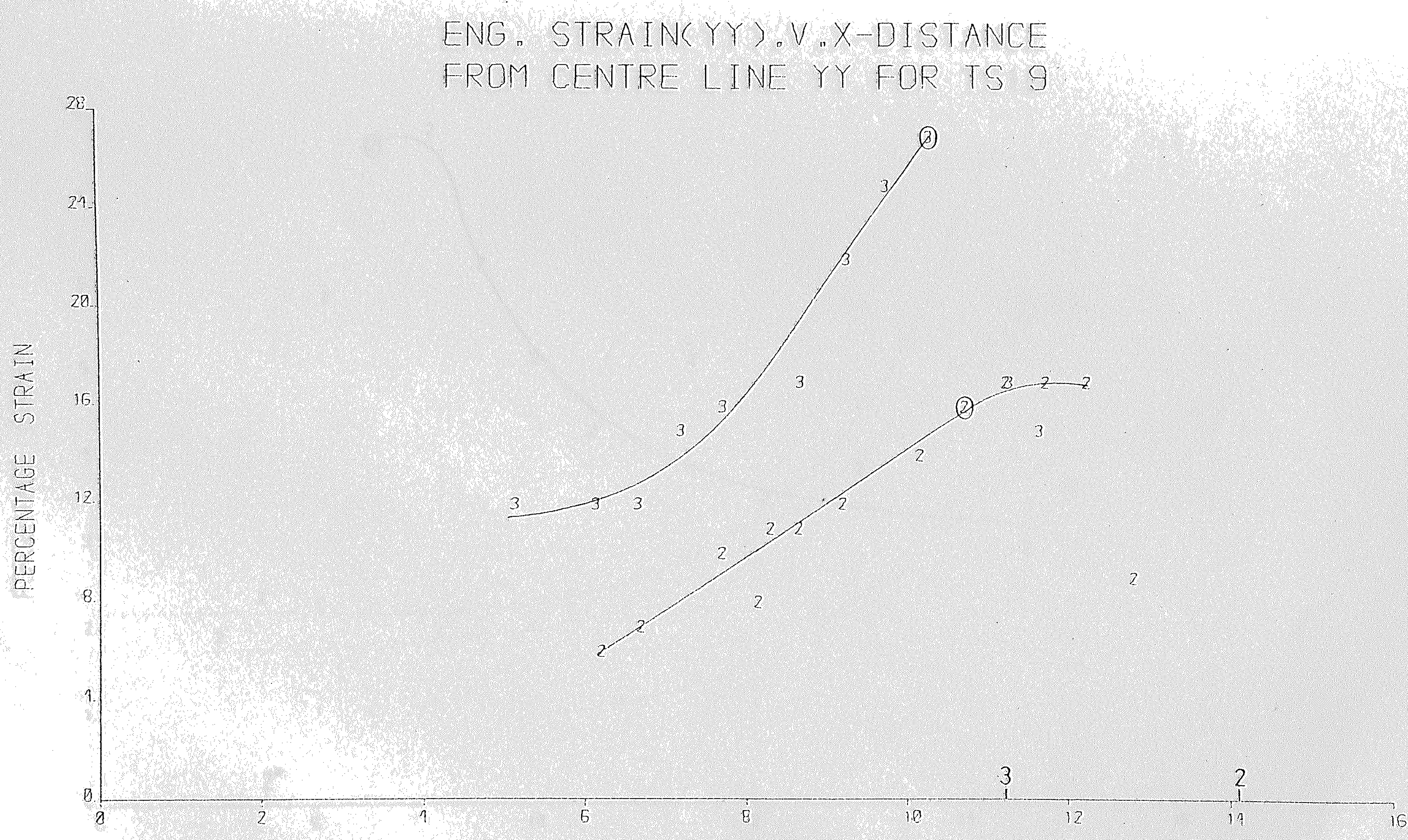
ENG. STRAIN(YY).V.X-DISTANCE
FROM CENTRE LINE YY FOR TS 9
PERCENTAGE STRAIN
DISTANCE FROM CL(MM)

FIG.4.15.9

ENG. STRAIN(YY).V.X-DISTANCE
FROM CENTRE LINE YY FOR TS10

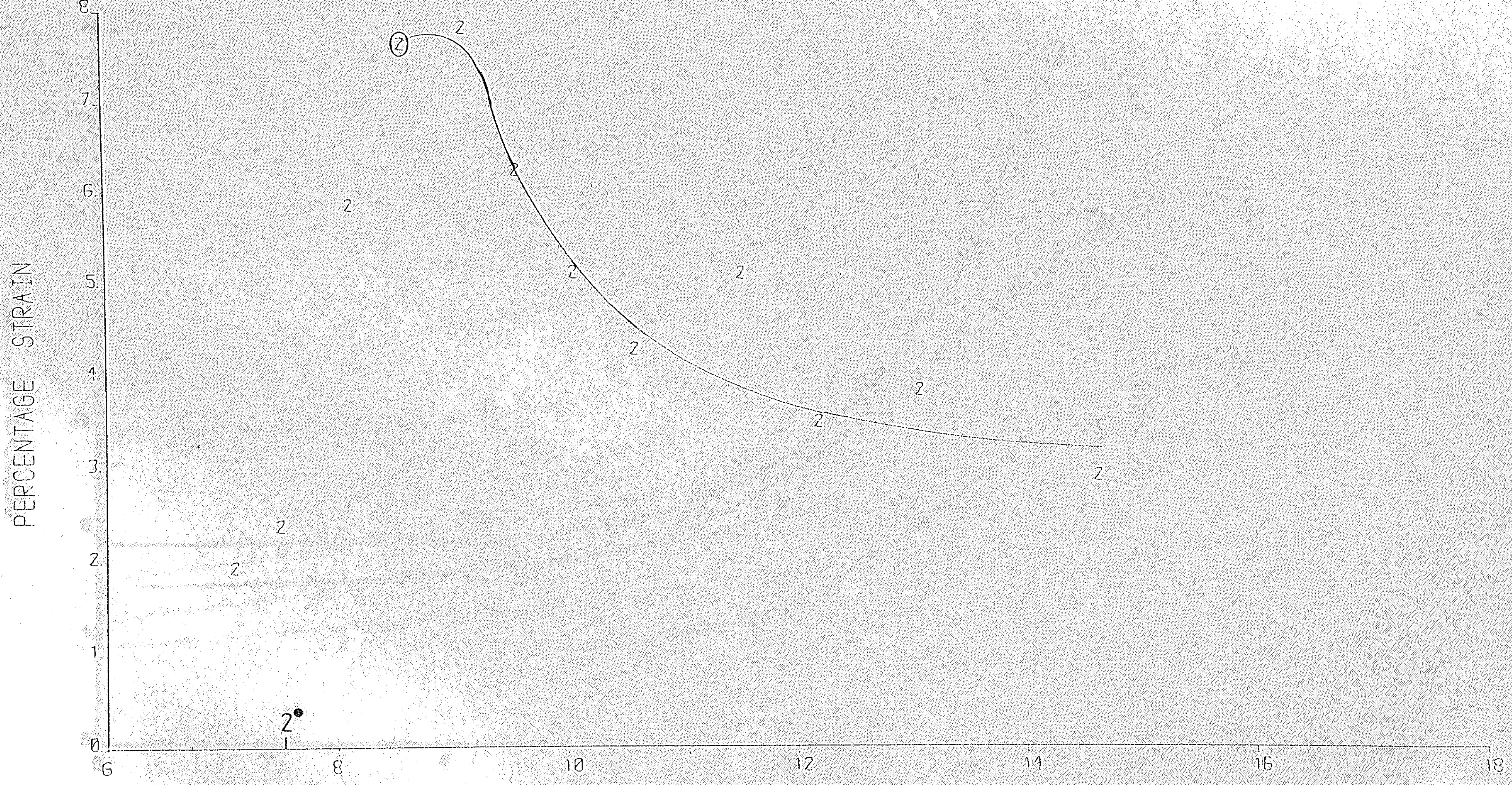

FIG. 4.15.10

ENG. STRAIN(YY).V.X-DISTANCE
FROM CENTRE LINE YY FOR TS11

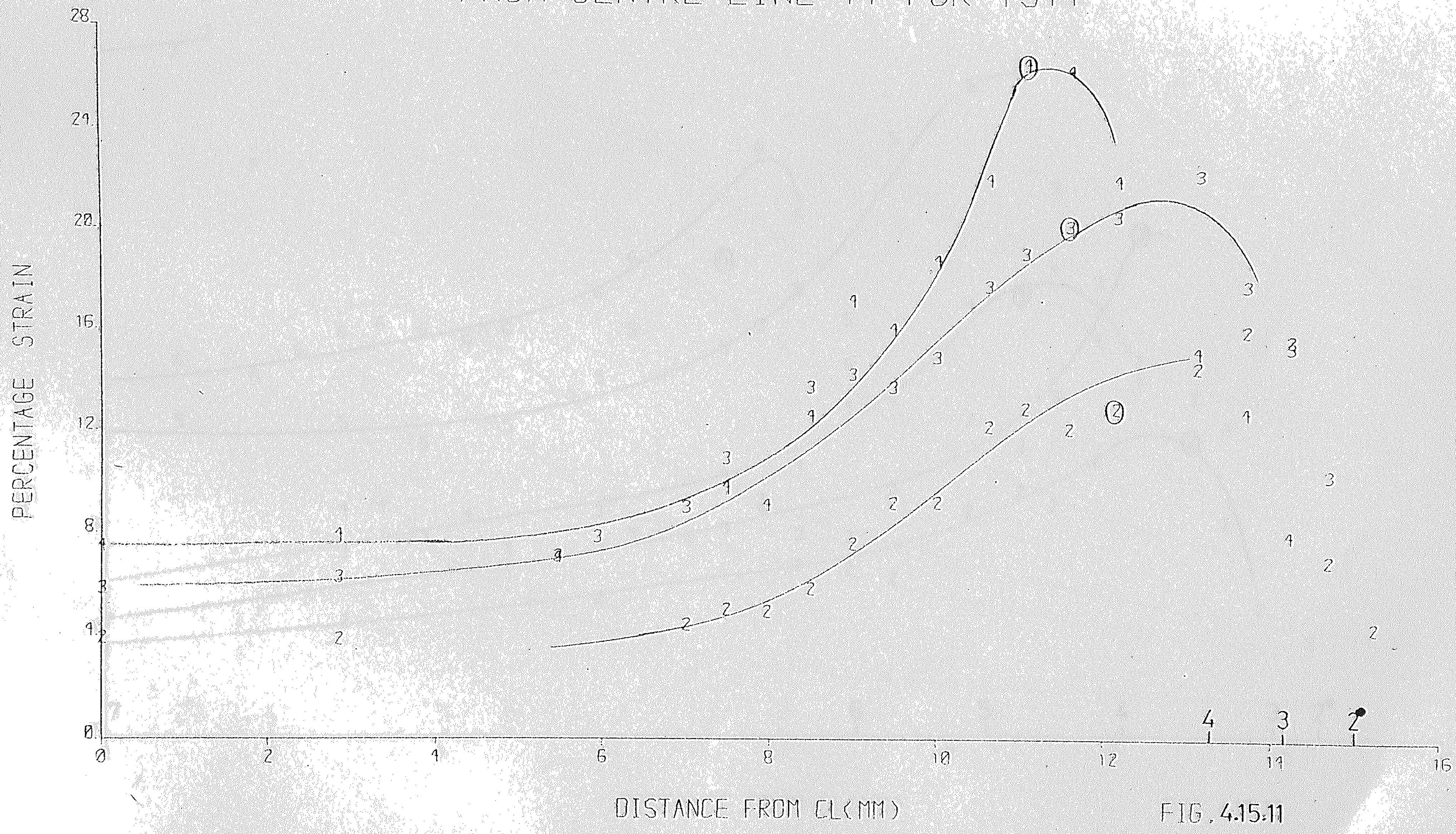

FIG. 4.15.11

ENG. STRAIN(YY).V.X-DISTANCE
FROM CENTRE LINE YY FOR TS12

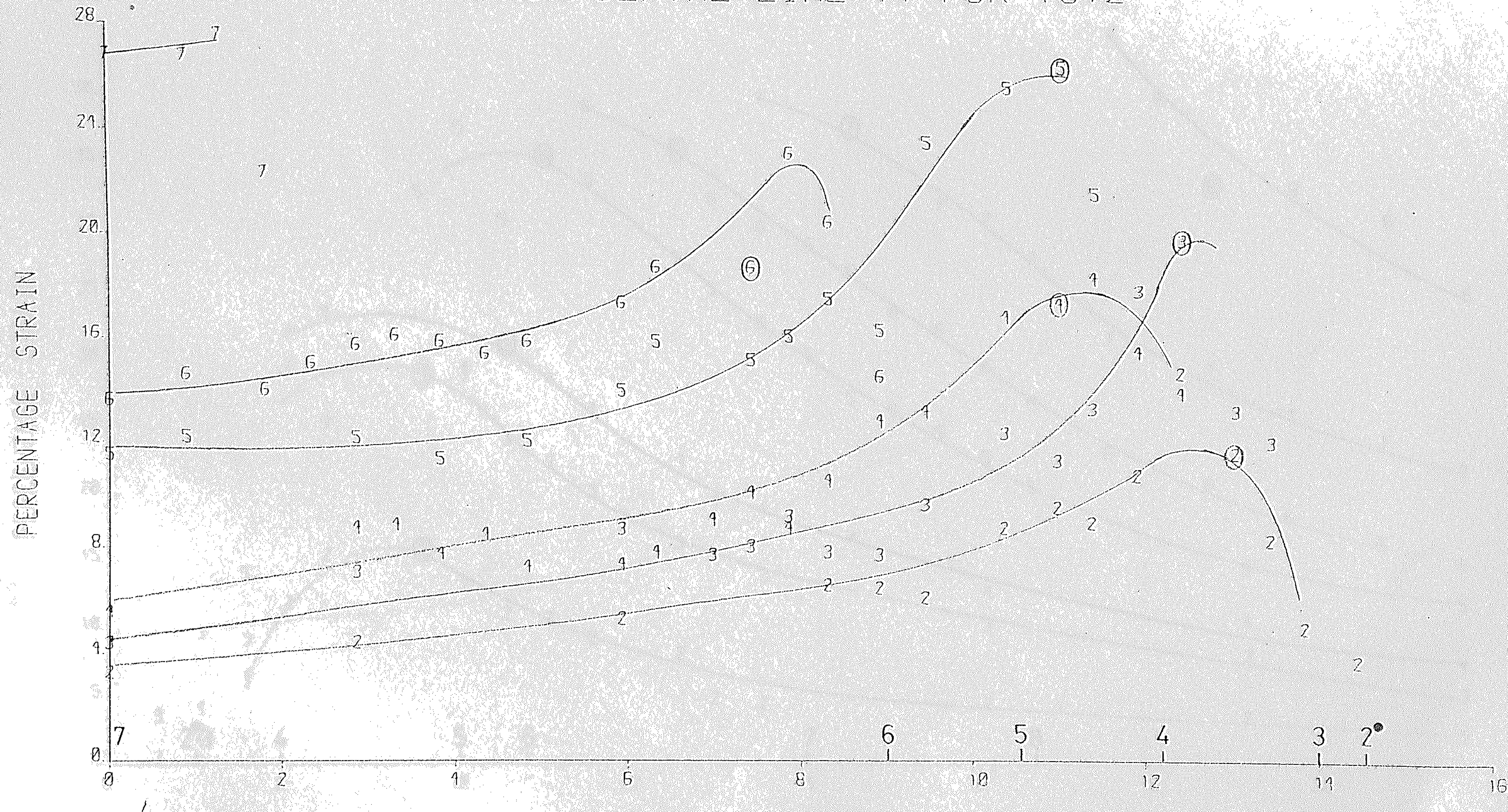

FIG.4.15.12

ENG. STRAIN(YY).V.X-DISTANCE
FROM CENTRE LINE YY FOR TS13

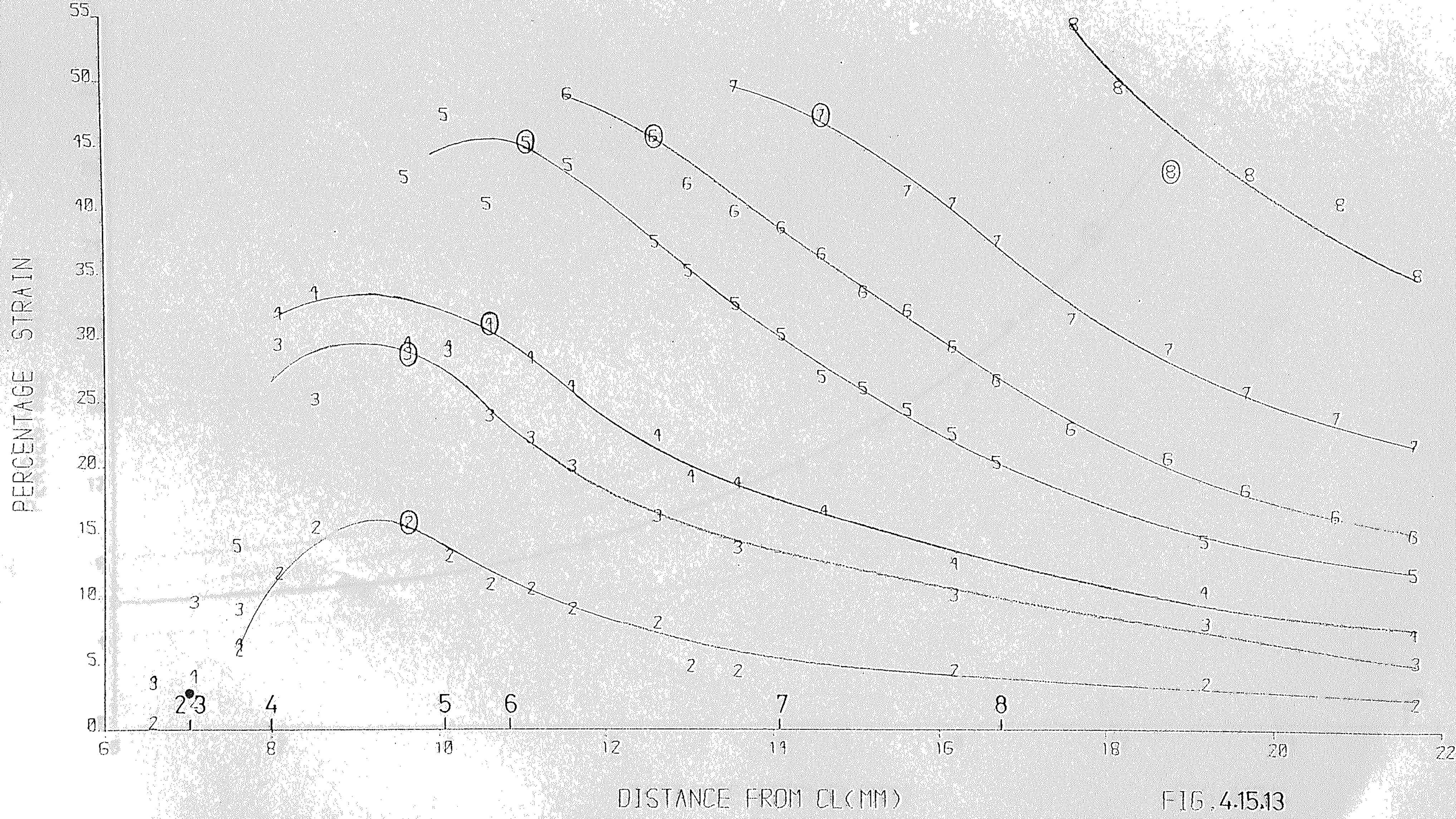

FIG. 4.15.13

ENG. STRAIN(YY).V.X-DISTANCE
FROM CENTRE LINE YY FOR TS14

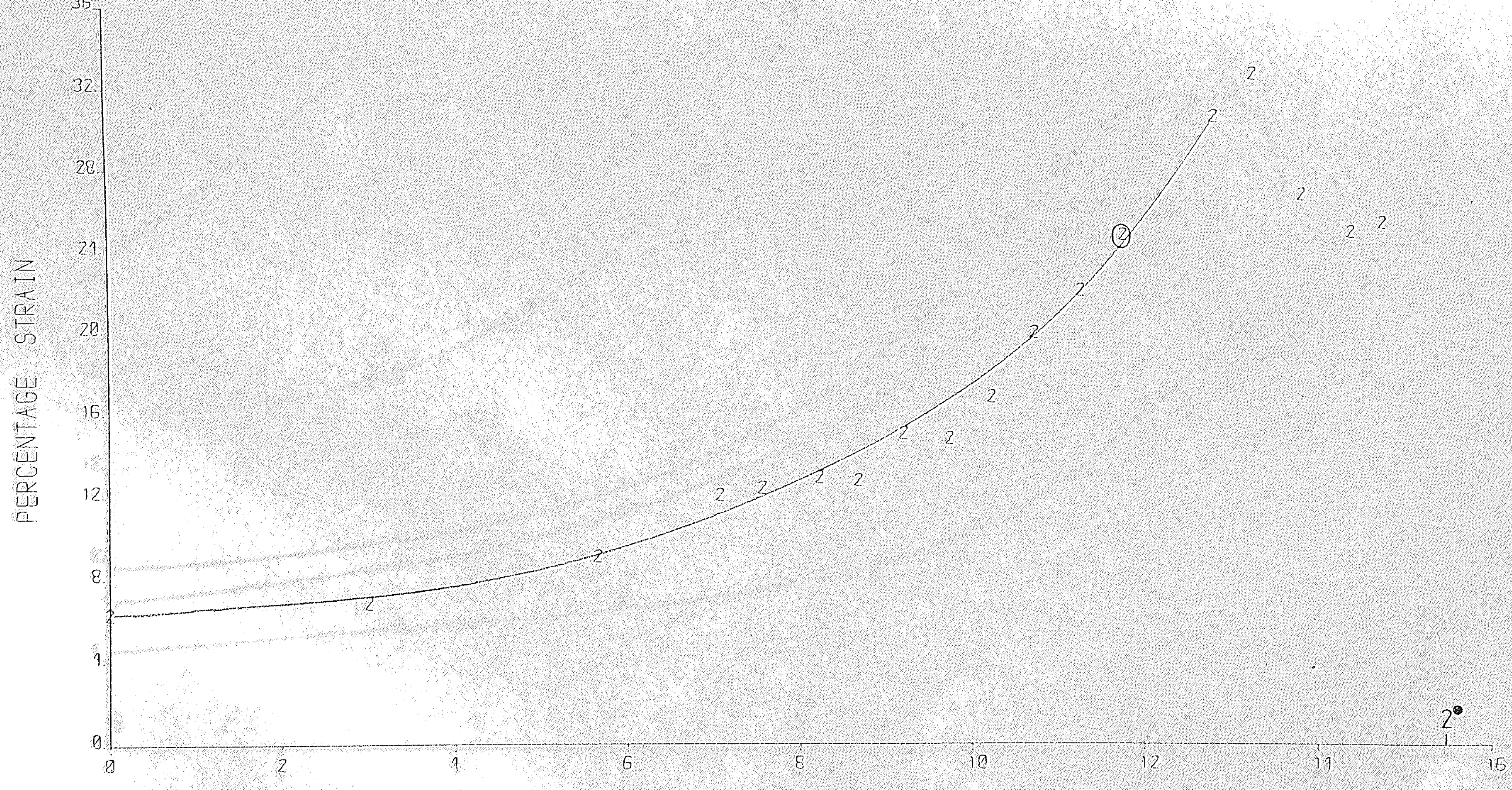

FIG. 4.15.14

ENG. STRAIN(YY).V.X-DISTANCE FROM CENTRE LINE YY FOR TS15

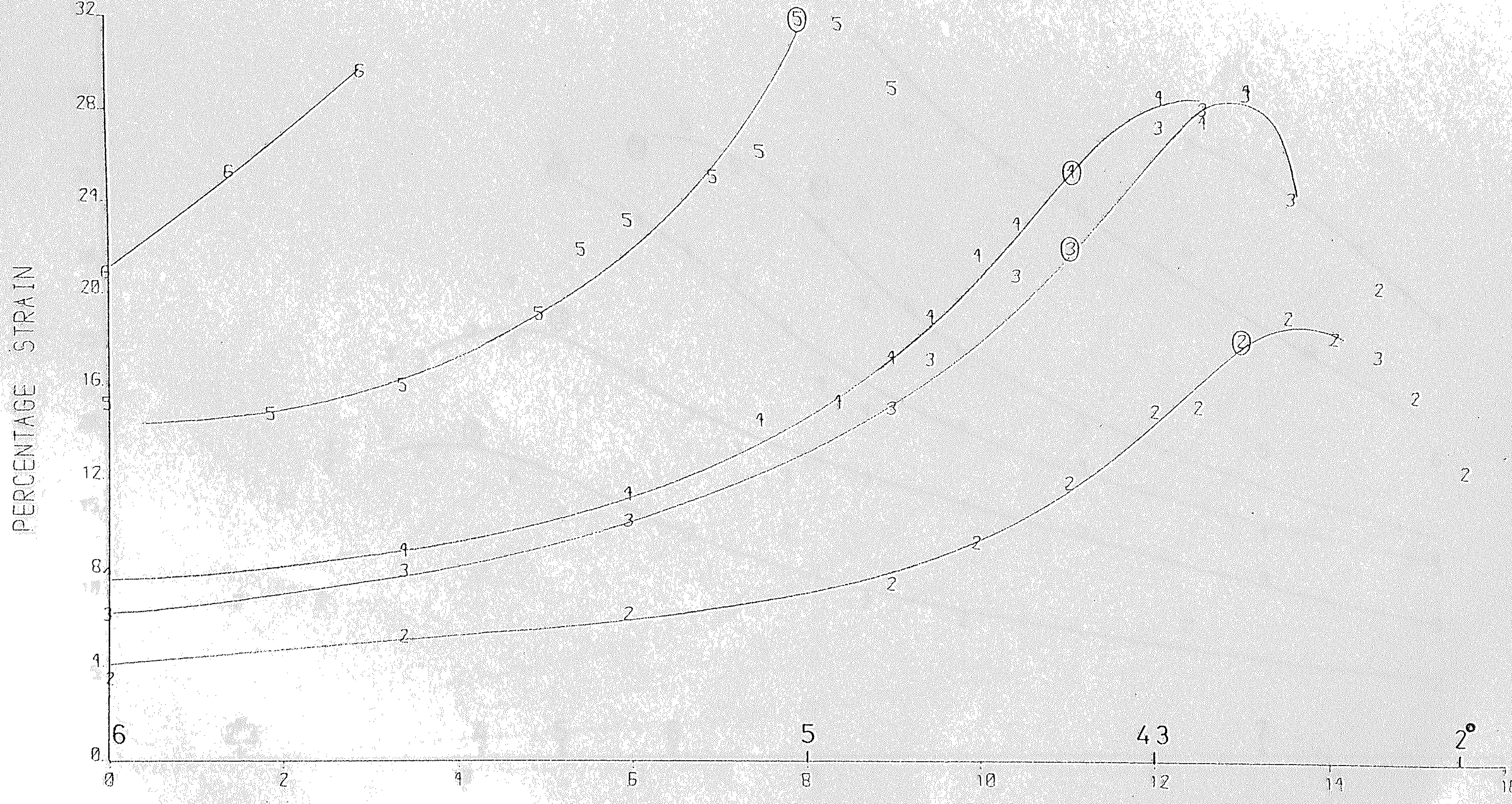

FIG. 4.15.15

ENG. STRAIN(YY).V.X-DISTANCE
FROM CENTRE LINE YY FOR TS16

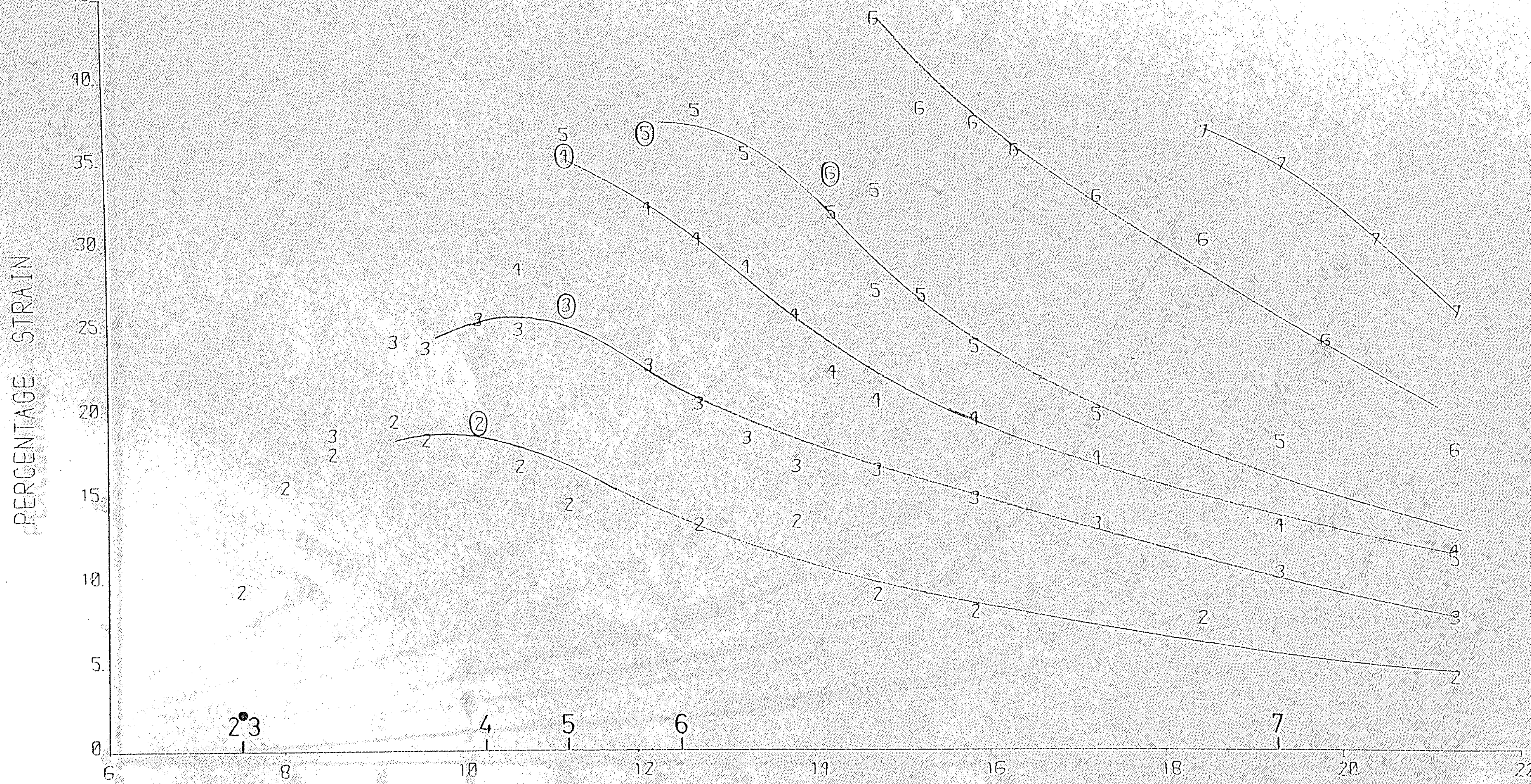

FIG. 4.15.16

ENG. STRAIN(YY).V.X-DISTANCE
FROM SPECIMEN EDGE FOR TS17

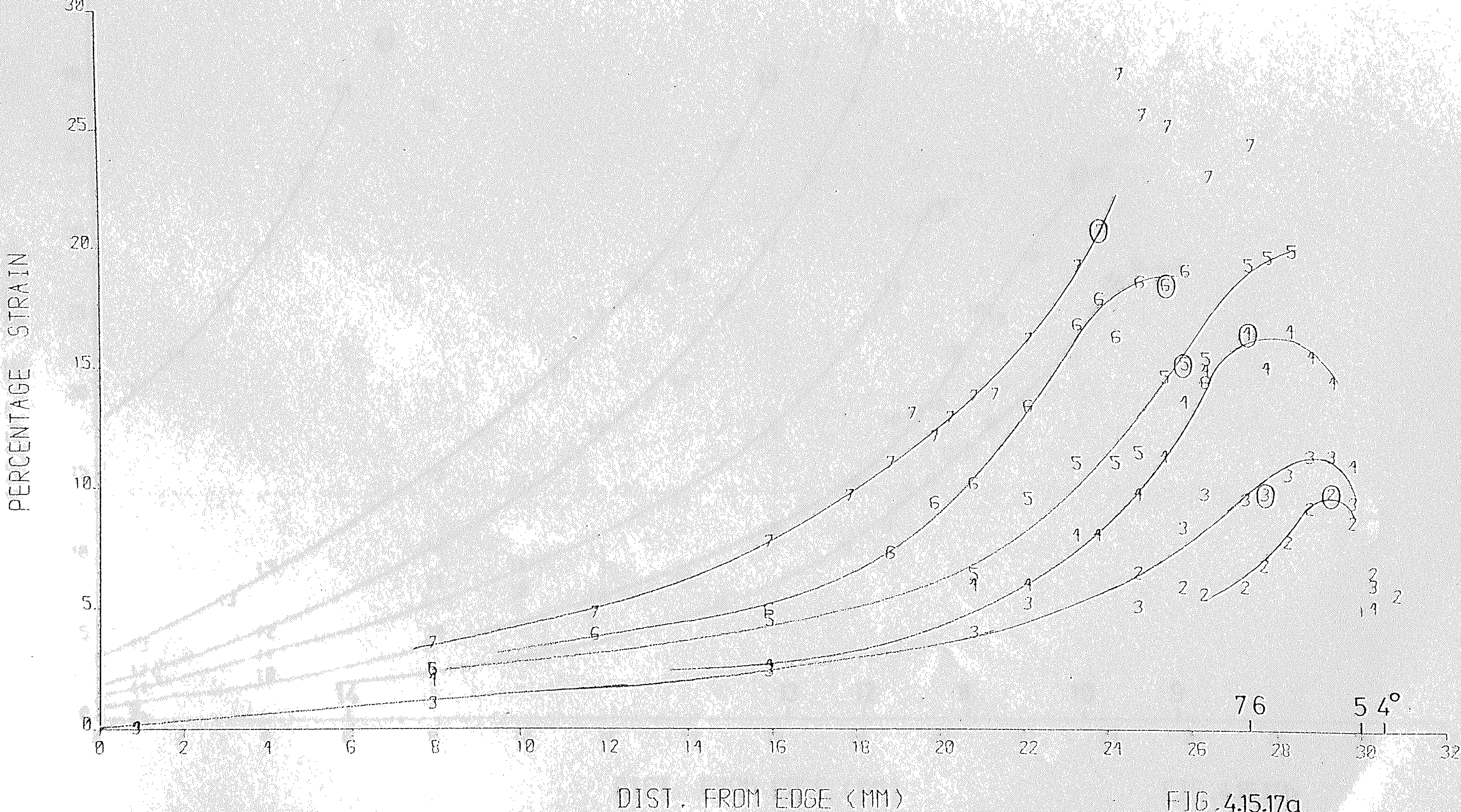

FIG. 4.15.17a

ENG. STRAIN(YY).V.X-DISTANCE
FROM SPECIMEN EDGE FOR TS17

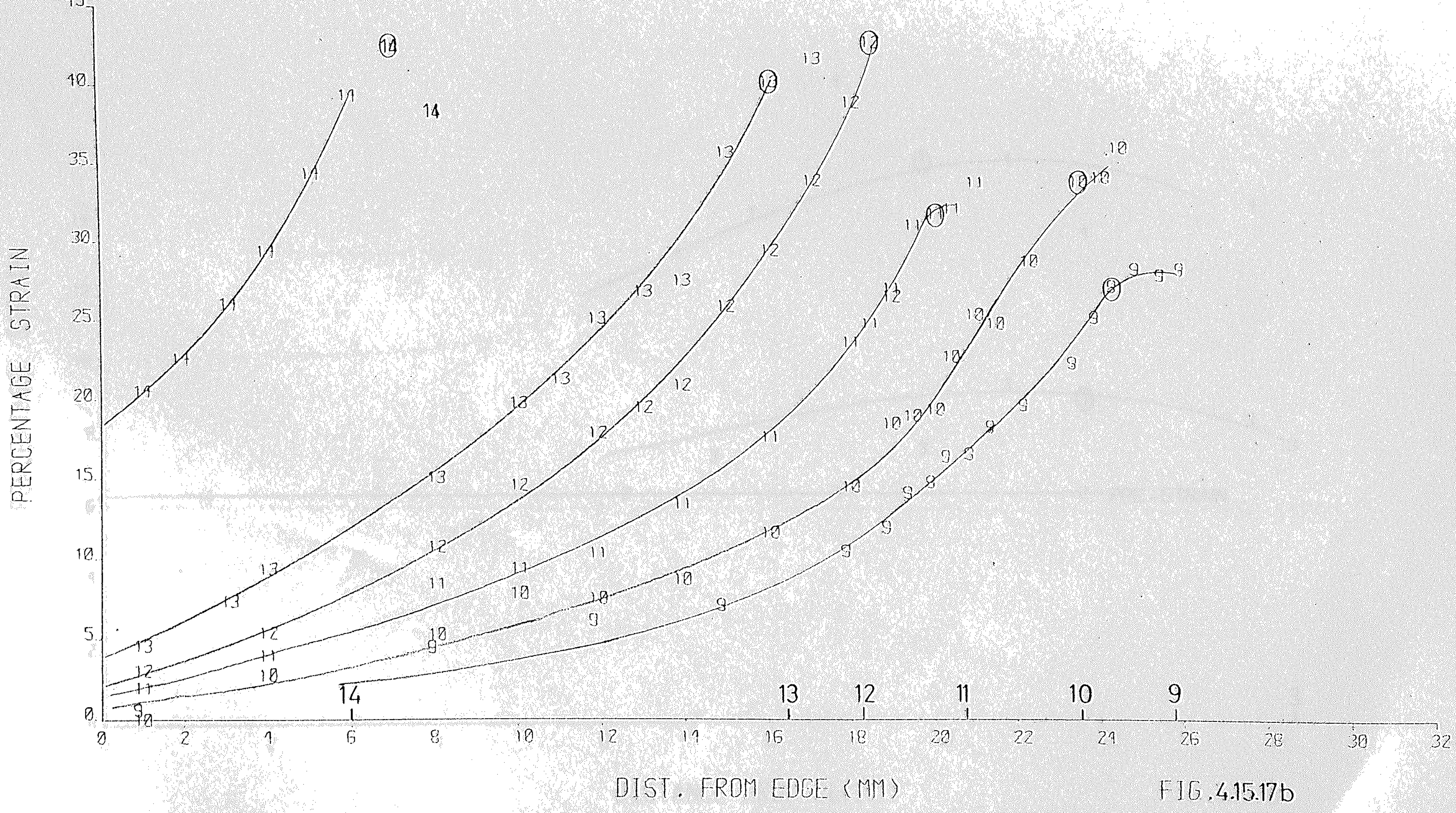

FIG. 4.15.17b

ENG. STRAIN(YY).V.X-DISTANCE
FROM CENTRE LINE YY FOR TS18

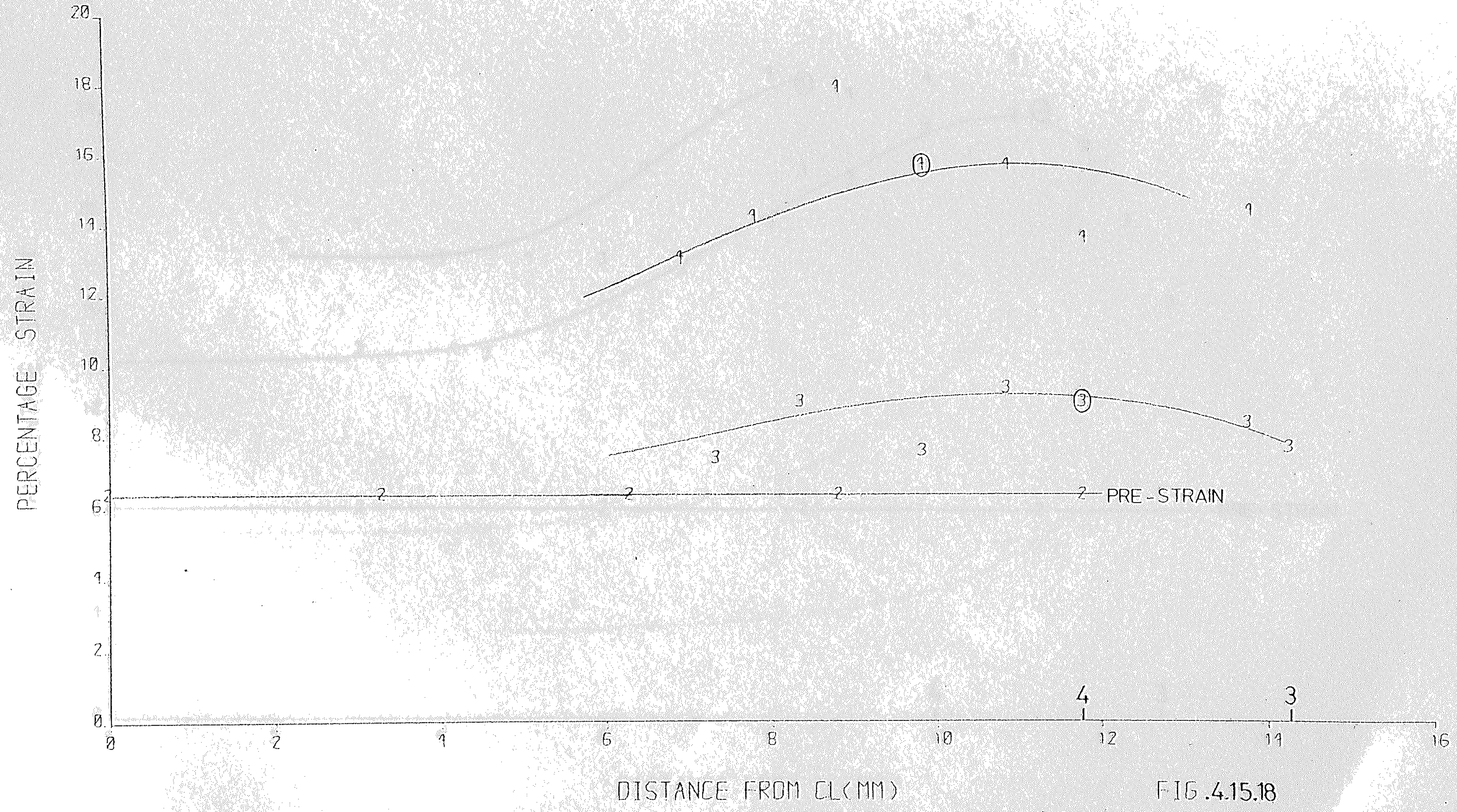

FIG.4.15.18

ENG. STRAIN(YY).V.X-DISTANCE
FROM CENTRE LINE YY FOR TS19

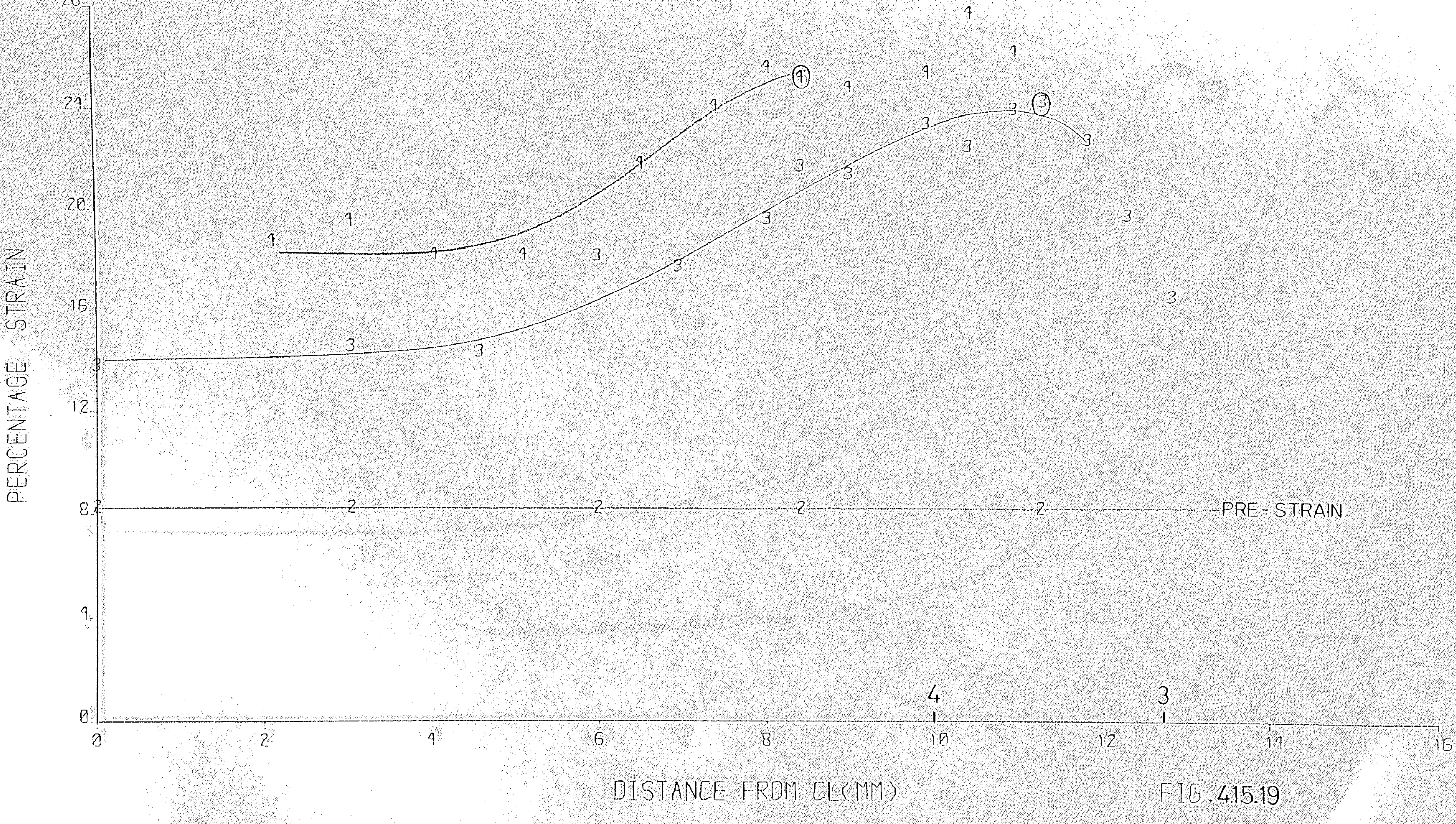

FIG. 4.15.19

ENG. STRAIN(YY).V.X-DISTANCE
FROM CENTRE LINE YY FOR TS20

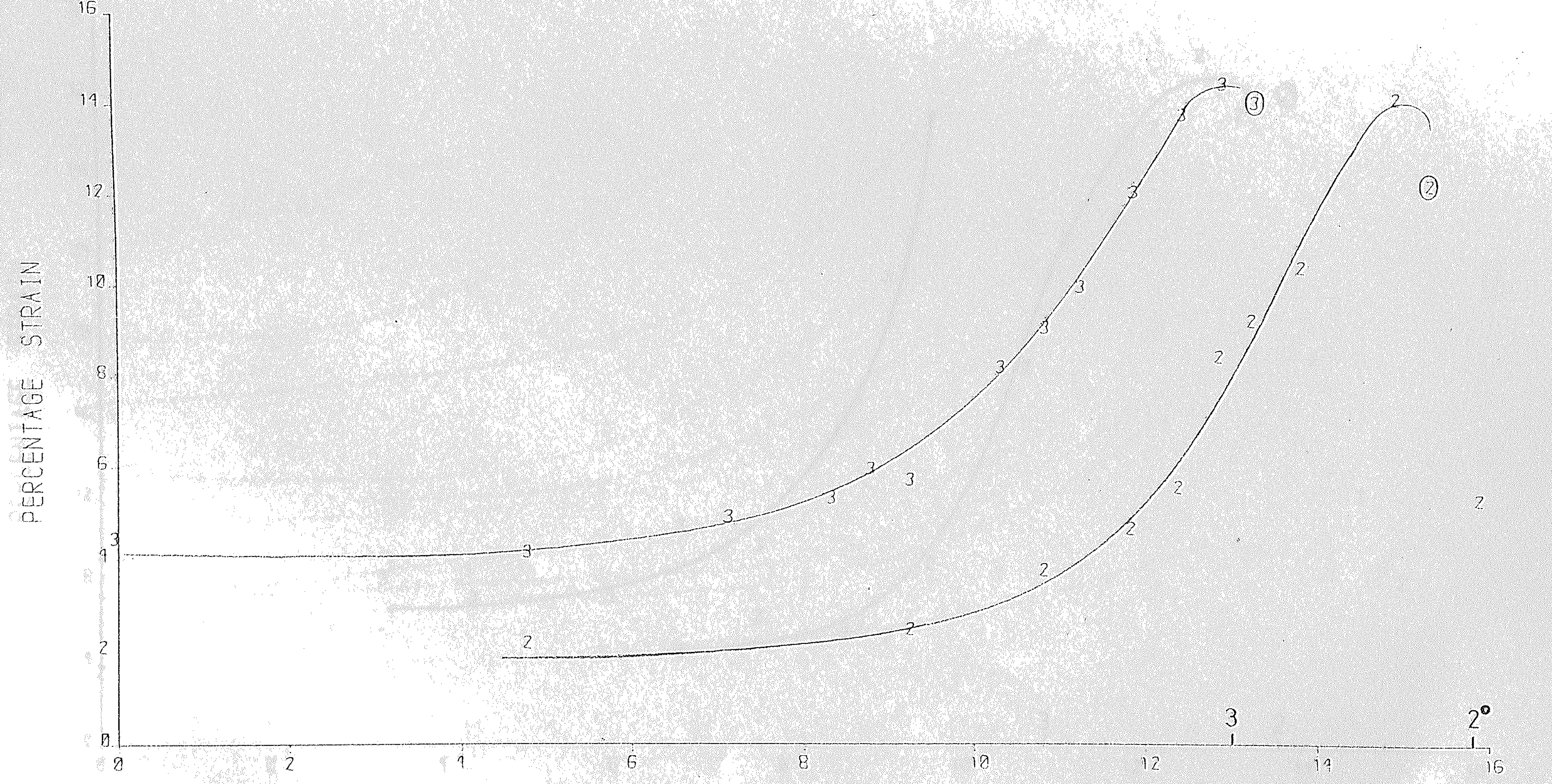

FIG. 4.15.20

ENG. STRAIN(YY).V.X-DISTANCE
FROM CENTRE LINE YY FOR TS21

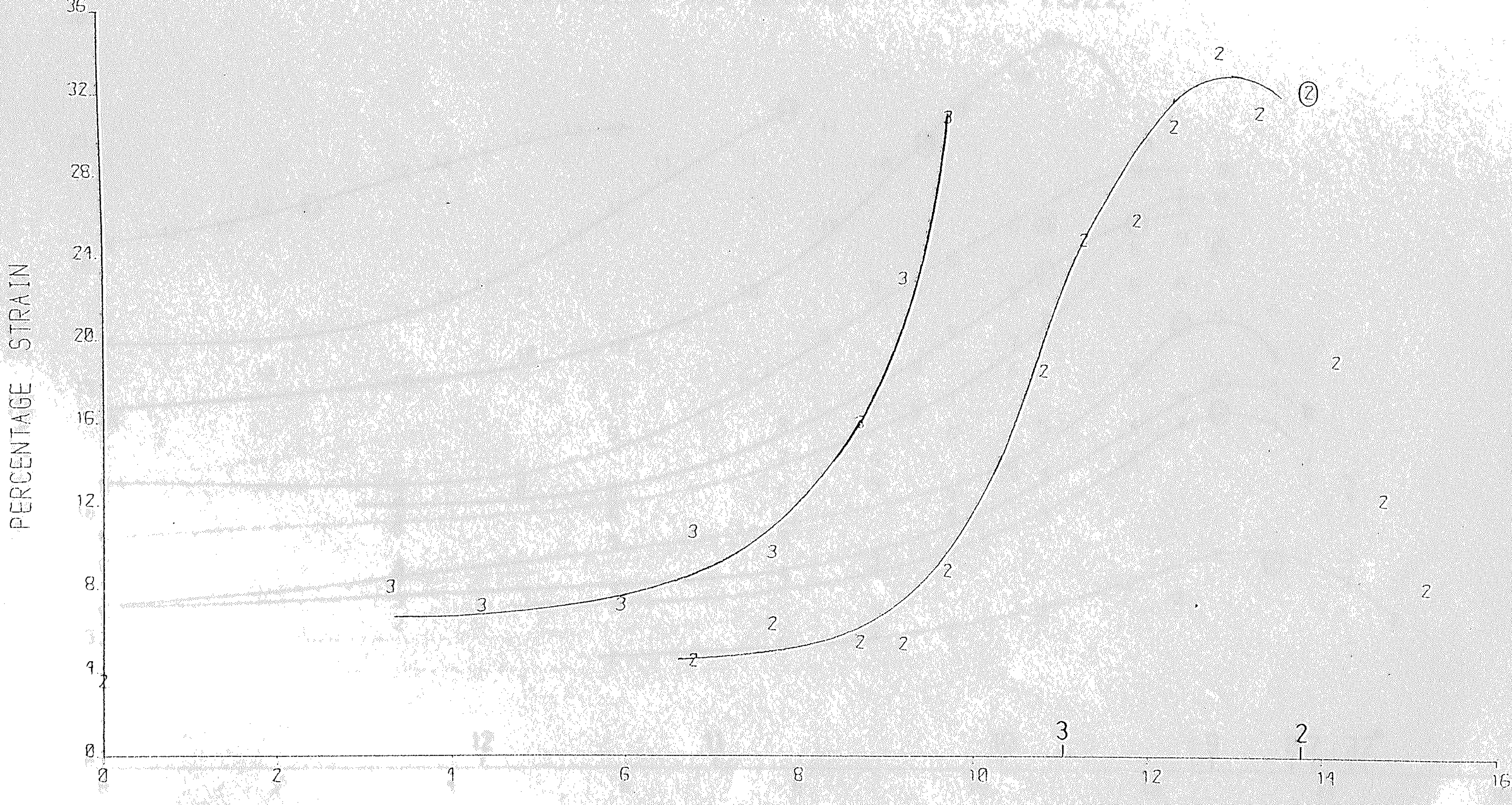

FIG.4.15.21

ENG. STRAIN(YY).V.X-DISTANCE
FROM CENTRE LINE YY FOR TS22

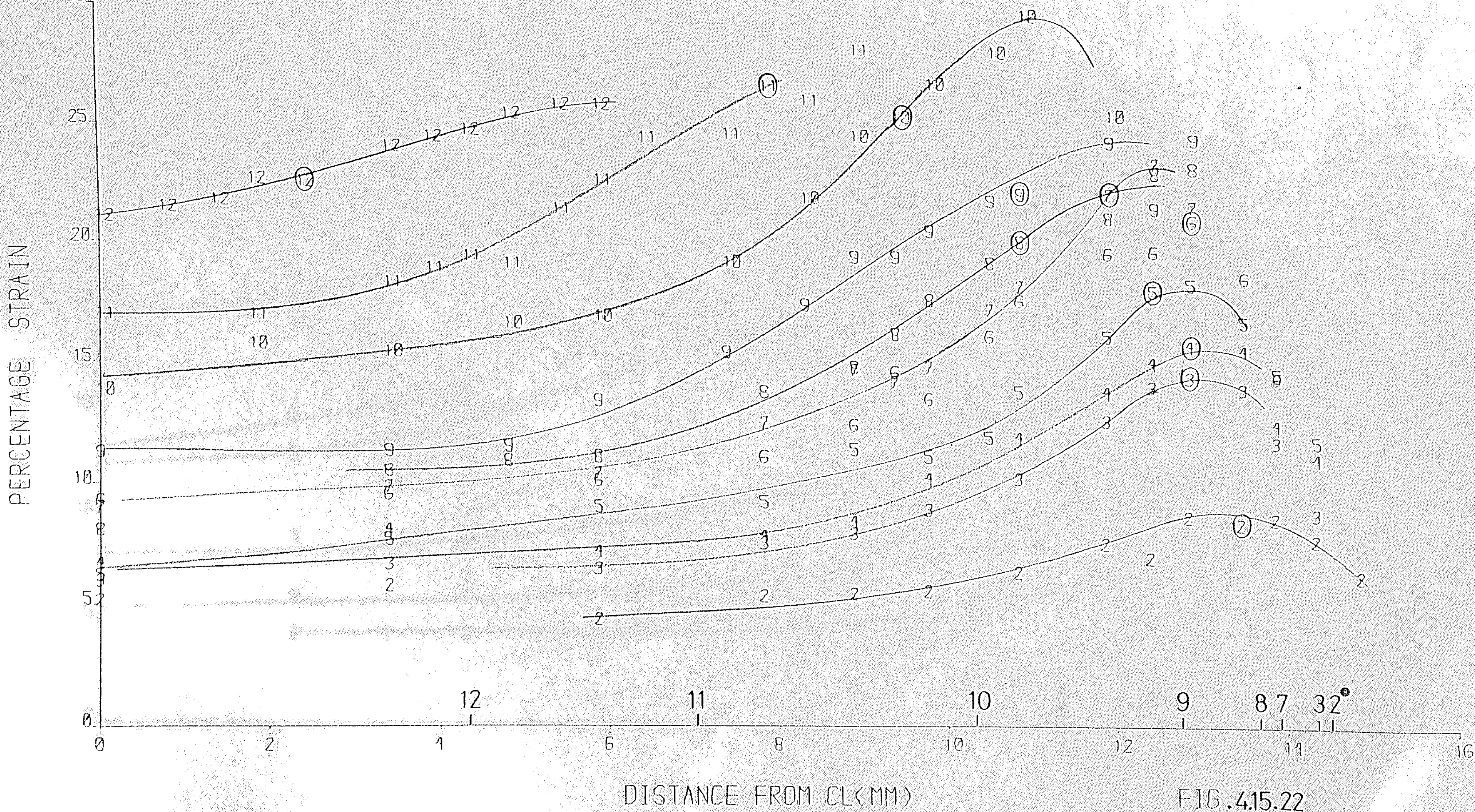

FIG. 4.15.22

ENG. STRAIN(YY).V.X-DISTANCE
FROM CENTRE LINE YY FOR TS23

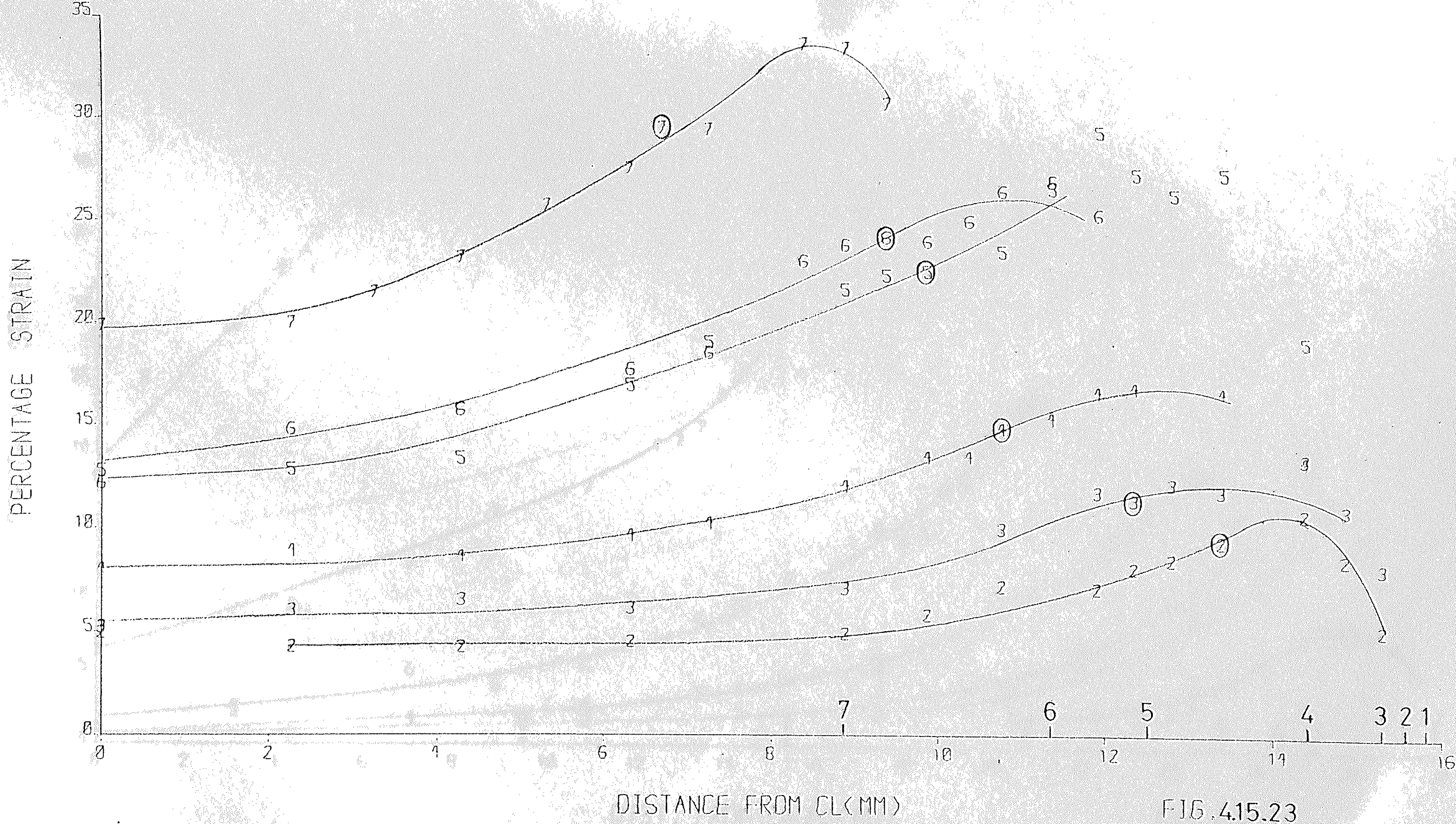

FIG.4.15.23

ENG. STRAIN(YY).V.X-DISTANCE FROM SPECIMEN EDGE FOR TS24

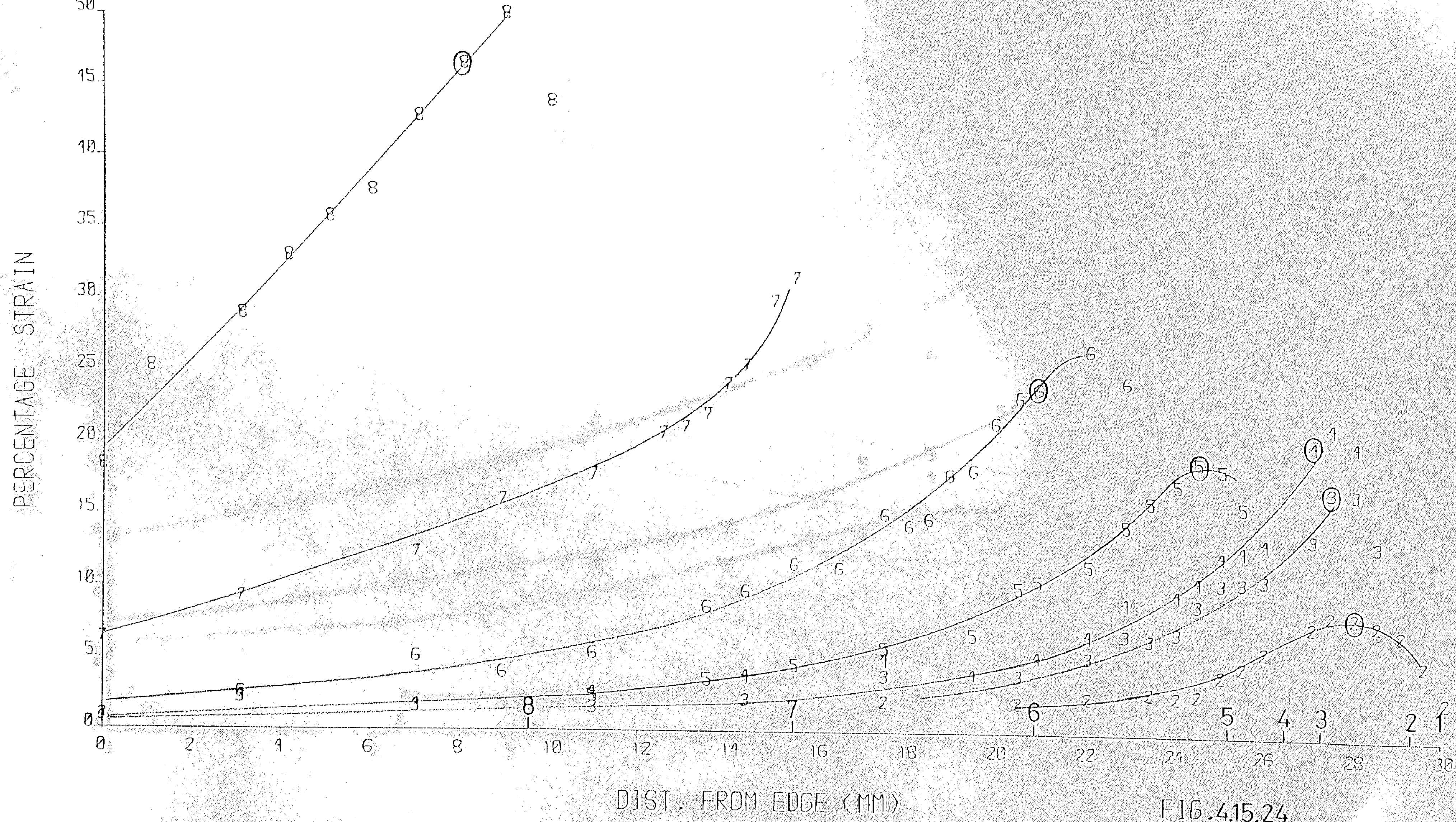

FIG.4.15.24

ENG. STRAIN(YY).V.X-DISTANCE
FROM CENTRE LINE YY FOR TS25

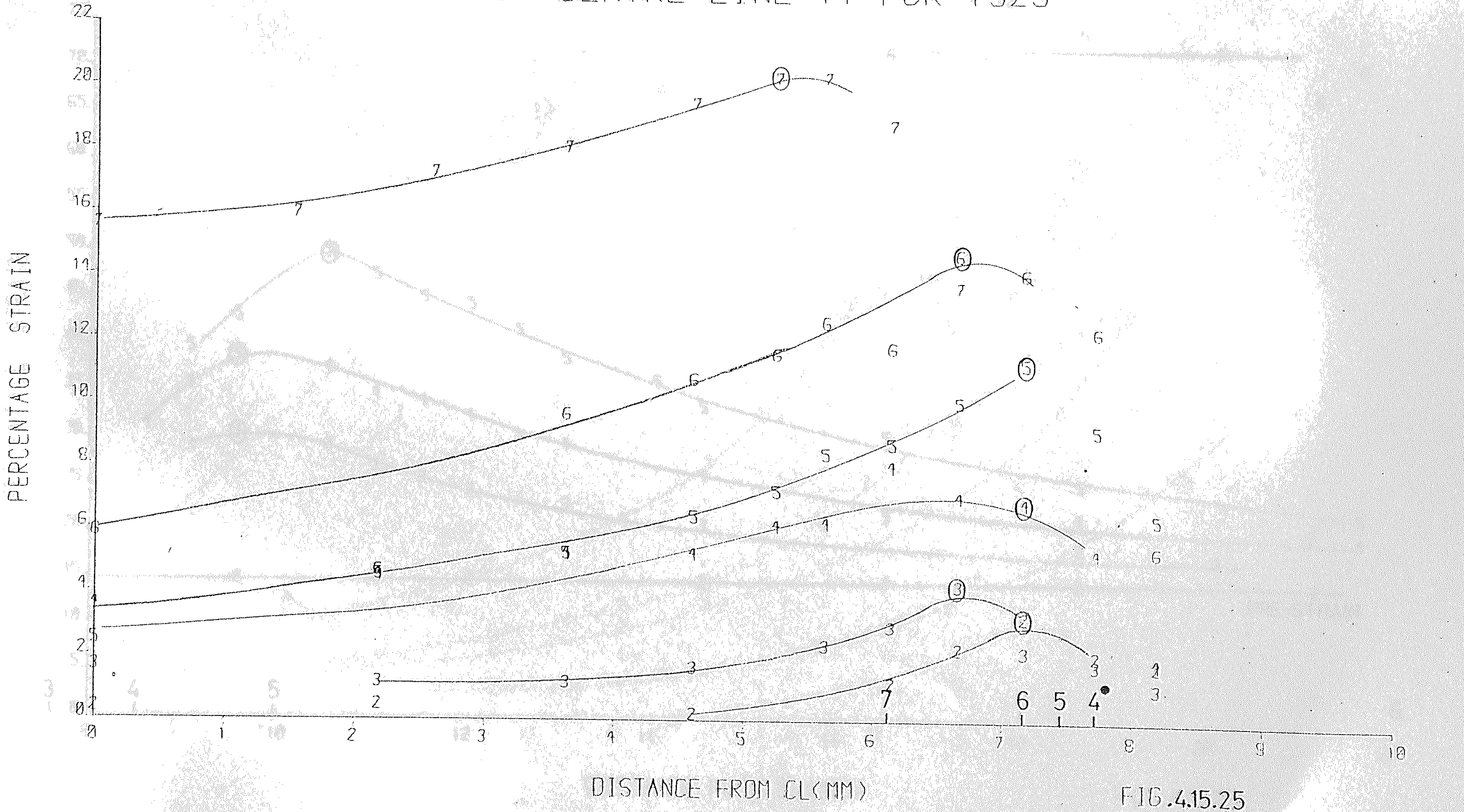

FIG.4.15.25

ENG. STRAIN(YY).V.X-DISTANCE
FROM CENTRE LINE YY FOR TS26

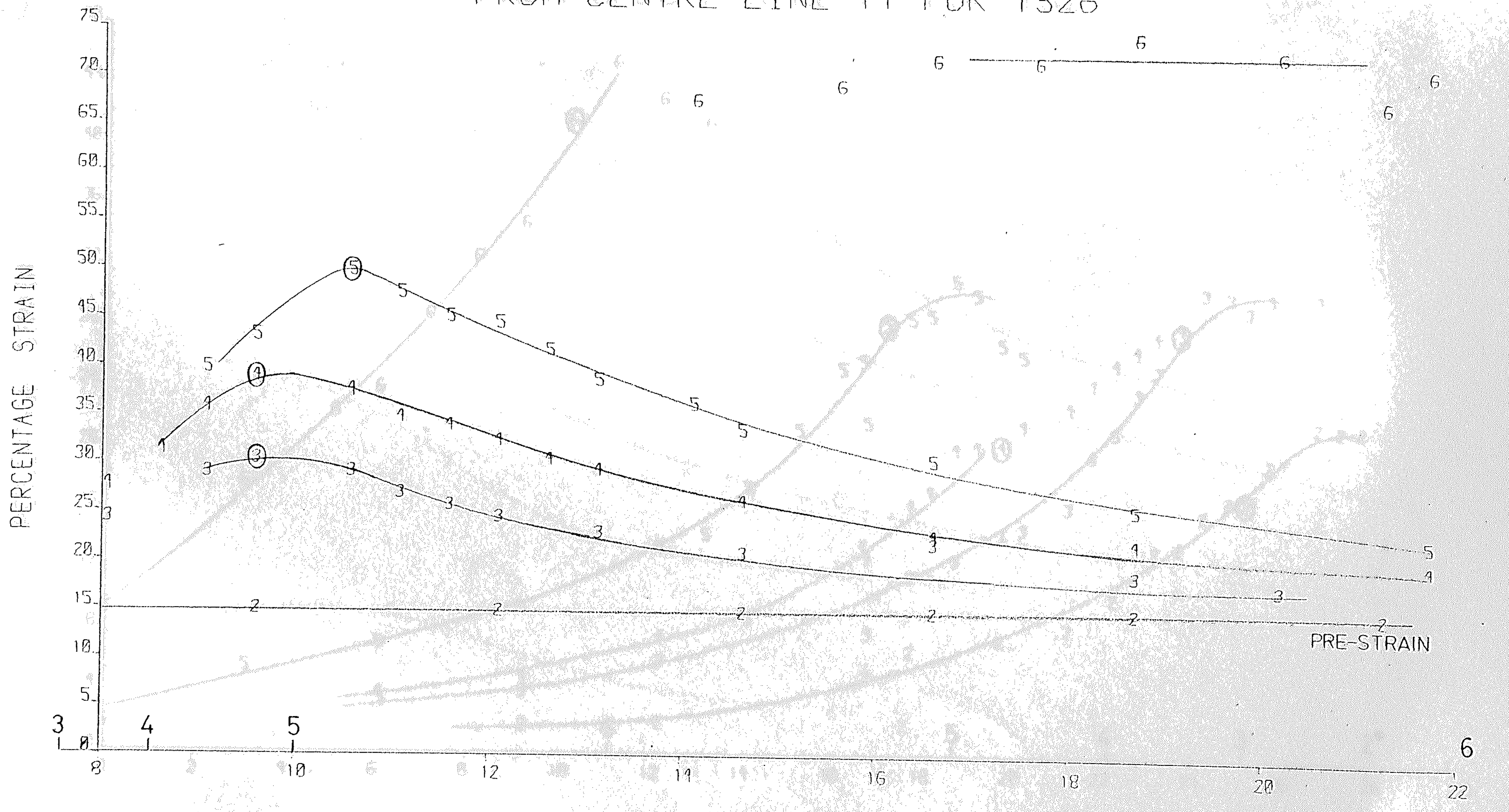

FIG.4.15.26

ENG. STRAIN(YY).V.X-DISTANCE
FROM SPECIMEN EDGE FOR TS27

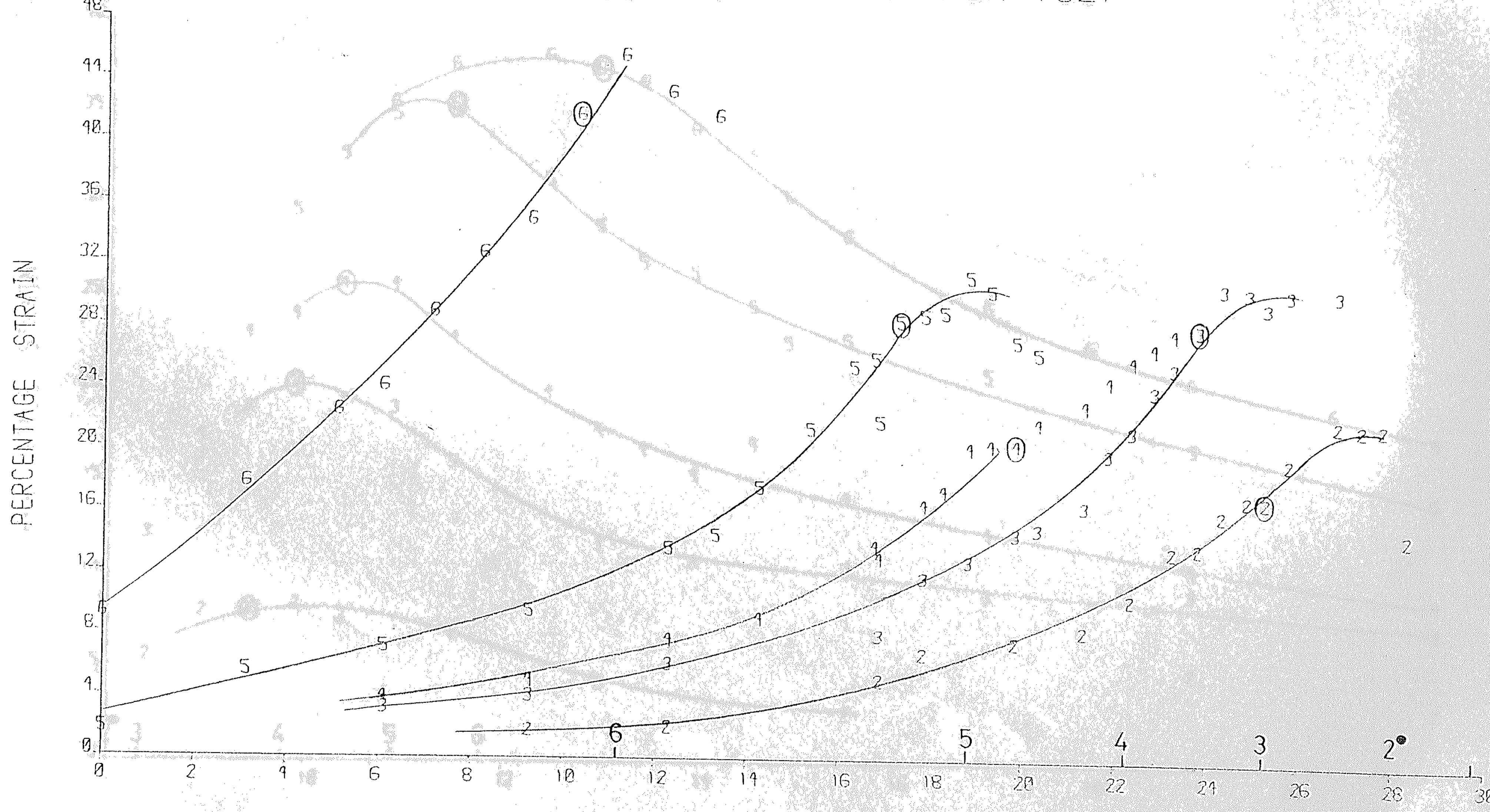

FIG.4.15.27

ENG. STRAIN(YY).V.X-DISTANCE
FROM CENTRE LINE YY FOR TS28

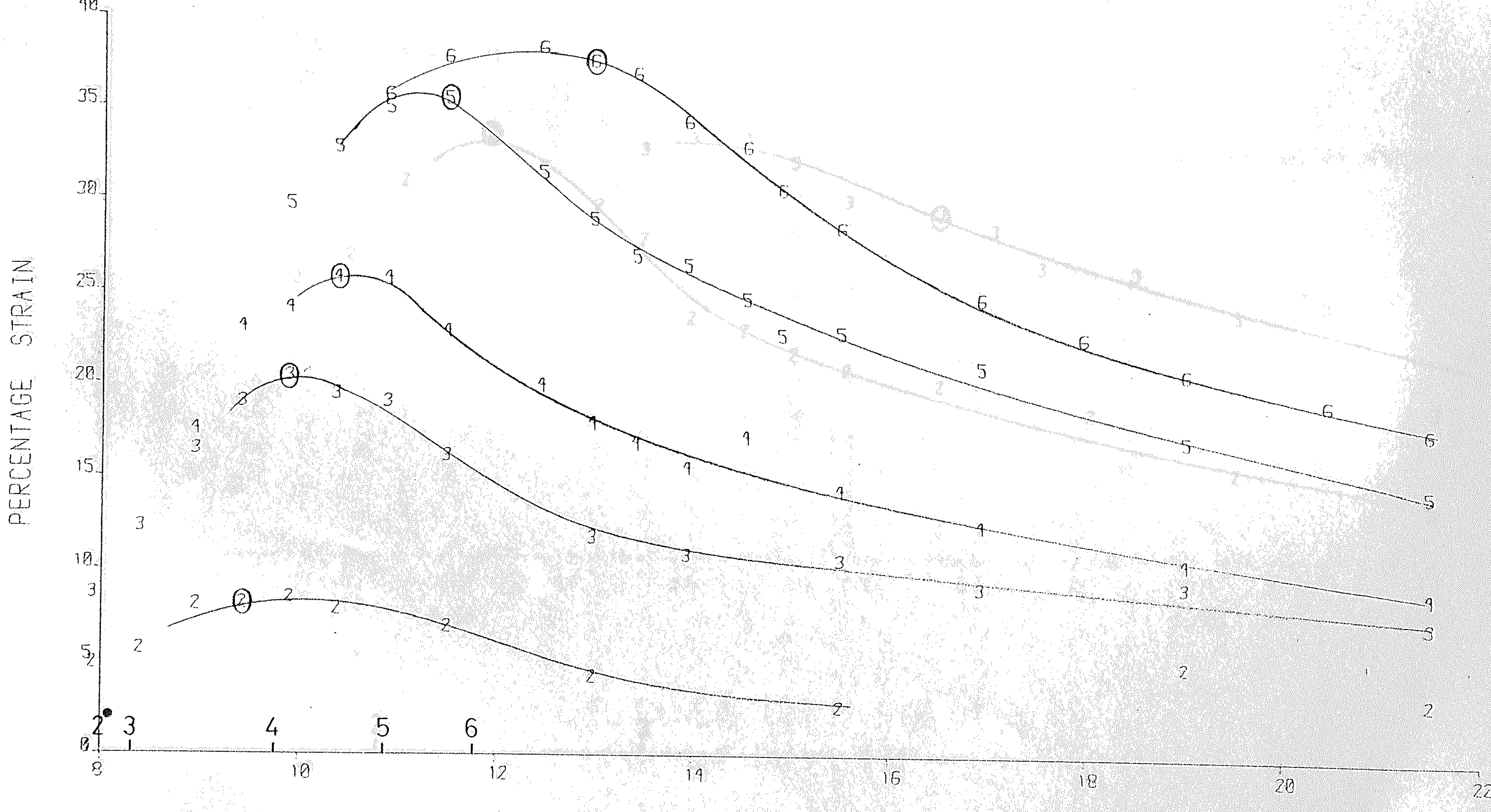

FIG.4.15.28

ENG. STRAIN(YY).V.X-DISTANCE FROM CENTRE LINE YY FOR TS29

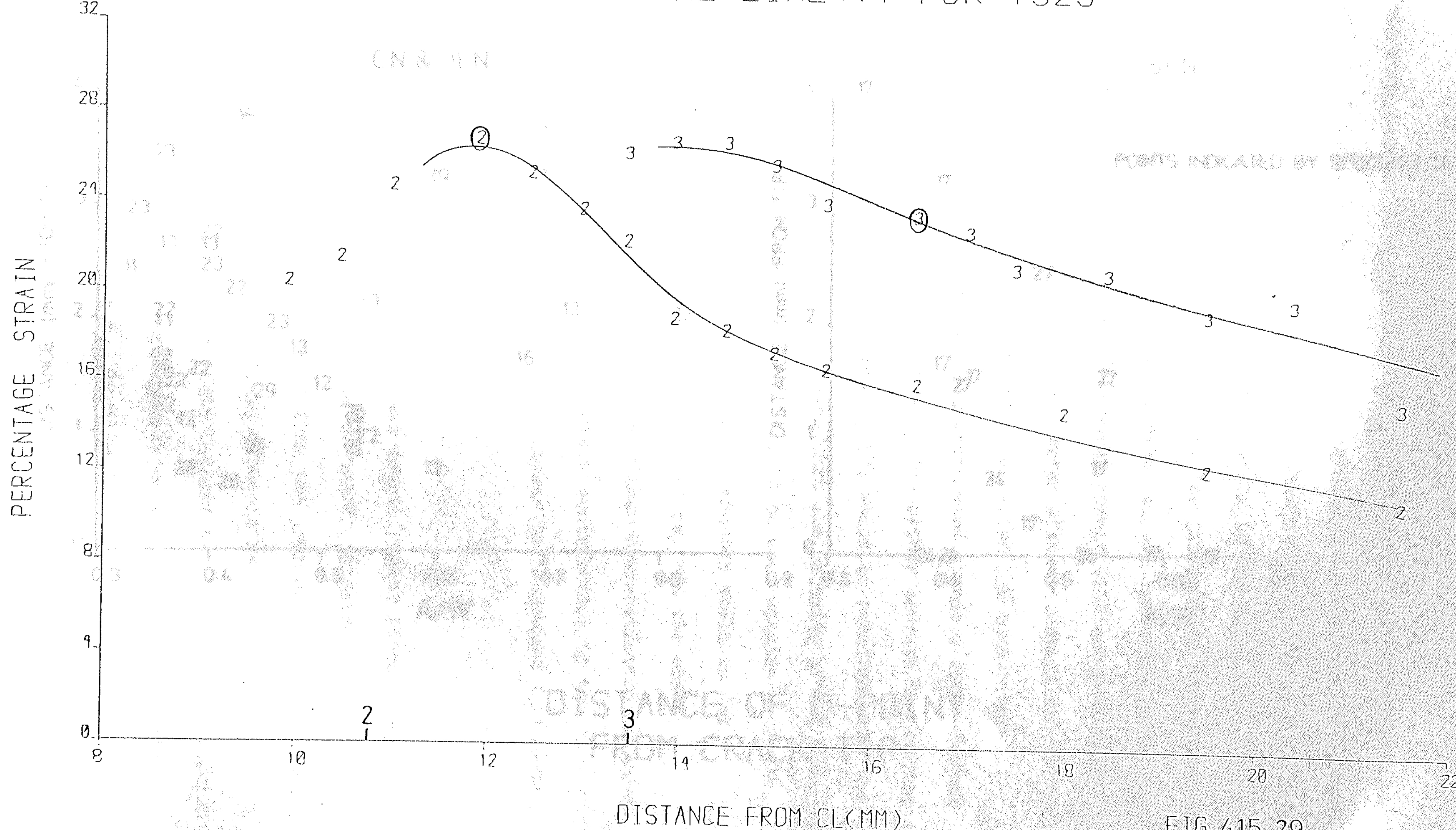

FIG.4.15.29

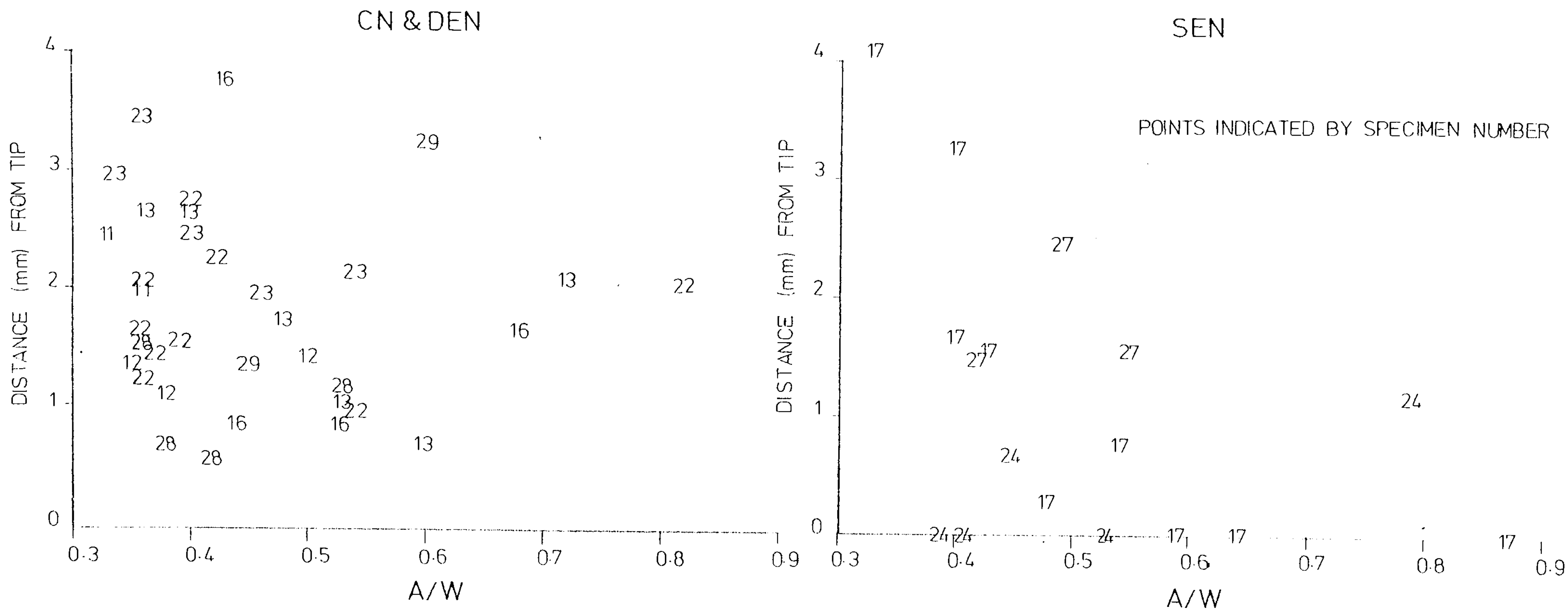

DISTANCE OF D-POINT
FROM CRACK TIP

FIG. 4.16

the displacement measurements. For a 15% strain the displacements will be between 0.15mm to 0.52mm. Magnification differences between photographs will introduce errors so attempts were made to minimise these wherever possible. A constant error in the magnification of all the photographs will not effect the gradient of displacement so these could be tolerated to a greater extent but where still kept to a minimum where possible. The worst errors will occur when by statistical chance the displacement error either accumulates or decreases with distance. If a line over which 15% strain had occurred had errors in measurement increasing linearly from -0.04mm at the XX centre line to +0.04mm at 3.5mm either side of the centre line, then a strain of approximately 17% would be obtained from the regression analysis. This indicates that the majority of all the strain values (i.e. more than 90%) should be well within ±2 of the indicated percentage as the more normal tendency would be for a random distribution of the measurement errors. On the other extreme, if all the measurements were either over-estimated or under-estimated by 0.04mm then the non-uniform contribution to the displacement (intercept value) would appear to be changed by 0.04mm accordingly.

The gradient of d_{xx} with distance was devoid of any linear region of the nature observed in the analysis of the ε_{yy} strain values. The displacements used were calculated from the average of 2 measurements. Fairly extensive plots of d_{xx} versus distance were prepared, especially in the region between the D-point and the crack tip, which assisted in showing up any particularly unreliable measurements. However the analysis of the ε_{xx} strains cannot be considered of compatible accuracy to the ε_{yy} values each of which was based on 6 measurements specific to that value. Also the ε_{xx} values were smaller than their Y-direction counterparts making them even more suseptible to errors from measurement.

The effect of vertical distance from the XX centre line on the ε_{xx} values has been observed throughout, but in particular in the earlier tests. The variation of ε_{xx} with increasing Y-distance from this centre line has defied exact quantification, possibly due partly to the inherent inaccuracy. Scans of d_{xx} across the ligament in the X-direction for increasing distances above the XX centre line were made. These showed an overall decrease in displacement for the CN geometry and over the range of distance from the XX centre line considered, an increase for DEN specimens. This is consistent with the observation in section 4.2.1 with regards the position of the region of maximum lateral contraction as shown in Fig. 4.5.

When comparing plots of displacement versus distance produced from measurement scans at different distances above and below the XX centre line the following was observed. The plots for a specimen were basically similar in appearance and would approximately superimpose if moved together in a horizontal direction by a distance roughly equal to the vertical separation of the scans. The plot from a measurement scan made further from the XX centre line would require to be displaced back towards the crack tip in order for it to superimpose with a plot from a scan nearer the XX centre line. This effect and the general shape of d_{xx} versus distance plots are shown schematically for the DEN and CN specimens in Fig. 4.17. The features of the profiles are also smoothed or averaged slightly as the distance from the XX centre line increases, but this is only really significant where very large changes in the gradient of displacement occur, such as at the

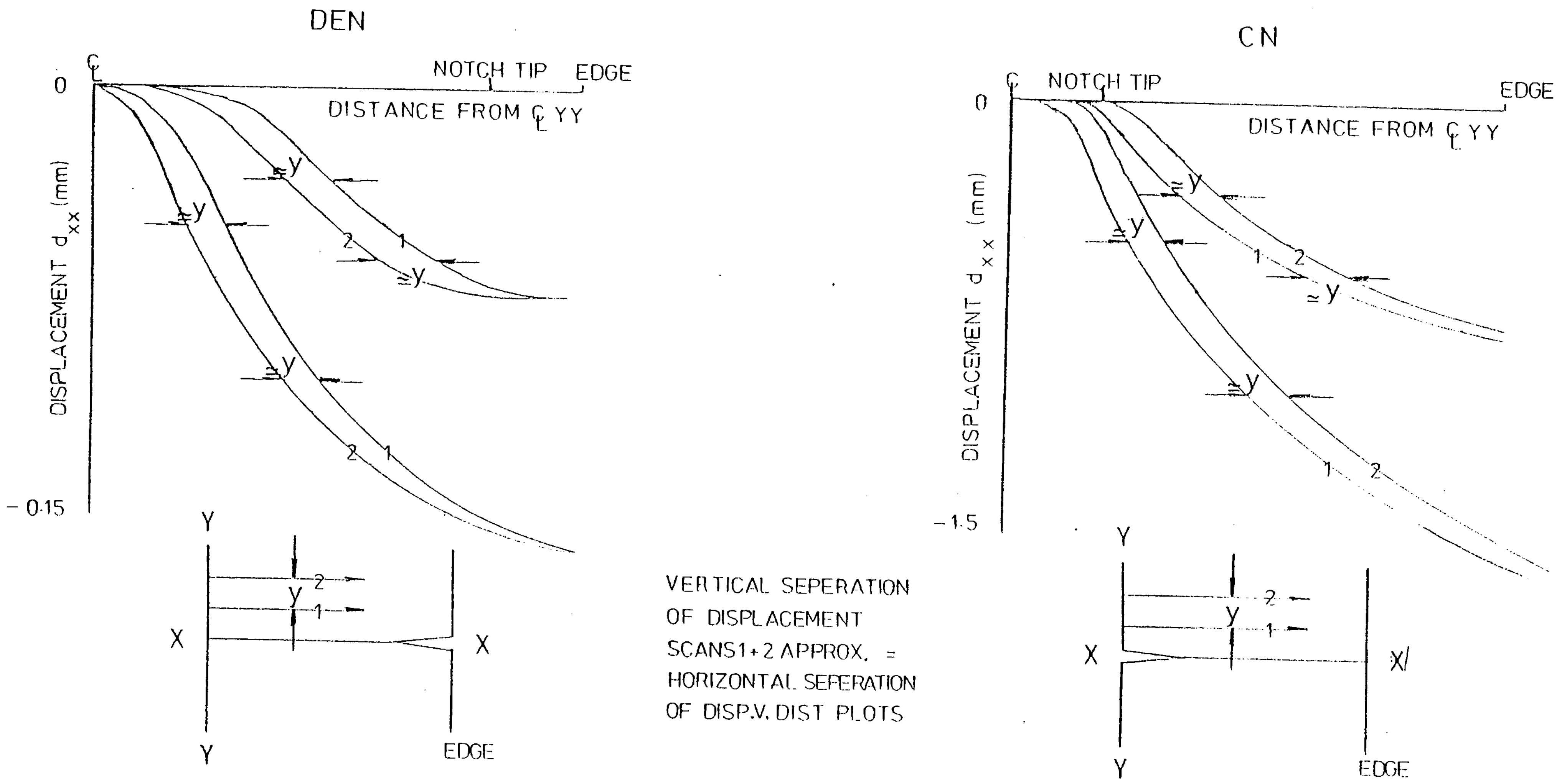

SCHEMATIC REPRESENTATION OF
HORIZONTAL DISPLACEMENT .V.
DISTANCE FROM YY-CENTRE LINE

FIG. 4.17

notch tip during crack initiation.

There were two basic reasons why the ε_{xx} and ε_{yy} strain distributions were determined. Firstly in order to gain evidence as to the parameters controlling crack advance by examining for critical strain or COD criteria and secondly in an attempt to evaluate the nature of the distribution of stress with increasing distance from the crack tip under creep conditions. These observations are reported under the headings of Major Strain Observations and Strain Profile Analysis respectively.

4.2.3.1 Major Strain Observations

Slow crack growth is consistent with the advance of the crack tip being controlled by the attainment of a critical strain or displacement, or with the attainment of a critical amount of damage which would probably be related to strain. To examine this possibility of crack growth being controlled by such a criterion the following true strain measurements, or parameters derived from true strain measurements have been plotted against the instantaneous position of the crack tip:

i) Maximum value of ε_{yy} for each position of the crack tip examined.

ii) D-point strain " " " " " " "

iii) ε_{xx} at the location of maximum ε_{yy}

iv) Equivalent strain at the location of maximum ε_{yy}

v) Arithmetic sum of ε_{yy} and ε_{xx} from i and iii above

vi) An indication of the deviation from normal Poisson contraction strain

vii) COD (equivalent) At the crack tip and at the position of maximum ε_{yy} from (i) above.

These are shown in Fig. 4.18a to 4.18g respectively. Considering each in turn.

Maximum value of ε_{yy} for each position of the crack tip

These values are the maximum values of ε_{yy} observed for each examination of a specimen strain profile. One value is shown for each determination of the strain distribution across a specimen ligament. The maximum value of ε_{yy} for a given strain distribution would normally occur a short distance ahead of the crack tip, or in the later stages of crack growth, very close to the crack tip. These values of ε_{yy} only represent the uniform strain component of the total displacement and do not include the non-uniform displacement represented by the intercept component observed in the near tip region.

Comparing the maximum values of ε_{yy} obtained for the different geometries, and the variation in these values with crack growth it can be seen that this quantity is geometry dependant. The CN and SEN geometries exhibited greater tensile ductility than the DEN specimens. The general trend of behaviour is shown schematically in Fig. 4.19.

Strong support was observed for the existence of a critical strain criterion for a particular geometry once growth was well established, that is, after about 0.42a/w. During earlier stages of crack growth lower values of maximum ε_{yy} were observed. Typically the DEN geometry stabilised at value of ε_{yy} around 20 to 25% and the other two geometries around 40%

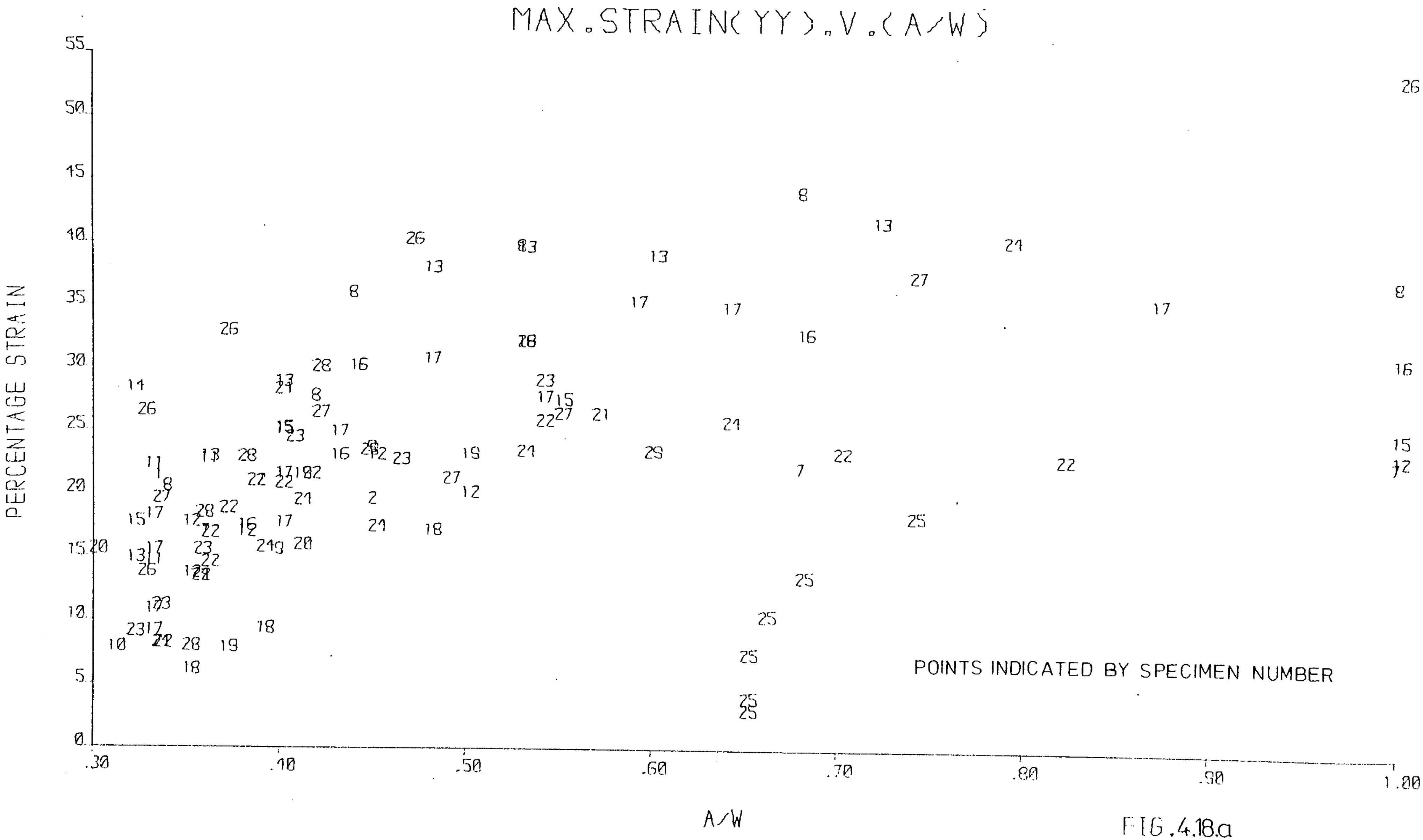
MAX.STRAIN(YY).V.(A/W)
PERCENTAGE STRAIN
A/W
POINTS INDICATED BY SPECIMEN NUMBER

FIG.4.18.a

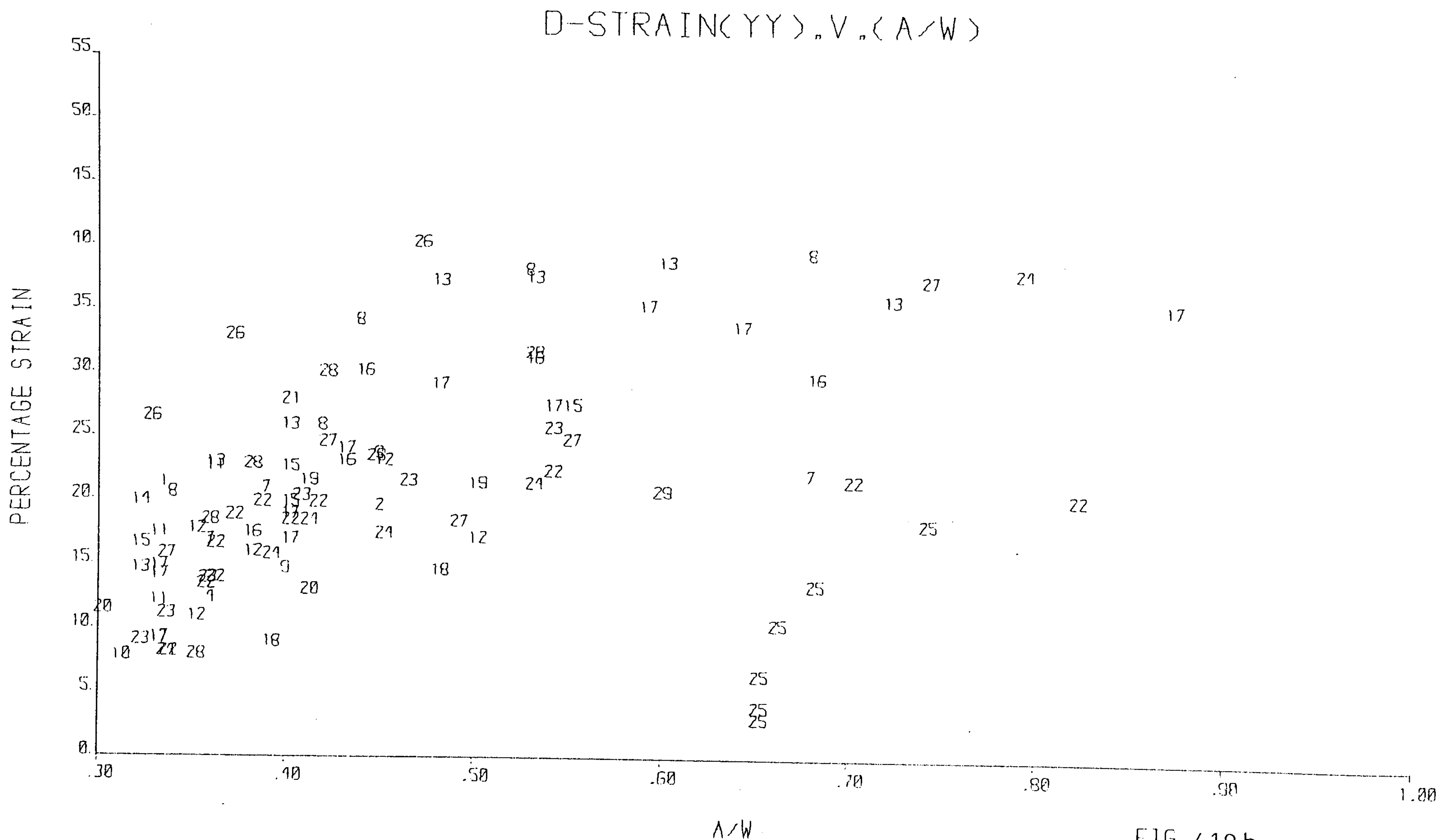

FIG.4.18.b

EQUIVALENT STRAIN.V.(A/W)

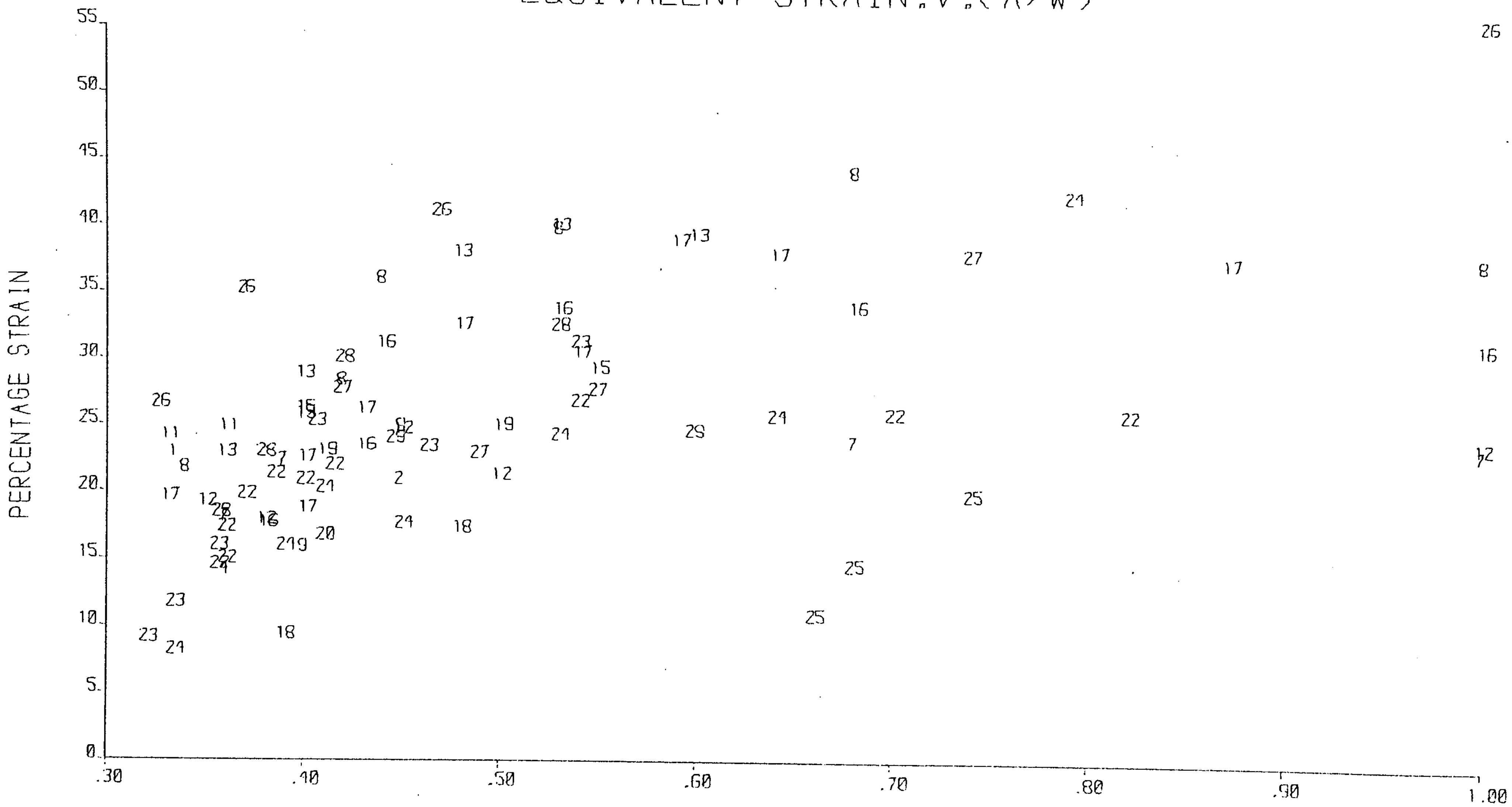

FIG.4.18.d

MAX.STRAIN(YY) + CORRESPONDING STRAIN(XX).V.(A/W)

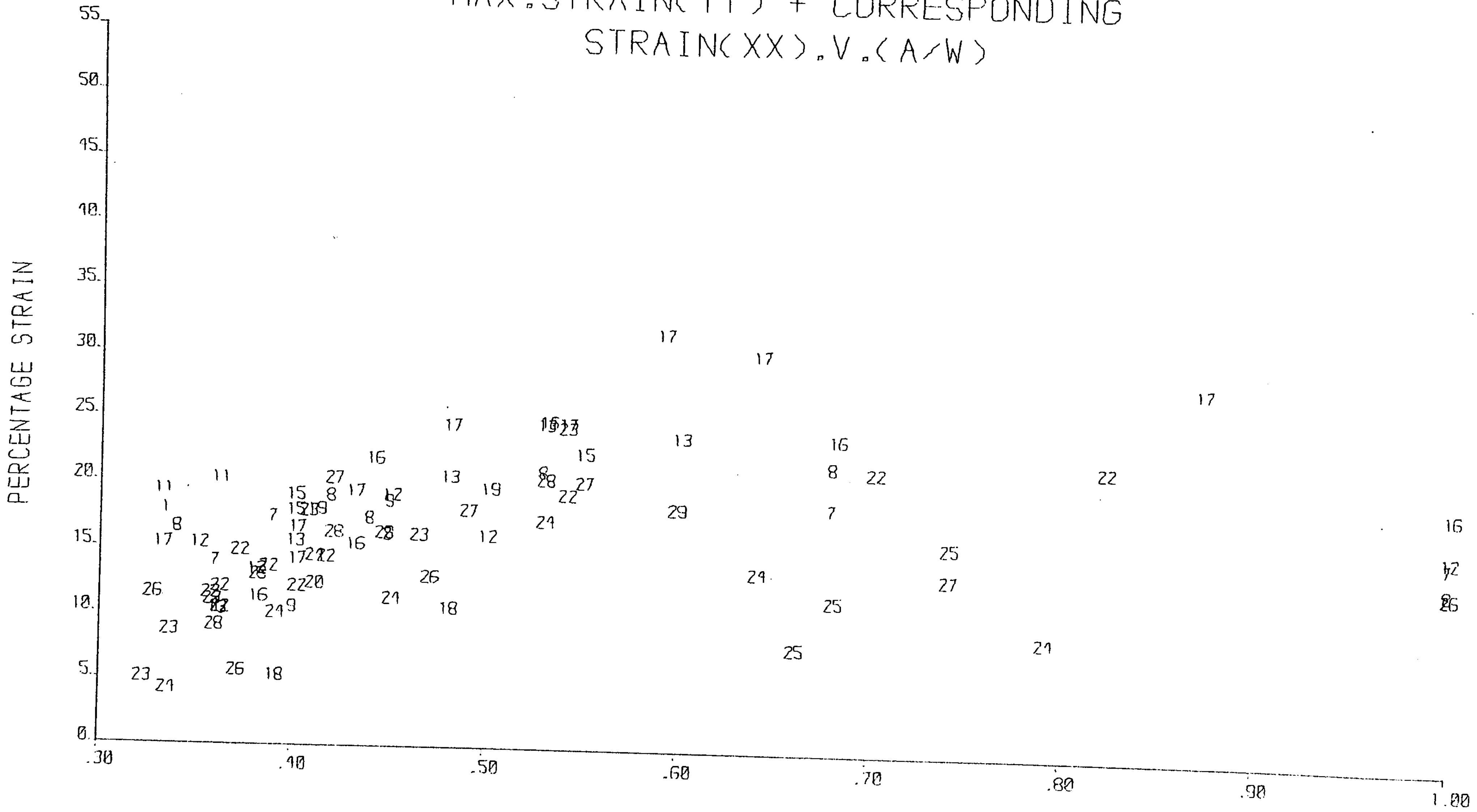

FIG. 4.18.e

FRACTIONAL DEVIATION FROM NORMAL POISSON CONTRACTION IN X-DIRECTION

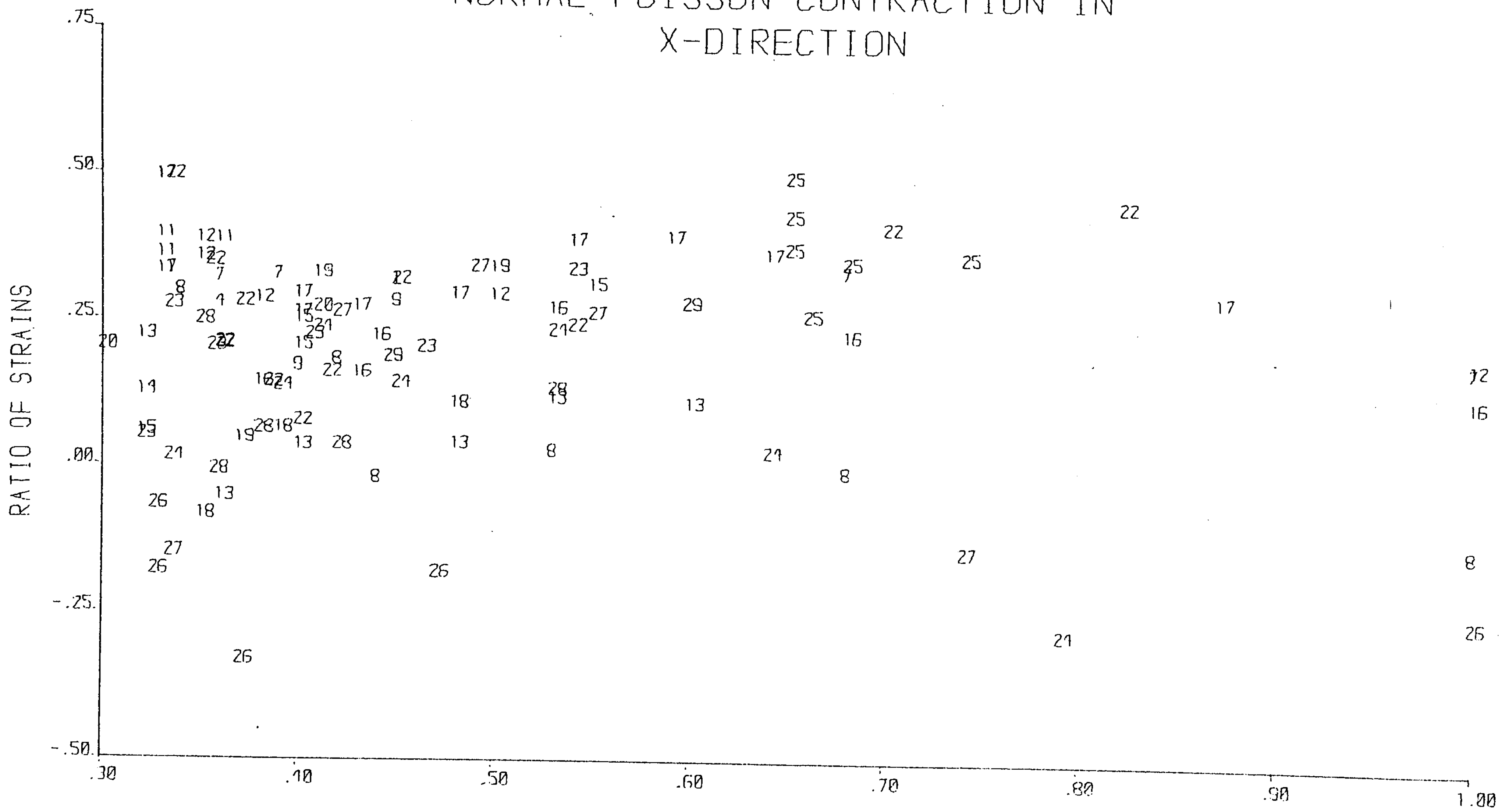

FIG.4.18.f

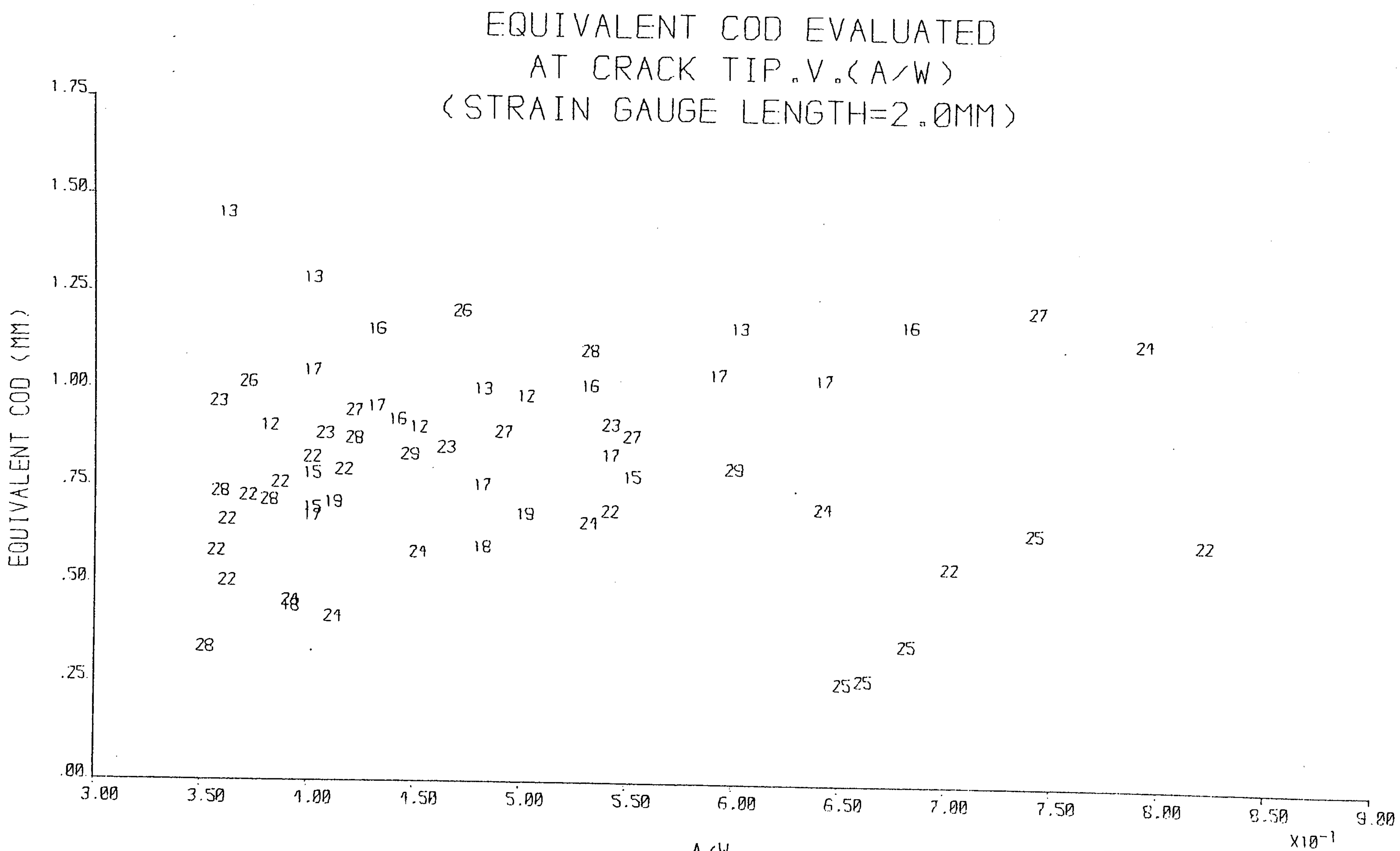
EQUIVALENT COD EVALUATED
AT CRACK TIP.V.(A/W)
(STRAIN GAUGE LENGTH=2.0MM)
EQUIVALENT COD (MM)
1.75
1.50
1.25
1.00
.75
.50
.25
.00
3.00
3.50
4.00
4.50
5.00
5.50
6.00
6.50
7.00
7.50
8.00
8.50
9.00
X10^-1
A/W

FIG.4.18g(i)

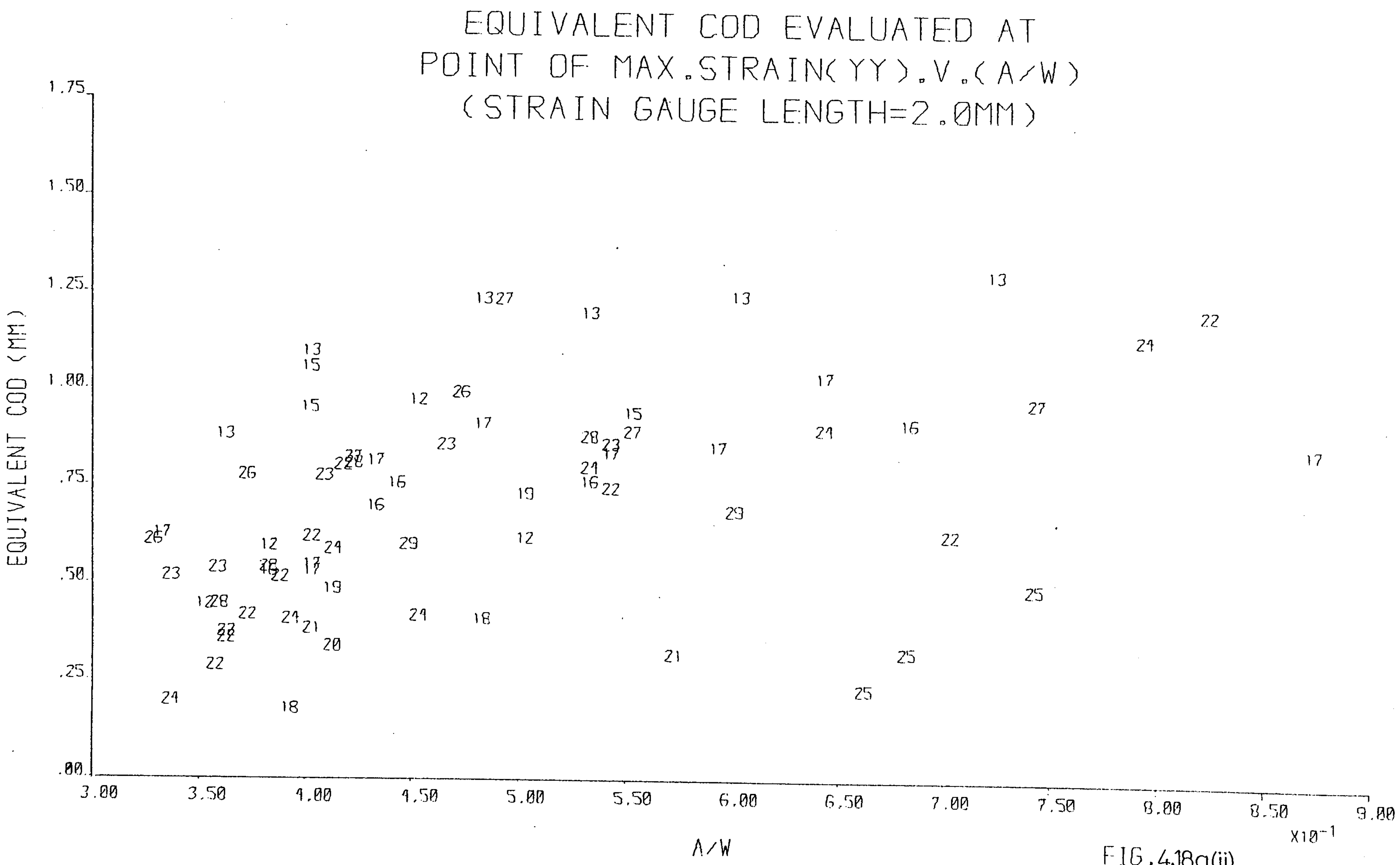
EQUIVALENT COD EVALUATED AT
POINT OF MAX.STRAIN(YY).V.(A/W)
(STRAIN GAUGE LENGTH=2.0MM)
EQUIVALENT COD (MM)
A/W
X10^-1

FIG.4.18g(ii)

SCHEMATIC REPRESENTATION
OF GEOMETRY DEPENDANCE
OF STRAIN(YY) VALUES

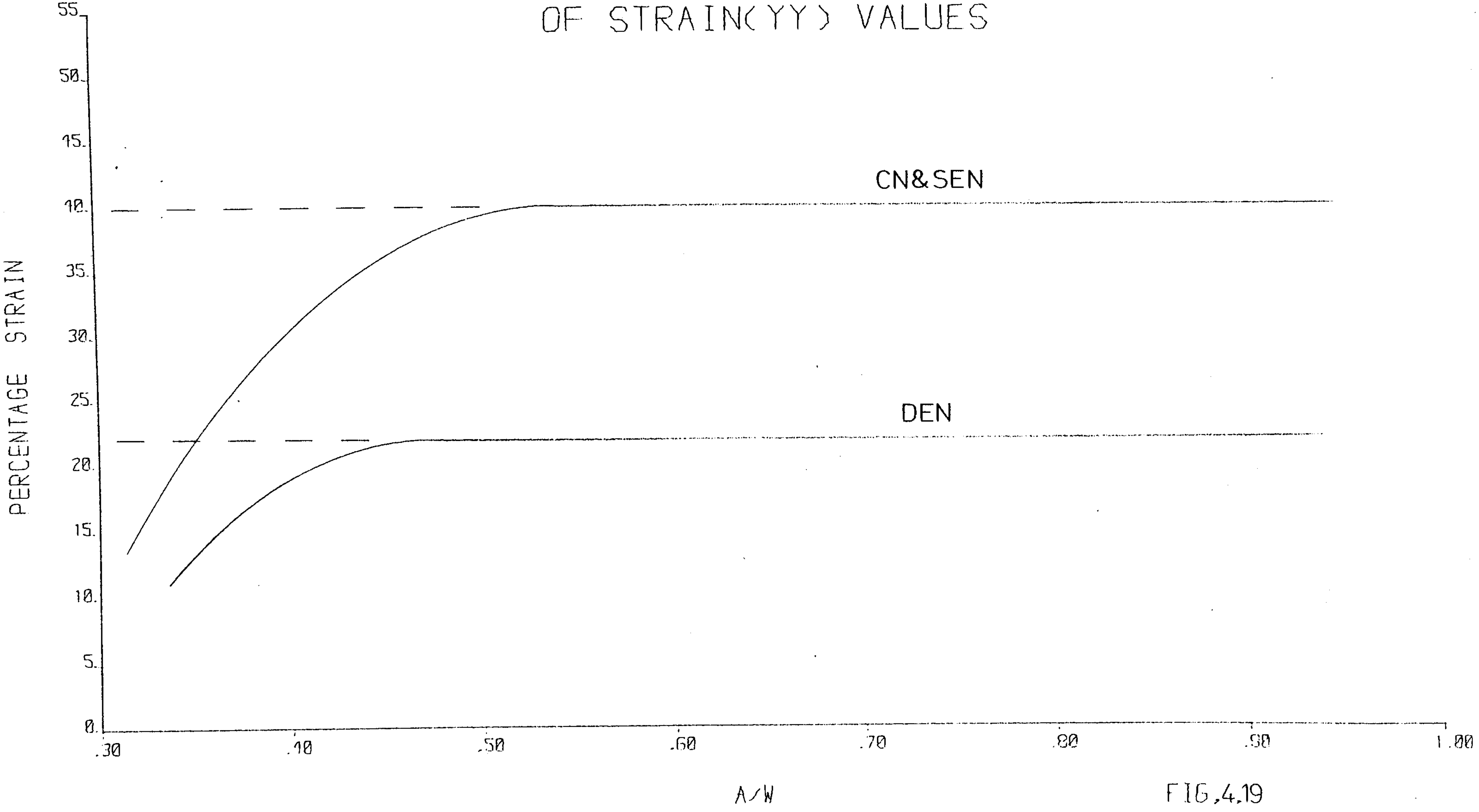

FIG.4.19

D-Point Strain for each position of the crack tip

The value of the strain at the D-Point (the last point when approaching the crack tip to exhibit a negligible non-uniform strain contribution) was typically only a few percent lower than maximum value of ε_{yy} during growth and in the very early stages of the initiation period approximately coincident with the ε_{yy} value. The characteristics of the D-point strain with crack length and geometry consequently closely resemble those of the maximum ε_{yy} values. This means that the schematic Fig. 4.19 will also describe the variation in D-point strain.

Values of ε_{xx} at the location of maximium ε_{yy}

These strains were evaluated at a distance of between 1 and 1.5mm either side of the specimen XX centre line. This was necessary because deformation in the near tip region was normally too intense to permit the grid markings to be distinguished. Increasing the vertical distance above or below the XX centre line was observed to shift the displacement profile to a similar extent horizontally. Using this observation the gradient of displacement d_{xx} was evaluated between the locations of maximum ε_{yy} and the D-point in order to compensate for not evaluating the strain along the XX centre line.

As expected from visual examination of the deformed specimens these strain values proved highly geometry dependant. The DEN geometry produced only small values of ε_{xx} with the CN geometry tending to produce much larger values. The SEN geometry was less consistent than the other two showing some quite moderate ε_{xx} strains and some very large strain values, particularly at higher a/w values. The basic trend of large strains with CN and SEN specimens and small strains with DEN specimens was basically maintained, especially at higher a/w values.

Equivalent strain at the location of maximum ε_{yy}

The equivalent strain was calculated from the following equation;

$$\bar{\varepsilon} = (\tfrac{2}{9}(\varepsilon_x - \varepsilon_y)^2 + \tfrac{2}{9}(\varepsilon_y - \varepsilon_z)^2 + \tfrac{2}{9}(\varepsilon_z - \varepsilon_x)^2)^{0.5} \quad 4.25$$

The values of ε_{yy} and ε_{xx} used were those already considered. The values of ε_{zz} were calculated on the basis of constant volume.

$$\varepsilon_x + \varepsilon_y + \varepsilon_z = 0 \quad 4.26$$

$$\varepsilon_x + \varepsilon_y = -\varepsilon_z \quad 4.27$$

Whilst appreciating that constant volume in unlikely to be a totally valid assumption any deviation due to effects such as grain boundary cavitation should be small and elastic dilatation will be negligible. For this approach, only those sequences after which initiation was considered to have occurred were included. The results still show the geometry dependance indicated by Fig. 4.19, that is the DEN specimens tended to produce substantially smaller strains (around 24%) than the other two geometries (around 40%). The equivalent strain approach showed approximately the same difference in the level of strain between the geometries as the maximum ε_{yy} approach. However, the equivalent strain values were generally greater than the maximum ε_{yy} values by up to an additional 3% and there is some evidence of the DEN specimens showing a more consistent tendency for such an increase compared with the CN geometry. This would be consistent with the DEN geometry showing a greater degree of lateral constraint than the CN geometry.

Summation of maximum ε_{yy} with the corresponding value of ε_{xx} for each position of the crack tip

In this case the arithmetic sum of maximum ε_{yy} and correspond ε_{xx} values were plotted against the instantaneous position of the crack tip. Again only sequences after crack initiation had occurred were included in the analysis. At constant volume this summation will equal -1 times the through thickness strain ε_{zz}. This approach proved the most successful of all those considered so far in bringing the results of all three geometries into a single common band. That is, this parameter was the least geometry dependant of all those considered so far.

Behaviour for the CN and DEN geometries could basically be described as follows. Initiation occurred at a fairly low value of through thickness strain (computed for the position of maximum ε_{yy}, just ahead of the notch tip). As crack growth continued the through thickness strain corresponding to the instantaneous position of maximum ε_{yy} increased to around 20% ± 5 after a fairly short increment of crack growth and then stabilised around this value. It is possible that a small decrease in this strain value may occur in the very final stages of fracture but evidence at high a/w values is sparse due to ligament collapse.

Not all the results of the SEN geometry fell within the scatter band of the results of the other two geometries. This deviation was more pronounced at a/w values between 0.6 and 0.7. However the results of the SEN geometry fell on both sides of the scatter band for the DEN and CN specimens, indicating that this geometry does not radically differ in behaviour to the other two with respect of this parameter.

Deviation from normal Poisson contraction

Under conditions of uniaxial tension from a stress σ_{yy}, an isotropic material at constant volume would be expected to produce equal strains in the X and Z direction, both equal to -0.5 times the strain ε_{yy}. Deviation from this behaviour indicates that a constraint exists in either the X or Z direction or in both directions but of differing magnitudes. It has been observed that the CN and DEN geometries exhibit very different ε_{xx} behaviour. This indicates differing degrees of lateral constraint. Consider the deviation from Poisson behaviour in the contraction in the X-direction, assuming constant volume and plane stress conditions:

The contractional strain ε_{xx} under normal uni-axial conditions would be given by,

$$\varepsilon_{xx} = -0.5\varepsilon_{yy}$$

Therefore the deviation will be given by,

$$\varepsilon_{xx} -(-0.5\varepsilon_{yy})$$

As a fraction of ε_{yy} the deviation P_d will be given by,

$$P_d = (\varepsilon_{xx} + \varepsilon_{yy})/\varepsilon_{yy} \qquad 4.28$$

If the deviation P_d given by equation 4.28 is positive then a constraint to contraction in the X-direction exists. A value of P_d equals 0.5 indicates that ε_{xx} is zero so contraction in the width direction is fully constrained. A value of zero indicates no constraint to lateral contraction or that the stresses opposing contraction are equal in the X and Z-directions. A negative value of P_d will arise if ε_{xx} is greater than that expected from Poisson contraction. This would imply that the resistance to through thickness contraction is greater than the resistance to width contraction and the conditions are not those of plane stress.

This parameter P_d has been evaluated using the values of maximum ε_{yy} and the corresponding values of ε_{xx} considered above. The results are shown in Fig. 4.18f. The results show an expected geometry dependance, the CN geometry (both n values but excluding pre-strained specimens) gave an average value of the P_d deviation factor of +0.12 (standard error of mean 0.02) and for the DEN geometry under the same restrictions, an average fractional deviation of 0.29 (standard error of mean 0.01). The SEN geometry produced an intermediate value for the average P_d value of 0.26 (standard error of mean 0.04). With the DEN and CN geometries there was no definitely detectable change in the value of the deviation parameter with increasing a/w. With the SEN geometry there was some evidence to suggest that a decrease in width constraint occurred with crack growth, this would not have been unexpected for this geometry. Unfortunately the number of SEN specimens tested was too few to definitely confirm whether or not a trend really does exist.

Fractional deviation values less than zero indicates that the resistance to thickness contraction is greater than any resistance to width contraction. These particular instances may be indicative of inaccuracy but it was noticed that all the pre-strained specimens, particularly the high stress cases, showed a greater tendency for width contraction than thickness contraction during pre-straining. That is, without notches complicating strain behaviour. This was confirmed by both measurements from the grids and from measurements of the specimens with a micrometer after pre-straining.

The fractional deviation from normal Poisson behaviour P_d was used to estimate the constraint stress σ_{xx} operative in the CN and DEN specimens. This was done by use of the Hencky[188] equations for plasticity. Under steady state creep conditions for each single instance of time the creep and plasticity laws can be shown to be analogous:

$$\varepsilon = A'\sigma^n \qquad \text{Plasticity} \qquad 4.29$$

$$\dot{\varepsilon} = A\ \sigma^n \qquad \text{Creep} \qquad 4.30$$

$$\varepsilon = At\sigma^n \qquad \text{Creep} \qquad 4.31$$

Hence the creep and plasticity laws are analogous if:

$$A' = At \qquad 4.32$$

This approach is similar in result to application of the Hoff analogue in which a creep situation under steady state conditions can be shown to be analogous to the non-linear elastic solution.

The assumption of steady state conditions is considered in detail in section 4.2.3.2. The validation of this assumption was particularly important in this section for the analysis of the variation of strain with distance from the crack tip.

For the CN and DEN geometries the fractional deviation from Poisson behaviour was observed to remain approximately constant throughout a test. This indicated that the applied tensile stress and the constraint stress (or stresses) remained in an approximately fixed proportion during initiation and growth. This observation enabled direct application of the plasticity equations to the creep case. Creep strain is given by the summation of a function of the stress for each instance of time, whilst the strain under plastic conditions is basically governed by the maximum level of stress attained.

$$\varepsilon_{creep} = \int_0^t A\sigma^n.dt \qquad 4.33$$

$$\varepsilon_{plastic} = A'\sigma^n_{max} \qquad 4.34$$

The problem of strain accumulation is hence considerably simplified if the ratio of the stresses under biaxial loading can be considered constant.

The Hencky equations assume the material to be homogeneous and isotropic so that the axis of principal stress and strain coincide. This should be reasonably true for the material over which the strains were measured but some cavitation may have been present. Proportional loading is also a requirement for the application of the Hencky equations. On the basis of the observation of approximately fixed proportionality between ε_{xx} and ε_{yy} for a given specimen, it was assumed that this requirement was satisfied.

$$\text{Let } \alpha = \frac{\sigma_2}{\sigma_1} \text{ and } \beta = \frac{\sigma_3}{\sigma_1}$$

Then

$$\varepsilon_1 = \left(\frac{\sigma_1}{C}\right)^{1/n'} \left(\alpha^2 + \beta^2 - \alpha\beta - \alpha - \beta + 1\right)^{(1-n')/2n'} \left(1 - \frac{\alpha}{2} - \frac{\beta}{2}\right) \quad 4.35$$

$$\varepsilon_2 = \left(\frac{\sigma_1}{C}\right)^{1/n'} \left(\alpha^2 + \beta^2 - \alpha\beta - \alpha - \beta + 1\right)^{(1-n')/2n'} \left(\alpha - \frac{\beta}{2} - \frac{1}{2}\right) \quad 4.36$$

$$\varepsilon_3 = \left(\frac{\sigma_1}{C}\right)^{1/n'} \left(\alpha^2 + \beta^2 - \alpha\beta - \alpha - \beta + 1\right)^{(1-n')/2n'} \left(\beta - \frac{\alpha}{2} - \frac{1}{2}\right) \quad 4.37$$

Where $n' = 1/n$

$c = \sigma/\varepsilon^{n'}$

Let R equal the ratio of $\varepsilon_{yy}/\varepsilon_{xx}$ i.e $\varepsilon_{yy} = R\varepsilon_{xx}$ 4.38

Thus

$$R\left(\alpha - \frac{\beta}{2} - \frac{1}{2}\right) = \left(1 - \frac{\alpha}{2} - \frac{\beta}{2}\right) \quad 4.39$$

Assuming plane stress conditions $\beta = 0$

$$R(\alpha - 0.5) = \left(1 - \frac{\alpha}{2}\right) \quad 4.40$$

$$\alpha = (1 + R/2)/(R + 0.5) \quad 4.41$$

Now consider the P_d value of 0.12 for the CN geometry and 0.293 for the DEN geometry. For unit strain in the Y-direction these deviations correspond to values of E_{xx} as follows:

$\varepsilon_{xx} = -0.5 + 0.12 = -0.38$ for the CN case

$\varepsilon_{xx} = -0.5 + 0.293 = -0.207$ for the DEN case

These correspond to R values of -2.63 and -4.83 respectively. Substitution in equation 4.41 produced the following values of α for the CN case 0.148 and for the DEN case 0.327. The SEN case has not been considered because it is expected that the degree of constraint may change significantly with crack growth for this geometry. The α values calculated correspond to:

$$\sigma_{yy} = 6.75\sigma_{xx} \text{ for the CN case}$$

$$\sigma_{yy} = 3.06\sigma_{xx} \text{ for the DEN case}$$

That is, if the use of the Hencky equations is permissible under the conditions considered, the DEN geometry produces a constraint to lateral contraction at the point where maximum ε_{yy} is observed over twice that observed in the CN geometry and equal to almost one third of the applied tensile stress at this point. Introducing a small through thickness constraint such that $\beta = 0.05$, then using the same values of R in equation 4.39:

$$\sigma_{yy} = 5.26\sigma_{xx} \text{ for the CN case}$$

$$\sigma_{yy} = 2.75\sigma_{xx} \text{ for the DEN case}$$

That is, the DEN geometry still shows around twice the lateral constraint seen with the CN case.

Crack Opening Displacement

It has been shown from the grid analysis that displacements near the crack tip, that is closer than the D-point, result from the combination of a uniform strain ε_{yy} and a non-uniform displacement I. The total displacement d along any vertical line across the XX centre line is given by:

$$d = I + H\varepsilon_{yy} \qquad 4.42$$

Where H = operative gauge length

The exact position at which the COD should be evaluated is open to some debate. The crack tip is initially the most obvious location. However, at this location the material is being observed in its final stage of a necking process and observations at this position would be unlikely to provide much insight into the controlling criteria for crack advance. The D-point marks the location of the onset of the non-uniform contribution which appears to arise from localised necking. The onset of this non-uniform contribution to displacement could be considered to represent the onset of the final failure process. The D-point is hence another position at which evaluation of the COD should be considered. A third possibility is the position at which ε_{yy} reaches its maximum value. The position of maximum ε_{yy} is roughly midway between the crack tip and the D-point. The summation of ε_{yy} and ε_{xx} at this point has already been shown to represent a good criterion for the crack advance in all three geometries. Also failure criteria for sheet forming under biaxial tension have shown that the onset of failure is started by the formation of a groove, but ultimate failure is controlled by the strain in the bulk sheet after the initial formation of this groove.[189] Hence the use of the position of maximum ε_{yy} for evaluating the COD has some justification.

Moving from the D-point to the position of maximum ε_{yy} and on to the crack tip the contribution of the non-uniform deformation to the COD value will be increasing in importance.

It is unlikely that all the displacement described by equation 4.42 for any one of these three locations could be described as the true COD as some of the displacement may occur outside the region bounded by the flanks. However, it seems reasonable to propose that the true COD may show some degree of proportionality to a quantity evaluated on this basis. Evaluations based on equation 4.42 shall be referred to as equivalent COD values. The main problem with this approach is in specifying the length of the gauge length H. For equivalent COD values at the D-point the gauge length is unimportant provided that it may be considered constant during crack growth. If H is constant then the equivalent COD is simply proportional to the D-point strain as the value of I is zero. This means the COD will be strongly geometry dependant as shown in Fig. 4.18b and schematically in Fig. 4.19. As the non-uniform displacement is only observed near the crack tip, this region can be considered similar to a plastic zone under LEFM conditions. If this zone can be considered circular then the non-uniform contribution can be considered to occur over a distance equal to the distance of the crack tip from the D-point. It would seem logical to adopt this length for the gauge length H for equivalent COD evaluations at both the crack tip and region of maximum ε_{yy}. For the CN and DEN specimens this distance was found to be approximately equal to 2mm. Equivalent COD values using a gauge length of 2mm are shown in Fig. 4.18g(i) for the crack tip position and Fig. 4.18g(ii) for the position of maximum ε_{yy}. Only cases for which initiation was considered to have occurred have been included.

Approaching the crack tip from the D-point the non-uniform displacement contribution to the equivalent COD becomes progressively more dominant and there is a marked decline in the geometry dependance of the COD values obtained. However even at the crack tip there was some evidence of slightly larger displacements with the CN specimens. The basic trends of the equivalent COD evaluations made at the crack tip and at the position of maximum ε_{yy} were similar.

As with the plots of maximum ε_{yy} and D-point strain etc. there was evidence of an initial increase in equivalent COD over the first 0.05a/w of crack growth. After this initial increase there was little further change in the equivalent COD values.

Although comparatively geometry independant the equivalent COD based on crack tip measurements is not considered a good criterion on which to assess crack advance. It appears that the geometry independance of this equivalent COD value at this position is due to the geometry independance of the necking phenomenon masking a geometry dependant uniform strain. This uniform strain will be the more useful description of the imminence of failure. Numerical techniques for predicting crack growth on the basis of stress and strain computations will be more able to deal with a critical uniform strain than a displacement arising from local necking.

It is interesting to note that the equivalent COD values at the crack tip, typically somewhat less than 1mm, are in fact smaller than initiation COD values estimated from measuring the opening of the notch flanks. These estimates are listed in Table 4.5 and were made by measuring the notch flank opening from photographs. This technique proved to open to a degree of personal interpretation and the results are only considered suitable for comparison with the equivalent COD values. For some specimens estimations of the COD values during growth were made by projecting the lines of the notch flanks forward to the position of the instantaneous crack tip and measuring the separation. Examples of the COD estimations made in this manner for a DEN and CN specimen are shown in Fig. 4.20 . For both geometries the estimated COD increases with crack length to an unrealistically high figure. The difference in the COD behaviour during growth

ESTIMATIONS OF COD FOR INITIATION

(FROM NOTCH FLANK OPENING)

SPECIMEN NUMBER	COD (mm)
7	1.7
8	2.6
9	2.5
11	2.0
12	2.2
13	2.5
16	2.2
17	1.5
18	1.0
19	1.3
22	1.3
23	1.0
24	1.4
25	1.6
26	2.0
28	2.2
29	1.2

TABLE.4.5

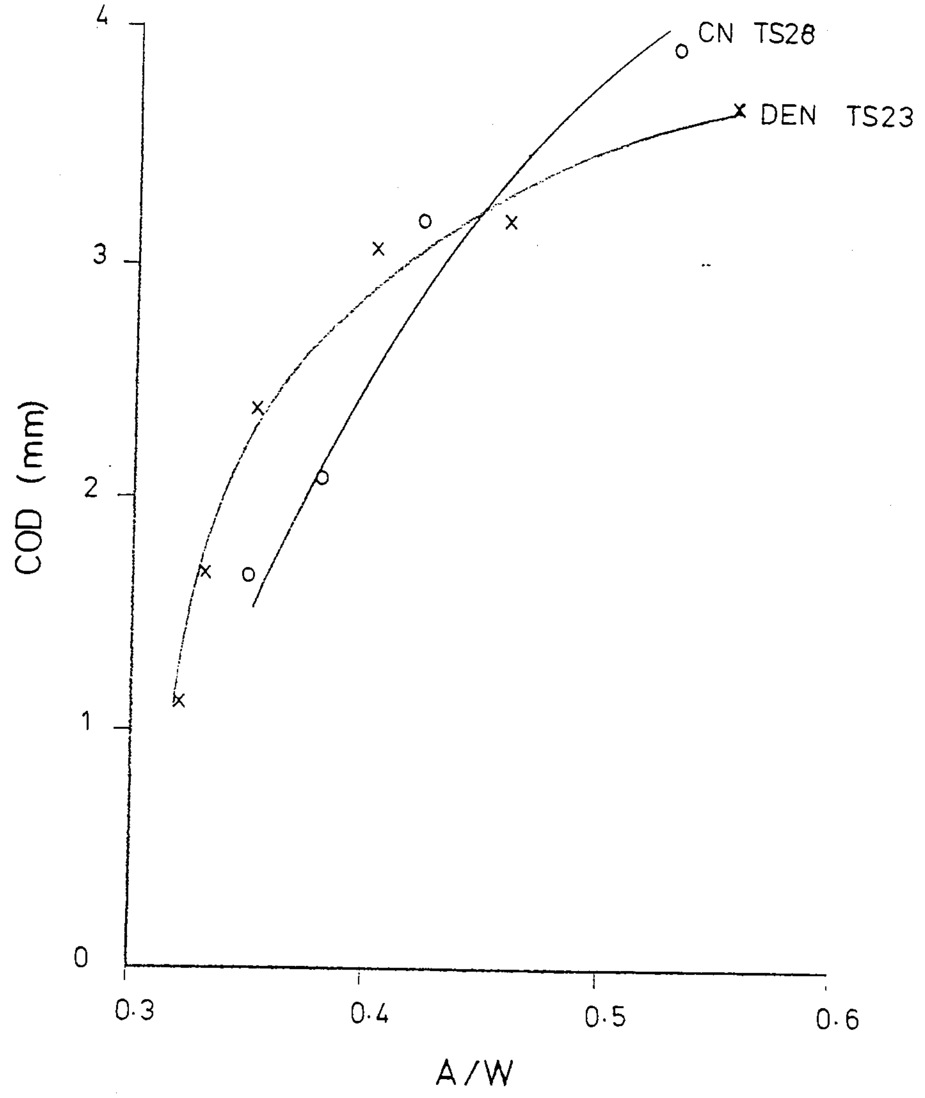

EXAMPLES OF COD VALUES ASSESED
FROM NOTCH MOUTH OPENING

FIG.4.20

depending on whether the evaluation of the COD is made by the notch flank projection method or by an equivalent COD approach is discussed in section 5.2.

Effect of test variables on major strain observation

The effect of basic specimen geometry (DEN, CN or SEN) has already been considered in the analysis of the major strain observations. The effect of some other variables will now be summarised. These variables include

stress level

thickness

creep pre-strain

notch root radius

starter notch length

Stress Level

There is little evidence to suggest that the level of the applied starting stress caused any significant effect on the magnitude of the strains observed. No changes correlating with starting stress level were detected in the equivalent COD values. This was also basically true of the values of the deviation from normal Poisson behaviour. However, it was noticed that the high stress pre-strained specimens TS 18 and 26 could account for a large proportion of the negative values for this parameter.

Test Specimen Thickness

The maximum values of ε_{yy} obtained for a DEN and CN specimen from each of the three thicknesses of sheet used are shown in Fig. 4.21. No definite trend with thickness could be identified from this figure. This is also basically true for the corresponding values of ε_{xx} but

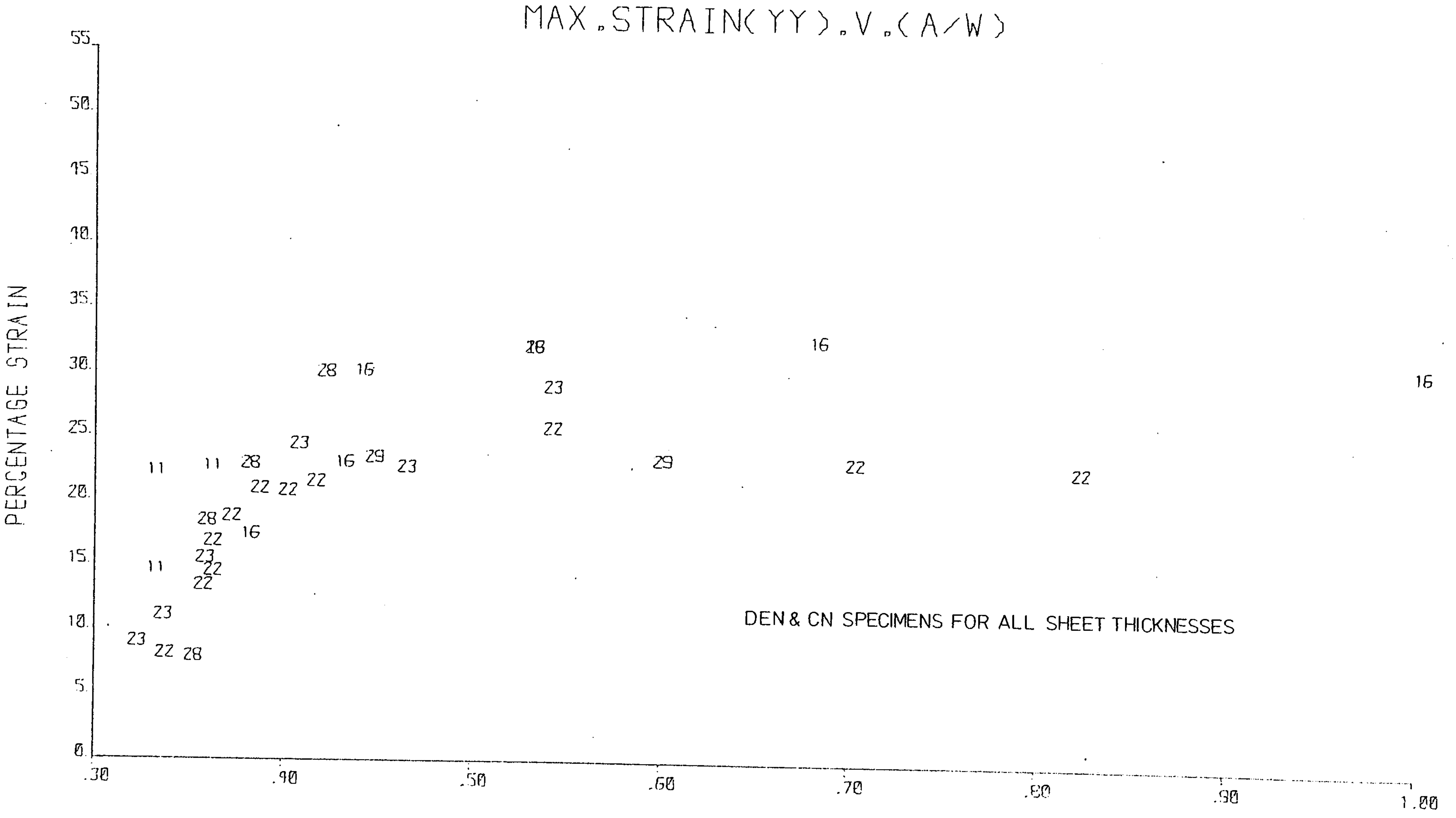

MAX.STRAIN(YY).V.(A/W)
PERCENTAGE STRAIN
A/W
DEN & CN SPECIMENS FOR ALL SHEET THICKNESSES

FIG. 4.21

trends with this parameter appear less easy to identify. The results of the 1.6mm specimens and the 6.2mm specimens all fall in the general scatter band of results for the summation of ε_{yy} and ε_{xx}. A trend for the thicker specimens to show a lower deviation from normal Poisson contraction than their thinner counterparts could exist. The significance of the observation is doubtful as the variation in P_d is not sufficient to cause the results of these specimens to deviate from the general band of scatter. The equivalent COD is the only parameter considered that is not calculated entirely from ε_{yy}, ε_{xx} or both. The equivalent COD values were free from any detectable correlation with thickness once crack growth was established but the equivalent COD values at the crack tip for the thicker specimens TS22 and 28 were lower than average during the very early stages of growth.

Creep Pre-Strain

These specimens would be expected to show a deviation from the normal ε_{xx} behaviour for their respective geometries due to the lack of constraint from the notches during pre-straining. This was particularly noticable for TS26 which was of the CN geometry and extensively pre-strained (14.3%). The results of the summation of the maximum value of ε_{yy} and the corresponding value of ε_{xx} for these specimens fell close to the results for the specimens that had not been pre-strained. This would not be the case if only that strain accumulated after pre-straining was considered.

Notch Root Radius

The principal effect of increasing notch root radius appeared to be a reduction in the lateral constraint during initiation and in the first stages of crack growth, but the effect appeared to become fairly insignificant after a short length of crack is established. The reduction in lateral constraint was apparent from the three specimens with very large root radii all showing larger value of ε_{xx} and smaller values of P_d than was typical for their respective geometries. However, on the basis of the sum of the ε_{yy} and ε_{xx} strains the behaviour of these specimens was consistent with that shown by the other specimens.

Starter Notch Length

One specimen TS25 was tested with starter notch lengths corresponding to 0.65 a/w as opposed to around 0.33 a/w. During initiation this specimen exhibited an above average deviation from normal Poisson behaviour. As crack growth became established in this specimen all the strain parameter values and the equivalent COD values were observed to approach those typical for the DEN geometry. Unfortunately ligament collapse occurred in this specimen after only a short interval of crack growth.

4.2.3.2 Strain Profile Analysis

In order to predict the rate of advance of a creep crack in a material it will be necessary to know the criteria controlling crack advance and also the nature of the stress distribution ahead of the crack tip. This will enable an estimate to be made of the rate at which the criteria controlling crack advance are satisfied.

Functions predicting the variation of stress with distance from the tip of a creep crack have been proposed as follows (see Section 2.4.2)

$$\sigma \propto x^{-(1/2n)} \qquad 4.43$$

$$\sigma \propto x^{-(1/n+1)} \qquad 4.44$$

From Nortons law it can be seen that these relationships correspond to:

$$\dot{\varepsilon} \propto x^{-(n/2n)} \qquad 4.45$$

$$\dot{\varepsilon} \propto x^{-(n/n+1)} \qquad 4.46$$

It was decided to compare the strain behaviour of ε_{yy} observed in practice with that predicted from these relationships. The strain distributions considered were those profiles of strain versus distance derived from the analysis of the specimen grids. Only that part of the experimental profile further from the crack tip than the D-point was considered suitable for analysis. This excluded the immediate near tip region and also ensured that the uniform strain could describe all the creep deformation observed at each point considered. During the very early stages of a test the D-point would tend to be close to the position of maximum ε_{yy}. In such cases the analysis only included that part of the strain profile for which there was a continued increase in the rate of change of strain with distance, approaching the crack tip.

Usually only a section of profile covering a distance of 6mm was analysed. Theoretical analyses of problems of a similar type have been considered to apply for a distance d, approximately equal to either one half of the crack length or one half of the remaining ligament length, which ever is shorter.[183] The minimum value of d seen during a test between 0.33 and 0.7 a/w equals 6.8mm for the SEN case and 3.4mm for the DEN and CN geometries. Hence for the latter two cases 6mm exceeds the minimum value of d, but it was considered necessary to use a section of profile around this length in order to obtain a representative impression of the strain distribution. Experimental strain profiles for high a/w values, where compliance with this requirement is likely to be more important due to edge effects or interacting stress profile effects, are in the minority for both the DEN and CN cases.

The theories proposing stress distribution of the type to be considered require the material to be deforming under steady state conditions. It has been assumed that this is the case at all times in this work. This assumption of steady state was made on the basis of two observations. Firstly, the distribution of the difference in strain between sequential strain profiles were plotted out against distance from the specimen YY centre line. These strain difference values were then normalised so that the mid-range value for each profile was the same. It was then observed that for a given specimen these profiles were all of a similar shape. By moving the profiles in a horizontal direction (along the distance axis) all but the profiles from very high a/w values would approximately superimpose. Examples from sample specimens are shown in Fig. 4.22. As can be seen the superimposition would not be perfect but is considered a reasonable indication of steady state deformation, especially when account is taken for the fact that each strain difference profile covers different intervals of crack growth and time. Also this approach is compounding the errors of two experimental profiles in each case. If an error of say , +2 on the percentage strain distibution was carried over to the strain diference distribution it would represent a considerably larger fractional error here than with the original strain distribution. Consideration of these factors has in fact necessitated a rather indirect means of analysing the strain profiles observed during growth.

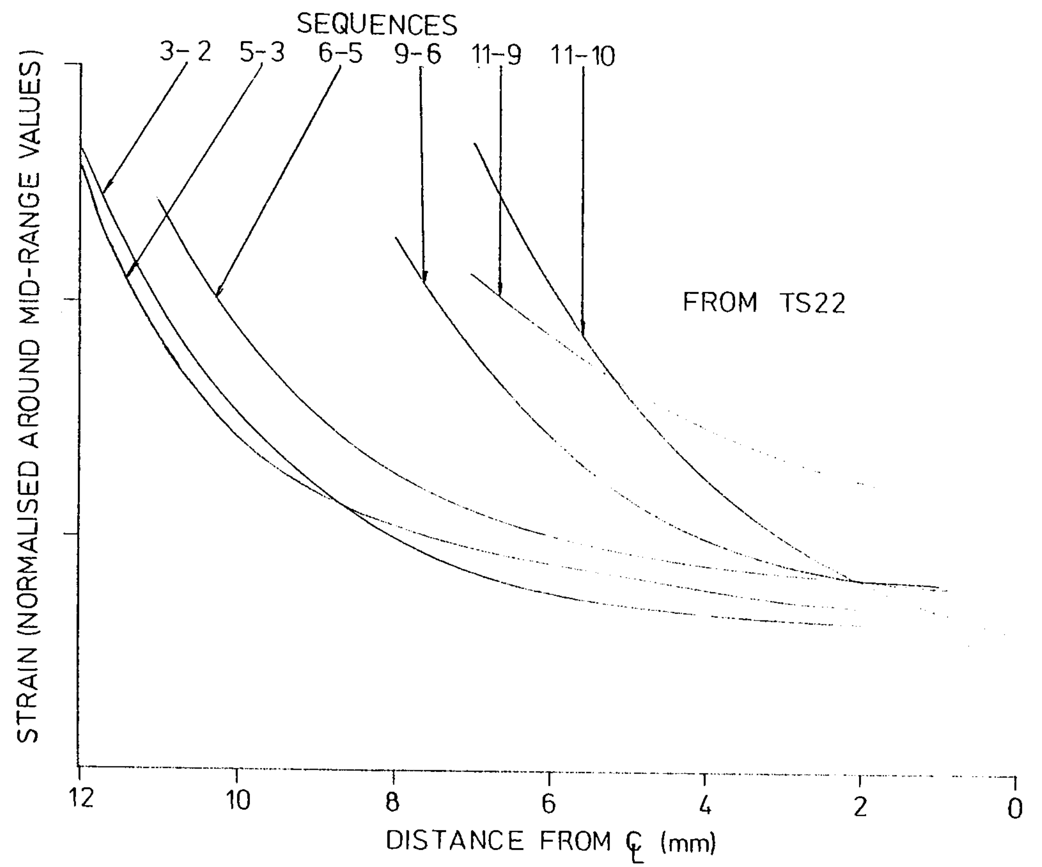

DIFFERENCE IN STRAIN PROFILES
FOR SUCCESSIVE TIME SEQUENCES
(TYPICAL EXAMPLE)

FIG.4.22

The second observation supporting the general assumption of steady state deformation is from the results of the smooth bar creep tests shown in Table 4.1. The results of these tests indicated that the interval over which the primary creep regime was observed represented less than 20% of the typical notched rupture test initiation time for the respective starting stress levels. Also the contribution to the creep deformation resulting from the primary regime, additional to the strain that would have been accumulated if deformation was entirely of the type seen during the secondary regime, was small. This contribution was less than 1% for a starting stress of $5MNm^{-2}$ and around 4% for a starting stress of $20MNm^{-2}$. In addition, the variation in the contribution from the primary creep regime over the stress gradient expected would be compatible with, or less than, the experimental error.

Elastic strains have been neglected throughout. The Young's modulus of Magnox AL80 at the test temperature of $300^{\circ}C$ is given[11] as approximately $35GNm^{-2}$. Hence, even a stress of $35MNm^{-2}$, close to the short term UTS of the material at this temperature, would produce an elastic strain of only about 0.1%.

The analysis of the experimental strain profiles was split into two parts, i) initiation ii) during growth, the latter between 0.35 and 0.7 a/w as it was considered doubtful that near steady state conditions could prevail at higher values of crack length and crack growth rate.

Initiation

In elastic-plastic fracture mechanics the presence of a plastic zone displaces the origin of the σ_{yy} stress distribution from the crack tip to the mid point of the plastic zone. As the presence of a non-uniform deformation zone has been observed for all specimens, in all sequences, it was considered probable that such a displacement may occur here as well. This means that it cannot be assumed that the position of x=0 for the stress distribution is located at the crack tip.

During initiation it can be considered that the stress distribution will be stationary and hence the function describing strain rate will also describe strain. To compensate for the uncertainty in the position corresponding to x=0 for the stress and strain rate distributions, the strain dependance on distance was evaluated for a range of positions of x=0, see Fig. 4.23. Regression analysis of log.ε versus log. distance from the present position of x=0 were performed. The positions of x=0 were recorded for which correlations were obtained corresponding to the following:

$$\varepsilon \propto x^{-(1/2)} \qquad 4.47$$

$$\varepsilon \propto x^{-(n/n+1)} \qquad 4.48$$

The results are shown in Table 4.6 and can be summarised as follows. Normally good correlations were obtained with both strain dependancies on x. (i.e. regression coefficients better than 0.96 absolute). The position of x=0 for the correlation for the exponent equal to -(1/2). Equation 4.47, averaged 1.78mm from the crack tip (standard error of the mean 0.18). The correlations for the -(n/n+1) exponent and equation 4.48, averaged 0.97mm from the crack tip (standard error of the mean 0.21).

<u>Growth</u>

Analysis of the strain distributions observed during crack growth

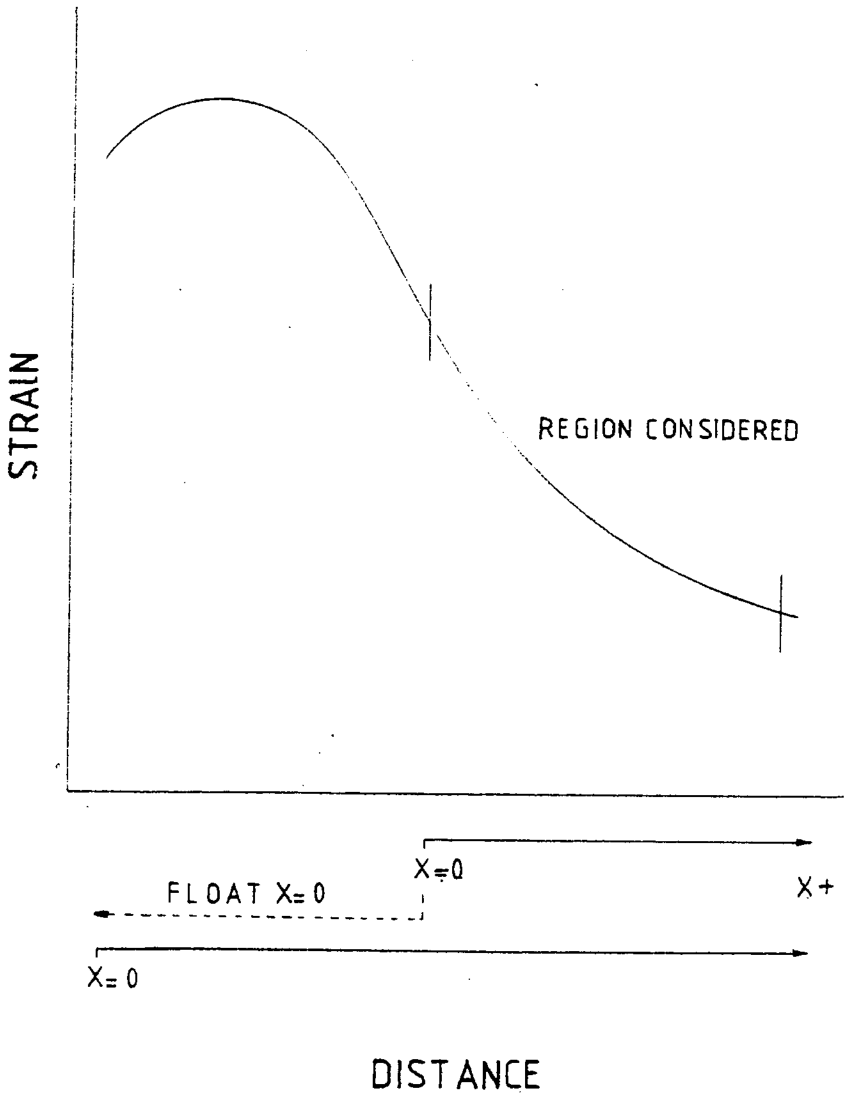

SCHEMATIC REPRESENTATION OF
ASSESSMENT OF STRAIN
DISTRIBUTION

FIG.4.23

TABLE OF STRAIN DISTRIBUTION CORRELATIONS DURING INITIATION

SPEC.	SEQU.	DISTANCE OF POINT x=0 AHEAD OF NOTCH TIP	
		$\varepsilon \propto x^{-(n/2n)}$	$\varepsilon \propto x^{-(n/n+1)}$
9	2	2.4	1.14
10	2L	0.6	0.24
10	2R	1.82	0.9
11	2	1.2	0.4
12	2	0.86	/
12	3-2	/	1.26
13	2	2.22	0.72
13	3	1.4	/
13	3-2	1.8	/
14	2R	2.4	0.
14	2L	2.2	0.24
15	2	0.63	/
16	2	2.26	0.26
16	3	2.8	0.4
16	3-2	2.52	0.
17	3-2	2.64	1.24
17	4	/	2.64
17	5	/	3.2
17	5-4	/	3.2
19	3-PS	1.66	0.
22	3	0.5	/
22	3-2	/	0.75
23	2	0.75	/
24	2	/	1.7
25	3	1.25	0.3
25	4	0.3	/
25	3-2	1.5	0.25
26	3-PS	2.0	1.5
27	2	4.2	1.9
28	2	2.0	0.

TABLE.4.6

was less simple than for during initiation. The creep crack growth tests were conducted under constant load conditions and hence the nett section stress increased as the crack grew. Also, as the crack tip moved, the position corresponding to x=0 for the stress distribution would also advance. Hence, at any stage during crack growth the strain profile observed had accumulated according to a range of positions for x=0. Arising from this, direct regression analysis of strain profiles observed during growth would not give a true indication of the instantaneous strain rate dependance upon distance. Subtracting consecutive strain profiles was not considered a feasible method of overcoming this problem. For there to be sufficient strain difference between the profiles for accurate analysis a fairly substantial time interval would have to elapse, with an associated increase in crack length and change in position of x=0. Also as mentioned in the verification of steady state conditions earlier, the subtraction of sequential strain distributions would compound the errors of both the profiles under consideration.

The simplest way in which to determine whether the observed strain distributions resembled those expected from a stress distribution of the type shown in either equation 4.43 or 4.44 was to compare experimental strain profiles with profiles derived theoretically for these two stress distributions.

Theoretical strain profiles were computed by the method shown schematically in Fig. 4.24. A profile representing the typical accumulation of strain just after crack initiation was required. Rather than using a theoretically derived profile for this purpose it was considered preferable to average several suitable experimental strain profiles. This should ensure that the theoretically derived accumulation of strain with crack growth started from as realistic initiation strain distribution as possible. The following profiles were used to construct this composite starting profile:

specimen	sequence
8	2
12	3
13	3
22	3
23	3&4
28	3

These profiles were all beyond initiation and were between 0.34 and 0.36 a/w. The composite profile resulting from averaging the above profiles is shown in Fig. 4.25. It is considered that this profile is fairly typical of that which would be observed with either a CN or a DEN specimen at 0.35 a/w from either exponent level. This profile was not typical of that expected for the SEN geometry. For this geometry experimental profiles from TS17 and 24 were used according to the creep exponent level (n=3.5 for TS17 and n=7 for TS24).

An equation relating crack length to time was required. Relationships predicting crack growth rate from the nett section stress were used to derive crack length/time relationships in the same manner as in section 4.2.2.2. The values of the exponent used in the crack growth law were the same as applied for Nortons law and the following damage corrections were included:

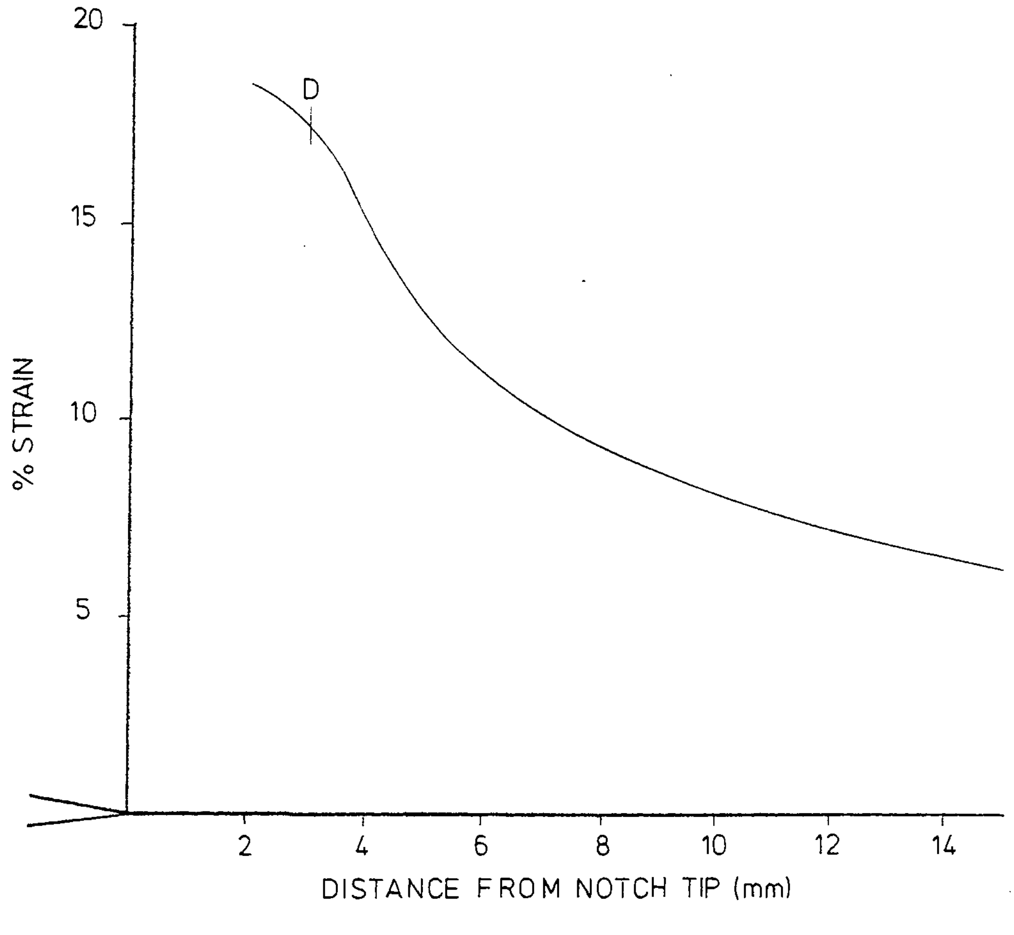

STRAIN PROFILE USED FOR START
OF NUMERICAL INTE~~R~~GRATION

FIG.4.25

SEN geometry	n=3.5 & n=7	no damage correction
CN & DEN	n=3.5	0.29 a/w equivalent damage at 0.7 a/w(none at 0.35 a/w)
CN & DEN	n=7	0.1 a.w equivalent damage at 0.7 a.w(none at 0.35 a.w)

These relationships were used only because experimental results indicated that they gave a reasonable representation of experimental behaviour.

Now consider the actual process of numerical integration by which the theoretical accumulated strain profiles were produced. For the SEN case the ligament considered represented the entire specimen width. For the DEN and CN geometries the ligament considered in the theoretical analysis represented only half of the specimen width, from an edge to the YY centre line. The theoretical ligament was divided into 45 points, that is, each spaced at 0.5mm for the DEN and CN geometries and at 1mm intervals for the SEN geometry.

The crack growth from 0.35 to 0.7 a/w was originally performed in 100 steps but for cases of n=7 substantial growth was occurring for each time interval at the high a/w values. It was decided to reduce the step size from unity to 0.25 (400 steps) to overcome this problem. This step size was standardised upon despite the observation that the larger step size caused only minor differences in the strain profiles produced, and then only for large values of a/w.

Initially the strain integration was performed with the position of x=0 for the stress distribution at the calculated location of the crack tip for that instance of time. For each step in time, stress values were calculated for each point across the ligament from a distance corresponding to 1mm immediately ahead of the position of x=0. This was done using both the equations predicting the distribution of stress with distance from the crack tip, i.e.

$$\sigma \propto x^{-(1/2n)} \tag{4.43}$$

$$\sigma \propto x^{-(1/n+1)} \tag{4.44}$$

where x=0 at the crack tip

These stress values were then scaled so that their sum across the ligament for each of the stress distributions was equal to a constant. Neglecting the 1mm region ahead of the x=0 position this simulated constant load conditions. Using the scaled stress values, and Norton's law, the strain accumulated for that time step at each point was calculated and summed to that already accumulated there. The constant in Norton's Law was set so that the value of the accumulated strain at 2 points from the position of x=0 was typical of the D-point strains seen in practice. The crack length corresponding to the next step in time was then calculated and the entire process repeated. This continued until a crack length of 0.7 a/w was obtained.

The entire operation was repeated with the position of x=0 for the stress distributions displaced ahead of the crack tip by 1mm. Examples of the strain profiles resulting from these numerical integrations for which the position of x=0 was displaced by 1mm from the crack tip are shown in Fig. 4.26.

A criterion was required on which to compare the theoretical and experimental accumulated strain profiles. The need to produce the theoretical profiles arose because during growth the strain at a point

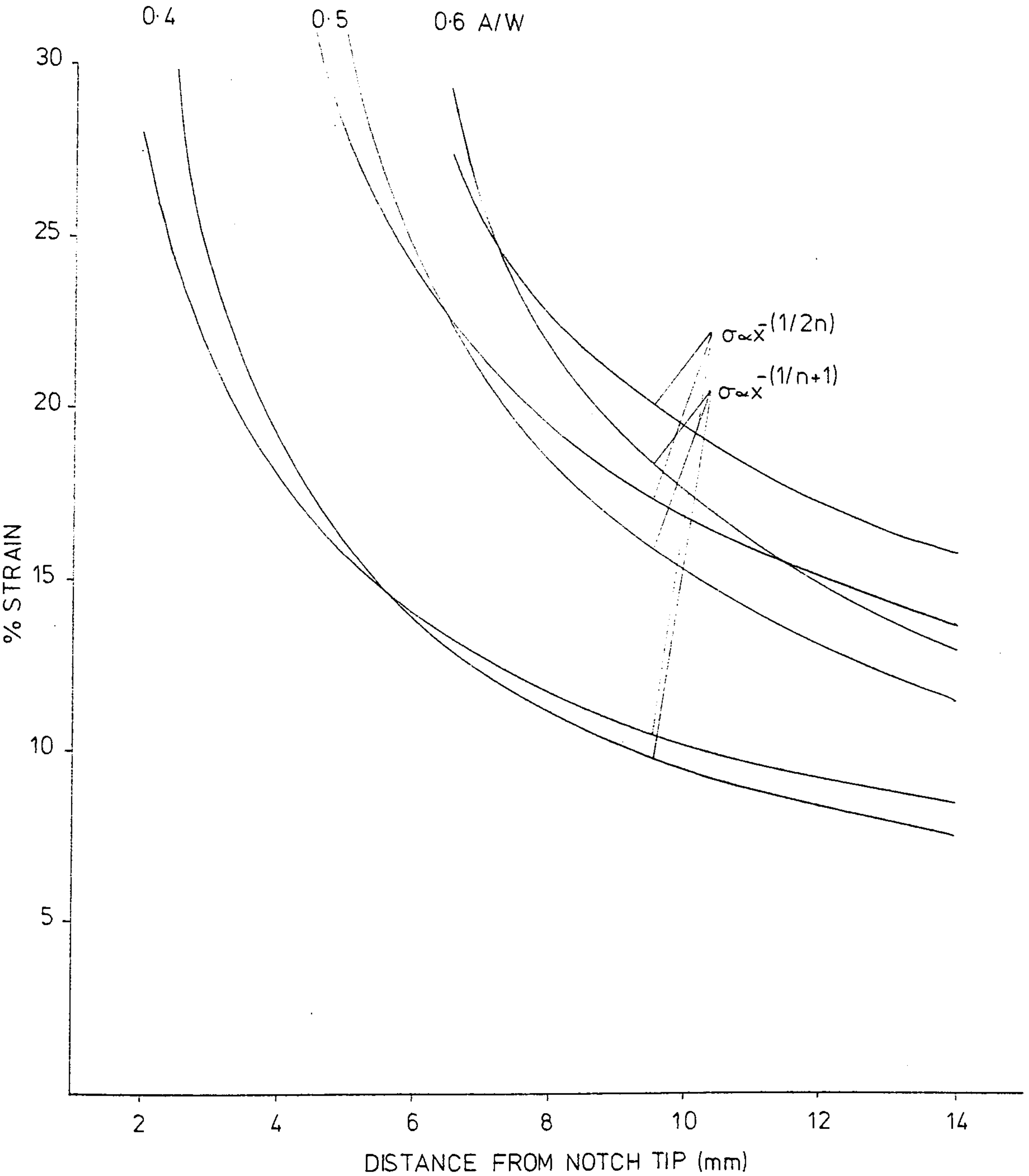

EXAMPLES OF STRAIN PROFILES
OBTAINED FROM NUMERICAL
INTE~~R~~GRATION (N=3.5)

FIG.4.26a

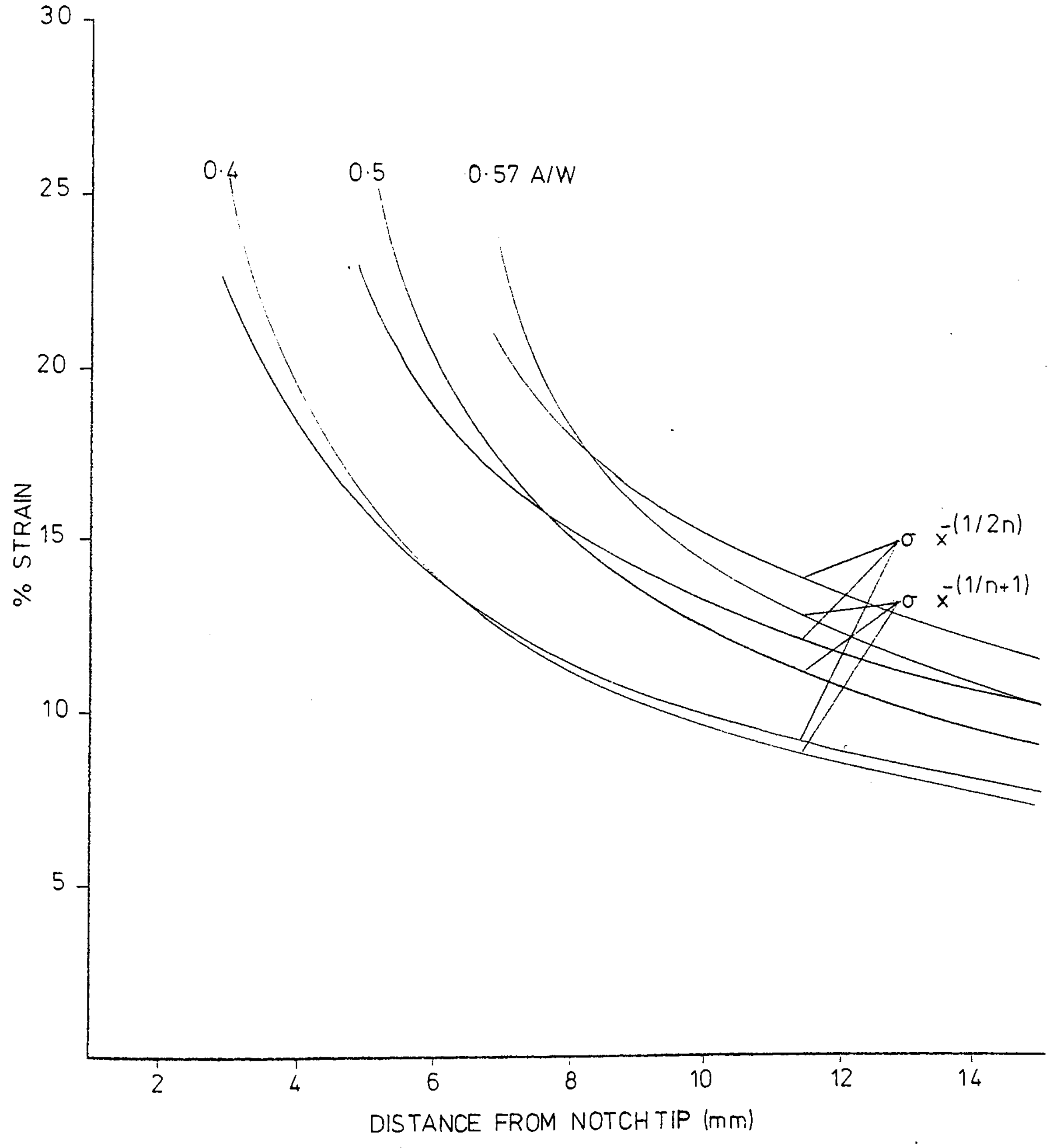

EXAMPLES OF STRAIN PROFILES
OBTAINED FROM NUMERICAL
INTER~~R~~GRATION (N=7)

FIG.4.26b

along the XX centre line is accumulating at an ever decreasing distance from the instantaneous crack tip. Hence if the stress distribution is given by:

$$\sigma = Ax^{-p}$$

Then the distribution of strain from the crack tip will not be given by:

$$\varepsilon = A'x^{-pn} \qquad 4.49$$

but by

$$\varepsilon = A''\int_0^t x^{-pn}.dt \qquad 4.50$$

where $x = f(t)$

The numerical integration has been an evaluation of equation 4.50. To compare these integrations with the experimental strain accumulation profiles it was required that both the theoretical and experimental strain distributions were expressed in the form of equation 4.49. Regression analyses of log.accumulated strain against log.distance from a point $x_1=0$ were made on the theoretical profiles using a range of positions of $x_1=0$ for each crack length. The technique used to do this was the same as for evaluating the experimental profiles during initiation. Only a section of profile was considered for each crack length. The section of each profile started two points ahead of that corresponding to x=0 for the stress distribution at that crack length. The interval covered corresponded to 6.5mm for the DEN and CN geometries and 8mm for the SEN case. An exponent of -0.5 correlating distance and strain was selected on a purely arbitory basis such that:

$$\varepsilon \propto x_1^{-0.5} \qquad 4.51$$

Given the correct location for $x_1=0$ it was found that a correlation of this type would represent a reasonable description of the general shape of all the sections of the accumulated strain profiles under consideration. Correlation coefficient values of better than 0.98

absolute were obtained with the theoretical profiles in all cases. It was decided to use the position of $x_1=0$ that was required to obtain an exponent of -0.5 from these regression analyses of the accumulated strain distributions as the criterion for comparing the theoretical and experimental strain profiles.

The approach proposed for comparing theoretical and experimental results may seem somewhat indirect. However, the approach has the advantage of being less susceptible to experimental errors than comparing the regression correlations obtained at say the crack tip or mid-way between the crack tip and the D-point.

Regression analysis was performed over sections of the experimental strain profiles of around 6mm in length. The position of $x_1=0$ required to produce a correlation between strain and distance through an exponent of -0.5 as in equation 4.51 was recorded for each profile. For pre-strained specimens, only that strain accumalated after pre-straining was considered in the profile analysis.

The effect of changes to the starter profile used in the computation of the theoretical strain profiles was considered. The numerical integration was repeated using two starter profiles for which each point in the original starter profile had beem multiplied by, in the first case 0.7 and in the second case 1.3. These changes to the magnitude of the original starter profile resulted in negligible change in position of $x_1=0$ for the correlation used for comparison.

For the analyses for which n=3.5 the maximum value of the stress observed at any point along any section of strain profile considered in regression analysis was less than $14MNm^{-2}$. Stresses approaching this value were only observed at higher values of a/w. The creep exponent

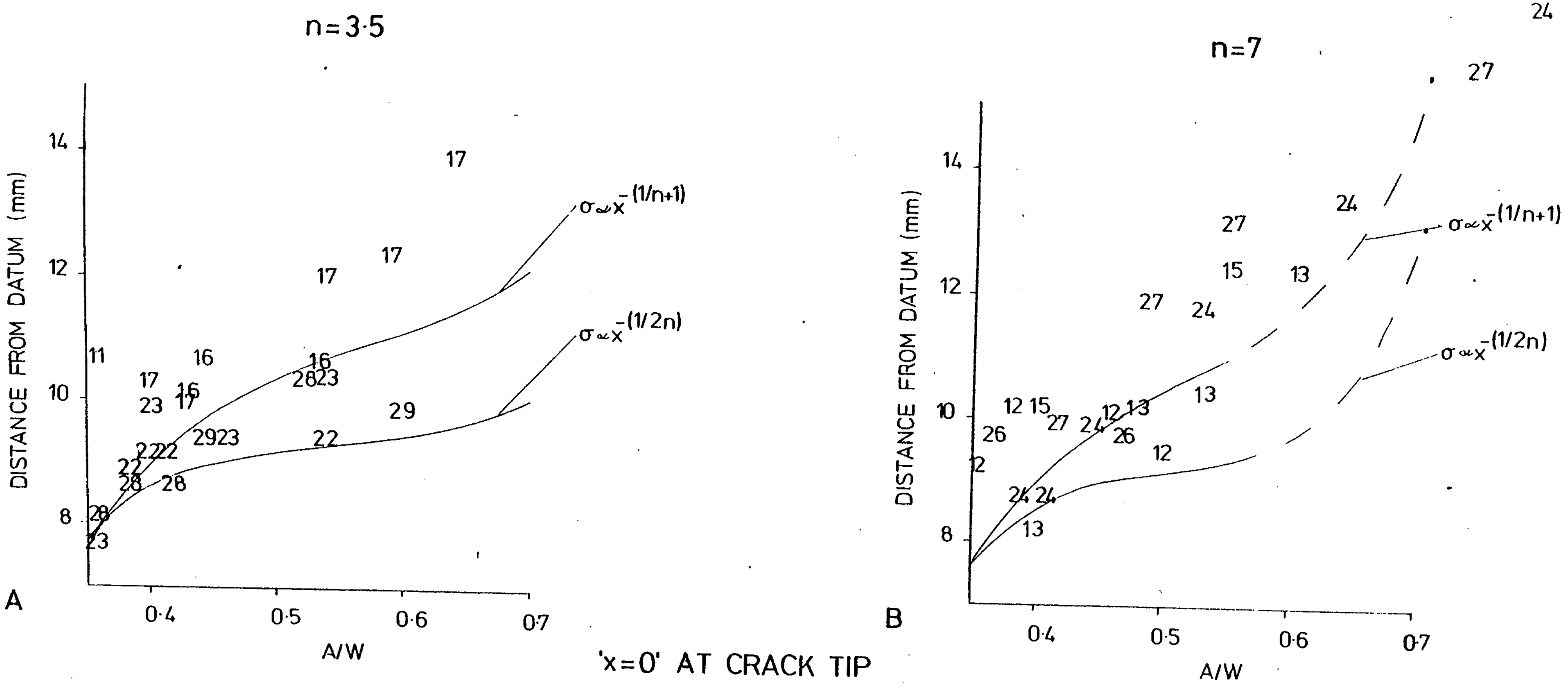

COMPARISION OF LOCATION OF POSITION OF $x_1=0$ TO FIT A $\varepsilon = A x_1^{-(0.5)}$ TYPE CORRELATION TO EXPERIMENTAL AND THEORETICALLY DERIVED STRAIN PROFILES FOR VARYING DEGREES OF CRACK GROWTH

FIG.4.27 CONT'D OVER

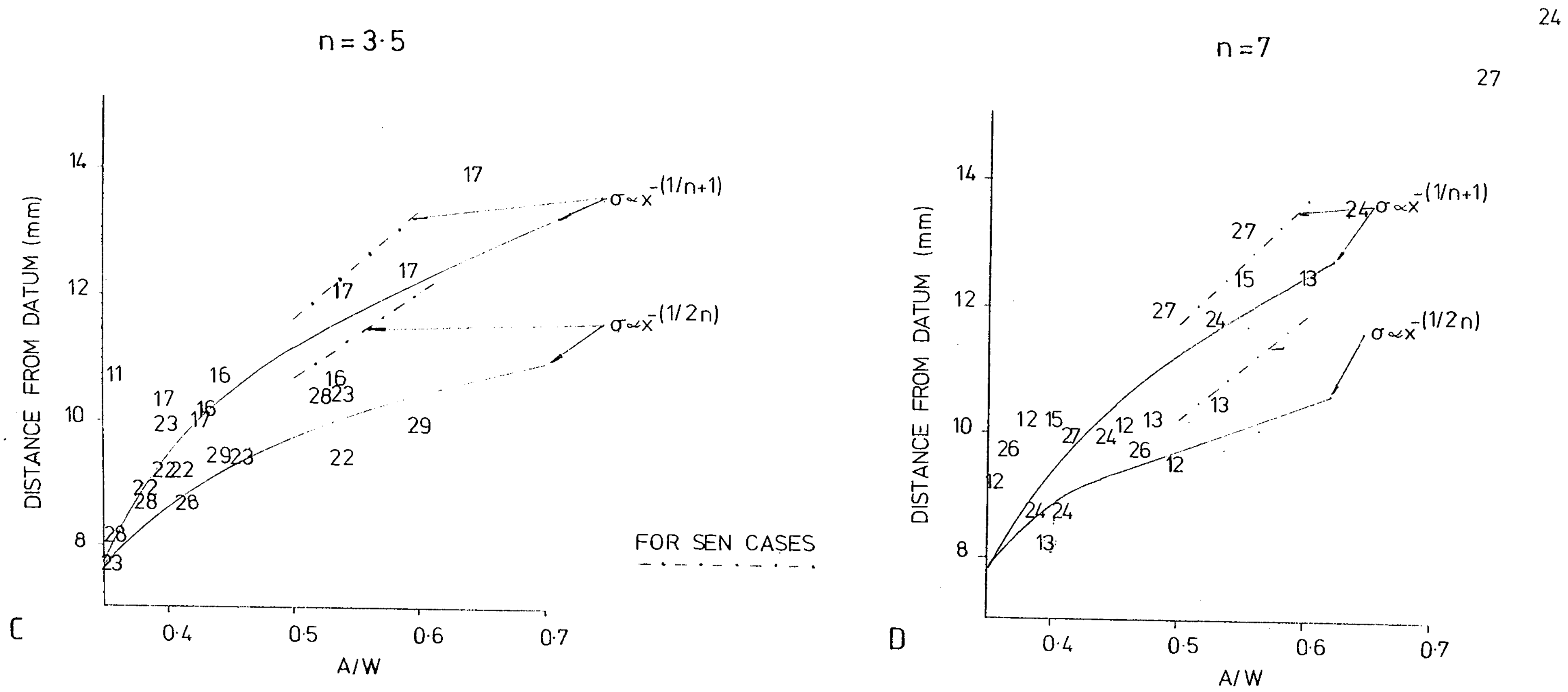

'x=0' DISPLACED AHEAD OF CRACK TIP

FIG. 4.27 contd

for Magnox AL80 is considered to increase from $n=3.5$ to $n=7$ at around a stress level of $15.5MNm^{-2}$. It is appreciated that the transition to the higher exponent level is likely to occur over a range of stress level. However, on the basis of the observations with regards the predicted stress level and the absence of many experimental profiles at high a/w values, it is considered unlikely that the transition in the level of the creep exponent will adversely effect the comparison of the theoretical and experimental strain profiles for the low stress specimens. The starting stress for the high stress specimens was $20MNm^{-2}$ and hence always above the transition threshold. The strain profiles for specimens from the intermediate stress regime were not included in the analysis. This was because of the proximity of the starting nett section stress ($10MNm^{-2}$) for these specimens to the exponent transition level.

The comparisons between the theoretical and experimental profiles are shown in Fig. 4.27 on the basis of the position of $x_1=0$ in order to produce a correlation of the type shown in equation 4.51. The position of $x_1=0$ is described differently for each geometry. For the DEN case it is the distance from the specimen edge to the position $x_1=0$ and for the CN case it is the distance from the specimen YY centre line. Although differing in definition these represent equivalent measurements for the two geometries relative to the notch. The SEN case is shown as half the distance from the notch mouth to the position $x_1=0$. This is also equivalent to the definition used for the other geometries.

Considerable scatter is observed with the experimental results. The results with $x=0$ for the theoretical stress distributions located at the crack tip are shown in Fig. 4.27a and b. There is reasonable agreement with both the $x^{-(1/n+1)}$ and $x^{-(1/2n)}$ stress distributions but the former shows the overall better fit with the experimental points. Displacing x=0 for the stress distributions 1mm ahead of the crack tip for the DEN and CN specimens improved the general agreement between the theoretical and experimental points for both stress distributions. However, the $x^{-(1/n+1)}$ type stress distribution still gave the better agreement with the experimental results. The improved agreement between experimental and theoretical results using a displaced position of x=0 indicated the validity of such a correction. For the SEN geometry it appeared that the best agreement between experiment and theory would be obtained with the position of x=0 for the $x^{-(1/n+1)}$ stress distribution displaced less than 1mm. The large notch diameter specimens TS15 and 27 appear to warrant a larger correction in the x=0 position than the other specimens.

There is some evidence to suggest that for the DEN and CN specimens at high a/w values the strain accumulation ceases to be consistent with the operation of either the theoretical stress distributions considered. This is supported by visual observation of some high a/w cases in Fig. 4.15. Although this cannot be considered conclusive this would not be entirely unexpected at high crack lengths due to the possibility of severe material degradation leading to tertiary creep deformation. Also with the DEN geometry there is the possibility of interaction of the stress profiles from the two crack fronts.

Analysis of the σ_{xx} Stress Distribution

The distribution of the stress σ_{xx} was examined via the ε_{xx} strain distributions. It has already been observed that the values of the

ε_{xx} strains were more susceptible to inaccuracy than the corresponding ε_{yy} values. From consideration of the accuracy of the ε_{xx} values it was not considered realistic to attempt to compare these strain distributions with theoretically derived profiles as was done for the ε_{yy} profiles. Instead it was considered preferable to compare the distributions of σ_{yy} and σ_{xx} by comparing the distributions of ε_{yy} and ε_{xx}. A measure of the σ_{xx} constraint stress can be obtained from the deviation from the normal Poisson contraction in the X-direction expected for uniaxial tension. This deviation P_d was calculated as in section 4.2.3.1 from equation 4.28. Constraint in the X-direction is indicated by a positive value.

The deviation from normal Poisson behaviour is an indication of the ratio between the stress time integrals in the X and Y-directions. If the deviation was found to be constant along corresponding sections of ε_{yy} and ε_{xx} distributions it would indicate that σ_{xx} is proportional to σ_{yy} for this region and hence both σ_{xx} and σ_{yy} follow the same dependance on distance, assuming plane stress conditions.

As discussed earlier the ε_{xx} strain profiles were evaluated from displacements made along lines between 1 and 1.5mm either side of the XX centre line. To simulate the strain distribution expected along the XX centre line 1mm was subtracted from the distance of each point from the crack tip. This displaced the strain profile back towards the crack tip by approximately the distance that the strains were assessed above and below the XX centre line. The deviation from normal Poisson behaviour P_d was then evaluated for points along each pair of ε_{xx} and ε_{yy} profiles. The results from specimens where reasonable distributions of ε_{xx} could be obtained are shown in Fig. 4.28 As expected, due to the inaccuracy of the ε_{xx} determinations the results

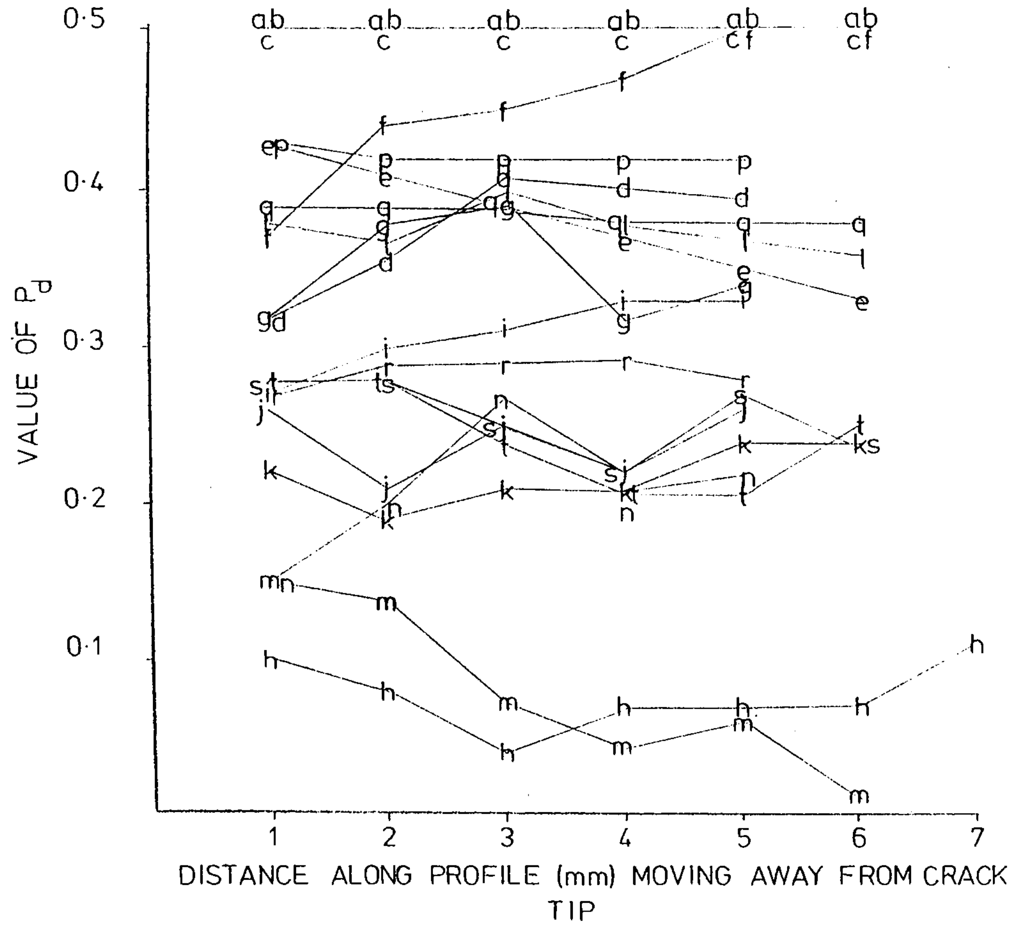

KEY	SPECIMEN	SEQUENCE
a	22	3
b	22	5
c	22	7
d	23	5
e	23	3
f	24	5
g	24	6
h	24	7
i	9	2
j	28	3
K	28	4
l	12	3
m	13	3
n	13	4
p	17	11
q	17	13
r	16	3
s	16	4
t	16	5

VARIATION OF POISSON DEVIATION ALONG PROFILE SECTIONS

FIG.4.29

showed a degree of inconsistency. However, there is reasonable support for the suggestion that the deviation from normal Poisson behaviour is constant for a particular pair of ε_{xx} and ε_{yy} distributions, and hence σ_{xx} is proportional to σ_{yy}. The DEN geometry shows a higher level of σ_{xx} than the CN case, the average values of the deviation corresponding approximately to 0.4 and 0.2 respectively. From equation 4.41 these deviations from normal Poisson behaviour correspond to stresses of $0.42\sigma_{yy}$ and $0.23\sigma_{yy}$ for the DEN and CN geometries respectively, assuming plane stress conditions.

There is no real evidence from the DEN and CN specimens that as the crack length increases the deviation from Poisson behaviour changes significantly. However, the SEN geometry showed a similar or greater deviation from Poisson behaviour compared with the DEN geometry at short crack lengths but this constraint was observed to decay as the crack length increased.

4.2.4 Notched Tensile Specimen Metallography

Notched tensile specimens showing various degrees of crack growth have been examined both optically and by means of the SEM. As observed with the smooth bar creep tests cavitation was more pronounced at the low stress regime. For all stress regimes damage was observed to be at a concentrated level in the near tip region. However, it was normally observed to continue to some extent right across the ligament. Damage was observed in the form of cavitation principally along grain boundaries perpendicular to the tensile stress axis. Many of the cavities were associated with boundaries between more than two grains Fig. 4.29. However, the length of these cavities was such that it was difficult to determine if these multiple grain junctions represented the initiation site of the cavity. Indications of grain deformation in the form of slip lines were visible in some areas particularly with the high stress regime specimens, see Fig. 4.30.

There was some evidence with the CN and SEN geometries that although the cavities were preferentially orientated along boundaries roughly perpendicular to the tensile stress axis, they were observed in greater numbers along the slip bands radiating at 45° from the crack tip. This effect is visible in Fig. 4.31 which shows a CN crack tip (low stress, $5MNm^{-2}$) at low magnification. Fig. 4.32a shows a field 4mm in front of this crack tip on a line along the notch plane (XX centre line). Fig. 4.32b shows a field 4mm above the previous field in the Y-direction, that is at 45° to the crack tip. As can be seen from comparing Figs. 4.32a and b the damage is marginally more extensive away from the centre line. A similar observation was made when considering the corresponding field at 45° to the crack tip on the other side of the centre line.

Fig. 4.33a and b show fields along a vertical line 3mm from the crack tip of a DEN specimen. Fig. 4.33a shows the field on the line XX and Fig. 4.33b represents those fields at 45° to the crack tip. The difference in the extent of the damage is less pronounced in this case than for the CN example. Fig. 4.34 shows a low magnification photograph of the crack tip of the DEN specimen.

Examination of fracture surfaces showed high ductility and evidence of cavitation. The failure mode was considered to be the void-sheet mechanism with ductile tearing between cavities taking a path that may have been at least in part trans-granular. The fracture surfaces of the low stress regime specimens took on a slightly coarser appearance than those from the high stress regime. Evidence of the presence of cavitation was clearly visible. Figure 4.35 shows a typical fracture surface viewed from two angles.

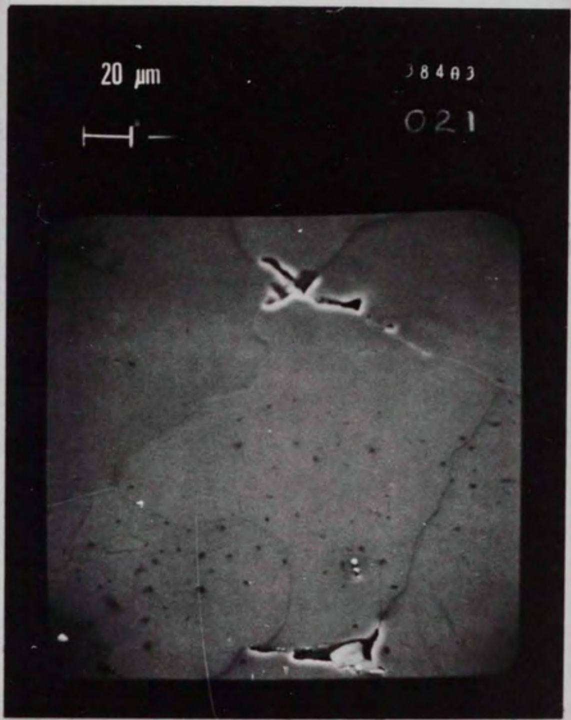

CAVITATION AT MULTIPLE
GRAIN JUNCTIONS

FIG.4.23

EVIDENCE OF CRYSTAL DEFORMATION

FIG.4.30

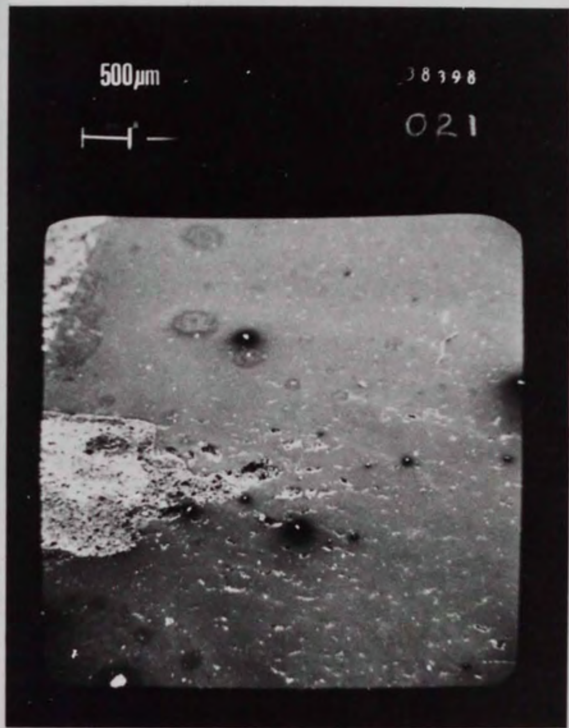

NEAR CRACK TIP REGION (CN)

FIG.4.31

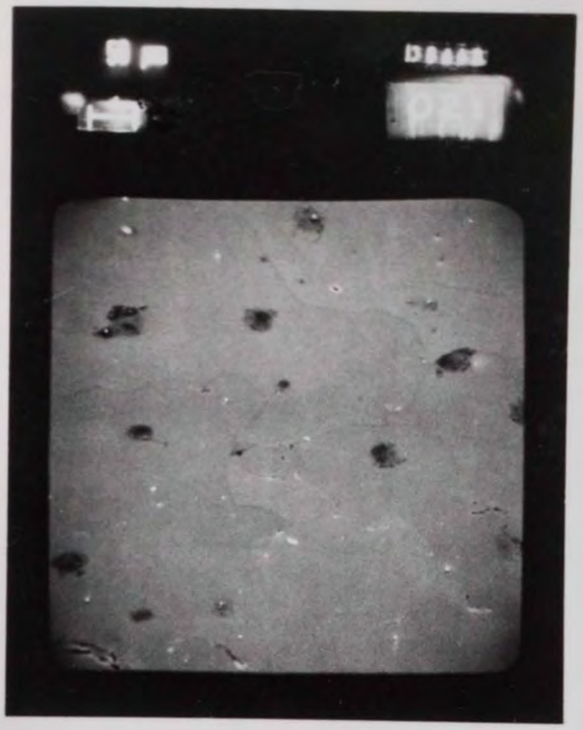

A

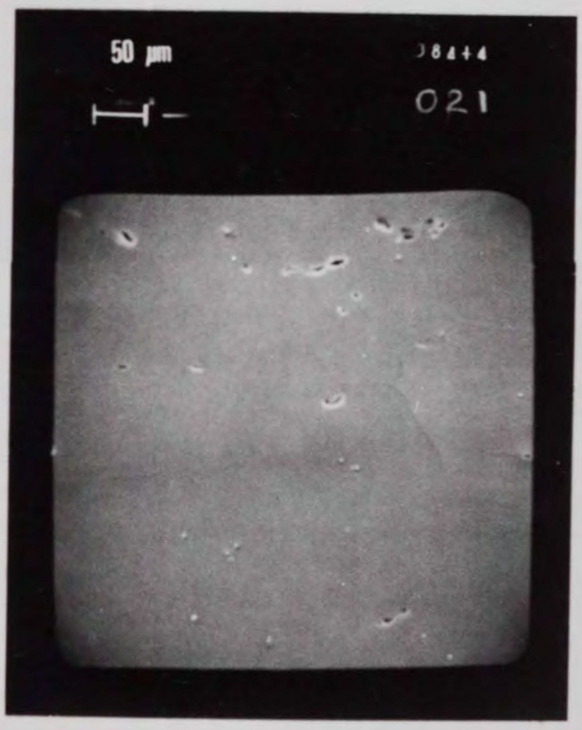

B

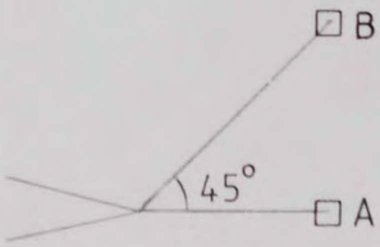

CAVITATION IN A CN SPECIMEN AHEAD OF THE CRACK TIP ON AND ABOVE THE CENTRE LINE XX

FIG.4.32

A

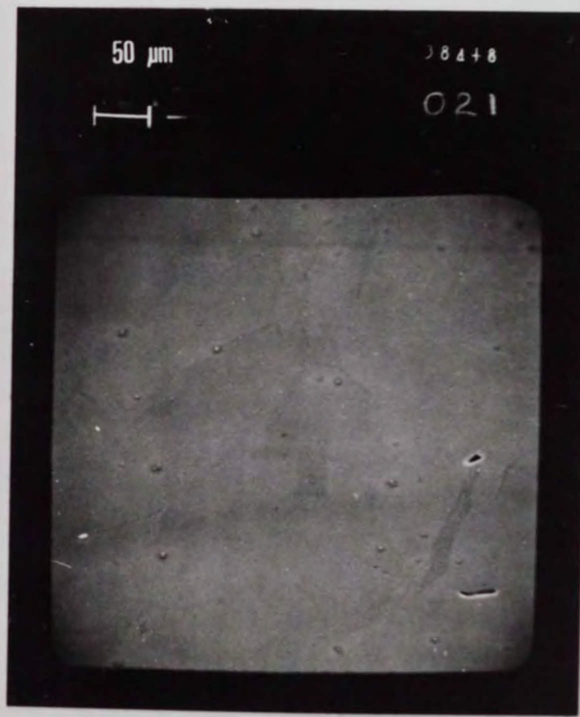

B

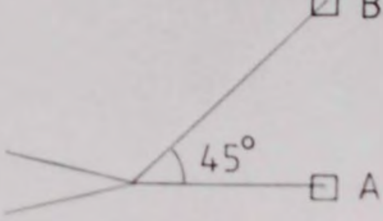

CAVITATION IN A DEN SPECIMEN AHEAD OF THE CRACK TIP ON AND ABOVE THE CENTRE LINE XX

FIG.4.33

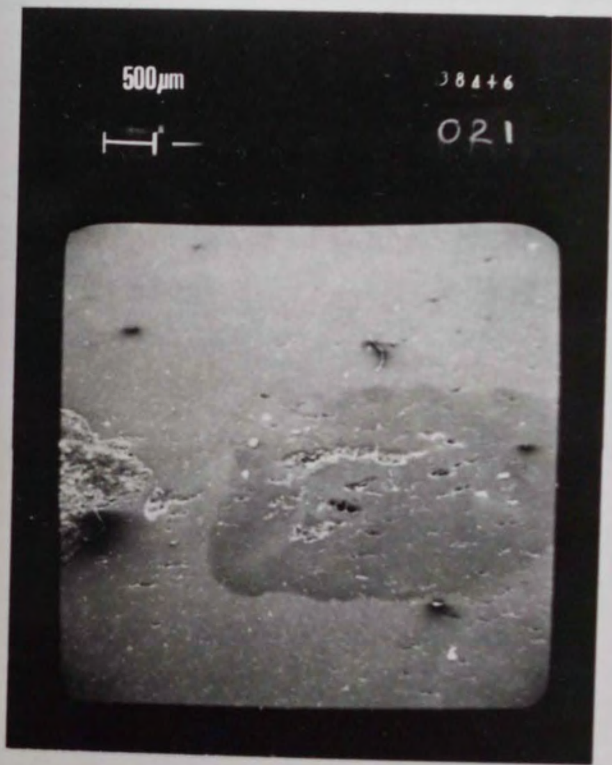

NEAR CRACK TIP REGION (DEN)

FIG.4.34

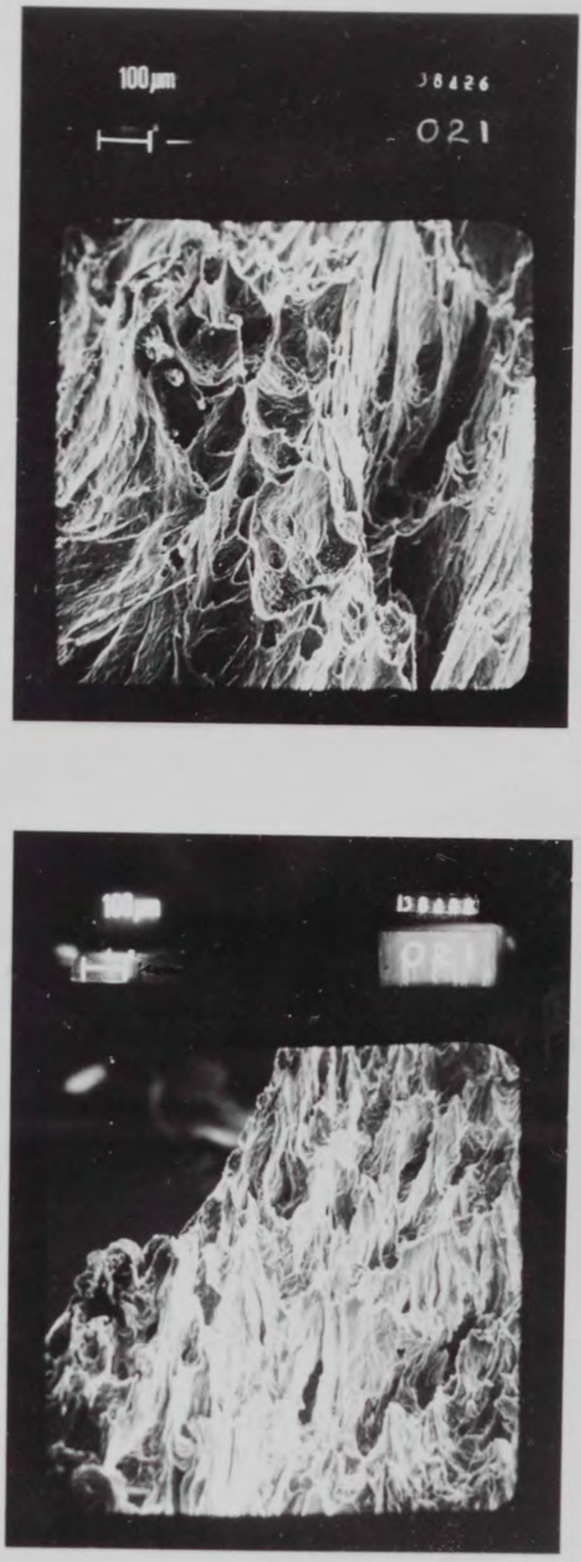

TYPICAL FRACTURE SURFACE (LOW STRESS)

FIG.4.35

5. DISCUSSION

The ductile behaviour of Magnox AL80 resulted in fracture showing more resemblance to a ductile tearing process than to a cracking process in the conventional sense. This must cast some question on the validity of the work to the general problem of crack growth. However it was shown in sections 2.33 and 2.45 that the parameters describing fracture cannot always be predicted on the basis of ductility and that correlation with the various growth laws were observed for a range of ductilities. This suggests that the concepts examined in this study may find some level of applicability in less ductile situations. The high ductility of Magnox AL80 ensured adequate opportunity for creep relaxation prior to the onset of creep crack growth. This has enabled information to be obtained as to the nature of the steady state stress distribution resulting from creep relaxation. The high ductility has also facilitated the study of the strains and displacements in the near crack tip region.

5.1 Considerations with Respect to Specimen Geometry

Throughout this study it has become apparent that there are 3 basic factors concerning the differences in specimen geometry which must be considered when reviewing the experimental results of the notched tensile tests.

These are:

i) The differences in the K-calibration curves for the different geometries. Combined with these differences, allowance must also be made for the presence of a bending moment opening the crack mouth with the SEN geometry.

ii) The difference in the slip line field patterns

iii) The difference in the lateral constraint in the form of differing values of σ for the three geometries.

i) The K-calibration compliance curves for the three geometries are shown in Fig. 5.1. As can be seen from this figure, over the range 0.35 to 0.7 a/w the CN and DEN specimens have very similar K-calibrations. This means that the variation in K with crack length for these specimens will be very similar. The variation in σ_{nett} with crack growth is of course identical for these specimens. The SEN geometry has much higher values for the K-calibration than the DEN or CN and as shown in section 4.2.2.2 the SEN K-calibration shows the greatest percentage increase as the crack length increases. Also the SEN geometry has the additional complication of a bending moment. The magnitude of the bending moment is proportional to the perpendicular distance of the loading points to the neutral axis and will hence become progressively more significant as the crack length increases. However the tendency of the specimen to rotate around the pins will cause the moment to relax.

ii) Despite the similarity in K-compliance for the DEN and CN geometries the slip line field patterns for the two geometries vary considerably, as is shown in Fig. 5.2. The slip lines for the DEN case are focused back towards the crack plane, but with the CN geometry they simply fan out at 45^{o} from the crack tip. The pattern expected for the SEN case is similar to that for the CN case.

iii) The variation in the lateral constraint became apparent from the experimental work. Provided that the assumptions made with respect to the application of the Hencky equations are valid, then remote from the near tip region σ_{xx} for the CN geometry was ≈ 0.55 the σ_{xx} value for the DEN geometry. In the location of the maximum value of ε_{yy} the difference in the two geometries was ≈ 0.45, the DEN again giving

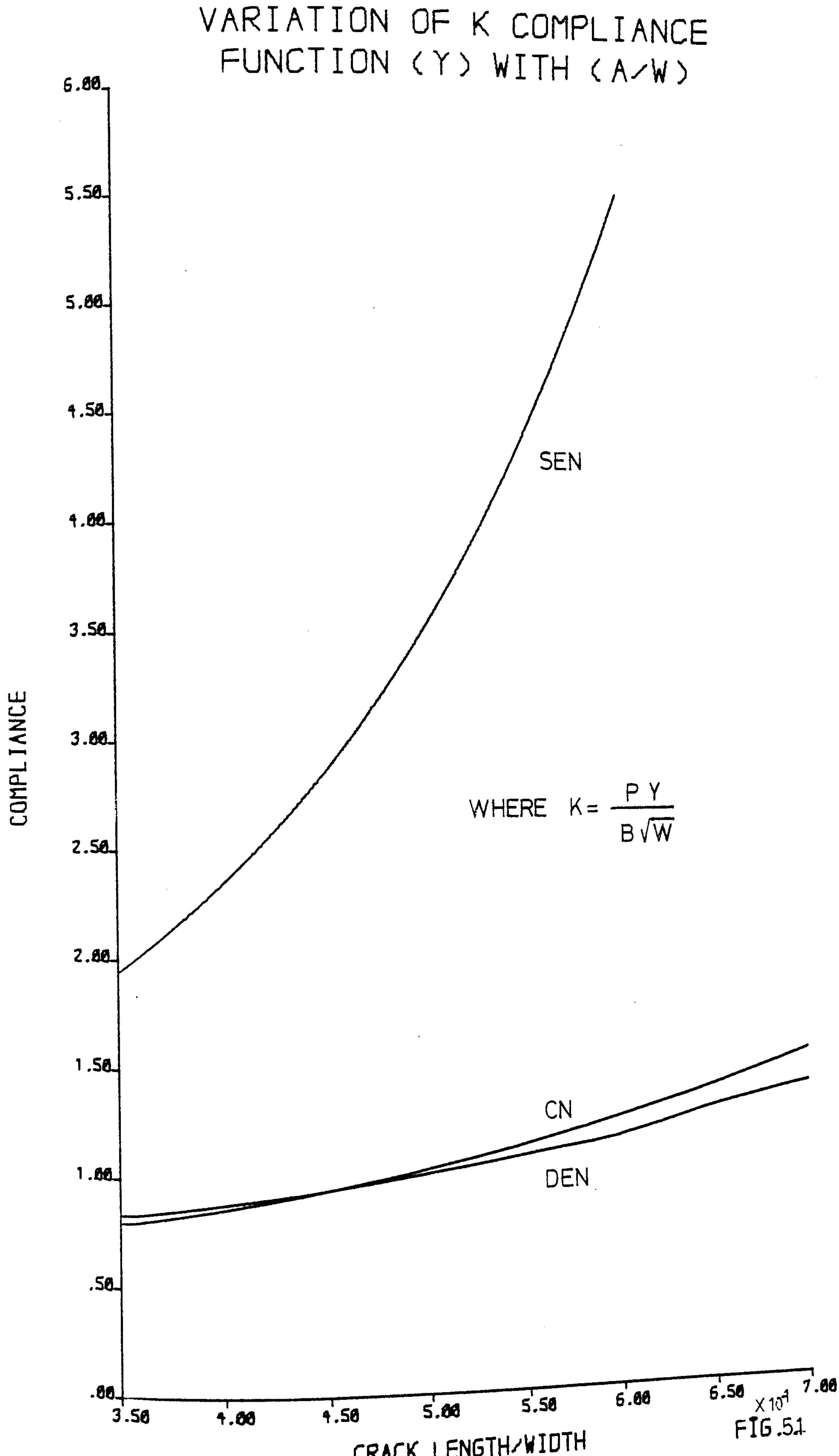

VARIATION OF K COMPLIANCE
FUNCTION (Y) WITH (A/W)
6.00
5.50
5.00
4.50
4.00
3.50
3.00
2.50
2.00
1.50
1.00
.50
.00
COMPLIANCE
SEN
WHERE $K = \frac{P Y}{B \sqrt{W}}$
CN
DEN
3.50
4.00
4.50
5.00
5.50
6.00
6.50
7.00
$\times 10^{-1}$
CRACK LENGTH/WIDTH

FIG.5.1

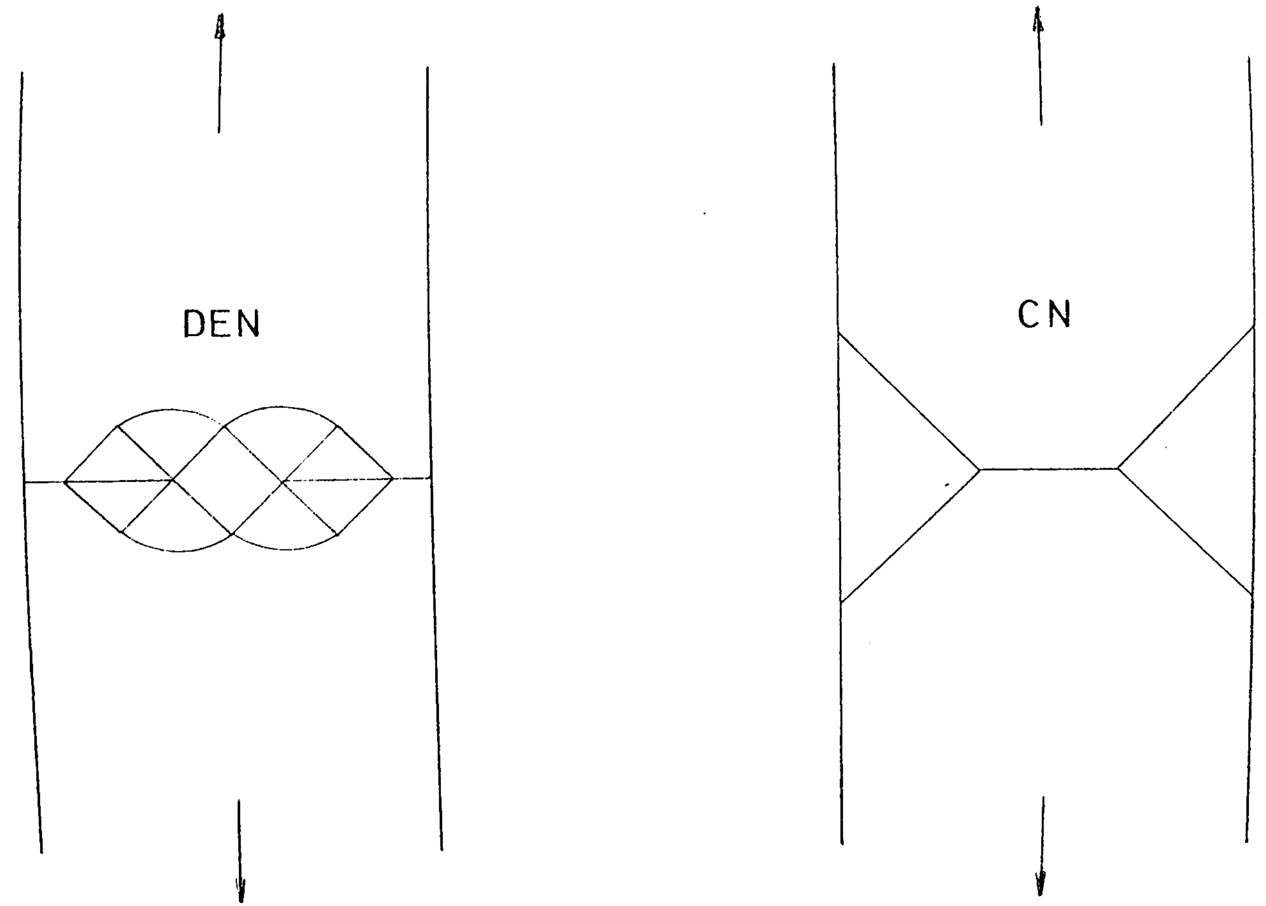

SLIP LINE FIELDS FOR CN AND
DEN GEOMETRIES

FIG.52

the higher constraint. For both geometries the constraint stress σ_{xx} was lower in the near tip region. This decrease was not entirely unexpected due to the presence of a region of non-uniform deformation in the near tip region. The evaluation of ε_{yy} is such that the value obtained only represents the uniform strain and excludes any non-uniform displacement. This is not the case with the ε_{xx} strains and these may be increased in value due to unstable behaviour near the crack tip. This means that in the near tip region the ratio of ε_{xx} to ε_{yy} may be higher due to the inclusion of strain from the non-uniform displacement in ε_{xx} but not in ε_{yy}. For analysis in the ligament beyond the D-point this discrepancy will not arise as there is no non-uniform displacement.

A decrease in the constraint would also be expected from LEFM considerations. A decrease in σ_{xx} is predicted near the crack tip due to the presence of a traction free surface.

The observation of a higher constraint stress with the DEN geometry than the CN case is quite rational. The CN geometry will not develop a high constraint stress as the edges of the specimen are free from traction and can deform towards the crack tips in response to longtitudinal displacement. With the DEN specimen the relatively low stressed material constituting the notch flanks will tend to inhibit lateral contraction on the plane of the notches. This constraint will be balanced by the presence of a notch on each side of the specimen, which in effect will pull outwards against each other.

It might be expected that the constraint should increase for the DEN geometry as the crack length increases as there is a greater area of low stressed notch and crack flank. An increase in constraint was not apparent. It seems likely that this tendency for increase was offset by the notch flank rotating outwards around the crack tip which would reduce their efficiency in constraining lateral contraction. This is also consistent with the observation of a high P_d value for the long notch specimen TS25, during the early stages of initiation but a tendency for this value to decrease with notch opening.

Evaluation of the σ_{xx} constraint values for the SEN geometry was not attempted because it was felt that the constraint with this geometry was likely to be prone to change. Initially the combination of very long notches and an expanse of ligament remote from the crack could lead to a constrained condition. As crack growth became extensive the tendency for the notch free surface to deform towards the crack tip would increase as the length of ligament separating them decreased. The bending moment increasing in magnitude with crack length may also assist in reducing the constraint at high crack lengths. The bending moment will certainly promote an opening rotation of the crack flanks which will reduce constraint. Consideration of the differences in K, slip line patterns and constraints will influence much of the discussion to follow.

5.2 The Criteria Controlling Crack Advance

The possibility that creep crack growth was controlled by local displacements was originally proposed by Wells & McBride[171] and this proposal has since received much attention. In a situation of cumulative damage such as in the creep regime this approach clearly has good grounds for examination. In this work it has been found more advantageous to consider the total displacement contributing to fracture in terms of a strain acting uniformly over a gauge length, plus an additional displacement that is concentrated at the XX centre line, that is on the line of the notch plane. The observation of fracture proceeding at a constant value of ε_{yy} for a particular geometry is a clear indication of the fracture process being strain or displacement controlled. COD evaluations were made at three locations. In the first case, at the D-point, only a uniform strain component was present and so the COD and strain were directly proportional. The COD's evaluated at either the crack tip or the position of maximum strain ε_{yy} were not directly related to the uniform strain at these points as they also included a non-uniform component to the total displacement. It is felt that the inclusion of the non-uniform displacement detracts from the usefulness of the analysis and that to consider only the uniform strain contribution is a realistic approach. The non-uniform displacement arises from localised necking down of the material. Once this necking phenomenon starts, the material will lose its load bearing capacity in the same way as the load drops in a tensile test once the UTS is exceeded. The equivalent COD evaluated at the crack tip was seen to be fairly independant of geometry but this was only considered to be the case because the necking phenomenon was masking a geometry dependant uniform strain. When this uniform strain reached a limiting value uniform material deformation gave way to instability. For purposes of theoretically describing crack advance the uniform strain measurement is by far the most useful. Finite element computations of stress and strain distributions will be modelling the build up of this uniform strain and the fact that final through fracture includes a geometry independant contribution to displacement through a necking phenomenon is of little interest. The important factor for successful prediction of creep crack growth rates will be the criterion which represents the limiting capacity of the material for uniform behaviour. Beyond this limiting criterion the material will either crack or neck down and then tear.

The values of ε_{yy} were geometry dependant, due to the difference in constraint. The most successful way in which to balance the effect of the constraint was not by use of an equivalent strain approach as was anticipated but simply by the summation of ε_{yy} and ε_{xx} which at constant volume will equal the $-1 \times \varepsilon_{zz}$. This is in fact, a common empirical criterion for sheet forming under bi-axial tension. With the sheet forming case the material is strained to an extent where upon a groove is observed to form. Marciniak[189] showed that through failure of the material in the groove occurs when the material of the bulk sheet reaches a limiting value of the summation of ε_{xx} and ε_{yy}. This is very similar to the case here, where a region of localised necking is observed immediately in front of the crack tip. This region tears through in correlation with the bulk material either side of the necked region reaching a limiting strain. Failure controlled by a critical thickness strain can be represented in terms of the relative values of ε_{xx} and ε_{yy} by the failure diagram shown in Fig. 5.3. The summation of ε_{xx} and ε_{yy} was performed for the values at the point of the maximum value of ε_{yy}. From observations of the strains considered it could reasonably be expected that the summation of the D-point strain ε_{yy} and the strain ε_{xx} at the D-point would also produce a critical strain summation value, capable of describing crack advance.

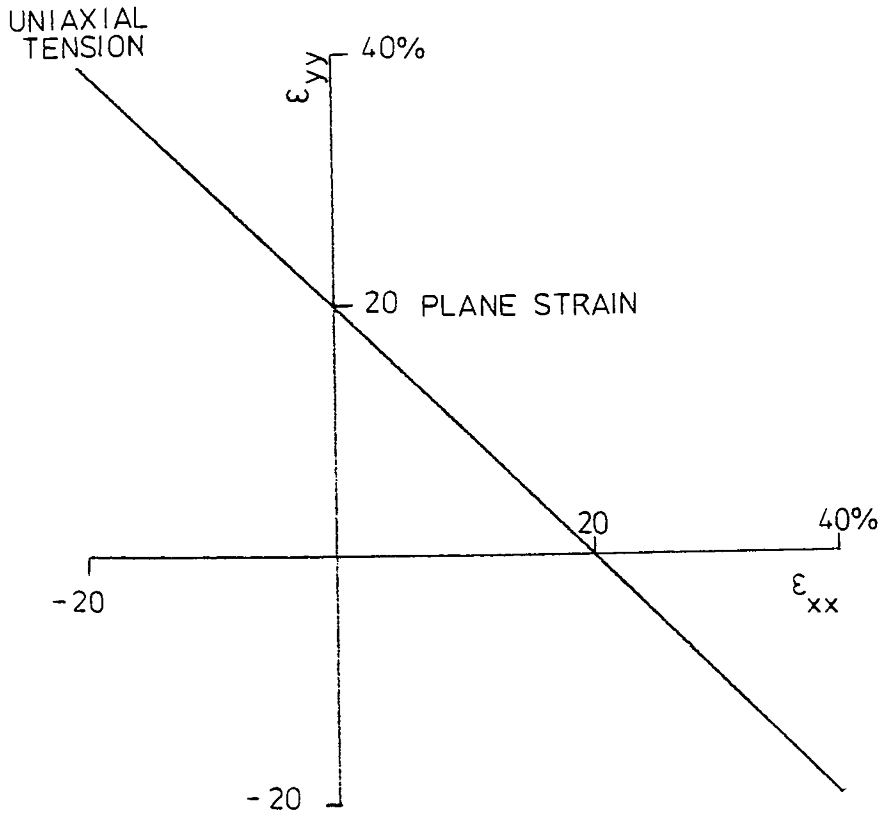

FAILURE MAP OF CRITICAL STRAIN
SUMMATION CRITERION

FIG.5.3

The observation that even the pre-strained specimens failed at approximately the same summation of ε_{yy} and ε_{xx} is further support of strain controlled fracture. It appears that strain accumulated during pre-strain contributes to that required for failure under crack growth.

The large notch specimens are a further indication of the effect of lateral constraint on the failure strain. The principal effect of the large notch root radii appears to be to reduce the extent of the lateral constraint in the near tip region bounded by the projection of the lines from the notch flank. The constraint typical of the specimen type reappeared with the establishment of normal crack flanks. This would be expected when the crack flanks as opposed to the notch flanks become the principal constraining influence.

The absence of any detectable trend between the strain and the stress level was not unexpected. Magnox AL80 is noted for its constant elongation to failure over a very wide range of stress around the temperature range used. Fig. 5.4 shows a plot of elongation to failure versus stress for AL80,[11] this plot indicates that over the stress range considered an increase in ductility of around 4% would be expected for uniaxial tension. This is less than the scatter band width for all the strain parameters considered so it is not really surprising that any effect has been well masked, especially as high stress specimens are in the minority.

As already discussed reservations are held with respect to the usefulness of the equivalent COD values which are computed from measurements taken close to the crack tip so that they include a

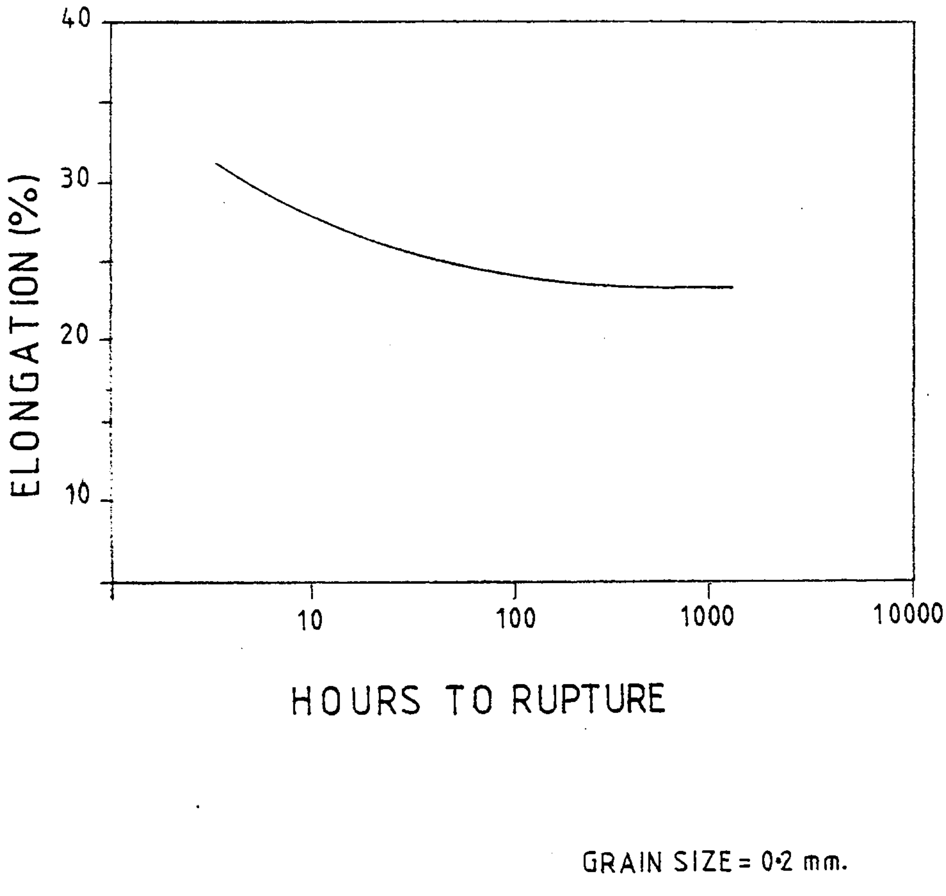

FAILURE ELONGATION.V.TIME TO RUPTURE FOR MAGNOX AL80.

FIG.5.4

contribution from material instability. However, it is considered that the equivalent COD approach provides a more valid description of the control of crack growth than estimates of the COD from the notch flank opening approaches favoured by other workers.[103, 154, 173] The equivalent COD method gives an indication of the displacement at the instantaneous crack tip. The projection from the notch flank produces a progressively larger value of the COD as the crack grows.

Visual examination of failed specimens showed pronounced thinning just ahead of the notch tip, extending above and below the XX centre line to some distance. This thinning produced a gentle hollow in the specimen surface just ahead of the crack tip. This indicates that material flow from behind the notch flanks was contributing to the COD seen by measuring the notch flank displacement. This effect will be progressive with time and because of this, growth will occur with apparently increasing COD values using the flank displacement method. Strain is occurring over the entire uncracked ligament but strain in the low stressed notch flanks is far less significant. This results in an increased volume of material flowing into the region bounded by the lines of projection of the notch flanks and the COD is being assessed effectively over a progressively larger gauge length. Further deformation in any of this increasing volume will contribute to the COD observed. This effect is indicated by the curved nature of the fracture surface of a failed DEN specimen, see Fig. 5.5 Failure has been shown to occur at approximately constant strain so this curviture can only arise from progressive flow of material remote from the XX-centre line.

The use of COD measurements from notch flank opening seems distinctly

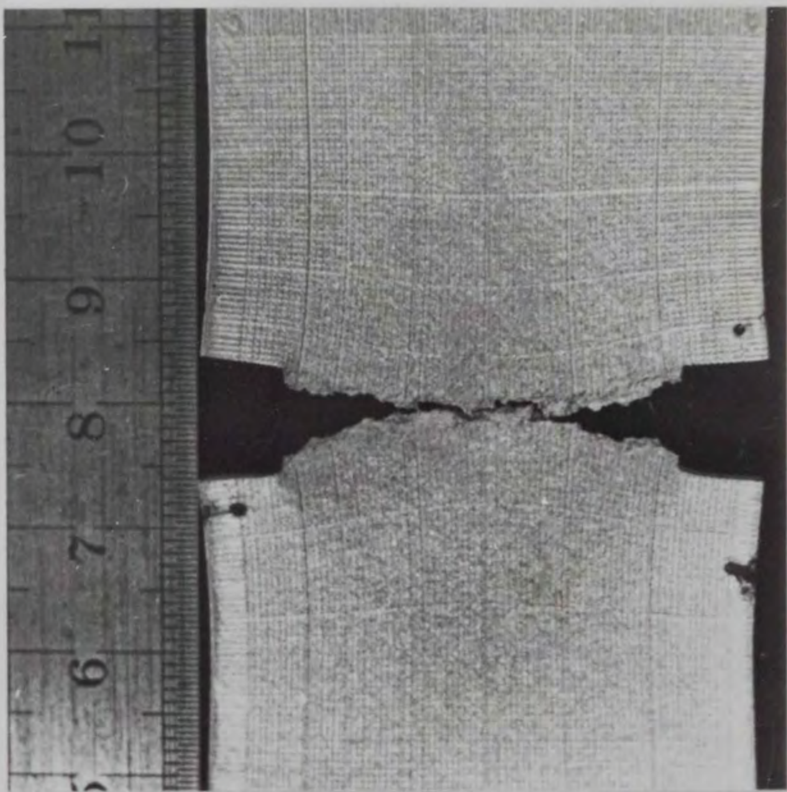

FAILED DEN SPECIMEN

FIG.5.5

limited, except possibly during initiation where the material under examination is that immediately adjacent to the notch tip. These measurements during growth will be geometry dependant according to whether the notch flanks rotate on opening as with the edge notched geometries or open in a roughly parallel manner as with the embedded crack of the CN case. It is considered doubtful that correlations obtained with this parameter are even evidence of displacement controlled growth. This is because the growth rate will be dictating the stress/time integral and hence the extent of creep flow contributing to the apparent increase in COD. Correlations between notch mouth opening and crack growth rate are to be expected regardless of whether a stress or displacement parameter is controlling fracture. Analysis of actual displacements in the material near the crack tip is considered to provide the best indication of crack advance being displacement controlled. Unfortunately such analyses are not without disadvantage as at present they are labour intensive and not amenable to continuous monitoring.

Another problem with the equivalent COD approach is in setting the value of the operative gauge length. For the estimations of the initiation COD from the notch flank opening, it appears that the gauge length equal to the average distance of the D-point from the crack tip was an under-estimate and that displacement in material even further away is contributing to the COD. This illustrates the very severe error in Haighs[154] assumption of all the COD displacement occurring along the crack plane. Cottrell's[142] approach of the COD gauge length equalling twice the notch root radius is also inadequate under creep conditions where extensive material flow can occur in some cases.

Theoretical approaches based on crack growth following a constant crack tip displacement typically only consider the uniform strain contribution, and use an equation for the COD of the type[175, 183]

$$COD = H\mathcal{E}$$

The strain $\mathcal{E}$ is usually $\mathcal{E}_{yy}$ or this could be taken as $\bar{\mathcal{E}}$, the equivalent strain. In either case, in this work these have been shown to be geometry dependant. However provided the gauge length H is constant these theoretical predictions should provide a valid description of crack growth in a single geometry provided the other assumptions made in the analyses are valid.

The initial tendency for the major strain measurements to show an increase in ductility over the first 0.05 a/w to 0.07 a/w (1.1 - 1.6mm for DEN and CN) of crack growth is considered to be due to the crack moving out of the influence of the relatively undeformed notch flanks. Material ahead of that immediately adjacent to the notch flanks can undergo a thickness strain with little constraint. As the crack grows, material ahead of this thinned region can progressively thin down to the same extent with little difficulty. However, the material immediately adjacent to the notch tip, the first material through which the crack will pass is constrained from through thickness contraction by the notch flanks so an overall reduction in ductility is expected in this region, see Fig. 5.6. Following this line of reasoning the large notch root radii specimens would be expected to show initiation at a through thickness strain close to that observed during growth. This is because the wide spacing of the notch flanks would reduce their effectiveness in constraining through thickness contraction. It can be seen from the summation of $\mathcal{E}_{xx}$ and $\mathcal{E}_{yy}$ (Fig. 4.19e) that points for the large notch root radii specimens TS15 and 27 occur on the top edge of the scatter band when between 0.4 and 0.42 a/w but were

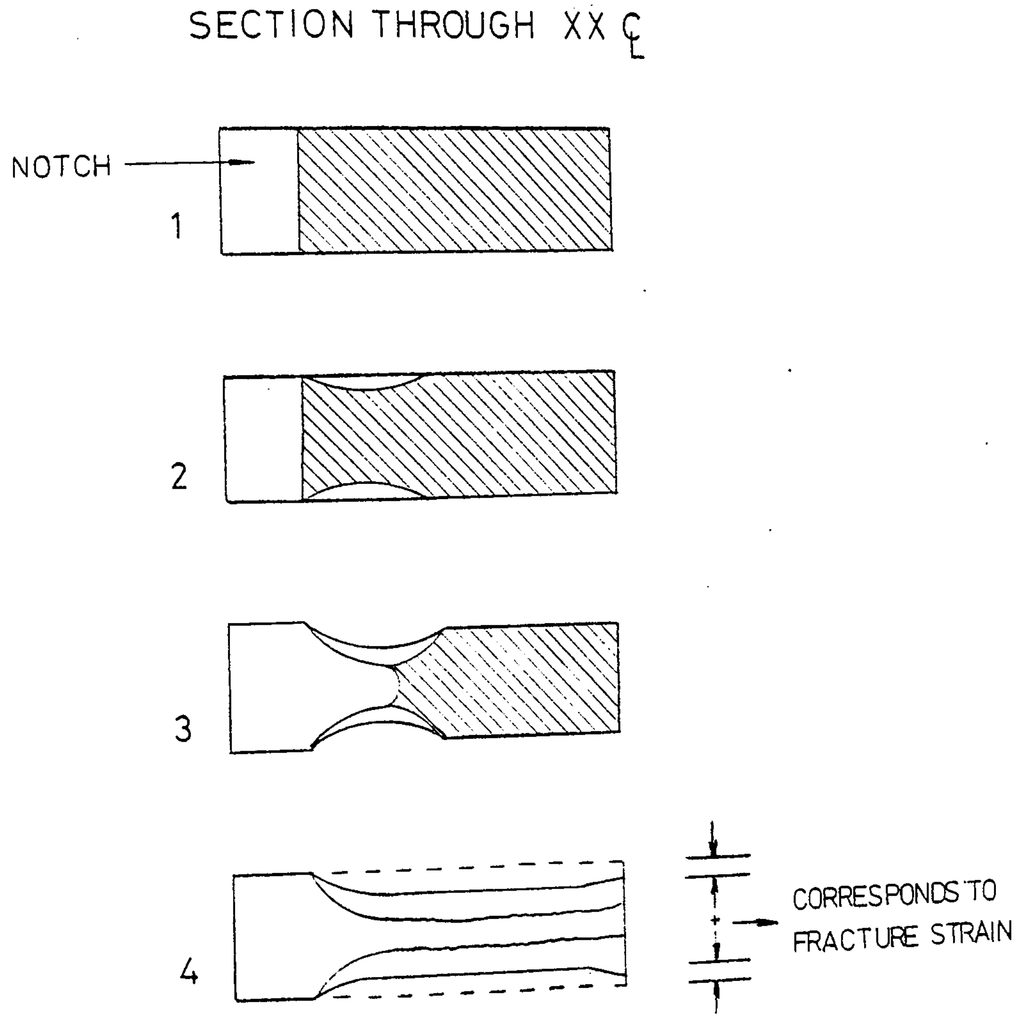

PROGRESION OF THROUGH
THICKNESS STRAIN
IN NEAR TIP REGION

FIG.5.6

mid-range of the scatter band at higher a/w values.

Having shown that crack advance is controlled by the attainment of critical strain logically the next step will be examine the factors that will control how fast this strain is obtained. This will be controlled by the nature of the stress distribution existing ahead of the crack tip.

5.3 Stress Distribution Preceding Creep Cracks

The results of the strain analysis show that the stress distribution σ_{yy} observed ahead of a creep crack can be described by the expression

$$\sigma \propto x_1^{-(1/n+1)} \qquad 5.1$$

Where x_1 is the distance from some point ahead of the crack tip

This is analogous to the results of the theoretical analysis by Barnby & Nicholson[125] but with the addition of a displacement to the position of the point x=0 for the theoretical distributions, moving this point to a little ahead of the crack tip. It is considered that this equation provides a reasonable description of the operative stress distribution for most of the creep life but not in the final stages of crack growth.

The need to displace the position of x=0 for the theoretical distributions away from the crack tip was not unexpected. A similar displacement to the stress distributions is required in LEFM fracture mechanics to compensate for the presence of a plastic zone.

During initiation the position of x=0 for a stress distribution of the type $x^{-(1/n+1)}$ was observed to be roughly half way between the crack tip and the D-point. Consider the situation for crack growth. Fig. 4.16 shows the distance between the crack tip and the D-point for the notched tensile specimens at various crack lengths. The average of this distance for the DEN and CN specimens together is 1.88mm and for the SEN specimens it is 0.98mm. Half these respective distances would correspond to sensible estimates of the suitable displacement of the theoretical stress distributions from the crack tip. That is, 1mm for the DEN and CN specimens and 0.5mm for the SEN specimens.

It would appear that the region between the crack tip and the D-point may function in redistributing the near tip stresses in a similar manner as the plastic zone under LEFM conditions. One fundamental difference does exist between the D-point region and a conventional plastic zone. That is, the plastic zone is strongly dependant in size upon the level of the applied stress, but the extent of the D-region, does not appear to be significant affected by the stress level. Even an increase in stress level by a factor of x4 failed to cause a consistently observable change in the size of the D-region. This suggests that the D-region is more of a geometrical effect than a stress effect. It is possible the D-region is principally where non-uniform behaviour occurs to accommodate the opening of the crack flanks. It will be related to the materials capacity for uniform strain and the ability for local through thickness contraction to accommodate the concentration of deformation in the near tip region bounded by the notch flanks.

These results are basically compatible with the experimental results of Barnby & Nicholson[125] who also found it necessary to displace the position of x=0 for a $x^{-(1/n+1)}$ type stress distribution away from the crack tip in order to obtain agreement with experimental results. Although they recognised the importance of such a displacement they were unable to correlate its magnitude with any observed characteristic. Nicholson[172] considered the displacement to be strain rate dependant and attempted to define the displacement by use of a stress function. This is not consistent with the observations here. Nicholson worked on stainless steels such as **AISI 316**. It is possible that with these less ductile materials the near tip zone may respond to the stress level in a manner more similar to a conventional plastic zone rather than to the geometrical considerations proposed here for the D-zone in an extremely ductile case, where the response of the entire ligament is already plastic.

It was observed that the stress σ_{xx} remained approximately proportional to σ_{yy} over the region of the strain profiles considered. This also was not totally unexpected. The σ_{yy} gradient along the X-direction produced a gradient of strain ε_{yy}. Greater flow in the Y-direction being associated with the larger values of σ_{yy}. Under constant volume conditions this strain ε_{yy} must be accompanied by contractions in the other two directions. The requirement for X-direction flow or strain ε_{xx} will hence follow a similar gradient in the X-direction as ε_{yy}. The lateral flow of material near the crack tip will be constrained by the material progressively further from the crack tip. This will result in a gradient of σ_{xx} of a similar nature to that describing the variation in σ_{yy} with distance in the X-direction. The magnitude of the constraining stress gradient will be geometry dependant for the reasons discussed earlier in section 5.1.

Some decrease in σ_{xx} was reported in the region close to the D-point. A similar decline is observed under LEFM conditions as the σ_{xx} value decays to zero at the traction free surface of the crack tip. The stress σ_{xx} must decay to zero at a traction free surface so under creep conditions where flow is possible a decline in the σ_{xx} constraint in the near tip region would not be unexpected.

The observation of proportionality between σ_{xx} and σ_{yy} means that if plane stress conditions can be assumed ($\sigma_{zz} = 0$) then the equivalent stress follows the same dependance on distance as was proposed for σ_{yy}. Consider the equivalent stress given by:

$$\bar{\sigma} = \frac{1}{\sqrt{2}} \left((\sigma_1 - \sigma_2)^2 + (\sigma_2 - \sigma_3)^2 + (\sigma_3 - \sigma_1)^2 \right)^{0.5}$$

Of $\sigma_3 = 0$ and $\sigma_2 = M\sigma_1$ then:

$$\bar{\sigma} = \frac{1}{2} \left((\sigma_1 - M\sigma_1)^2 + (M\sigma_1)^2 + (-\sigma_1)^2 \right)^{0.5} \qquad 5.2$$

$$\bar{\sigma} = \sigma_1 (1 - M + M^2)^{0.5} \qquad 5.3$$

As it has been shown that for each specific case M is a constant for the stress distribution along the XX centre line, if:

$$\sigma_{yy} \propto x^{-(1/n+1)} \quad \text{then} \quad \bar{\sigma} \propto x^{-(1/n+1)} \qquad 5.4$$

5.4 Crack Initiation

It has been proposed on the basis of a critical COD approach that crack initiation time should correlate with K^{-m}. This was not found to be a good description of crack initiation in this study. The regression analysis showed the principal factor controlling crack initiation to be the nett section stress although the importance of specimen geometry is accepted. Regressing initiation time against either just K or just σ_{nett} gave better correlations with σ_{nett}. From approaches splitting the K function into stress and geometrical features, the stress feature was always the more significant factor both from the basis of a larger exponent value and from the T tests. Use of correlations with the stress term related to σ_{gross} rather than σ_{nett} improved the significance of geometry term. This is because σ_{nett} takes account of the principal geometry feature, the crack length and hence σ_{nett} and the Y function are not totally independant.

The most probable reason for failure of the theoretical predictions is that they rely on small scale yielding. In practice the near tip deformation was extensive, and probably modified the near tip stress distribution to a greater extent than allowed for in theory.

For a given crack length around 0.35 a/w the DEN geometry will have a marginally higher K value than a CN specimen for the same nett section stress. The observation of the tendency for a DEN specimen to initiate in a longer time than a CN specimen under similar conditions tends to reflect the importance of the difference in lateral constraint present with the two geometries. The higher constraint with the DEN specimen will slow down the accumulation of strain and could effect initiation.

Increasing the constraint, for instance increasing starter notch length, would be expected to increase initiation time further as was observed with TS25.

The consideration of the constraints can be applied to the examination of the variation in initiation time with specimen thickness. One explanation as to the tendency of the thinner sheet to initiate first is that the 1.6mm material has a significant finer grain size than the others. From Equ. 2.2 this would be expected to result in a faster creep rate which lead to faster initiation. However, this is not the only consideration. For these specimens no significant trends concerning the maximum values of $\dot{\varepsilon}_{yy}$ or the corresponding values of $\dot{\varepsilon}_{xx}$ could be determined corresponding to specimen thickness. There was inconclusive evidence of a possible trend for the deviation from normal Poisson behaviour to be smaller with the thicker specimens. This would not be unexpected. It is considered that this effect is not due to a decrease in the lateral constraint σ_{xx} but to an increase in the through thickness constraint σ_{zz}. An increase in the through thickness stress would reduce the effect of the lateral stress in preventing contraction in the X-direction. Based on observations of ε_{xx} and ε_{yy} there would be an apparent decline in σ_{xx} if the increase in σ_{zz} was not taken into account. Increasing specimen thickness would be expected to increase through thickness contraint particularly in the vicinity of the notch. This is due to the increase in the area of the low stressed notch flanks in the plane of the notch. As this low stressed area increases in size with specimen thickness the constraint to thickness contraction in the area immediately adjacent to the notch flank is bound to increase see Fig. 5.7. As stresses are acting in the X and Y-directions this thickness constraint would give rise to a hydrostatic stress component and would hence reduce the rate of accumulation of strain ε_{yy}. As failure in all the specimens was successfully characterised by the summation of ε_{yy} and ε_{xx}, this hydrostatic component would be expected to delay initiation. One point emerging from this is that the damage leading to failure is more strongly correlated with strain than with a hydrostatic stress component. If the hydrostatic stress was the primary factor controlling damage accumulation leading to fracture, then the thicker specimens would be expected to initiate first and at a lower value of the strain summation.

The factor controlling initiation would appear to be the constraints to the accumulation of strain, in particular ε_{yy} as ε_{yy} will dictate the total level of strain in the other directions. To describe initiation an approach will be required that will take account of the variation in constraint due to geometry. An approach at correlating initiation times whilst considering the σ_{xx} constraints observed was attempted by using the equivalent stress. Using the values of σ_{xx} $= 0.33\sigma_{yy}$ for the DEN specimens and $0.15\sigma_{yy}$ for the CN specimens and by substitution in the equation 5.3 the following relationships were obtained:

$$\bar{\sigma} = 0.883\sigma_{nett} \text{ for DEN} \qquad 5.5$$

$$\bar{\sigma} = 0.93\sigma_{nett} \text{ for CN} \qquad 5.6$$

The stress concentration at the crack tip was ignored on the basis of that the near tip stress redistribution would probably ensure that it was of a similar level for both geometries especially as the K values would be similar anyway.

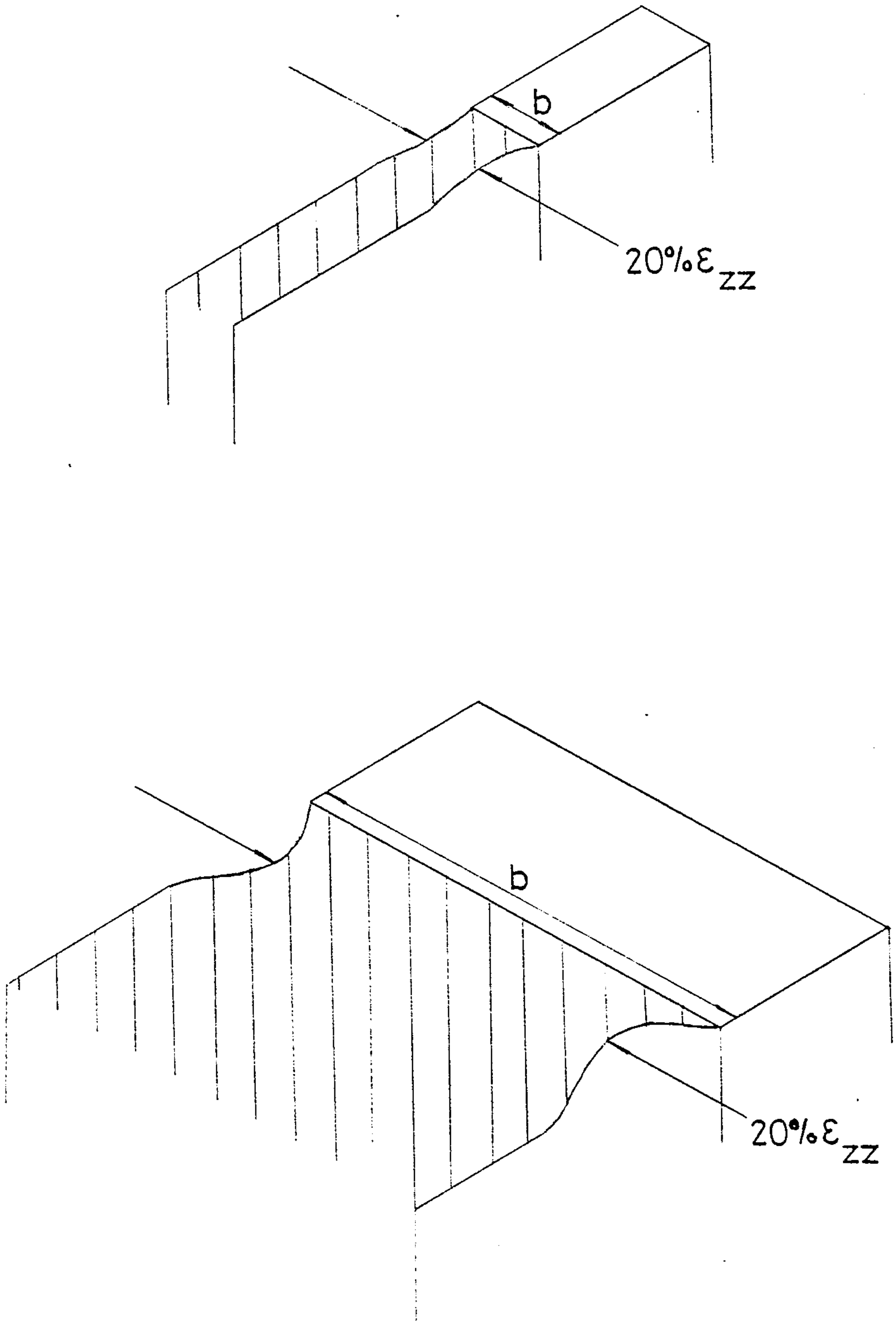

EFFECT OF INCREASING THICKNESS
ON THE CONSTRAINT TO THROUGH
THICKNESS CONTRACTION

FIG .5.7

From these values the following regression was obtained for $n = 3.5$

$$t_i = 2.1 \times 10^{5} \bar{\sigma}^{-3.77} \qquad r = 0.97 \qquad 5.7$$

This is a better correlation than with either just σ_{nett} or just K and predicts the initiation time for DEN specimens to be approximately 20% greater than for CN specimens of the same nett section stress, which is compatible with experimental results. It is interesting to note that the stress exponent in equation 5.7 is very close to the creep exponent n. This again would tend to indicate strain control of the initiation event, as initiation time and the accumulation of strain have the same stress dependance. The SEN geometry has not been included in this $\bar{\sigma}$ analysis because of the uncertainty in the level of the stress arising from the bending moment. Any stress contribution due to bending will raise the level of σ_y and hence also the equivalent stress and result in faster initiation as is observed with this geometry. The level of lateral constraint present with the SEN geometry is also uncertain. It is probable that some effect of the much higher K value associated with this geometry will be at least in part responsible for the reduced initiation time seen with these specimens. This suggests that the most complete description of initiation may be derived from an expression of the type:

$$t_i = AY^{B_1 n} \bar{\sigma}^{B_2 n}$$

The residual importance of K is supported by the initiation times of the large notch root radii specimens. These specimens showed comparatively long initiation times for their geometries. The low value of constraint stresses σ_{xx} and σ_{zz} would be expected to result in fairly fast initiation time but the initially low K value associated with these notches has obviously reduced the level of the equivalent stress in the near tip region.

For 0.33 a/w and the same nett section stress the K value for a SEN specimen is over twice that of a DEN specimen. Assuming similar degrees of lateral constraint (i.e. same ratio of σ_{xx}/σ_{yy}) and that the ratio of the near tip stresses are the same as for the K values (from equation 2.27). Equations 5.7 estimates the difference in initiation time as follows:

$$t_{i(SEN)} = 0.05t_{i(DEN)}$$

In practice $$t_{i(SEN)} = 0.18t_{i(DEN)} \quad \text{approx.}$$

Hence the redistribution of stress under creep conditions must reduce the difference in local stress reflected through K. This is consistent with the low exponent values for the Y-function in the regression equations 4.12 - 4.16 (these exponent values were around - 0.9 for n=3.5 and around -0.3 for n=7).

5.5 Crack Growth Behaviour

The results of the crack growth work show that neither

$$\frac{da}{dt} = AK^{m}$$

or

$$\frac{da}{dt} = B\sigma^{m}_{nett}$$

will provide a universal description of creep crack growth behaviour in Magnox AL80, regardless of the value of m selected, even when considering results for a single value of the creep exponent n. From examination of the results it would appear to be possible to correlate individual specimens with one or both of these growth laws by manipulation of the exponent, but such correlations would be distinctly local, that is, specific to that specimen and not a description of the behaviour of other specimens.

The process of crack advance has been shown to be strain or displacement controlled. This suggests that it would not be unrealistic to expect crack growth to show a similar dependance on stress as is shown by normal creep deformation. This means that the exponent for the stress function in any law describing crack growth would be expected to be related to or equal to the creep exponent. Arising from this consideration the K approach or the σ_{nett} approach could not be expected to constitute more than approximations of the observed behaviour. This is because the results indicate that the stress distribution preceding the crack tip is only defined by K for values of m=1 and by σ_{nett} for values of m = infinity. Despite this observation correlations with both K and σ_{nett} have been reported by several workers.

A point which should be emphasised first is that the method used here to compare crack growth behaviour is basically comparing the change in growth rate with change in crack length rather, than comparing the relationship of growth rate with crack length i.e.

$$\frac{da^2}{d^2t} \quad \text{versus a or t} \qquad 5.9$$

rather than $$\frac{da}{dt} \quad \text{versus a or t} \qquad 5.10$$

The increase of σ_{nett} and of the finite geometry K functions for the DEN and CN with increasing crack length are very similar as can be seen from Fig. 4.9. This provides a possible explanation why good simultaneous correlations with both σ_{nett} and K_{finite} are not uncommon.

The strain analysis section of this work has clearly shown the existence of a steady state stress distribution ahead of the creep crack tip. It has also shown that a significant accumulation of strain far in advance of the near crack tip region can occur particularly for the DEN and CN geometries. Crack advance has been shown to be strain controlled. The accumulation of strain ahead of the crack tip must influence the rate of crack advance in that as the time increases the crack tip will be growing into progressively more pre-damaged material. The effect of accumulating damage is endorsed by the creep pre-strained specimens. The results of the pre-strain tests showed that strain accumulated in the material prior to the arrival of the crack tip is contributory to the total required for fracture. The failure to take account of accumulating strain is a major weakness of most of the theoretical approaches to predicting creep crack growth rates.

The inclusion of a damage allowance to the theoretical σ_{nett} distributions was seen to improve agreement with experimental results. The level of the damage correction necessary to enable approximate agreement between the theoretical and experimental results was not consistent with the predicted level of the loss of ligament observed due to cavitation. The loss of ligament due to cavitation was estimated on the basis of the stress and strain levels from the quantitative metallographic results of the smooth bar creep tests. This suggests that damage should be considered in terms of the exhaustion of strain capacity rather than simply the loss of load bearing ligament.

With higher exponent values there will be a tendency for a pronounced accumulation of strain in the near tip region, declining rapidly to an asymptotic level. Lower creep exponent values will show a more gradual decline in the level of strain from the concentrated level near the crack tip, (compare Figs. 4.26a and b). The more gradual decline in strain level with lower creep exponent values means that on a strain exhaustion basis the lower exponent crack growth results would be expected to require a greater damage correction than their high exponent counterparts. This is because the effect of damage accumulation well ahead of the near tip region will be more pronounced for the low exponent case.

The type of damage correction applied here is not particularly appropriate for compensating for damage in the form of strain exhaustion. For allowing for loss of ligament due to cavitation the correction was valid apart from ignoring the fact that damage close to the crack tip will have the most influence on crack growth rate. On a loss of ligament basis the correction represented the same extent of damage at both exponent levels which is not the case if it is correcting for strain exhaustion. A damage correction in the form of additional crack length at n=7 will be equivalent to a greater amount of strain exhaustion damage than with n=3.5. This is because the extra crack length represents additional nett section stress and at a high value of the creep exponent a change in stress has considerably more effect on strain and strain rate than the same change at a low exponent. For instance, say for a small finite distance, strain accumulation has reduced the amount of further strain required for fracture over this interval by half. This can be expected to approximately halve the time taken for the crack tip to cross this interval. This could be compensated for in the σ_{nett} growth law by doubling the strain rate arising from the applied stress To double the strain rate at n=7 the stress must be increased by $\times 1.10$ and at n=3.5 by $\times 1.22$. Deterioration in the form of strain exhaustion does however excuse the tendency of the damage correction method to make the increase in damage with crack growth very pronounced.

In general it would be expected that correlations with the theoretical crack growth relationships would have exponent values slightly higher than the creep exponent values. This will accommodate the greater change in growth rate due to damage accumulation than is predicted theoretically without considering this phenomenon. For reasons already discussed this effect will decrease as the creep exponent increases.

The occurrence of ligament collapse close to 0.7 a/w was unfortunate in that it limited the extent over which crack growth could be observed. However it does represent the extreme limit of damage accumulation. It seems probable that tertiary effects are almost certain to be responsible for some of the acceleration in growth rate observed leading to ligament collapse. The onset of tertiary behaviour is supported by the deviation of the strain accumulation at high a/w values from that predicted by the theoretical stress distribution. This suggests that a breakdown in steady state conditions may be occurring at high a/w values. Also the strain level at the edge of a CN specimen at around 0.7 a/w would be around 30%. The CN geometry is that most resemblant of a smooth bar specimen in respect to the lateral constraint stresses. A strain of around 30% in a smooth bar specimen would suggest that tertiary behaviour could be expected. In addition, the high stress specimens will be approaching the UTS of the material for uniaxial tension around 0.7 a/w. The biaxial stressing will elevate the UTS to some extent but the onset of unstable behaviour would be impending.

It was observed that reducing the crack growth interval in order to eliminate the effects of ligament collapse as much as possible did not dispel certain trends in crack growth behaviour, such as:

i) The tendency for the SEN geometry to show very little change in crack rate

ii) The effect of creep pre-strain to reduce the change in growth rate

iii) The effect of increasing specimen thickness to increase the change in growth rate.

Consider the tendency for the SEN geometry to exhibit a much more even growth rate than the other geometries. A similar tendency has been observed by Bain in HK40 [164] over a range of temperatures. There are two factors which may contribute to this effect i) the ability of the SEN geometry to confine the strain remote from the crack tip to a low value ii) the tendency for this geometry to exhibit shorter crack initiation times compared with the DEN and CN cases.

Unfortunately the number of SEN specimens tested was rather limited but both of the factors above are consistent with the observed crack growth behaviour.

The ability of the SEN geometry to confine strain accumulation and hence damage close to the crack tip will mean that the crack will be continually growing into material of a more uniform condition than for the other two geometries, for the same change in a/w. Damage accumulation prior to the arrival of the crack tip has been shown to contribute to crack growth and so this effect must reduce the tendency for the SEN crack to accelerate.

Also the SEN geometry tends to initiate a through thickness crack in a shorter time than the other geometries. This rapid initiation would allow a greater interval for growth before tertiary effects started to cause a significant increase in growth rate.

Consider the large notch root radius SEN specimen TS27. This specimen will have a very low K value prior to initiation. This specimen showed a very long initiation period and a change in crack growth rate with crack length that was greater than for the conventional SEN specimen but still less than was seen with the DEN and CN specimens. This suggests that both the strain distribution and the initiation periods are important.

Another point to consider is the 'real time' interval between initiation and failure. These time intervals will be inversely proportional to the average crack growth rate. These times are shown in Table 4.5. The SEN specimens for n=3.5 showed an overall faster growth rate than the DEN and CN equivalents, but for n=7 the reverse is true even to the extent of offsetting any reduction in crack initiation time so that the total time to fracture was in fact longer. The stress intensity factor is more likely to be influential under a low creep exponent value. This follows from the stress following an $x^{-1(1/n+1)}$ type distribution and hence resembling the K distribution more at low exponent values and σ_{nett} more at high values. This can explain the tendency for the SEN geometry to show rapid crack growth at n=3.5 as the high K value for this geometry may still be partially effective. The tendency for slower than average crack growth for the SEN geometry at n=7 is not explained by consideration of the difference in K values for different geometries. This slower than average crack growth is most likely to be due to the tendency of this geometry not to cause extensive strain accumulation and hence creep damage other than in the near tip region. It should be remembered that the SEN crack has to cross twice the length of ligament compared to one crack of a DEN and CN specimen for the same a/w change.

Consider the observations with regards the effect of specimen thickness on crack growth behaviour. Thicker specimens were observed to show more change in crack growth rate than their thinner counterparts. From Table 4.4 it is seen that thinner specimens initiated faster and the growth interval leading to final fracture is also reduced. A short initiation time and rapid growth would tend to reduce the chance of tertiary effects in the ligament causing a substantial increase in the crack growth rate during the final stages. This is consistent with the thin specimens showing least change in crack growth rate. If increasing the thickness resulted in a uniform thickness constraint across the ligament there should be no change in the normalised growth rate. That is, the true growth rate will be slower for thick specimens but the normalised time representations of crack growth should be identical. This would be the case if the only effect of thickness constraint was due to the grain size variation. However thicker specimens showed a distinct tendency for greater acceleration in crack growth rate at high a/w values. This suggests that ligament damage effects are inhibited differently and less severely than the accumulation of strain at the crack tip. The accumulation of strain in the ligament will be inhibited in the thicker specimens by the larger grain size which will reduce the creep rate. The accumulation of strain at the crack tip will be affected by grain size but it will also be affected by any change in through thickness constraint due to the notch flanks. This through thickness constraint is bound to increase with specimen thickness, but the effect will only be apparent in the near tip region, (as discussed in section 5.4 with respect to crack initiation).

The pre-strained specimens tended to show less change in growth rate than was normal for their respective geometries. The effect of creep pre-strain would be to give the ligament a uniform distribution of damage. When a stress gradient is superimposed onto this evenly damaged ligament crack initiation would be expected to occur fairly rapidly. As the crack would then be growing through evenly damaged material the rate of growth would be expected to be fairly rapid and also even as there would be reduced opportunity for further significant strain accumulation far ahead of the crack tip. This argument is consistent with the short initiation time (after pre-straining) and short growth time interval seen for TS19 for which n=3.5. However the evidence is not so immediately convincing for n=7. For the high stress regime pre-strained specimens the initiation and growth intervals appeared relatively unaffected by the pre-straining treatment. Inadequate allowance for the time to re-establish a temperature approaching 300°C after pre-straining may be responsible for an over-estimate in the initiation time after pre-straining. For the high stress regime tests the initiation interval is short so that an error or even 0.25 hours in this estimate could be significant when comparing the initiation times of pre-strained specimens and corresponding specimens without this treatment. However, the principal reason for the apparent lack of change in initiation time or crack growth interval after pre-straining is considered to be because of the level of the applied load after pre-straining. After pre-straining the load applied was such that the nett section stress was the typical starting stress used for that exponent level (i.e. $5MNm^{-2}$ or $20MNm^{-2}$). For instance for TS26 a load of 3380N was used instead of 4000N had the specimen not been pre-strained. This ensured that both the specimens without pre-strain and those with pre-strain started notch rupture testing with a similar nett section stress (approximately $20MNm^{-2}$). As fracture is strain controlled both the pre-strained specimen and the specimen without pre-strain would continue to deform until a similar failure strain is reached. To reach this point the specimen without pre-strain will have to deform to a greater extent, with greater changes to the cross section area, as the pre-strained specimen is already strained to a significant fraction of the failure strain. The specimen without pre-strain will hence be under a greater nett section stress at the time of initiation. At n=7 the affect of this anomaly will be very pronounced as the high value of the creep exponent will mean that a small change in the stress will cause a very noticable effect on the strain rate.

5.6 Metallographic Observations

Creep damage in the form of cavitation was a common observation. The cavities in the smooth bar tests were observed to lie on grain boundaries perpendicular to the stress axis and resembled those predicted as forming through a vacancy condensation process.

With the notched specimens, the observation of cavitation to favour the shear bands at 45° to the crack tip for the CN and SEN specimens and the tendency for the final fracture path of these geometries to run up the shear bands suggests that cavitation may be influenced by the slip line fields. However, cavitation was still observed to favour grain boundaries normal to the principle stress axis. The observation that a hydrostatic stress component arising from specimen thickness did not reduce the critical value of the summation of ε_{yy} and ε_{xx} supports the need of displacement in order to produce creep damage leading to failure.

Where cavities were observed they usually occupied a large proportion of the boundary on which they were situated and consequently often included a multiple grain boundary. Examples such as Fig. 4.29 tend to suggest that grain boundary decohesion in the form of wedge cracking may be responsible for some of the cavitation but this would not explain the distinct tendency for cavities to orientate at around 90° to the tensile axis. A wedge cracking mechanism would be expected to produce cavities orientated at 90°, 70° and 45° to a principal tensile axis. The observation of cavities to orientate predominantly at around 90° to the tensile axis suggests that diffusion processes are influencing growth. Deformation nucleation processes are consistent with the lack of observation of many small isolated cavities. In a ductile material such as this flow around small grain boundary obstacles will reduce the probability of decohesion at these points due to grain boundary sliding. It seems very probable that cavitation is influenced by both deformation and diffusion processes.

The observation of less cavitation in the higher stress specimens is considered to be due to deformation at this stress range being less dependant upon grain boundary sliding. This cannot be supported by any measurements of the relative fractions of grain boundary strain contributions and grain deformation contributions. However this possibility is supported by the observation of a greater evidence of grain deformation with the high stress specimens in the form of higher slip band densities.

It is considered that the as supplied material has a fairly strong grain orientation texture. During prestraining a noticable tendency for lateral contraction as opposed to through thickness contraction was observed in the pre-strain specimens, especially at the higher stress level. The pre-strain specimens TS18 and 26 represent the majority of the **values** of P_d less than zero. Whilst it is considered that in some cases value of P_d less than zero could be indicative of error this is not the case for these pre-strained specimens. The effect was more noticable at the higher exponent, probably because the contribution of grain deformation to the total was greater and because there was less chance of the texture being lost by a prolonged time at 300°C.

A given level of cavitation at a high exponent value will have a greater effect on strain rate than for a low exponent. The cavitation represents a loss in load bearing ligament and hence an increase in stress on the remaining ligament. From Norton's law this increase in stress will have a much greater effect on strain rate at high exponent values. This can account for the materials tolerance of higher levels of cavitation at the lower stress levels.

The fracture mechanism appeared to be ductile tearing between the creep cavities. This is again consistent with the importance of shear deformation. The mechanism appears to be basically the void sheet mechanism. However it is inconclusive whether or not the intercavity tearing was entirely transgranular or mixed transgranular and inter-granular. This type of failure has been observed in several materials under creep conditions, particularly where reasonable ductility exists including AISI 316. This emphasises the probability that many of the observations made in this work on AL80 may be applicable to more common engineering materials.

5.7 Summary of Creep Crack Growth Behaviour

Very briefly the following observations summarise creep crack growth in Magnox AL80. The advance of the crack tip is controlled by the attainment of strain. A critical value of the summation of ε_{yy} and ε_{xx} proved to be a good criterion for describing crack growth in all the geometries and the variations on the geometries considered. The influence of stress on crack growth is through its effect on the rate at which strain is accumulated. This is true not only for σ_{yy} but also for the constraint stresses σ_{xx} and σ_{zz}. The stress varies with distance from just ahead of the crack tip as $x^{-(1/n+1)}$. There is extensive stress redistribution of stress in the near tip region. This inhibits K from providing a description of crack initiation time. To describe crack advance the effect of strain accumulated prior to the arrival of the near crack tip region must be considered. Cavitation features in the fracture process. The formation of this cavitation is certainly dependant at least in part on deformation processes but the allied importance of diffusion processes is suggested.

5.7.1 Theoretical Prediction of Creep Crack Growth

Having experimentally examined the criteria controlling creep crack advance a brief attempt can be made to assemble these in a theoretical approach for predicting creep crack growth rates. The following observations have been employed, failure occurs at a critical strain and the stress distribution preceding the creep crack is given by $\sigma_y \propto x^{-(1/n+1)}$. Also σ_{xx} is proportional to σ_{yy} for a particular geometry and so in this approach the stress is considered to be the equivalent stress $\bar{\sigma}$. The failure strain is correspondingly set at 40% (20% through thickness strain under uniaxial conditions) but in fact the magnitude of the failure strain used in this approach will have no effect on the shape of a crack length/normalised time distribution.

Let initiation be characterised by the point one unit of distance ahead of the crack tip reaching the failure strain. At initiation the stress distribution can be considered stationary so the strain profile will be given by:

$$\varepsilon_{yy} = 40x^{-(n/n+1)}$$

This is shown in Fig. 5.8. The crack tip will reach point $x=x_1$ when the strain at the point x_1 has risen from its value at initiation to the failure value. The time for this to occur will be given by:

$$t = \frac{\varepsilon_{fail} - \varepsilon_{x_1 t_i}}{\text{Average } \dot{\varepsilon}_{x=x_1}} \qquad 5.11$$

Where $\varepsilon_{x_1 t_i}$ = strain at point $x=x_1$ and time t_i (initiation)

Average $\dot{\varepsilon}$ = average strain rate at $x=x_1$ between $t=t_i$ and $t=t$

The strain rate $\dot{\varepsilon}$ at the point $x=x_1$ will increase as the crack tip advances towards the point $x=x_1$. Mathematical solution of this

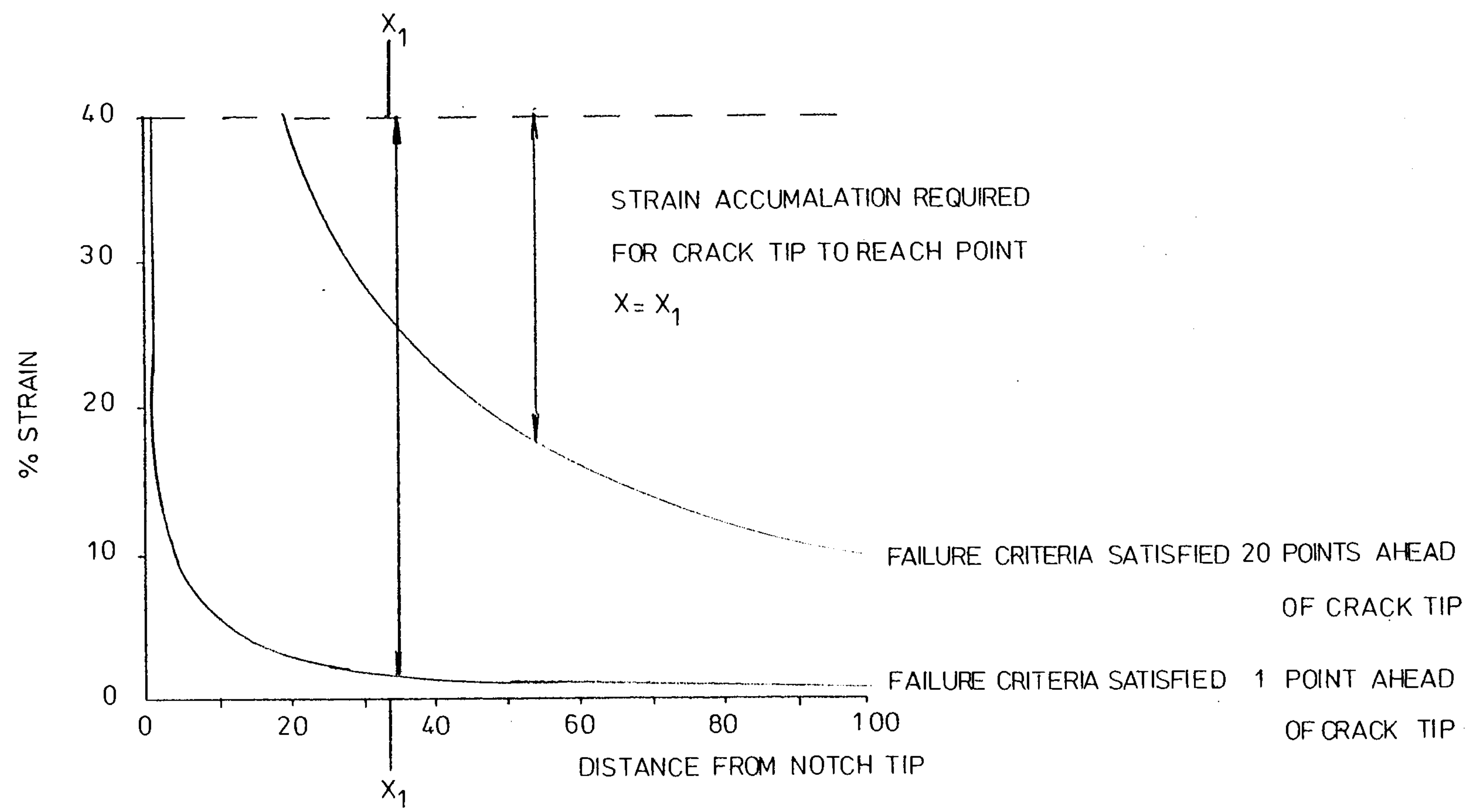

STRAIN DISTRIBUTION AT
TIME OF INITIATION

FIG. 5.8

problem was not forthcoming so a numerical solution was adopted, using the following method:

1) Determine the strain at each point across the ligament at initiation using $\varepsilon = 40x^{-(n/n+1)}$

2) Calculate the stress at each point across the ligament ahead of the crack tip from $\sigma = Ax^{-(1/n+1)}$. The stress for each point from x=1 is summed across the ligament in order to determine the constant A from A = 1/(sum of stresses for each point). This corresponds to constant load conditions.

3) Apply Norton's law to each point for unit time so that $\varepsilon_{x_1} = B\sigma^{n}_{x_1}$ and add this strain to that already accumulated at the point.

4) Test to establish how many points across the ligament have accumulated strain values in excess of the failure strain. The last point having an accumulated strain level above 40% corresponds to the position of the crack tip. The position of x=0 is moved accordingly.

5) Return to 2 and repeat until the crack tip has crossed the ligament.

The process was also repeated with the failure event being based on the points x=5, 10, 15 and 20 reaching the failure strain. This was to make some allowance for the deviation of the near tip region from the theoretical stress distribution. In these cases the summation of the stress across the ligament was performed from half way between the point x=0 and the failure strain point to the end of the ligament (x=100).

The most striking observation of this approach is that it produces a plot of crack length versus normalised time almost identical to that predicted for constant load over the same growth interval from:

$$\frac{da}{dt} = A\sigma_{nett}^{n}$$

(See Fig. 5.9). This was true for both n values and regardless of the value of the failure strain selected. This is especially of interest as the strain accumulation approach uses a steady state stress concentration. Moving the position of x at which the failure criteria must be satisfied had only a minor effect on the resulting relationship between time and crack length. It is considered that these minor changes arise due to the changes in the nett section stress resulting from summing the stresses over a marginally shorter interval and not due to any changes in the strain behaviour. Modifying the starting strain distribution to include uniform pre-strain across the ligament did produce a minor decrease in the change of growth rate observed, consistent with experimental results.

This theoretical model fails to predict the same increase in growth rate that was observed with the experimental specimens. It is considered that this is due to the theoretical approach describing deformation purely by Norton's law and hence not accommodating any tertiary effects. At high a/w values in practice it is probable that a substantial portion of the ligament was exhibiting tertiary behaviour. This is consistent with the agreement between theory and practice being poorer for n=3.5 as for this exponent level the change between secondary and tertiary deformation is more pronounced then for n=7.

The similarity in crack growth behaviour predicted from σ_{nett} and strain accumulation does provide an explanation for correlations

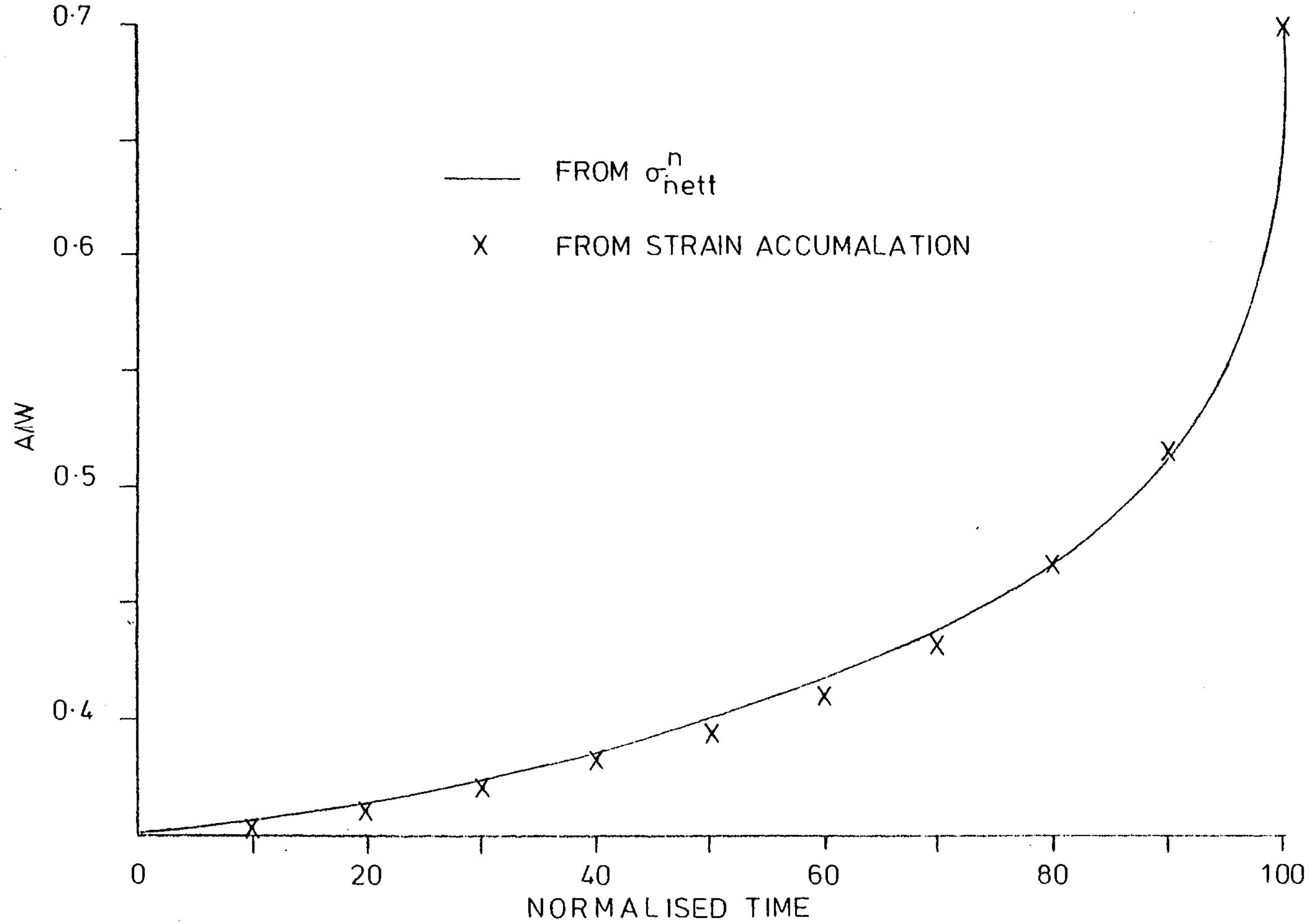

COMPARISION OF STRAIN
ACCUMALATION AND NETT SECTION
STRESS APPROACHES

FIG.5.9

with σ^n_{nett} especially for materials that fracture with little tertiary behaviour. The reason for this similarity is worth considering
The crack length versus time plot for σ_{nett} control is derived from:

$$t = \int_{a_1}^{a_2} \frac{1}{\sigma^n_{nett}} .da$$

A dominant feature of the accumalating strain model is:

$$\int_{a_1}^{a_2} \frac{1}{\dot{\varepsilon}_{x_1}} .da$$

Strain rate $\dot{E}$ would correlate to σ^n_{nett} so a link between the approaches can be seen here. However this argument ignores an important point. As the crack grows the point x_1 lies at an ever decreasing distance from the crack tip. This means that its position along the stress concentration varies and hence the ratio of the stress at x_1 to σ_{nett} will also vary. The extent of this variation will depend on the original distance of point x_1 from the crack tip. It appears from the analysis that the difference in the level of strain accumulation required at different points across the ligament at t_i offsets this effect. Unfortunately this has not been mathematically verified.
It should be noted however that with the strain accumulation approach, crack growth rate for a given value of σ_{nett} will be dependant to some extent on the amount of prior crack growth. This dependance on prior crack growth is not predicted by the empirical growth law based on σ^n_{nett}. This means that the σ_{nett} law may not be predictive of growth rates from other starting crack lengths and stresses.

The strain accumulation approach to crack growth prediction layed out here is an over simplification. However the approach is based on theoretically proposed criteria which have been experimentally verified by this work. This is a definite deviation from the empirical application of parameters such as σ_{nett} or K with possible explanations as to their applicability being proposed later.

Most of the attempts to predict creep crack growth rates have failed in their inability to relate results from one geometry to different geometries. The finite element approaches are the most successful in this respect.[190] However even these tend only to prove predictive in a retrospective manner when some of the parameters can be set on the basis of observed behaviour. The finite element techniques calculate stress distributions within a finite body. These are then related to growth rates through empirical relationships, or alternatively, strains resulting from these stress distributions can then be calculated and crack growth can then be predicted on the basis of a critical failure strain. This work has illustrated the importance of taking account of the constraint stresses and it is in this capacity that the finite element technique has an advantage over most other methods. This work has provided details of the strain behaviour during crack growth which may provide a first step towards understanding how the failure parameters may be set accurately for finite element predictions of crack growth. For materials where creep failure is strain controlled prediction of creep crack growth will ultimately be performed using refined versions of the simple approach used here. The stress system may be calculated on the basis of a finite element approach but crack advance will be determined by assessing the strain accumulated, possibly using more complete descriptions of strain rate than Norton's law. The knowledge of how failure strain varies with multiaxial stress will be of very vital importance to the success of these approaches with real geometries. The apparent applicability of an established sheet forming criterion for biaxial tension (critical bulk sheet thickness strain) for Magnox AL80 is encouraging as it is very easy to apply. Verification as to whether or not this approach is applicable to more common engineering materials under biaxial creep conditions would be useful. Also a fuller examination of the effect of tertiary stress states is important. Use of Magnox AL80 for such a study would not be totally unrealistic as although this knowledge for AL80 does not represent an immediate service requirement, the good ductility of the material enables easy study of the effect of the stress system on ductility.

6. CONCLUSIONS

1. The advance of a creep crack in Magnox AL80 at 300°C is controlled by the attainment of a critical strain. Failure of specimens of 3 different geometries was characterised by the same value of the summation of ε_{yy} and ε_{xx} at the location of the maximum value of ε_{yy}.

2. Strain accumulated prior to the arrival of the crack tip is contributory to the accumulation of the critical failure strain. This factor must be considered when predicting creep crack growth rates in materials where crack advance is strain controlled.

3. Assessing the COD from the notch flank opening can be misleading and may indicate different growth behaviour for edge cracks compared to embedded cracks. Material a considerable distance either side of the plane of the notch contributes to the COD seen between the notch flanks. Measurements of the strains in this material will provide the best description of the criterion controlling crack advance. The equivalent COD evaluated at the crack tip was found to be basically independant of geometry and relatively constant during growth. However the geometry independance arises by virtue of a dominance of the contribution to total displacement from material instability. It is hence not a good indication of the criterion controlling crack advance. If the COD is evaluated at the D-point which marks the onset of material instability the COD will be geometry dependant.

4. The parameter K was not a good description of the time taken to produce a through thickness crack. This is due to the extensive

near tip deformation redistributing the stress in this region. The principal factor controlling initiation appears to be the nett section stress, however geometry does have some influence. Allowing for the difference in lateral constraint between the DEN and CN specimens by use of an equivalent stress approach described the difference in initiation time for these geometries seen in practice.

5. A stress distribution of the form $\sigma_{yy} \propto x^{-(1/n+1)}$ gives a fair description of that deduced from experimental measurements of strain distributions, both during initiation and growth. An allowance for near-tip behaviour is required, which appears to approximate to displacing the position of x=0 by half the distance between the crack tip and the D-point (the point at which non-uniform near tip displacement is first observed). This correction is analogous to the displacement of the point x=0 to the centre of the plastic zone for the stress distributions under LEFM conditions.

6. From strain measurements it was deduced that σ_{xx} follows the same stress distribution as σ_{yy} except in the region close to the crack tip. The ratio of σ_{xx} to σ_{yy} is geometry dependant. DEN specimens produce around twice the lateral constraint seen for a CN specimen. As σ_{xx} and σ_{yy} are proportional, under plane stress conditions the equivalent stress distribution will also follow an $x^{-(1/n+1)}$ type distribution.

7. The principal effect of increasing notch root radius appears to be to reduce the lateral constraint stress σ_{xx} during initiation and the early stages of crack growth.

8. Neither the nett section stress nor K provide a valid description of crack advance in Magnox AL80. From consideration of the stress distribution ahead of a creep crack neither of these approaches could constitute more than approximations unless the creep exponent n=1 for K control or infinity for σ_{nett} control. Even then they would be failing to accommodate accumulating damage.

9. Failure of the material was by the void sheet mechanism. Deformation processes are important in cavity initiation but the allied importance of diffusion is not discounted. Estimations of creep damage should not be based on the extent of cavitation but on the extent of accumulated strain.

ACKNOWLEDGEMENTS

Appreciation is expressed to the Project Supervisor Professor J.T. Barnby for his guidance throughout the project. Thanks are also expressed to the external supervisors Dr. R.B. Jones at Berkeley Nuclear Laboratories and Dr. R.D. Nicholson now at Marchwood Engineering Laboratories, for their much valued advice and for the supply of the test material plus use of B.N.L. facilities.

REFERENCES

1. A.H. Cottrell, ISI Special Report 70 London 1961

2. Royal Commission Report on Environmental Pollution, 6th report HMSO September 1976

3. Nuclear Power Reactors UKAEA Publication

4. E.F. Emley, Principles of Mg. Tech. Pergamon Presss 1966

5. G.F. Hines, V.J. Haddress & R.E. Jones, Proc. Inf. Conf. Phys. Met of Reactor Fuel Elements Sept. 1973

6. Calder Hall Symposium, J. Brit. Nucl. Eng. Conf. 1957,2,2

7. British Patent 776649

8. E.F. Emley, J. Brit. Nuch. Eng. Conf. 2,1957,254

9. R.A.U. Huddle & L. Wyatt ibid 2,1957,110

10. L. Grainger & A.B. McIntosh ibid 2,1957,121

11. Magnox Data Sheet 16 Nuclear Eng. 1961

12. J.E. Harris & R.B. Jones, Berkeley Nuclear Labs. Report. RD/B/R.144 unpub.

13. J.E. Harris & R.B. Jones & G.W. Greenwood, CEGB Report, R.D./B/N172 1963

14. J.E. Dorn, J. Mech. Phys. Solids 3,1954,85

15. C.M. Sellars & A.G. Quarrel, J.I.M. 90,1961-62,329

16. O.D. Sherby Acta Met. 10,1962,135

17. R.N. Rhines, NPL Symp. Creep & Fracture of Metals at High Temps. HMSO 1954,47

18. E.R. Parker & J. Washburn ASM 1956 Creep & Recovery P.227

19. C. Herring, J.APPL. Phy. 21,1950,437

20. F.R.N. Nabarro Report on Conf. Strength of Solids Bristol 1948

21. I.G. Crossland & R.B. Jones, Met. Sci. J. 6,1972,162

22. B. Burton, Met. Sci. J. 5,1971,11

23. A.T. Churchman, Proc. 3rd. Int. Conf. Peaceful uses of atomic energy United Nations 1964,156

24. J. Weertman, Trans. AIME 218,1960,207

25. R.B. Jones, Berkeley Nuclear Labs, Private Communications 1978

26. J.N. Greenwood, D.R. Miller & J.W. Suiter, Acta Met. 2,1954,250

27. C.H.M. Jenkins, J.Inst. Met. 70, 1944,57

28. J.N. Greenwood, JISI, 171,1952,380

29. C. Zener, Fracturing of Metals ASM Cleveland, 1948

30. J.N. Greenwood, D.R. Miller & J.W. Suiter, Acta Met. 2,1954,250

31. J.O. Stiegler & K. Farrell, BTM Loh. & H.E. McCoy Trans. AMSM 60,1967,494

32. D. McLean, J. Inst. Met. 85,1956-7,468

33. R.D. Stacey, Metallurgia 58,1958,125

34. T.J. Heal, Proc. Int. Conf. Peaceful Uses of Atomic Energy United Nations 5,1959,208

35. R. Eborall, Proc. Symp. Creep & Fracture of Metals at High Temps Teddington, 1954

36. H.C. Chang & N.J. Grant, Trans. AIME 206,1956,544

37. I.S. Servi & N.J. Grant, Trans. Met. Soc. AIME 191,1951,909

38. A.A. Griffith, Phil. Trans. Roy. Soc. A221,1921,163

39. A.N. Stroh, Proc. Roy. Soc. A223,1954,404

40. D. McLean, Grain Boundaries in Metals. Oxford Univ. Press 1957

41. A.N. Stroh, Advances in Physics 6,1957,418

42. F.E. Hauser, P.R. Landon, J.E. Dorn AIME, Trans. 206,1956,589

43. E. Smith & J.T. Barnby, Met. Sci. J. 1,1967,56

44. J.E. Harris, Trans. Met. Soc. AIME 233,1965,1509

45. R.G. Fleck, D.M.R. Taplin, C.J. Beevers, Met. Sci. J. 9,1975,49

46. T. Johannesen & A. Tholen, Met. Sci. J. 6,1972,189

47. C.W. Chen, E.S. Machlin, Acta Met. 4,1956,655

48. R.W. Baluffi & L.L. Seigle, Acta Met. 3,1955,170

49. R. Raj, Acta Met. 26,1978,995

50. R.G. Fleck, D.M.R. Taplin, C.J. Beevers, Acta Met. 23,1975,415

51. E. Smith & J.T. Barnby, Met. Sci. J. 1,1967,1

52 C.W. Weaver, J. Inst. Met. 88,1959-60,296

53. D.G. Morris D.R. Harries Met. Sci. J 12,1978, 532

54. R. Eborall, ISI Symp. Structural Processes in Creep, London 1961

55. J.E. Harris Met.Sci. J. 12,1978,321

56. P.W. Davies & K.R. Williams, Met. Sci. J. 3,1969,48

57. A.E.B. Presland & R.I. Hutchinson, J.Inst. Met. 92,1963-64,264

58. G.W. Greenwood, Phil. Mag. 19,1969,423

59. R.T. Ratcliffe & G.W. Greenwood, Phil. Mag. 12,1965,59

60. C.E. Price, Acta. Met 14,1966,1781

61. J. Intrater & E.S. Machlin Acta. Met 7,1959,140

62. R.C. Boettner & W.D. Robertson, Trans. AIME 221,1961,613

63. A. Gittins, Met. Sci. J. 1,1967,214

64. P.R. Oliver, L.A. Girifalco Acta. Met. 3,1955,605

65. D.A. Woodford, Met. Sci. J. 3,1969,234

66. B.F. Dyson & D. McLean Met. Sci. J.8,1974,261

67. H.E. Evans, J.S. Waddington, Phil. Mag. 20,1969,1075

68. C.K.L. Davies, P.W. Davies, B. Wilshire, Phil. Mag. 18,1968,197

69. N.G. Needham, J.E. Wheatley & G.W. Greenwood, Acta Met. 23,1975,23

70. C.H.M. Jenkins, Symp. Creep Fracture of Metals at High Temps. Teddington, 1954

71. R.W. Baluffi & L.L. Siegle, Acta Met 5,1957,449

72. D. Hull & D.E. Rimmer Phil Mag. 4,1959,673

73. D.M.R. Taplin, L.J. Barker Acta Met. 14,1966,1527

74. J.A. Williams, Phil. Mag. 15,1967,1289

75. R. Soderberg, Proc. 2nd. Inf. Conf. on Fracture, Brighton 1969

76. J.S. Waddington & J.A. Williams, Acta Met 15, 1967,1563

77. N.G. Needham & G.W. Greenwood, Met. Sci. J. 9,1975,258

78. D. McLean, J.Australian Inst. Met. 8,1963,45

79. I.G. Crossland, J.E. Harris Met. Sci. J 13,1979,55

80. P.W. Davies, R. Dutton Acta Met. 14,1966,1138

81. D.M.R. Taplin & R.C. Gifkin, Acta Met. 15, 1967, 650

82. P.W. Davies, K.R. Williams, Met. Sci. J. 3,1969,220

83. Y. Ishida & D. McLean, Met. Sci. J. 1,1967,171

84. J. Hancock, Met. Sci. J. 10,1976,319

85. F.A. McClintoch, Trans. ASME series E 35,1968,363

86. D. McLean, B.F. Dyson & D.M.R. Taplin, Fracture 77, Waterloo Canada.

87. J.A. Williams 1975 Proc. Conf.. The Mechanics & Physics of Fracture, Cambridge

88. P. Rama Rao, V.V.P. Kutunba Rao, M.C. Pandey, JISI 211,1973,801

89. S. Goods & W.D. Nix Acta Met. 26,1978,739&753

90. D.W. Matlock & W.D. Nix J. Nuc.Mat. 56,1975,145

91. K. Erlich, H. Bohn & C. Wassiler ASTM STP 480,1971,495

92. B.J. Cane Met. Sci.J. 12,1978,102

93. W. Beere & M.V. Speight Met. Sci. J 12,1978,172

94. R.S. Gates, Mat. Sci. Eng. 27,1977,115

95. F.A. McLintock ASM Seminar on Ductility 1967

96. T.J. Heal, Proc. Int. Conf. Peaceful Uses of Atomic Energy United Nations 5,1959,208

97. D.G. Morris, Met. Sci. J. 12,1978,19

98. G.J. Cocks & D.M.R Taplin, Metallurgia 75,1967,229

99. R. Soderberg, Met.Sci. J. 9,1975,275

100. C.J. McMahon, Fracture 77, Int. conf. Waterloo, Canada

101. J.F. Knott, ibid

102. S. Goods & W.D. Nix,ibid

103. C.L. Jones & R. Pilkington, ibid

104. A.E. Johnson, Recent Progress in Applied Mech. (ed. Broberg)

105. A.E. Johnson & J. Henderson, Complex stress creep relaxation of metallic alloys, HMSO Edinburgh 1962.

106. R. Sumerling & E.D. Hyam, The Metallurgy of Beryllium, Inst. of Metals Monograph 28,1961

107. A.L. Wingrove & D.M.R. Taplin, J. Mat. Sci.4,1969,789

108. W.F. Brown & G. Sachs, NACA, Tech. Note 2433,1951

109. M.J. Manjoine, J. Basic Eng 84,1962,220

110. M.J. Manjoine, Proc. Int. Conf. on Creep, London 1963

111. R.M. Goldhoff, ibid

112. H.R. Voorhees, J.W. Freeman, J.A. Herzog, J. Basic Eng. 84,1962,207

113. D.K. Hanik, H.R. Voorhees, J. Basic Eng. 84,1962,233

114. E.A. Davies, M.J. Manjoine, ASTM Tech. Pub. 128,1952

115. W.F. Brown, M.H. Jones & D.P. Newman ibid.

116. F. Garofalo Proc. ASTM 1959,957

117. S. Taira & R. Ohtani Proc. Conf. Creep & Fatigue in elevated temp. application, Philadelphia, 1973.

118. D.R. Hayhurst & F.A. Leckie Univ. of Leicester Eng. Dept. 75-2, April 1975.

119. D.R. Hayhurst, J.T. Henderson, Univ of Leicester, Eng. Dept. Rep. 76-3,May 1976

120. D.R. Hayhurst, F.A. Leckie Proc. Royal Soc. A360, 1978,243

121. G.R. Irwin, Trans. ASME J. App. Mech. 24,1957, 361

122. H.M. Westergaard, App. Mech. 61,1939,A49

123. J.R. Rice & G.F. Rosengren, J. Mech. Phy. of Solids 16,1968,1

124. J.T. Barnby, Eng. Frac. Mech. 6,1974,627

125. J.T. Barnby & R.D. Nicholson, J. Mat. Sci. 12,1977,2099

126. N.J. Hoff, Q. Appl. Mat. 12,1954,49

127. H. Neuber, Trans. ASME 1961,544

128. M.P. Harper, E.G. Ellison J. Strain Analysis 12,1977,167

129. V. Vitek, Int. J. Frac. 3,1977,39

130. B.A. Bilby, A.H. Cottrell & K.H. Swinden, Proc. Roy. Soc. A272 1963,304

131. G.R. Irwin, Fracturing of Metals, ASM Cleveland 1948

132. E. Orowan, Progress in Physics, 12,1949,185

133. E. Orowan, Weld. J. Res. Supp. 20,1955,157S

134. F.R. Irwin & J.A. Kies ibid 17,1952,95S

135. G.R. Irwin J. App. Mech. 24,1957,361

136. G.R. Irwin 9th Int. Congr. App. Mech. Brussels 1957

137. G.R. Irwin Eng. Frac. Met. 1,1968

138. G.R. Irwin, Sagamore Ordance Mat. Conf. 1961

139. A.A. Wells, Crack Propagation Symp. Cranfield 1961,210

140. D.S. Dugdale, M. Mech. Phys. Solids 8,1960,100

141. F.M. Burdekin & D.E.W. Stone, J. Strain Analysis 1,1966,145

142. A.A. Cottrell, Proc. Roy. Soc. A285,1965,10

143. J.R. Rice, J.Appl. Mec. Trans. ASME. 35,1968,379

144. P. Price & F. Erdogan, J. Basic Eng. 85,1963,528

145. H.G. Popps & A. Coles, Proc. U.S. Air Force Conf. Fatigue & Fracture, 1970,71

146. M.J. Siverns & A.T. Price, Nature,228,1970,760

147. C.B. Harrison & G.N. Sandor, Eng. Frac. Mech. 3,1971,403

148. L.A. James, Int. J. Frac. Mech. 8,1972,347

149 K. Robson, Int. Conf. on Creep Resistance in Steels, Dusseldorf 1972

150. D.V. Thornton, G.E.C. (Whetstone) Rep. CML 1972-18

151. G.J. Neate & M.J. Siverns, Int. conf. on Creep & Fatigue in Elevated Temp. Apps. Philadelphia 1973

152. J.L. Kenyon, G.A. Webster, J.C. Radon & C.E. Turner, ibid

153. E.G. Ellison & D. Walton, ibid

154. J.R. Haigh, Mat. Eng. Sci. 20,1975, 213 & 225

155. G.J. Neate, C.E.G.B. Report. SSD Mid/R.12/74

156. R. Pilkington, P. Hutchinson & C.L. Jones, Met. Sci. J. 8,1974,237

157. G.A. Webster, Proc. Conf. Mech. Phy. of Fracture, Cambridge 1975

158. R.D. Nicholson & C.L. Formby, Int. J. Frac. 11,1975,595

159. R. Koterazawa, Int. J. Frac. 11, 1975,1060

160. E.G. Ellison & M.P. Harper, J. Strain Anal. 13,1978,35

161. K. Sadananda & P. Shaninian, Met. Trans. A8, 1977,439

162. J.D. Landes & J.A. Begley, ASTM STP 590,1976

163. D.J. Gooch, Mat. Sci. Eng. 29,1977,227

164. M.D.M. Bain, Thesis, Aston 1979

165. R.J. Dimelfi & W.D. Nix, Int. J. Frac. 13,1977,214

166. K.M. Nikbin, G.A. Webster, Proc. Joint Meeting, Prediction of Life of High Temp. Components London 1975

167. C.E. Turner, G.A. Webster, Int. J. Frac. 10,1974,455

168. J.D. Landes, J.A. Begley, ASTM, Spec. Tech. Pun. 560 1974

169. K.M. Nikbin, G.A. Webster, C.E. Turner Fracture 77 Int. Conf. Waterloo, Canada 1977

170. K.M. Nikbin, G.A. Webster, C.E. Turner ASTM STP 601

171. A.A. Wells, F.H. McBride, Can met. Quart. 6 1967,347

172. R.D. Nicholson, PhD. thesis (Aston) 1975

173. D.J. Gooch Mat. Sci. Eng. 27,1975,57

174. S. Floreen, R.H. Kane Met. Trans 7A 1976,1157

175. D.J.F. Ewing Int. J. Frac. 14,1978,101

176. D.R. Hayhurst, F.A. Leckie, C.J. Morrison J. Appl. Mech. Trans. ASME Series E 42,1975,613

177. J.T. Barnby, Eng. Frac. Mech. 7,1975,299

178. J.A. Williams, A.T. Price, Trans, ASME (H) 97 1975,214

179. D.J. Gooch, J.R. Haigh, B.L. King, Met. Sci. J. 11,1977,545

180. H.P. Van Leeuwen Eng. Frac. Mech 9,1977,951

181. V. Vitek, Acta Met. 26,1978,1345

182. V. Vitek Mat. Sci. Eng. 27,1977,209

183. H. Riedel, Mat Sci. Eng. 30,1977,187

184. L.M. Kachanov, Problems of Continium Mechanics, Soc. for Industrial & Applied Maths. Philadelphia, 1961

185. Shiro Kubo, Kitosugo Ohji and Keiji Ogura, Eng. Frac. Mech. 11,1979,315

186. D.M. Gilbey & S. Pearson, R.A.E. (Farnborough) Tech. Report. 66402, 1966

187. D.G. Widgery & J.F. Knott, Met. Sci. J, 12,1978,8

188. J.H. Faupel, Engineering Design, Page 375, Wiley 1964

189. Z. Marciniak, Aspects of Material Formability, MacMasters Univ.

190. W. Laidler, Thesis, University of Aston 1978